OBSERVATIONS IN A SEDIMENT-LADEN FLOW BY USE OF LASER-DOPPLER VELOCIMETRY

Thesis by

Catharine van Ingen

In Partial Fulfillment of the Requirements

for the Degree of

Doctor of Philosophy

California Institute of Technology

Pasadena, California

1982

(Submitted October 29, 1981)

ACKNOWLEDGEMENTS

This thesis is hardly the work of a single individual, but rather results from a collaboration of a number of people. To thank all of the contributors adequately is not possible; I am sincerely grateful for all of the time, tolerance, assistance and friendship from the many people named and unnamed upon whom I have relied.

First, and foremost, I would like to express gratitude and appreciation to Professor Norman Herrick Brooks for guidance, encouragement, and funding during this investigation. Dr. Brooks suggested the topic and was my principal advisor. His never failing optimism was always an inspiration and he was always able to transform my Sanskrit into intelligible English.

I am also indebted to Professor E. John List for numerous discussions on the analysis and physical interpretation of the data. His many suggestions and insights over the years were invaluable to this study.

The instrumentation could not have been built without the unique assistance of Elton F. Daly and Joe Fontana. From the smallest precision mirror mount to the major alterations of the flume support truss, Elton always had a better way.

The simple approach to laser velocimetry used in this study depends on the analog electronics contributed by Professor Ricardo Gomez. I have learned electronics by example; the formative lessons were most generously given by Professor Gomez. The Gomez magic boxes will never cease to amaze me.

Others also contributed to the development of the processing electronics. E. J. Siskind taught me about the brute force approach to grounding and the controlled approach to interfacing an external device to a computer. Discussions with Alan Barnes, John Gord, and Robert Landau yielded many, many helpful suggestions and comments. The electronics were constructed with the help of Sven Sondergaard, James Campbell, Jean Armistead, and Leonard Montenegro.

I would also like to thank the following people who, asking nothing in exchange, gave me access to their computer time, their computer facilities, and their computer expertise: Mark Bartelt, J. Blinn, K. Crandall, K. Clardy, DELCO-PEP, R. Feenstra, R. Flagan, W. Kropac, F. Nagy, C. L. Senior, and B. A. Zimmerman.

The continuing friendship and help of Joan Mathews, Pat Rankin, Pat Houseworth, Debbie Brownlie, Adelaide Massengale, Rayma Harrison, Gunilla Hastrup, and Melinda Hendrix-Werts is greatly appreciated. This thesis and other previous manuscripts could not have be prepared without them. Dave Byrum, Teresa Fall, and Phil Dubé provided help with the drawings and illustrations.

Discussions with fellow students have provided much needed support and camaraderie. I would especially like to thank Greg Gartrell, William Brownlie, Steve Wright, Derek Goring, Lisa Anderson, Jim Young, and Phil Roberts.

I have received much encouragement throughout the years from the Hydraulics faculty of the University of California, Berkeley. Initially instructors, now colleagues, Professors H. B. Fischer,

R. L. Wiegel, J. A. Hammack, and J. A. Harder remain valuable mentors.

The completion of this thesis required the special support given only by close friends. For assistance above and beyond that which can be considered normal, I would especially like to thank the Bunch, the Proprietors of Rent-A-Room, South, the staff of New York Consulting Buffoons, Inc., the Barracuda-in-Penguin-Clothing, and my favorite Sheep.

Financial support for this research was provided by the California Institute of Technology, which provided the laboratory facilities and a Graduate Teaching Assistantship during 1976 amd 1977, and the National Science Foundation under Grants ENG 75-15786, ENG 77-10182, and CME 79-20311.

ABSTRACT

The laser-Doppler velocimetry technique was adapted for use in sediment-laden flows. The developed instrumentation was used to make one-dimensional, instantaneous measurements of both fluid and sediment grain velocities throughout the water column in such a flow. The velocimetry results were obtained in a steady, uniform flow over a natural sediment bed in the high-transport, flat bed regime.

Laser-Doppler velocimetry is particularly attractive for use in sediment-laden flows as no calibration is required and no probe is introduced into the flow field. Measurements of the fluid velocity and the occurrence and velocity of individual sediment grains are possible with the instrumentation developed in this study. The major difficulties encountered are the possible conditional sampling, hence possible biasing, of the fluid velocity data and the failure of the instrumentation to record or resolve individual sediment grains at higher sediment transport rates. The instrumentation employed in this study is still in the developmental stages and suggestions for its improvement are given.

Despite the difficulties encountered, the data obtained in this study give some insights into the mechanics of suspension and entrainment of sediment during transport by water. The longitudinal turbulence intensity does not seem to be significantly affected by the presence of suspended sediment; the turbulence intensities observed in the sediment-laden flow of this study do not differ greatly from the values reported by previous investigators for clear fluid flows. The mean and standard deviation of the sediment

grain velocity were observed to be less than those for the fluid velocity in the lower portion of the flow, but respectively greater near the water surface.

The data demonstrate the shortcomings of the continuum approach to the mechanics of the suspension of sediment. The length (or time) scales of the fluid turbulence are smaller than the length (or time) scale of a set of sediment grains required to define suspended sediment concentration. Near the water surface, where the velocimeter acts as a grain counter, the probability density functions of the sediment grain inter-arrival times, the time between the detection of successive sediment grains, were observed to be negative exponentials. The transport of individual sediment grains might be modeled as a Poisson process.

This work is the foundation of an ongoing experimental program of direct measurements of the fine-scale, time-fluctuating characteristics of sediment-laden flows. This study developed and implemented instrumentation capable of making such measurements and established a conceptual framework for the subsequent interpretation of the data obtained. Two-dimensional measurements, with improved instrumentation, will give additional insights into the mechanics of sediment transport.

TABLE OF CONTENTS

LIST OF FIGURES

LIST OF TABLES

NOMENCLATURE

a	reference distance above the sediment bed
c	time-averaged sediment concentration at a point
$\bar{c}$	depth-averaged sediment concentration
$C(M)$	simple lag correlation coefficient
d	flow depth
dA	cross-sectional measurement area
d_g	geometric mean sediment grain size
f	Doppler frequency shift
f_b	friction factor of the sediment bed
f_j	fraction of the j^{th} sediment grain which passes through the laser beam intersection volume
f_m	measured value of f
$\frac{\Delta f}{f}$	relative error in Doppler frequency
$F(\nu)$	true Fourier transform
$F_N(\nu)$	discrete Fourier transform
F_R	Froude number = $\frac{u}{\sqrt{gd}}$
k	von Karman constant
M	lag index
m	mass of a sediment grain
m_j	mass of the j^{th} sediment grain
N_I	number of fluid velocity observations
N_J	number of sediment grain velocity measurements
$P(\nu)$	true power spectral estimate
$P_N(\nu)$	discrete power spectral estimate

P_s	stream power
P_{sw}	power to suspend sediment
Q	flow discharge
q	fluid flux per unit area
Q_s	total sediment transport rate
q_s	sediment discharge per unit area
R	hydraulic radius
$R(\tau)$	true auto-correlation coefficient
R_e	Reynolds number = $\frac{4Ru}{\nu}$
S	slope of the flow energy grade line
T	measurement period
t_i	time of measurement of the i^{th} fluid velocity event
t_j	time of measurement of the j^{th} sediment grain velocity event
u	longitudinal velocity component
u_i	i^{th} fluid velocity measurement
$\tilde{u}$	longitudinal sediment slip velocity
$\overline{u}$	mean fluid velocity
$\sqrt{\overline{u'^2}}$	longitudinal fluid turbulence intensity
u_{g_j}	j^{th} sediment grain velocity measurement
$\overline{u_g}$	mean sediment grain velocity
$\sqrt{\overline{u'^2_g}}$	sediment grain velocity standard deviation
u_*	fluid shear velocity
u_{*_b}	bed shear velocity
v	vertical velocity component
$\tilde{v}$	vertical sediment slip velocity
v_s	settling velocity of sediment grains

y	distance in the vertical direction
y_o	reference position of the sediment bed
z	Rouse exponent = $v_s/k\beta u_*$
α	constant
β	constant of proportionality $\beta = \varepsilon_s/\varepsilon_m$
$\gamma_N(\nu)$	power spectral window function
δ	Kroneker delta function
ε_m	turbulent diffusion coefficient for momentum
ε_s	turbulent diffusion coefficient for sediment
Δt	determined observation time
$\overline{\delta t_g}$	mean sediment grain inter-arrival time
$\sqrt{\overline{\delta t_g'^2}}$	sediment grain inter-arrival time standard deviation
$\delta_N(\nu)$	Fourier transform spectral window function
σ_g	geometric standard deviation of sediment grain size
λ	wavelength of laser light
$\psi_M(\tau)$	probability density function of lag time τ at lag interval M
ρ	fluid density
ρ_s	sediment density
η	frequency
ν	frequency
ν_s	sampling frequency
ϕ	half angle of laser beam intersection
τ	lag time
τ_o	boundary shear stress

overbar ($\overline{\quad}$)	mean value of a quantity
prime (')	fluctuating part of a quantity

Subscripts

g	denotes sediment grain value
i	fluid measurement index
j	sediment grain measurement index
k	integer index

CHAPTER 1

INTRODUCTION

After decades of laboratory and field research, the fundamental fluid mechanics of sediment transport is still only partially understood. As a result, predictions of gross flow parameters, friction factor and sediment discharge are difficult for uniform, steady flows and nearly impossible for non-uniform or non-steady flows. Until the small-scale time-fluctuating nature of sediment-laden flows is understood, the river engineer will be limited to the empirical methods now used to make such predictions.

Previous investigations have, for the most part, been limited to time-averaged measurements of flow variables due to lack of instrumentation. The effect of suspended sediment on the turbulent structure of the fluid has been theorized from measurements of sediment concentration and fluid velocity which were averaged over long sampling times and large sampling volumes. Also, most measurements have been made with some type of probe. The introduction of a probe into a sediment-laden flow deforms the flow field by deflecting the individual sand grains which collide with the probe and inducing local scour of the movable sediment bed.

In this study, a laser-Doppler velocimeter was developed and used to make instantaneous measurements of both fluid and sediment grain velocity throughout the water column. No probe was introduced into the flow field. The flow was not artificially distorted. Furthermore, the instrument needs no calibration for velocity measurements. The motions of individual sediment grains in the transporting fluid were observed.

The laser-Doppler technique has become well established for velocimetry of homogeneous fluid flows. Applications of the technique to two-phase flows are still relatively new. There are unique difficulties and limitations of the technique when applied to sediment-laden fluid flows. The instrumentation described in this study is clearly still in its developmental phase.

This new ability to make such fine scale measurements forced an examination of the traditional thinking about sediment transport. The motion of individual sediment grains, as well as collections of such grains, must be considered; sediment transport mechanics may be viewed as sediment grain kinetics. The traditional continuum approach, based on sediment concentration and its fluctuations, cannot adequately describe the experimental data. In fact, discussing sediment entrainment and suspension in terms of concentration may well obscure some of the fundamental mechanics of sediment-laden flows.

A review of previous theoretical and experimental investigations of the basic mechanics of sediment transport is given in Chapter 2. The traditional thought about suspension and entrainment of sediment by water is traced. Relevant experimental results are summarized.

A discussion of the meaning of fluid turbulence and an approach to sediment transport mechanics from the kinetics of individual sediment grains is given in Chapter 3. The form of the raw laser velocimetry data is presented. How such data can be processed to give insight into the basic mechanics of sediment transport is discussed. The meaning of sediment concentration and its relationship to individual grain motions is explored.

The application of the laser-Doppler velocimetry to sediment-laden flows is detailed in Chapter 4. The particular difficulties encountered in this study are discussed.

Chapter 5 enumerates and explains the velocimetry data analysis procedures. The errors inherent in the technique and the details of the data processing are discussed.

The experimental apparatus is briefly described in Chapter 6. A general description of the experimental flow conditions and the procedures followed is given in Chapter 7. The processed data are presented in Chapter 8 and discussed in Chapter 9. Suggestions for further work are also given in Chapter 9. The summary and conclusions of this study are presented in Chapter 10.

This work is the first portion of on ongoing experimental program to investigate the fine-scale time-varying characteristics of sediment-laden flows. The goal of this portion was two-fold. First was the development and implementation of instrumentation capable of observing these characteristics. Second was the development of a conceptual framework for the interpretation of the data obtained and to relate this new data to the results of previous investigations. This thesis reports on the development of the one-dimensional velocimetry system and the results obtained. The conceptual framework for the anticipated two-dimensional observations is established here. The necessary modifications to existing instrumentation are being made to implement the two-dimensional velocimetry system for continued research following this thesis.

CHAPTER 2

LITERATURE REVIEW

Previous investigations on the basic mechanics of turbulent sediment suspensions, including the effects of sediment grains on turbulent flow characteristics, have been primarily experimental. The relevant literature includes studies of flows transporting neutrally buoyant particles as well as studies of sediment-laden flows. This chapter reviews the various types of investigations relevant to the understanding of the entrainment and suspension of sediment in a turbulent fluid and relates that previous work to the present inquiry.

2.1 Theoretical studies of sediment suspension

A theoretical expression for the vertical sediment concentration distribution in a two-dimensional open channel flow was developed by O'Brien (1933) and expanded by Rouse (1937). By equating the upward diffusion of suspended sediment due to turbulence to the rate of settling due to gravitational force, they obtained the suspended load differential equation

$$v_s c + \epsilon_s \frac{\partial c}{\partial y} = 0 \qquad (2.1.1)$$

Here, y is measured vertically upward from the sediment bed, ϵ_s is the turbulent diffusion coefficient for sediment, c is the time-averaged suspended sediment concentration, and v_s is the settling velocity of the sediment grains in clear, stagnant fluid. In this form, the equation can only be solved if ϵ_s and v_s are known. If, following von Karman (1934), the diffusion coefficient for sediment is assumed proportional to the diffusion coefficient for fluid momentum, a

solution can be obtained. In a two-dimensional open channel flow, the momentum diffusion coefficient may be derived for the logarithmic velocity profile, giving

$$\epsilon_m = ku_*y(1 - \frac{y}{d}) \qquad (2.1.2)$$

where k is the von Karman constant, u_* is the fluid shear velocity ($u_*= \sqrt{\tau_o/\rho}$), d is the fluid depth, τ_o is the boundary shear stress, and ρ is the fluid density. Assuming that

$$\epsilon_s = \beta\epsilon_m \qquad (2.1.3)$$

where β is presumed to be a constant and substituting into equation 2.1.1 above, the solution is

$$\frac{c}{c_a} = (\frac{d-y}{y}\frac{a}{d-a})^z \qquad (2.1.4)$$

where c_a is the concentration at depth a and z is the "Rouse" exponent ($z=v_s/\beta ku_*$). The above equation was not expected to be reliable very near the bed (y=0) or very near the surface (y=d) as the velocity profile deviates from the logarithmic law in those regions.

Einstein and Li (1958) proposed an intermittent model of the laminar sublayer. The sublayer was supposed to behave cyclically, growing in thickness, then rapidly disintegrating. In this manner, velocity fluctuations could diffuse and extend throughout the flow. The entrainment of individual sediment grains from the bed would take place during the disintegration phase.

The intermittent behavior of the laminar sublayer was explicitly studied by Sutherland (1966). He made simultaneous observations of a dye streak near a flat sediment bed and the movement of individual

sediment grains. When the local dye line was disrupted, grains moved. He hypothesized that turbulence from the main flow impinges on the bed, disrupting the laminar sublayer and entraining sediment.

Large scale, coherent structures or bursts as the mechanism for sediment suspension were suggested by Jackson (1976). Observers of rivers have long noticed that the water surface is periodically disturbed by boils containing large amounts of suspended sediment. Recent developments in the study of turbulent shear flows (for example Offen and Kline (1975)) indicate that these boils may well be the result of large upward-tilted streamwise vortices. Thus, sediment grains may be periodically entrained at the bed and rapidly transported upward through the entire water column. Grains return to the bed relatively slowly, due to the action of gravitational forces. This argument was supported qualitatively by river data. Clouds of suspended sediment are also easily observed in flumes.

A theoretical treatment of particles suspended in turbulent flows was published by Hino (1963). A decrease in the von Karman constant with increased particle concentration was predicted. For neutrally buoyant particles, a predicted increase in root mean square turbulence intensity, $\sqrt{u'^2}$, agrees with the experimental data described below. The predicted slight decrease in $\sqrt{u'^2}$ for settling (negatively buoyant) particles is not in agreement with the prior experimental observations discussed in Section 2.3.

2.2 Experimental studies of mean properties in sediment-laden flows

The first experimental investigation of the effects of suspended sediment on the transporting flow was by Gilbert (1914). Contrary to his expectations, he noted that fluid discharge, sediment discharge and channel slope were not simply related.

The suspended load equation was experimentally verified by Vanoni (1946). Moreover, the experiments demonstrated that suspended sediment at alluvial concentrations affects the turbulent characteristics of the flow. Vanoni observed an increase in the slope of the velocity profile, or decrease in the von Karman constant, with increasing sediment load. Near the bed, the velocity profile departed from the logarithmic profile. Vanoni speculated that the presence of sediment suppressed or damped out turbulence, causing the mixing of momentum to be reduced, thus reducing the von Karman constant.

Vanoni's results were confirmed and expanded by his students, Ismail (1952), Brooks (1954) and Nomicos (1956). Ismail noted that the flow resistance in a sediment-laden flow was increased over that in a clear fluid flow only when bed forms occurred. He found that β was a function of sediment size (β=1.5 for d_g=0.10 mm, β=1.3 for d_g=0.16 mm).

In a more careful analysis, Brooks noted a variation in β of only 0.93 to 1.10 with sediment size. This analysis includes a decrease of the mean sediment size with elevation in the suspension due to selective sorting and reduction of the fall velocity due to particle interference. He concluded that β is very close to 1.0. This analysis demonstrated the need to consider sediment size variations with height

above the bed when applying the suspended load equation. For each sediment size fraction, a mean fall velocity is computed. The suspended sediment samples were sieved into separate size fractions and vertical sediment concentration profiles and z values were obtained for each size fraction.

Brooks also considered the meaning of the "sediment bed". To compute the total sediment discharge, the integral

$$\int_{y_o}^{d} u\, c\, dy \qquad (2.2.1)$$

where u is the fluid velocity is performed. Here, y_o is chosen to be small distance above y=0, as otherwise the integral diverges for $z \geq 1$. Four reasonable possibilities were proposed

$$y_o/d = \begin{cases} = 2d_{50}/d & 2d_{50} \text{ above the bed as lower limit of suspension} \\ = 11.6\nu/u_* d & \text{estimated laminar sublayer} \\ = e^{-ku/u_*} - 1 & u(y_o/d) = 0 \text{ by the logarithmic velocity law} \\ \left[\dfrac{c(y=\frac{d}{2})}{c_b}\right]^{1/z} & c(y_o/d) = \text{bed concentration} \end{cases} \qquad (2.2.2)$$

Brooks advocated the use of the maximum y_o. He also reported a deviation from the predicted suspended sediment profiles in the upper half of the flow. He concluded that in this region, where the shear stress and concentration gradients are small, the assumption that mixing of sediment is proportional to the mixing of fluid momentum is no longer valid.

Nomicos observed the effects of increasing sediment concentration on the flow. He formed a stable artificial flat bed of sediment in a

recirculating flume. Flows at the same discharge and depth with increasing, but small, amounts of sediment in the flume system were observed. His experiments showed that, with the flow Reynolds number and boundary roughness held constant, an increased sediment load decreased the friction factor. The velocity profile was observed to differ greatly from the logarithmic law near the bed.

Einstein and Chien (1952,1955) proposed modifications to the suspended load theory based on a mixing length concept. Their expression contained an unevaluated constant. Flume experiments did not help to evaluate the constant, and as such the expression is of little practical use. They also correlated the value of the von Karman constant to the ratio of the power to suspend sediment, P_{sw}, and the stream power, P_s. This ratio is given by

$$\frac{P_{sw}}{P_s} = \frac{(\frac{\rho_s}{\rho} - 1)\ v_s \bar{c}}{uS} \qquad (2.2.3)$$

where ρ is the fluid density, ρ_s is the sediment density, g is the gravitational constant, S is the slope of the flow energy grade line, and $\bar{c}$ is the depth-averaged concentration. The ratio can be used to predict k.

Bagnold (1954) suggested that collisions between individual sediment grains provide the shear to suspend sediment. He performed experiments using neutrally buoyant particles in the annular space between two concentric cylinders to confirm this. The intergranular stress was found to be very small when the concentration of sediment was below 0.25 per cent by volume. Thus, grain collisions may only be important near the sediment bed where the sediment concentration

approaches this value.

2.3 Experimental studies of fluctuating properties in sediment-laden and related fluid flows

In order to appreciate the effects of suspended sediment on turbulence characteristics, a knowledge of those characteristics in clear fluid flows is necessary. The first measurements of turbulent velocity fluctuations in a two-dimensional flow field were made by Laufer (1950). Data were obtained with a hot-wire anemometer in a wide rectangular air duct with smooth walls. He found that longitudinal turbulence intensity, $\sqrt{\overline{u'^2}}$, has a minimum at the centerline y=d/2 (analogous to the free surface in an open channel) and a maximum, approximately twice the wall shear velocity, at a small distance from the wall. As Reynolds number decreased, the relative turbulence intensity was observed to increase.

Turbulence measurements in a water flow in a flume were obtained by Raichlen (1967) using a hot-film anemometer. The relative longitudinal turbulence intensity, $\sqrt{\overline{u'^2}}/u$, was observed to be a maximum near the flume bottom and decreased toward the free surface. Neither a clear maximum in turbulence intensity nor a change in turbulence intensity with Reynolds number were noted. Turbulent length scales were found to be proportional to the flow depth.

Blinco and Partheniades (1971) used a hot-film anemometer to measure turbulence characteristics over smooth and rough boundaries (d_g=2.54 mm for the latter). They found that $\sqrt{\overline{u'^2}}$ was affected by the boundary roughness. A maximum in $\sqrt{\overline{u'^2}}$ was noted at some distance from the wall. The position of the maximum $\sqrt{\overline{u'^2}}$ was strongly related to

the boundary roughness; as the boundary roughness increased, the maximum was observed further away from the boundary.

Measurements in flows transporting neutrally buoyant particles were reported by Elata and Ippen (1961). An impact tube pressure transducer was used to measure longitudinal velocity fluctuations in flows with up to 0.25 per cent by volume polystyrene spheres. An increase in turbulence intensity and a decrease in von Karman constant were noted with increased particle concentration. A small increase in friction factor with increased particle concentration was reported. Elata and Ippen concluded that suspended particles do not damp turbulence, but rather change its structure. They speculate that the particles cause increased production of small scale eddies, on the order of the particle size. The major effect of suspended particles occurs near the flow boundary. Particle size is judged to be more important than particle buoyancy in altering the fluid turbulence. These results were confirmed by Daily and his co-workers (1961,1964,1966).

Bohlen (1969) made hot-wire anemometer measurements in flows transporting particles which were only slightly negatively buoyant. The experiments were made in an open channel, 3 cm deep, using silicon oil as the transporting fluid. Particle concentrations from 0.8 to 3.5 per cent by volume were observed. The mean particle fall velocity (d_g=0.595 mm) was 0.37 cm/sec. Bohlen reported a decrease in the von Karman constant and an increase in turbulence intensity. He noted that a maximum in $\sqrt{\overline{u'^2}}$ near the bed as in clear fluid flows did not exist in particle-laden flows. Turbulence intensity increases with particle

concentration throughout the depth, but particularly so near the boundary. Eulerian velocity fluctuation auto-correlations did not show any obvious effects of particle presence. Bohlen notes that particles colliding with the probe may introduce error in velocity fluctuation measurements due to vibration of the wire. At the low concentrations used, he judged the error to be negligible.

Hot-film anemometer measurements in sediment-laden flows were taken by Mc Quivey (1973). He reported higher turbulence intensity in flows transporting sediment than in clear water flows with the same flow depth, shear velocity and boundary roughness. His raw anemometer data contained large voltage spikes which he attributed to sand grains colliding with the probe tip. Peaks in the velocity auto-correlation due to collision-induced vibrations of the probe were also reported. Mc Quivey stated that these effects need not invalidate the data taken. He recommended a procedure of removing the spikes, and the application of a correction developed for fluid contaminated by dust or bubbles. Knowledge of the vibrational charateristics of the probe was said to allow better interpretation of the auto-correlation and power spectrum.

Investigators have applied the laser-Doppler technique to sediment-laden flows; however, such applications have been primarily for preliminary instrument development purposes rather than investigations of the physics of the fluid-sediment interaction. Müller (1973) compared measurements of mean velocity and longitudinal turbulence intensity in a movable bed sediment-laden flow (u=68.8 cm/sec, d=2.57 cm) with measurements in a clear fluid flow over a fixed sediment bed. A commercially available velocimeter with

conventional transmitting optics and a frequency tracker processor was used. An increase in turbulence intensity was reported. As explained in Chapter 4, the increase may be primarily due to the spectral broadening inherent in frequency tracker processor.

Müller and Glover (1977) proposed a method for avoiding saturation of the photodetector due to the larger light scattering by the sediment grains. A vertical sediment-laden flow of unreported concentration was used to test the method. Durst (1978) detailed a method used successfully in turbulent gas flows with glass spheres (d_g=100, 200, 400, and 800 μm). The concentration of the spheres was not reported. Complex receiving optics and electronics were used to separate the light scattered by the spheres from that by the gas flow tracer particles. The method is said to be applicable to sediment-laden water flows.

Luque and van Beek (1976) reported measurements of turbulent bed shear stress obtained by laser-Doppler velocimetry in flows near the threshold of motion. A slight decrease in root mean square bed shear stress, on the order of 10 per cent, was noted with the initiation of sediment motion. No direct velocity measurements were reported.

2.4 Summary

The interactions between suspended sediment and fluid turbulence have, for the most part, been surmised from measurements which are averaged over large spatial and temporal samples.

The relevance of measurements in flows with suspensions of neutrally buoyant particles to sediment-laden flows is limited. First, no fixed bed of the transported particles is formed. The bottom channel roughness is unaffected. Moreover, neutrally buoyant particles do not create a density gradient in the flow. Density, turbulence generation and turbulence dissipation are quite interrelated. The density is most affected in a sediment-laden flow near the boundary, the site of turbulence generation.

Measurements of turbulent flow characteristics in two-phase flows with hot wire and hot film anemometers are limited by calibration difficulties. The abrasion of the probe tip and the vibration of the probe due to particle impact creates long term drift in the velocity measurement. Also, any probe distorts the local fluid flow field especially near the sediment bed, which is scoured locally in the vicinity of the probe.

As the laser-Doppler velocimetry technique is still relatively new to the field of experimental fluid mechanics, few applications of the technique to particle-laden fluids have been reported. Most publications demonstrate the success of the application of an experimental apparatus to a flow situation, rather than exploring the fluid mechanics of that flow in detail.

To understand the fundamental mechanics of sediment-laden flows, measurements of the fine-scale, time-fluctuating flow characteristics are required. Laser-Doppler velocimetry is the most promising technique because it allows direct non-intrusive measurements of the flow velocity.

CHAPTER 3

FLUID TURBULENCE AND SEDIMENT GRAIN KINETICS

By use of laser velocimetry it is possible to observe directly the motion of individual sediment grains and the turbulent fluid which is transporting such grains. To make use of such data, the mechanics of sediment entrainment and suspension must be examined on a granular scale. Furthermore, this approach must be reconciled with the traditional continuum approach, utilizing the concepts of mean sediment concentration and turbulent diffusion in deriving the suspended load equation. The mean motion of a collection of sediment grains must be related to the motion of the individual grains.

This chapter discusses the general case of data available from a two-dimensional laser-Doppler velocimeter. The instrument developed during and employed in this study is a one-dimensional velocimeter, measuring only the streamwise velocity component. The one-dimensional results obtained are a subset of the two-dimensional results discussed.

The basic data received from a two-dimensional velocimeter consist of a set of four scalar time series

$$\begin{aligned} &u\,(t_i) \\ &v\,(t_i) \qquad\qquad i=1,2,3,\ldots,N_I \\ &u_g(t_j) \\ &v_g(t_j) \qquad\qquad j=1,2,3,\ldots,N_J \end{aligned}$$

where u and v are streamwise velocity and vertical velocity and the subscript g denotes sediment grain values. Note that the times of measurement t_i and t_j are not coincident. The raw data from a single experiment consists of a set of such velocity observations at each of

several vertical positions within the flow field, all on the flume axis.

3.1 A grain-by-grain approach to the mechanics of sediment-laden flows

Consider the sediment grain measurements at a single vertical position. The intersecting laser beams form a measurement volume with an effective frontal area, dA. Note that the effective frontal area is a function of the actual, optically determinable, laser beam intersection cross-sectional area, the geometry of the receiving optics, and size of the scattering particles. The effective area is small, on the order of a few times the cross-sectional area of a single sediment grain. If every grain which passed through this area generated a single good velocimetry signal, the velocimeter would be, effectively, a particle counter. The sediment mass flux through the effective frontal area would be given by

$$q_s(dA,\Delta t) = \frac{1}{\Delta t\, dA} \sum_{j=1}^{N_J} m_j f_j \qquad (3.1.1)$$

where f_j is the mean fraction of the volume of the jth grain which passed through the area dA, m_j is the mass of the jth sediment grain, N_J is the number of sediment grains observed in time Δt, $q_s(dA,\Delta t)$ is the sediment transport rate (mass/time/area), and Δt is the sampling time. To determine f_j, the exact trajectory through the beam intersection volume of the sediment grain must be known. This is not feasible. A grain need never be wholly contained within the volume yet will generate a valid velocimetry signal. A sediment grain may graze the volume without generating a valid velocimetry signal. If each

grain is assumed to have $f_j=1$, the sediment flux may be overestimated during the time that a grain is observed and underestimated during the time that no grain is observed. Averaging over a large number of grains, however, the contribution to the sediment flux by the grains which graze the beam intersection volume should balance the excluded portions of the grains which generate valid velocimetry signals. That is, in the mean, the two effects will tend to cancel. Thus, for a uniform sand, the above simplifies to

$$q_s(dA,\Delta t) = \frac{mN_J}{\Delta t\, dA} \qquad (3.1.2)$$

The effective frontal area, dA, remains to be determined. There is a physical surface area to the laser beam volume, but due to the small size of the volume, on the order of a few grains, the physical area is not the effective area. Most grains which generate good velocimetry signals will never be more than half contained within the physical beam intersection volume. To determine the effective frontal area, calibration is necessary. Thus, the mean sediment transport rate may be determined by the velocimeter only after calibration with traditional suction sampling tube measurements. The resulting calibration is only valid for the long time-averaged mean transport rate.

Unfortunately, the actual situation is more complex. While the effective scattering volume is small, it is large enough to allow multiple grains to pass through simultaneously. The probability of the scattering by multiple grains is a function of the scattering volume size, the grain size, and the local grain concentration. If every grain velocimetry signal is assumed to be generated by a single

sediment grain, the sediment flux will be underestimated. As the sediment flux increases, the probability of scattering by multiple grains increases, and the error in the estimate of the flux increases. The sediment transport rate may be determined by the velocimeter after calibration with traditional suction sampling tube measurements, but the calibration will not be linear.

From the above raw data, it is possible to compute a time series of sediment grain inter-arrival times, δt_{g_j}, and their mean, $\overline{\delta t_g}$.

$$\delta t_{g_j} = \frac{1}{2} (t_{j+1} - t_{j-1})$$

$$\overline{\delta t_g} = \frac{1}{N_J - 1} (t_{j=N_J} - t_{j=1}) \qquad (3.1.3)$$

Thus, the mean sediment transport rate is inversely proportional to the mean sediment grain inter-arrival time. Similiarly, fluctuations in the transport rate are related to fluctuations in the reciprocal of grain inter-arrival time. Periods of high relative transport are associated with relatively short grain inter-arrival times; low transport with long grain inter-arrival times.

The mean and variance of the grain velocity may be calculated for an ensemble of grains passing through the measuring volume. The grain data may also be split into two groups: upward-moving grains and downward-moving grains. Note that the mean grain velocity and inter-arrival time of the upward-moving grains need not be equal to the means of the downward-moving grains on the average over time. For the transport in the vertical to be in equilibrium, all that is required is that the number flux of the upward-moving grains be equal to the number flux of the downward-moving grains through the measuring volume. If

large scale turbulent bursts are a primary entrainment mechanism, it may well be that the mean velocity of the upward-moving grains is larger than that of the downward-moving grains.

Now consider the full data set. It is possible to relate fluid velocity measurements with sediment grain velocity measurements. The grain slip velocities, computed in this way, are given by

$$\tilde{u} = u_{g_j} - u_i$$
$$\tilde{v} = v_{g_j} - v_i \qquad (3.1.4)$$

The computation may be made for any t_i and t_j, but is only physically meaningful if the time lag between measurements, $/t_i - t_j/$, is small with respect to the turbulence time scale. The mean vertical slip velocity may be compared to the quiescent fall velocity (the average rate of fall of the grain in clear quiescent water) to determine the effects of turbulence and sediment transport on sediment grain settling. The grain record may be again split into upward-moving and downward-moving grains. Upward-moving grains should be associated with upward-moving fluid parcels, fluid parcels with positive vertical fluid velocity.

Correlations of grain inter-arrival times with fluid velocity may also be computed. The correlations of fluid velocity fluctuation with the inverse of sediment grain inter-arrival time have important physical interpretations. As noted above, the inverse of the sediment grain inter-arrival time is a measure of the sediment transport rate. Thus, the above are correlations of transport rate and fluid velocity. If these correlations are made with the divided grain record, with upward-moving and downward-moving grains, the correlations give insight into entrainment. If large scale turbulent bursts are a primary

entrainment mechanism, positive fluid velocity fluctuations should be associated with low sediment grain inter-arrival times. Settling, downward-moving grains should be diffuse, have longer inter-arrival times, and not be associated with strong positive fluid velocity fluctuations. A measure of the length scale over which the sediment grain is affected by the fluid turbulence may be made by computing the above at different lag times.

In summary, a sediment-laden flow is a mixture of flowing fluid and individual moving sediment grains. The motion of the grains is affected by and affects the fluid motion, but may be examined independently. The sediment transport rate may be considered independently of the fluid discharge or suspended sediment concentration. Direct measurements of grain motions give insight into certain details of the mechanisms of suspension and entrainment.

3.2 Sediment concentration and the continuum approach to the mechanics of sediment-laden flows

It remains to tie the laser velocimetry measurements and the grain-by-grain viewpoint to previous measurements and theory. Central to previous work is the concept of sediment concentration. Concentration is usually defined as the ratio of the sediment mass discharge through some sample area to the total volume flux through the same sample area. In alluvial flows, the total volume flux is effectively equal to the fluid volume flux. Thus, sediment concentration is given by

$$c(T) = \frac{q_s(T)}{q(T)} = \frac{1}{\bar{T}udA_s} \sum_{j=1}^{N_J} m_j \qquad (3.2.1)$$

where c(T) is the sediment concentration (mass/volume), dA is the inflow cross-sectional sampling area, m_j is the mass of the jth sediment grain, N_j is the number of grains collected, T is the sampling time, and $\bar{u}$ is the mean inflow velocity. For a uniform sand, this simplifies to

$$c(T) = \frac{mN_J}{T\bar{u}dA_s} \qquad (3.2.2)$$

Note that the concentration is not only a function of the sediment transport but also of the fluid volume flux.

Imbedded in the concentration approach is the assumption that a sediment-laden flow may be treated as a continuum. It is assumed that sediment grains may be treated as a tracer, similiar to dye, heat, or buoyancy. This approach is only valid if the length and time scales of the relevant fluid properties are on the same order of those of the tracer properties. For molecular tracers, such as dye, the validity is obvious. For sediment, the concept must be applied with care.

Mean sediment concentration must be defined over a large number of grains, a large sample volume and large sampling time. In the case of traditional sampling tube samples, which have a sample volume of one liter, the number of grains collected per sample typically ranges from one thousand to one million. The sampling time is on the order of three minutes. The sampling tube collects some large set of grains which is sampled and weighed. The sampling tube is, in effect, a grain counting device. Grains are not individually counted; however, the number of grains collected in a suction sample may be computed for sediments of known size distribution. The mass collected per unit time is the sediment flux through the sampling tube intake area. A sediment

concentration measurement is then derived from that measured sediment flux by dividing by the fluid volume flux. In analysis, that concentration "measurement" is then multiplied by the mean velocity measurement (at the same point) to compute the sediment transport rate. The sediment transport rate is the originally measured quantity. In other words, sediment concentration is not measured directly with a sampling tube; it is the sediment transport rate through the sampling tube tip which is observed.

Concentration fluctuations (c') must also be defined over some number of grains. Fluctuations in concentration are a function not only of the "instantaneous" sediment transport, but of the "instantaneous" volume flux. Usually, fluctuations in concentration are defined to derive an expression for fluctuations in transport. This is the case in the suspended load equation which expressed the vertical conservation of sediment flux as

$$\overline{(v_s + v')(c + c')} = v_s c + \overline{v'c'} = 0 \qquad (3.2.3)$$

The first term, $v_s c$, is the mean sediment transport due to gravity (negative for settling down). The second, $\overline{v'c'}$, is the net upward transport due to fluid turbulence. Both terms apply to averages over some volume of fluid which contains both upward-moving and downward-moving grains. It is not possible to assign individual grains to either term. The motion of an individual grain is determined by both effects.

The term $\overline{v'c'}$ is the correlation of the vertical fluid velocity fluctuations and the sediment concentraton fluctuations. If the length scales of the two processes are disparate, the expression losses its

physical significance. In alluvial flows, particularly in laboratory flumes, this is the case. Consider the case of fine sand, d_g=0.25 mm, in transport (u=50 cm/sec, d=7.5 cm). At common equilibrium concentrations, on the order of 0.3 grams per liter, the grains will be separated by about 20 grain diameters, approximately 5 mm. Measurements by Raichlen (1967) in a clear water flow may be used to estimate the turbulence length scales. Even if the "instantaneous" concentration is defined over a sample volume containing only ten grains, the volume required would be approximately three times that of a turbulent eddy with a diameter equal to the fluid turbulence micro scale (estimated as 0.1 times the depth).

The flow volume actually sampled is a long filament of the flow. In the case of a suction sampling tube, a one liter sample is typically a filament 90 meters in length. The cross-sectional area of the laser velocimeter is substantially smaller than that of a suction sampling tube. To sample a one liter volume of the flow, the velocimeter must observe a filament approximately 500 meters in length. To observe ten sediment grains, the velocimeter will sample a 5 cm filament. This length is on the order of the turbulence macroscale of the flow. The two processes, fluid velocity fluctuation and sediment concentration fluctuation, seem to have quite different length scales. This is an artifact of the relatively large length scale required to define sediment concentration fluctuations.

The suspended load equation is a statement of the competing effects, gravity and fluid turbulence, which suspend sediment. Computation of a $\overline{v'c'}$ term would not give insight into actual

entrainment mechanisms. Nor is there insight into the fine scale, time-varying structure of the fluid-sediment mixture. There are many complex small scale interactions in a sediment-laden flow which cannot be adequately described by time-averaged quantities and continuum concepts. However, grain motion measurements, together with fluid turbulence measurements, should yield valuable insight into the mechanisms of suspension and entrainment when examined on a grain by grain basis.

3.3 Fluid turbulence and Eulerian measurements of fluid velocity fluctuations

Consider first only the fluid velocity measurements. The data are similar to the majority of the existing experimental observations of turbulence. Comparision of the data obtained in a sediment-laden flow to similar data obtained in a clear fluid flow would seem to allow direct determination of the effect of transported sediment on the fluid turbulence. Unfortunately, such a determination is not simply possible.

Most experimental observations of turbulence in fluid flows are Eulerian. The fluid velocity is sampled at a single spatial location over some observation time which is long with respect to the time scales of any fluctuations in the flow. The data from several locations, obtained at non-coincident times, are used to infer the Lagrangian behavior of the flow field. The behavior of a fluid parcel as it moves through space is extrapolated from measurements of a number of fluid parcels which pass a set of known spatial locations.

The validity of inferring the Lagrangian nature of sediment-laden flows is questionable. A flow transporting sediment has, by necessity, a movable, deforming boundary. Even in the relatively simple case of transport in the flat bed regime, the flow boundary, the sediment bed, is continously in motion. In fact, the bed is defined primarily by convention, typically by the elevation observed in a quiescent flume. No rigorous determination of the location at which the fluid and sediment motion ceases has been made.

The motions of the flow boundary have two important consequences. First, the time required to observe all possible fluctuations of the flow is determined not only by the time scales of the fluid turbulence, but also by the time scales of the bed deformations. Observations over a few minutes are typically sufficient to characterize the fluid velocity fluctuations in fixed-boundary flows. In a sediment-laden flow, to characterize the bed motion adequately may require hours of observation. Second, a measurement location may be fixed at a point in space, but not fixed with respect to the boundaries of the flow field. This is most obvious if dunes are present.

The importance of the bed deformation on various flow properties is related to the magnitude of the deformation and the sensitivity of the selected flow property. Long term, spatially averaged properties, such as fluid discharge, are relatively insensitive to even large fluctations in bed elevation. Average fluid velocity at a point may be sensitive only to large changes in bed elevation. Fluid velocity fluctuations and local values of boundary shear may be sensitive to relatively small fluctuations in the bed elevation.

The order of magnitude of the change in fluid velocity due to small fluctuations in bed elevation may be estimated by a simple calculation. Assume the fluid velocity follows the logarithmic law and that the variation in the bed elevation is sinusoidal. The velocity at a fixed point in space will vary over the period of the bed oscillation. The observed standard deviation in the fluid velocity is shown in Figure 3.3.1 for various amplitudes of bed distortion. The fluctuations induced, even for the relatively small amplitudes considered, are of the order of the velocity fluctuations experimentally observed in turbulent flows.

Thus, it is not meaningful simply to compare velocimetry observations in movable boundary flows with observations in fixed boundary flows. In a fixed-bed flow, the velocity fluctuations are due solely to fluid turbulence. In a movable bed flow, the observed velocity fluctuations may also be due to deformations of the flow field. The turbulent kinetic energy of the fluid may be reduced with respect to that in a clear fluid flow due to the work done to suspend sediment, yet the fluid velocity fluctuations observed at a fixed point in space may be increased.

There exists an additional mechanism for the generation of fluid velocity fluctuations. Clear fluid flows with density stratification support internal waves. A fluid flow with suspended sediment is a density-stratified flow. The density gradient is a function of the sediment concentration gradient.

$$\frac{\partial \rho}{\partial y} = \left(\frac{s-1}{s}\right) \frac{\partial c}{\partial y} = -\left(\frac{s-1}{s}\right) cz' \left(\frac{d}{d-y}\right) \frac{1}{y} \qquad (3.3.1)$$

where ρ is the flow density, s is the specific gravity of the sediment

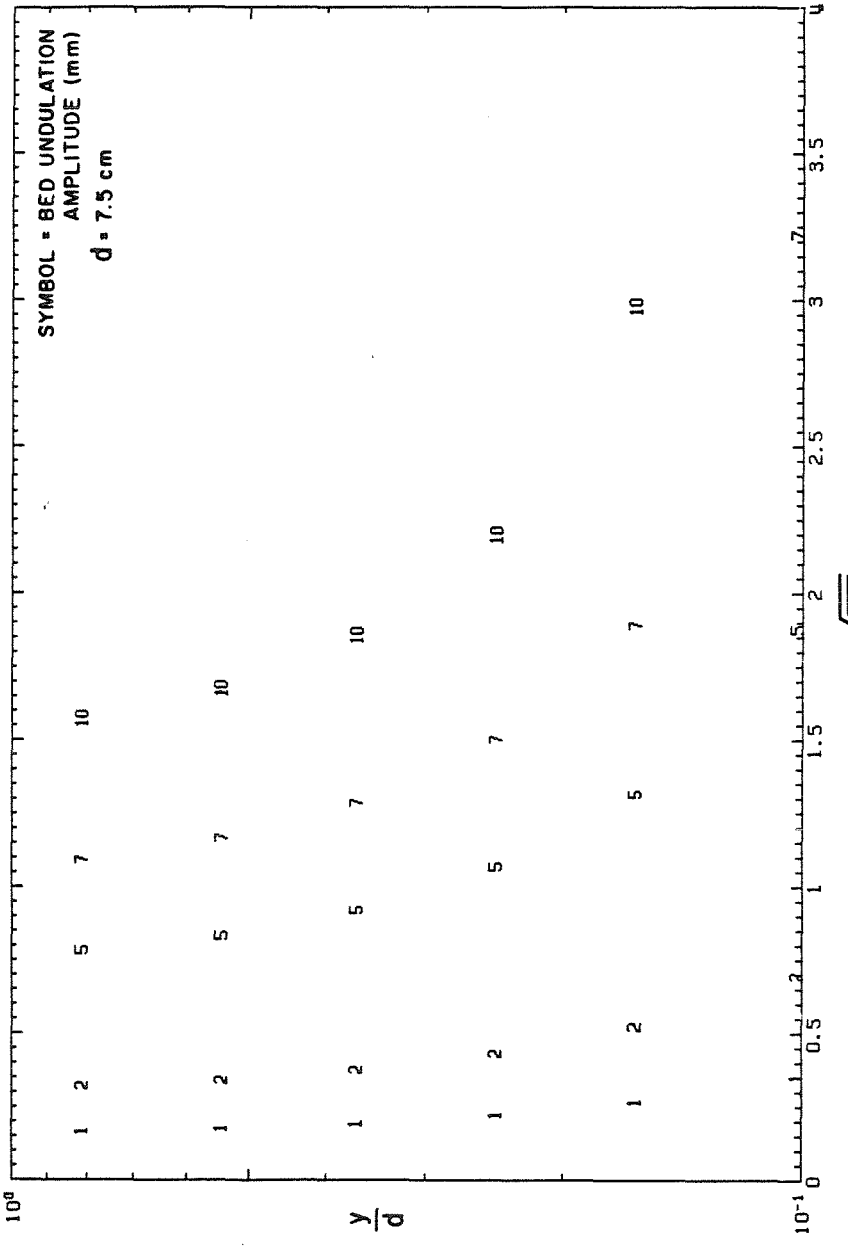

Figure 3.1.1 Computed velocity standard deviation due to oscillations of the sediment bed

and c is the sediment concentration (mass/volume). The time scale of such wave motion is determined by the Brünt-Väisälä frequency, given by

$$N^2 = -\frac{g}{\rho}\frac{\partial \rho}{\partial y} \qquad (3.3.2)$$

where N is the Brünt-Väisälä frequency and g is the acceleration of gravity. The frequency therefore will vary from 0 at the free surface to approximately 3 Hertz near the bed surface. Thus, velocity fluctuations with time scales on the order of the turbulence macroscale may occur due to internal wave motions.

In summary, the velocity fluctuations observed in a sediment-laden flow may be caused by migrating bed forms and internal waves in addition to fluid turbulence. Thus, it is not possible simply to determine the effects of sediment entrainment and suspension on the fluid turbulence. In fact, due to the long times required to characterize some bed forms, the quantity of data required to observe all existing fluctuations in the velocity may well be prohibitively large.

CHAPTER 4

LASER-DOPPLER VELOCIMETRY APPLIED TO SEDIMENT-LADEN FLOWS

The laser-Doppler technique has been used quite successfully in homogeneous fluid of two-phase gaseous flows. The technique does not distort the flow field and no calibration is required. Thus, it is particularly attractive for use in sediment-laden flows. There are, however, unique difficulties with the technique when applied to such flows. This chapter discusses the application of the technique to a sediment-laden flow. It is not intended to describe in detail the basic technique, but rather to give an overview of the specific system developed for use in sediment-laden flows in this study. For a general discussion of laser-Doppler velocimetry, see Durst, Melling and Whitelaw (1976). For a detailed description of the system developed in this study see Appendices A and B.

Due to lack of instrumentation, most previous investigations of sediment-laden flows have been limited to time-averaged measurements of flow variables. Also, most measurements have averaged over a large spatial volume. The interactions between fluid turbulent structure and suspended sediment have been theorized from the mean sediment concentration and mean velocity profiles. Hot-film anemometry has been done in sediment-laden flows, but the technique has real disadvantages. Sediment grains collide with the probe tip, seemingly causing short voltage spikes in the signal. Rapid abrasion of the probe tip gives long term calibration difficulties due to the changing thermal conductivity of the probe surface. Moreover, the local flow field is deformed by grain-probe collisions in two ways: vibrations of the

probe at its natural frequency are induced and the sediment grains are deflected from their natural trajectory. The gross flow field is also distorted, as the introduction of any probe in the vicinity of the movable sediment bed induces scour.

In homogeneous fluid flows, the laser-Doppler technique depends on the presence of small scattering particles. The flow is either seeded (particles are added to the fluid) or filtered to obtain a diffuse distribution of scattering particles. Ideally, at any instant only one particle is present in the measuring volume. The particles are chosen to be small enough ($\sim$10 μm) to follow the small scale fluid flow. In a sediment-laden flow, there are sediment grains also in suspension. These grains are quite large with respect to the small fluid tracer particles and need not follow the flow as the smaller particles do. The sediment grain concentration is determined by the flow mechanics; near the bed, the concentration becomes large and the grains are not diffuse.

For the laser-Doppler technique to be useful in a sediment-laden flow, the light scattered by the fluid tracer particles must be detectable and distinguishable from that scattered by the sediment grains. The measuring volume must be such that the sediment grains appear diffuse, that is, there are times in which only a fluid tracer particle is in the measuring volume.

Figure 4.1.1 shows the basic dual-scattering optical arrangement used in one-dimensional laser-Doppler velocimetry. The laser light beam is split into two beams of equal intensity, which are then made to intersect at a point within the flow field. When a particle passes

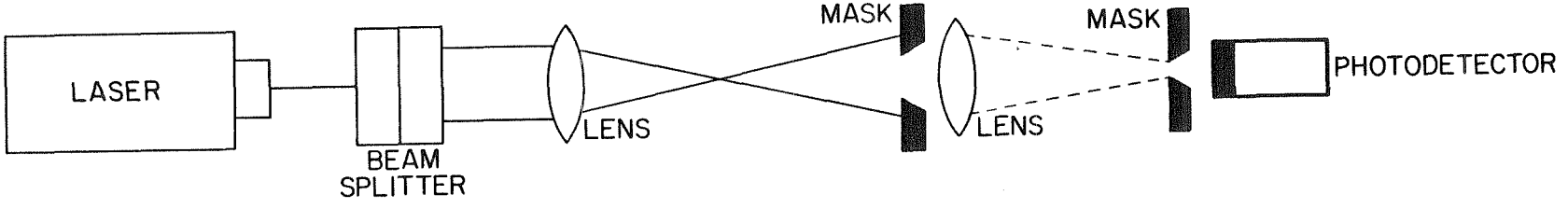

Figure 4.1.1 Basic one-dimensional dual-scatter optical arrangement for laser-Doppler velocimetry

through the laser beam, it scatters light which is frequency shifted according to the Doppler principle. The frequency shift, f, is given by

$$f = \frac{2u\sin\phi}{\lambda} \qquad (4.1.1)$$

where u is the particle velocity, 2ϕ is the beam intersection angle and λ is the wavelength of the incident light. The frequency shift is small with respect to the frequency of the incident light. The beam intersection volume is imaged on the surface of a photodetector by a collecting lens. When a particle passes through the beam intersection, it scatters light from both beams simultaneously. The collected light focused at the photodetector is a combination of light scattered from both beams. The response of a photodetector is slow with respect to the frequency of light, but not slow with respect to the difference frequency of the combined light.

The photodetector output current is proportional to the square of the intensity of the incident light. A typical photodetector output signal generated by a fluid tracer particle in a clear fluid flow appears in Figure 4.1.2.a. The signal consists of two parts: the pedestal or offset current and the Doppler modulated burst current. The offset current is caused by the Gaussian light intensity of the laser light beams. The total amplitude of the photodetector current is a function of the scattering particle size, the particle trajectory through the measurement volume and the geometry of the transmitting optics. The ratio of the pedestal amplitude to the Doppler burst amplitude is also a function of these factors.

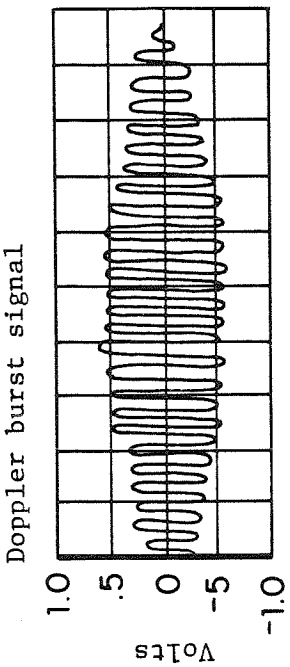

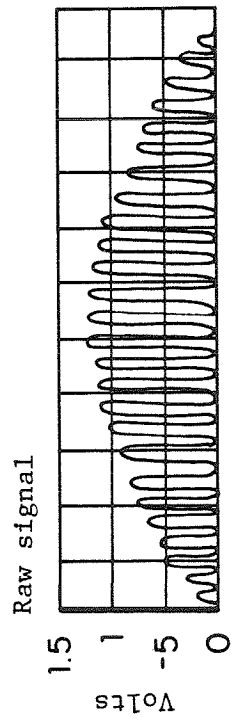

Figure 4.2.1.a Fluid tracer particle

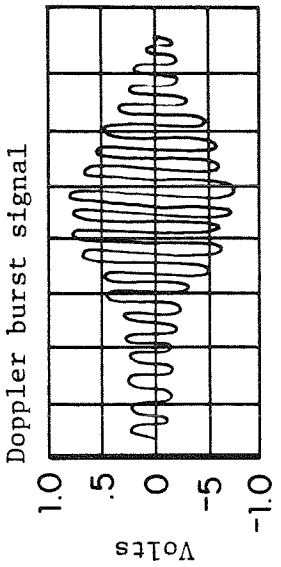

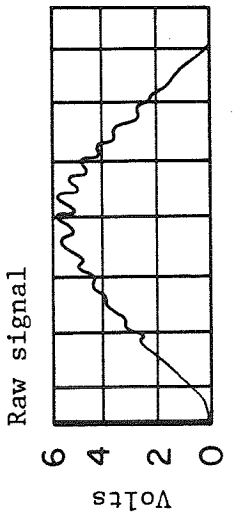

Figure 4.2.1.b Sediment grain

Figure 4.2.1 Typical photodetector output signals

A typical signal generated by a sediment grain using conventional dual-scatter optics is shown in Figure 4.1.2.b. That the light scattered by large particles is also Doppler scattered was demonstrated by Durst (1973) in experiments with steel balls. The signal shown in the figure was generated by a sediment grain cemented to a lucite disc. The disc was rotated at a known speed causing the cemented grains to pass through the measuring volume at a known velocity. Despite the non-sphericity of the grain surface, sediment grains do generate reliable Doppler modulated burst signals. It is therefore possible to measure directly the velocity of a sediment grain in situ.

In sediment-laden flows, the sorting of signals generated by sediment grains and fluid tracer particles can be accomplished by measuring the pedestal amplitude. Larger particles scatter more light. Since sediment grains are commonly on the order of 300 μm, they scatter much more light than the 10 μm fluid tracer particles. To distinguish various sediment sizes, however, is not simple. The exact particle trajectory through the measurement volume must be known. The preliminary experiments with the cemented grains on the rotating disc confirmed this. It is, however, quite simple to distinguish signals generated by sediment grains from signals generated by dust, polystyrene latex spheres, milk, latex paint particles, or other commonly used fluid tracer particles.

Sediment grains scatter so much more light than the smaller fluid tracer particles that detecting both types becomes a problem. The photodetector and processing electronics must be sufficiently sensitive to low amplitude scattering to detect the small particles, yet

sufficiently insensitive such that the large grains do not saturate the system. Also, a sediment grain which passes through a beam just outside the measuring volume scatters enough light to mask the scattering by a fluid tracer particle passing simultaneously through the beam intersection. This occurrence generates a burst of noise which must be distinguished from the Doppler burst generated by the particles and grains passing through the beam intersection. Thus, the transmitting optics must be such that there exist instants when not only are there no sediment grains within the measuring volume, but there are no grains in the beams near the volume.

In ordinary laser-Doppler applications, the angle of laser beam intersection is quite small ($\sim$2 degrees). This results in an elliptical measuring volume whose major diameter is on the order of fifty times the minor diameter. By increasing the beam intersection angle, thereby decreasing the ratio of the major diameter to the minor diameter, the measurement volume may be made smaller. If the minor diameter is then minimized, making it near the sediment grain diameter, the measuring volume becomes small enough to allow fluid velocity measurement. Sediment particles are sometimes absent from the measuring volume. A larger beam intersection angle also reduces the probability of the detection of light scattered by the sediment grains which pass through the beams just outside of the measurement volume. Thus, the scattering from water tracer particles can be detected. However, if the beam intersection angle gets too large, the scattering efficiency of the smaller fluid tracer particles lessens, making them quite hard to detect. Also, for the same particle velocity, a larger scattering angle generates a higher frequency Doppler modulated signal.

Doppler modulation frequencies up to 100 MHz have been successfully amplified and processed, but it is far simpler to process signals less than 1 MHz.

In this study, a beam intersection angle of 21.40 degrees was used. The major diameter of the beam intersection volume is therefore roughly five times the minor diameter. This angle was selected because the resulting beam intersection volume was estimated to be sufficiently small to allow the detection of both the fluid tracer particles and the sediment grains. The particular angle used may not be the most optically efficient. No serious attempt at optimization of the transmitting optical system was made.

Finally, the processing of the photodetector signal must be performed in a careful way due to the bursts of noise, caused by simultaneous scattering from multiple particles. As such bursts are far more likely in sediment-laden flows than in clear fluid flows, they must be identified and discarded prior to data analysis. If they are included in the data analysis, artificial, non-physical, broadening of the measured velocity spectrum will result. Realization of velocity must be made only when a single scattering particle is passing through the measuring volume. Each velocity realization must be independent of every other velocity realization. The photodetector signal must be regular in frequency before being processed. Simultaneous determination of the scattering particle type, whether a fluid tracer particle or a sediment grain, and particle velocity must be performed.

The above criteria imply either the use of a zero-crossing counter-processor or the direct digitization and computer analysis of

the photodetector signal. A frequency tracker should not be used due to the above probable causes of spectral broadening. Digitization of a 1 MHz signal at the Nyquist frequency for a period of several minutes results in excessive amounts of data which then must be reduced. Thus, the counter-processor method is preferable, as it generates far less data. The counter-processor used in this study is detailed in Appendix A. Suggestions for the use of this processor are given in Appendix B.

CHAPTER 5

ANALYSIS OF THE LASER-DOPPLER VELOCIMETRY DATA

This chapter discusses the acquisition and processing of the laser-Doppler velocimetry data presented in Chapter 8. Velocimetry data obtained in sediment-laden flows are quite irregularly spaced in time and care must be exercised in the data reduction and interpretation of the manipulated data. The methods are discussed for the one-dimensional data obtained in this study. Two-dimensional velocimetry data could be processed with an appropriate extension of these methods.

5.1 Data acquisition and preliminary data processing

The velocimetry data are obtained in real time using the laboratory mini-computer and the apparatus described in Chapter 6 and Appendix A. The procedures followed are detailed in Appendix B. Each piece of velocimetry data consists of a set of four numbers: the relative size of the scattering particle which generated the data, two independent realizations of the Doppler heterodyne frequency, and the time of the measurement.

The relative size of the scattering particle is determined by the relative amplitude of the light scattered by that particle. Sediment grains scatter much more light than fluid tracer particles. The velocimetry measurements are sorted into three basic size classes. In order of increasing signal amplitude, the sizes are: fluid measurements, measurements of scattering particles of unidentifiable size, and sediment grain measurements. Unidentifiable scattering

particles are those which scatter too much light to be fluid tracer particles, but not enough light to be sediment grains. The data associated with unidentifiable scatterers are discarded. The amount of such data is quite small.

A zero-crossing counter, described in Appendix A, was used to measure the Doppler heterodyne frequencies. The time required for a preset number of heterodyne signal zero-crossings to occur is determined. The signal frequency is then given by

$$f = \frac{N-1}{\Delta t} \qquad (5.1.1)$$

where f is the signal frequency, N is the preset number of zero-crossings, and Δt is the determined time. Two realizations of the Doppler heterodyne frequency are made to ensure that the observed frequency is regular. As discussed in Chapter 4, light scattered simultaneously from multiple particles, particularly when the flow is sediment-laden, generates velocimetry signals which are not regular in frequency. If the two determined frequencies do not agree and the scattering particle is not identified as a sediment grain, the measurement is discarded. If the particle is identified as a sediment grain, the measurement is retained in the data record, but tagged as unreliable. The detection of a sediment grain, regardless of its velocity, allows for more accurate computation of the sediment transport rate and later analysis for possible conditional sampling errors in the velocimetry process.

The velocity is computed from the heterodyne frequency by

$$u = \alpha f \qquad (5.1.2)$$

where u is the velocity (cm/sec), α is a coefficient determined by the wavelength of the laser light and the optical geometry of the system, and f is the observed heterodyne frequency (KHz).

The data record is then screened for multiple measurements generated by a single scattering particle. The Doppler modulated burst signal generated by a sediment grain is longer in duration and greater in amplitude than that generated by a fluid tracer particle following the same trajectory through the measurement volume. Each sediment grain may generate more than one velocity measurement. The data record is examined and measurements generated by a single scattering particle are consolidated as described in Appendix B.

Thus, the validated data obtained at a single vertical location within the flow field consist of a time series of velocity measurements, each of which is identified as either a fluid measurement or a sediment grain measurement. If the grain velocity is unreliable, it is so denoted. Each data record is not regular in time, nor does it include data from every scattering particle which passed through the velocimetry measurement volume.

5.2 Errors in laser-Doppler velocimetry

This section identifies and quantifies the principal sources of error inherent in the laser-Doppler method of velocimetry. The sources of errors include errors in the determination of the Doppler heterodyne frequency, determination of the velocity from the Doppler heterodyne frequency, and sampling errors.

The first source of error in the velocity measurement is the error in the determination of the Doppler heterodyne frequency. This error is due to the uncertainty in the signal processing electronics. As discussed by Gartrell (1978), the uncertainty in a zero-crossing counter processor system is at most one reference clock period, as a Doppler burst signal may arrive at any time within the clock cycle. The counter system used in this study has a reference clock frequency of 10 MHz, thus the relative error is given by

$$\frac{\Delta f}{f} = 10^{-4} \frac{fm}{N-1} \qquad (5.2.1)$$

where $\Delta f/f$ is the relative error in the frequency measurement, f_m is the measured frequency in KHz, and N is the preset number of zero-crossings. The measured frequencies were in the range 400 to 800 KHz. A minimum of 15 zero-crossings were counted. Therefore, the relative error due to the counter processor is, in the worst case, approximately 0.005. More commonly, 31 zero-crossings were used so that a typical relative error is approximately 0.002.

The uncertainties in the locations and directions of the intersecting laser beams result in a systematic error in the velocity measurement. The coefficient α in equation 5.1.2 is given by

$$\alpha = \frac{\lambda}{2\sin\phi} \qquad (5.2.2)$$

where λ is the wavelength of the laser light and 2ϕ is the beam intersection angle. As discussed in Chapter 6, the error in α was estimated to be 0.025 degrees. Using this value, the relative error in the velocimetry data is found to be 0.002.

The accuracy of the fluid velocity measurements is also dependent on the ability of the fluid tracer particles to follow the small scale fluid flow. Tracer particles which are too large may not follow the fluid particle trajectories. To measure turbulence with significant power at a frequency of 1 KHz in water, fluid tracer particles smaller than 15 μm are required (Durst et al., 1976). The size distribution of particles (excluding sediment grains) found in the flume water was measured (Hunt, 1980). The particles found in the flume water satisfy Durst's criterion as no particles greater than 10 μm were found in the size analysis, and no significant errors in the fluid velocity measurements resulted from this source.

The accuracy of the sediment grain velocity measurements may be affected by rotation of the sediment grains. Each sediment grain is a unique non-spherical, geometric light scattering particle. As each grain passes through the beam intersection volume, laser light is scattered from the illuminated portion of the grain surface. If the grain rotates or spins significantly, the characteristics of the light scattered by the illuminated portion of the grain surface may also change significantly. The detected Doppler burst frequency may not accurately reflect the desired component of the grain velocity. A typical time required in this study for the determination of the Doppler heterodyne frequency was 50 μsec. For a particle to rotate one degree during that time, a 55 rotations per second rate is required. Previous investigations of fluid turbulence indicate little fluid kinetic energy at such frequencies, particularly on length scales on the order of the size of a sediment grain. Significant rotation of a sediment grain during the time required for the determination of the

Doppler heterodyne frequency seems highly unlikely. No significant errors in the sediment velocity measurements were attributed to this source.

Lastly, the data from a laser-Doppler velocimeter do not form a continuous record, even in homogeneous fluid flows. The data record is a series of measurements made over discrete intervals. It has been well documented that such velocimetry measurements of fluid velocities may be statistically biased (Mc Laughlin and Tiederman, 1973, Dimotakis, 1976, Mc Dougall, 1980). The mean fluid velocity as measured is greater than the actual mean fluid velocity. If the fluid tracer particles are homogeneously distributed in the fluid, the probablity that an individual tracer particle will pass through the beam intersection volume is proportional to the local instantaneous volume flux. Relatively fast-moving fluid parcels have higher fluid volume flux, relatively higher numbers of fluid tracer particles, and generate relatively more measurements.

In sediment-laden flows, the fluid velocity data may be biased in a more complicated manner. Whenever sediment grains are within or very near the measurement volume, the generation of a fluid velocity measurement is not possible. A sediment grain which passes sufficiently close to the beam intersection volume scatters enough light to obscure the scattering by a fluid tracer particle passing simultaneously through the volume. The fluid velocity data record is therefore necessarily conditionally sampled. For example, suppose that all relatively fast-moving fluid parcels contain a significantly higher number of sediment grains. Even though such a fluid parcel also has a

relatively high number of fluid tracer particles, the light scattered by the smaller tracer particles will tend to be obscured by the light scattered by the sediment grains. The resultant fluid velocity data record is not biased by measurements of a relatively larger number of fast-moving fluid tracer particles.

Because of this possible conditional sampling of the fluid velocity data record, it is difficult to justify the selection of any one of the existing velocimetry correction procedures. All three of the above correction procedures were applied to the data in this study.

No bias correction procedure need be applied to the sediment grain velocity record. Barring any systematic pre-selection of the grains which generate velocimetry measurements, the mean sediment grain velocity is the mean velocity of the observed grains. Sediment grains are discrete particles; the behavior of a continuous medium is not being inferred.

Even if the grains which generate good velocity measurements are pre-selected in some way, the nature of the correction required is not evident. For example, if sediment grain velocity is positively correlated with the sediment transport rate, the observed mean sediment grain velocity may be less than the actual mean sediment grain velocity. When the sediment transport rate is relatively high, more sediment grains are in the vicinity of the beam intersection volume and the occurrence of simultaneous scattering by multiple particles increases. The likelihood that a given sediment grain which passes through the volume will generate a valid velocimetry data event decreases. There is, however, no physical basis on which to predict, a

priori, a correlation between sediment grain velocity and sediment transport rate. Furthermore, if such a correlation did exist in the flow, it may not be apparent in the observed, biased, velocimetry data record. The character and magnitude of any bias in the sediment grain velocity observations cannot be estimated until more is known about the time-fluctuating characteristics of the sediment grain motion.

5.3 Initial Data Analysis Procedures

This section describes the initial data analysis performed on each of the validated velocimetry data records. Each data record consists of an irregularly spaced time-series of velocity measurements. Each velocity measurement is identified as either a fluid measurement or a sediment grain measurement. If the grain velocity measurement is unreliable, it is so tagged.

Some simple statistics of the fluid and valid sediment grain velocity measurements are first computed. The number of measurements, mean velocity, and velocity standard deviation are determined. The standard deviation of the fluid velocity is the longitudinal turbulence intensity. Note that the number of valid fluid and the number of valid sediment grain measurements will differ in each data record. The three bias correction procedures are applied to the fluid velocity measurements to compute the corresponding corrected mean and standard deviation of the fluid velocity. The probability density functions of the fluid velocity and the sediment grain velocity are determined.

The above statistics obtained for the fluid velocity measurements are compared to those obtained for the sediment grain velocity

measurements at each location. Comparisons are also made between the results obtained at the various measurement locations throughout the water column. Mean velocity and velocity standard deviation profiles for both the fluid and the sediment grains are plotted. The fluid velocity results may be compared to observations in clear water flows by previous investigators to determine the effects of the suspended sediment on the fluid turbulence. The fluid and the sediment grain results will be similiar if the sediment grains are moving with the surrounding fluid and if the grains are not associated with a selected subset of fluid parcels.

Similiar statistics of the computed sediment grain inter-arrival times, the time intervals between successive sediment grain detections, are then obtained for each data record. The determinations are made for those sediment grains which generated valid velocity measurements and for all of the detected sediment grains. The number of measurements, mean inter-arrival time and inter-arrival time standard deviation are determined. Profiles of mean and standard deviation of sediment grain inter-arrival time are plotted. The mean inter-arrival time at each location is compared to the sediment transport rate at that location as measured by suction sampling tube. If the laser velocimeter acts as a grain counter, the mean grain inter-arrival time is inversely proportional to the sediment transport rate. The standard deviation of the sediment grain inter-arrival time gives a measure of the time variability in the sediment transport. The probability density functions of the sediment grain inter-arrival time data are computed for each data record. The physical interpretation of the probability density function is discussed in Section 5.5.

After the initial analysis, the data are then subjected to some time-series analysis procedures. Because of the irregular time spacing of the velocimetry data, the time-series analysis procedures used in this study differ from those applied to regularly spaced data. Additionally, the time spacing of the sediment grain data has a physical meaning. The techniques employed and the subsequent physical interpretation of the results are discussed in depth in the next sections.

5.4 Consequences of irregular time spacing of the fluid velocity data

As noted previously, laser-Doppler velocimetry data is a series of discrete measurements, irregularly spaced in time. If the mean data acquisition rate is rapid with respect to the frequencies of the fluid turbulence with significant energy, this irregularly spaced data may be interpolated to yield regularly spaced data. In homogeneous fluid flows, it is usually possible to construct such a regularly spaced data record. In sediment-laden flows, this is not simply possible. Significant gaps in the fluid velocity data record are created by the passage of sediment grains through or near to the beam intersection volume. Computation of fluid velocity auto-correlations and power spectra must be performed with the irregularly spaced data record. Although such computations are relatively straightforward, the subsequent interpretation of the computed correlations and spectra must be done with care. This section reviews the relevant computation techniques and interpretation guidelines applied in this study. For a detailed discussion of time-series analysis of unequally spaced data, see Deeming (1975), Roberts and Gaster (1980), and Shapiro and

Silverman (1960).

Turbulent flow data are subjected to time-series analysis in an effort to identify and characterize the time-dependent properties of the turbulence. Correlations of velocity fluctuations define the time scales, and by convention, the length scales of the turbulent kinetic energy and shear. The Fourier transforms of these correlations, when properly normalized, show the distribution of turbulent kinetic energy and shear among the various time scales.

Auto-correlations or cross-correlations of a function sampled at random time intervals may be computed by several different methods. The primary difficulty encountered is that the correlation is smeared. At a given lag time, the computed value of the correlation depends on the values of the correlations at the neighboring lag times. Additionally, the error in the computed correlation is a function of the lag time.

Consider the velocity at a point, u(t), sampled at random sample times, t_k. The simple lag velocity correlation coefficients, C(M), are given by

$$C(M) = \frac{1}{N-M} \sum_{k=1}^{N-M} u(t_k)\, u(t_{k+M}) \qquad (5.4.1)$$

where M is the lag index (M=1,2,...) and N is the number of observations. If the sample times are regular, the simple lag auto-correlation is equivalent to the true auto-correlation. In the general case

$$C(M) = \sum_{k=1}^{M} R(\tau j)\ \psi_M(\tau j) \qquad (5.4.2)$$

where t_k is the kth lag time, $R(\tau_*)$ is the true auto-correlation and $\psi_M(\tau_*)$ is the probability density function of lag time τ_* at lag interval M. Thus, given the simple lag correlation coefficients and the relevant inter-arrival time probability density functions, the true auto-correlation may be computed.

The Fourier transform of a continuous-valued function of time differs from the Fourier transform of discrete observations of that function. The discrepancy is due to the finite length and time spacing of the observed data record. The observed Fourier transform, $F_N(\nu)$, is the convolution of the true Fourier transform, $F(\nu)$, with a spectral window function, $\delta_N(\nu)$. Thus,

$$
\begin{aligned}
F_N(\nu) &= F(\nu) * \delta_N(\nu) \\
F_N(\nu) &= \sum_{k=1}^{N} u(t_k) e^{2\pi i \nu t_k} \\
F(\nu) &= \int_{-\infty}^{\infty} u(t) e^{2\pi i \nu t}\, dt \\
\delta_N(\nu) &= \sum_{k=1}^{N} e^{2\pi i \nu t_k}
\end{aligned}
\qquad (5.4.3)
$$

where ν is frequency and $\delta_N(\nu)$ is the spectral window function. It must be noted that, strictly speaking, the fluid velocity at a point within a sediment-laden flow is not a continuous function of time. During the periods when sediment grains pass through that point, the fluid velocity is not defined. At alluvial concentrations, these periods are not that common, less than one per cent of the time. Furthermore, the time of flight of a sediment grain through the measurement volume is small with respect to the turbulent time scales with appreciable kinetic energy. In this study, the fluid velocity at a point is assumed to be a continuous function of time.

The spectral window function is all important in the interpretation of the calculated transform. It pinpoints any pathology of the distribution of the data acquisition times. The spectral window function does not depend on the observed data values but only on the times of observation. The observed Fourier transform may contain aliases, spurious subsidiary peaks which are artifacts of the data sampling. These subsidiary peaks are not physically meaningful, and must be identified prior to the interpretation of the transform. The spectral window function identifies any aliasing in the computed transform.

Similiarly, the observed power spectrum is proportional to the convolution of the true power spectrum with the power spectral window function. Thus,

$$P_N(\nu) = P(\nu) * \gamma_N(\nu)\sigma_u \qquad (5.4.4)$$

$$F_N(\nu)\,\overline{F_N(\nu)} = \sigma_u P(\nu) * [\delta_N(\nu)\overline{\delta_N(\nu)}]$$

where $P(\nu)$ is the true power spectrum, $P_N(\nu)$ is the computed power spectrum, $\delta_N(\nu)$ is the power spectral window function, $\overline{\ }$ denotes complex conjugate, and σ_u is the variance of the function u(t). Again, the power spectral window function identifies any aliasing in the computed power spectrum.

As an example, consider a simple sine wave sampled at regular time intervals. The power spectral window function reduces to

$$\gamma_N(\nu) = \left\{ \sum_{k=1}^{N} e^{2\pi i\nu(k-1)/\nu_s} \right\} \left\{ \sum_{k=1}^{N} e^{\overline{2\pi i\nu(k-1)/\nu_s}} \right\} \qquad (5.4.5)$$

$$= \frac{\sin^2\left(\pi \frac{\nu N}{\nu_s}\right)}{\sin^2\left(\pi \frac{\nu}{\nu_s}\right)}$$

where ν_s is the sample frequency. As $N \to \infty$, the spectral window function approaches a set of delta functions equally spaced at intervals of ν_s. Aliasing at integral multiples of the sampling frequency, the familiar result, is predicted. As $\nu \to 0$, the spectral window function approaches N^2. The observed power spectral estimate will be aliased at low frequencies by the finite length of the data record. For a sinusoidal function, $u(t)=\sin(2\pi\eta t)$, the observed power spectral estimate is given by

$$P_N(\nu) = \left[\sum_{k=1}^{N} \sin\left(2\pi\frac{(k-1)\eta}{\nu_s}\right)\sin\left(2\pi\frac{(k-1)\nu}{\nu_s}\right)\right]^2 + \left[\sum_{k=1}^{N}\sin\left(2\pi\frac{(k-1)\eta}{\nu_s}\right)\cos\left(2\pi\frac{(k-1)\nu}{\nu_s}\right)\right]^2 \qquad (5.4.6)$$

where η is the signal frequency of the sine wave. As $N \to \infty$, the observed spectral estimate approaches a set of delta functions

$$P_N(\nu) = \delta(\eta + i\nu_s) \qquad (5.4.7)$$

where i is any integer. The observed spectral estimate is the true spectral estimate, a single delta function located at $\nu=\eta$, convoluted with the spectral window function.

The observed power spectral estimate and the power spectral window function computed for the case of a 2 Hz sine wave sampled at 20 Hz are plotted in Figure 5.4.1. The length of record was 42.5 seconds. The frequencies for the computation were chosen to appear evenly spaced

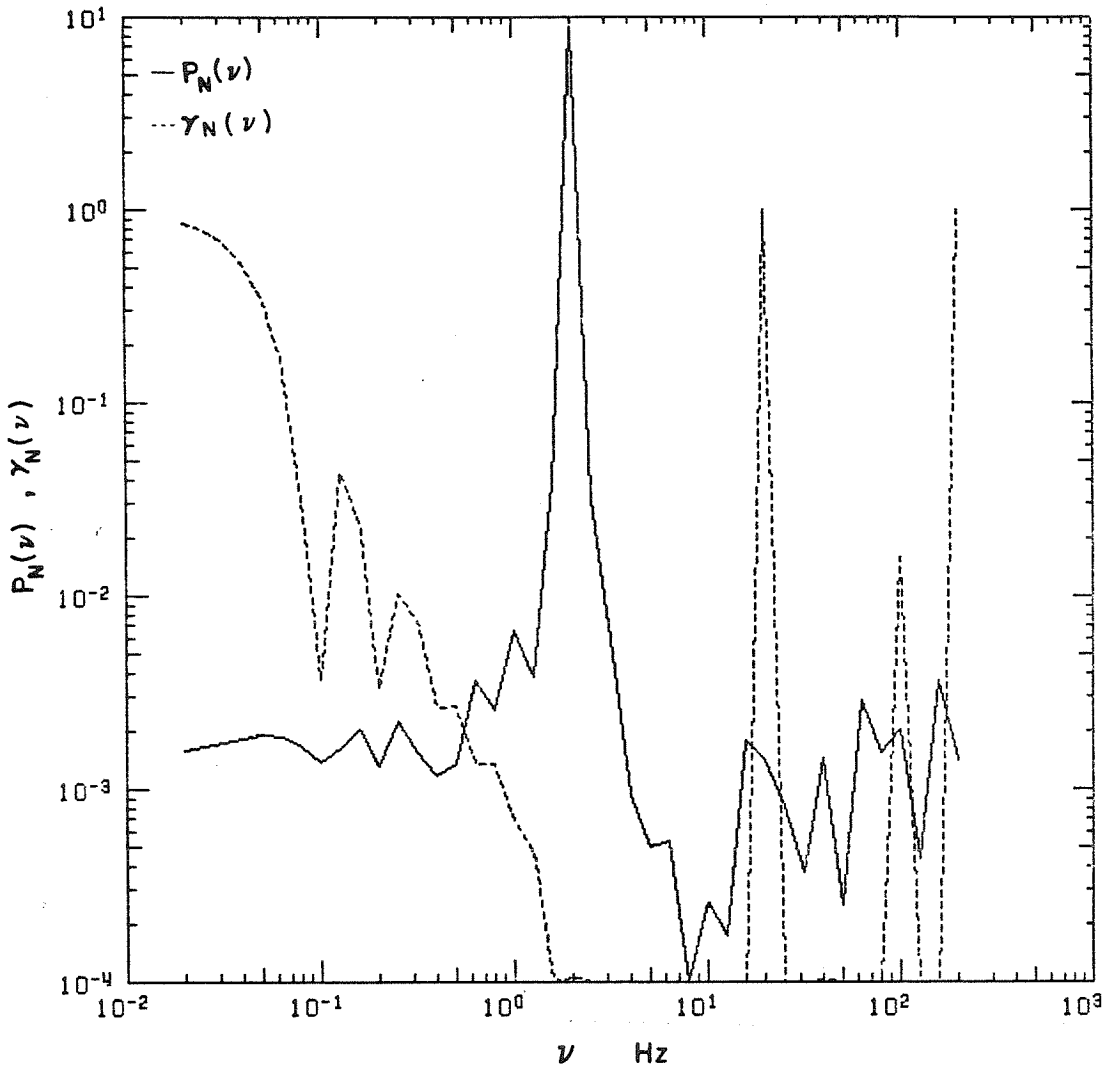

Figure 5.1.1 Sample calculation of power spectral estimate and power spectral window function

when plotted on a logarithmic axis. Forty-one computational frequencies in the range 0.02 to 200 Hz were used. The power spectral estimate appears as the solid curve; the power spectral window function as the dotted curve.

For regularly sampled data, the Nyquist, or cutoff frequency is one-half of the sampling frequency. Any fluctuations existing in the measured system at frequencies higher than the Nyquist frequency cannot be determined from the resultant sampled data record. The Nyquist frequency for the example considered is 10 Hz. Aliasing of the power spectral estimate due to the data record spacing occurs only at frequencies greater than the Nyquist frequency. The example calculation was performed for frequencies greater than the Nyquist frequency so that the aliasing would be apparent. No simple cutoff frequency can be defined for random time sampled data. The reliability of the computed spectral estimate must be gauged by examination of the power spectral window function.

As predicted by Equation 5.4.6, the computed spectral window function exhibits strong peaks at 20, 100, and 200 Hz, all of which are integral multiples of the sampling frequency. However, no such peaks are apparent at 40, 60, or 80 Hz. The peaks are absent because these frequencies were not among the chosen computational frequencies. The computed spectral window function is a discrete function of frequency. The observed spectral window function may change markedly in response to a small shift in the selected computational frequencies, particularly if only a few computational points are used. The number of chosen frequencies is generally limited by the relatively large

computational effort required for each frequency. The spectral window function may sometimes be smoothed by judicious partitioning of the data record, computing the spectral window function for each partition, then averaging the results obtained for each partition. When the sampling times are highly erratic, however, the partitioned, averaged spectra are often less smooth, more variable, than those computed from the entire data record.

All of the above problems in the computation of the spectral window function are encountered in the computation of the power spectral estimate. The expected error in the computed spectral estimate is equal to the value of the estimate. If the signal frequency is not sufficiently close to one of the chosen computational frequencies, the corresponding peak will be lacking in the resultant spectral estimate. Also, all aliasing of the computed spectral estimate may not be predicted by the computed spectral window function. Since aliasing results from a convolution of the spectral window function and the true power spectrum, a spurious peak in the observed spectral estimate is not coincident with its related peak in the spectral window function. The chosen computational frequencies may include the frequency of the spurious peak in spectral estimate, but not the frequency of the related peak in the spectral window function.

Summarizing, time series analysis of irregularly sampled data must be done with care in both computation and interpretation. The spectral window function must be examined when performing spectral analysis. While aliasing can be predicted in advance for regularly sampled data,

it must be analysed after the fact for irregularly spaced data.

5.5 Consequences of irregular time spacing of the sediment grain velocity data

Sediment grain velocity at a point is not a continuous function of time. Rather, it consists of a sequence of discrete values at discrete times. The sediment grain velocimetry record is a subset of these values. The data record is not regular in time. The irregularity in the data spacing has physical significance as it reflects the mechanics of the sediment motions. Thus, sediment grain velocity data are different from fluid velocity data. While it is appropriate to manipulate the sediment velocity data record in the same manner as the fluid velocity data record, the subsequent interpretation of this manipulation differs.

The computed sediment grain inter-arrival times, regardless of the grain velocity, also form a time series of discrete values. If the velocimeter acts as a grain counter, the probability density functions of the sediment grain inter-arrival time reflect the mechanics of the sediment motions. To identify any physical mechanisms which may cause sediment grains to group or cluster, it is desirable to perform some type of time-series analysis on the inter-arrival time data records. The grain inter-arrival time data records may be treated similiarly to the fluid velocity data records, but the meaning of such manipulation differs.

If the passage of each sediment grain through the velocimetry measurement volume is viewed as an independent stochastic event, the time series of sediment grain inter-arrival times might be modeled as a

Poisson process. The probability density function, $\psi(\delta t_g)$, of the sediment grain inter-arrival times, δt_g, would then be given by

$$\psi(\delta t_g) = \nu_g e^{-\nu_g \delta t_g} \qquad (5.5.1)$$

where ν_g is the mean frequency of the sediment grain arrivals. The standard deviation of the sediment grain inter-arrival times would be equal to the mean. Computation of the probability density function for the experimentally observed sediment grain inter-arrival time data records allows this model to be tested. The approach does assume that successive passages of individual sediment grains through the volume are independent events. Time series analysis of the sediment grain inter-arrival times must be performed to check this assumption.

The simple lag correlation coefficients of sediment grain velocity and sediment grain inter-arrival times may be computed as described in Section 5.4. The lag correlation coefficients relate the motion of a given sediment grain to the motion of the Mth successive sediment grain. Just as the auto-correlation of the fluid velocity fluctuations are used to define time scales of the fluid turbulence, the lag correlation of the sediment grain inter-arrival times may be used to define grain number scales of the sediment motions. The number of grains, or lag, at which the grain inter-arrival times are no longer correlated is a measure of the number of grains which move as a group. If little or no correlation is observed, the motion of each sediment grain may be assumed to be independent of the motions of all other sediment grains.

The lag correlation coefficients may also be used to compute the true auto-correlation functions of lag time. Time scales of sediment

grain velocity fluctations and sediment transport rate may be defined by analogy with the time scales of the fluid turbulence. The physical interpretation of such time scales is not exactly analagous to that of the fluid time scales, however. The sediment grain velocity at a point in space can only be defined when a grain is present at that point. Comparison of the time scales of the fluid turbulence and the sediment grain inter-arrival times may give a qualitative description of the time scales of the turbulence which are important in sediment suspension.

The power spectral window function of the sediment grain observations also contains information about the time scales of the sediment motion. The power spectral window function reflects the frequency distribution of mean sediment grain inter-arrival time. A peak in the observed grain spectral window function implies the existence of a dominant sediment grain inter-arrival frequency. The fluid spectral window function has no such direct physical significance. The time spacing of the fluid velocity measurements is an artifact of the measurement technique. The time spacing of the detection of sediment grains reflects the transport of the sediment.

Interpretation of the time-series analysis of a function which is discontinuous in time is not straightforward. Suspended sediment, when viewed on the granular scale, is not a continuum. Sediment grain velocity measurements are recorded at random time intervals because sediment transport is an inherently intermittent process.

5.6 Summary

This chapter has presented the errors inherent in the technique and the methods of data analysis used in this study. Careful analysis and interpretation of laser-Doppler velocimetry data obtained in sediment-laden flows is not simple. Each velocity realization must be validated and multiple realizations of the same scattering particle must be eliminated. The resultant data record is irregular in time, and the any physical interpretation of such data must be done with care. With such care, the small scale, time varying mechanics of sediment-laden flows may be observed without flow disruption.

CHAPTER 6

EXPERIMENTAL APPARATUS

The experiments on turbulence and sediment grain transport in open channel flow reported in Chapter 8 were performed in the W. M. Keck Laboratory of Hydraulics and Water Resources. Most of the hydraulic apparatus used is similiar to that used in several previous experimental investigations of sediment transport in the Keck Laboratory. In addition, a laser-Doppler velocimeter was developed for use in sediment-laden flows. This chapter describes all of the apparatus used in this study.

6.1 The 13-meter flume

The experiments were conducted in the 13-meter tilting flume located in the Keck Laboratory. A schematic diagram of the flume is shown in Figure 6.1.1. The flume has been described in detail in Taylor (1971).

The flume is 26.7 cm (10.5 in) wide and 25.4 cm (10.0 in) deep. The flume discharge (sediment and water) is recirculated from the outlet section to the inlet section through a 10.2 cm (4.0 in) return pipe by an axial flow pump. The pump is connected to a two-speed electric motor through a variable-speed drive. The flume, pump, motor and return pipe are mounted on a tiltable truss.

The truss is supported at two points: on a pivot point near the downstream end and on a manually operated, screw-type jack near the upstream end. Thus, the flume slope may be varied continuously from

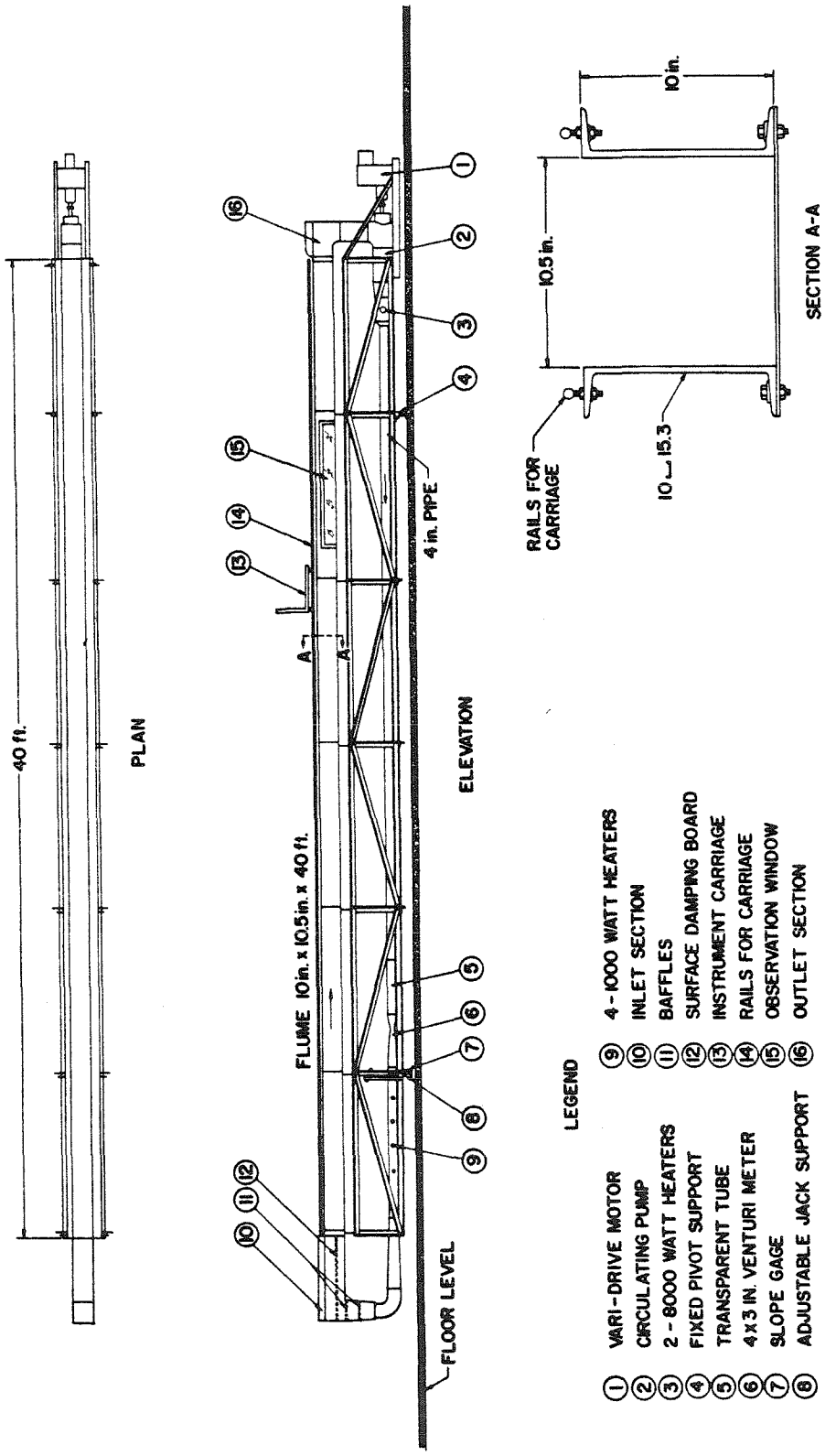

Figure 6.1.1 13-meter flume schematic drawing

-0.001 to +0.038 and is read directly from a scale (with vernier) located near the jack.

The flume consists of two steel channel beams bolted to a bed plate. The inside surfaces are painted with a bitumastic paint and are nearly hydrodynamically smooth. A window, 1.47 m in length, is installed 8.6 m from the inlet box and 2.1 m from the outlet box. Two precision stainless steel round bars mounted on top of the flume side wall beams act as rails for a metal instrument carriage. Gearing of the instrument mount on the carriage allows positioning of the mounted instrument to within 0.2 mm in the vertical or transverse directions. A point gage, Pitot tube, and sediment sampler were interchangeable on the instrument mount.

At the flume inlet, a series of baffles was used to damp large scale turbulence and secondary currents generated in the return pipe, and in the inlet and outlet sections. Two rectangular grids made from glued lucite strips (strip width=1.27 cm; opening=1.27 cm) were placed horizontally in the vertical portion of the inlet section. Two 0.30 cm mesh and two 0.16 cm mesh screens were placed vertically across the end of the inlet section at the upstream end of the flume. A plywood board was floated just downstream of the screens to damp surface disturbances. A 0.16 cm mesh screen was located at the downstream end of the flume.

The original flume truss was modified to accommodate the carriage for the laser-Doppler velocimeter. The cross brace located under the glass window was cut and replaced by two braces to provide the necessary clearance for the velocimeter carriage. Panels of lucite and

wood were made to cover the top of the flume to prevent dust from the laboratory ventilation system from entering the flume.

6.2 Sand characteristics

The sand used in this study has a geometric mean grain size, d_g, of 0.245 mm, a geometric standard deviation, σ_g, of 1.22, and a density, ρ_s, of 2.65 g/cm . The size analysis is shown in Figure 6.2.1. The material is one of the size fractions obtained by Taylor (1971) in a fall velocity separation of a natural alluvial sand. The sand was discharged into a water flume flow (mean velocity=12 cm/sec, depth=56 cm) using a dry sediment hopper. Slot dividers were positioned along the flume bed downstream of the hopper. The sediment which accumulated between each pair of slot dividers was removed. The resulting separated sands have size distributions which are not strictly log-normal, but are slightly bimodal as seen in Figure 6.2.1. The deviation from log-normal is not large and was judged not important in this study.

6.3 Measurements of time-averaged flow characteristics

Although these experiments were directed at observing the time-fluctuating characteristics of a sediment-laden flow, measurements of time-averaged flow quantities of the more traditional type were also made.

Flume discharge was measured by a Venturi tube connected to an air-water differential manometer. The Venturi was located in the return pipe near the upstream end. The manometer can be read to the

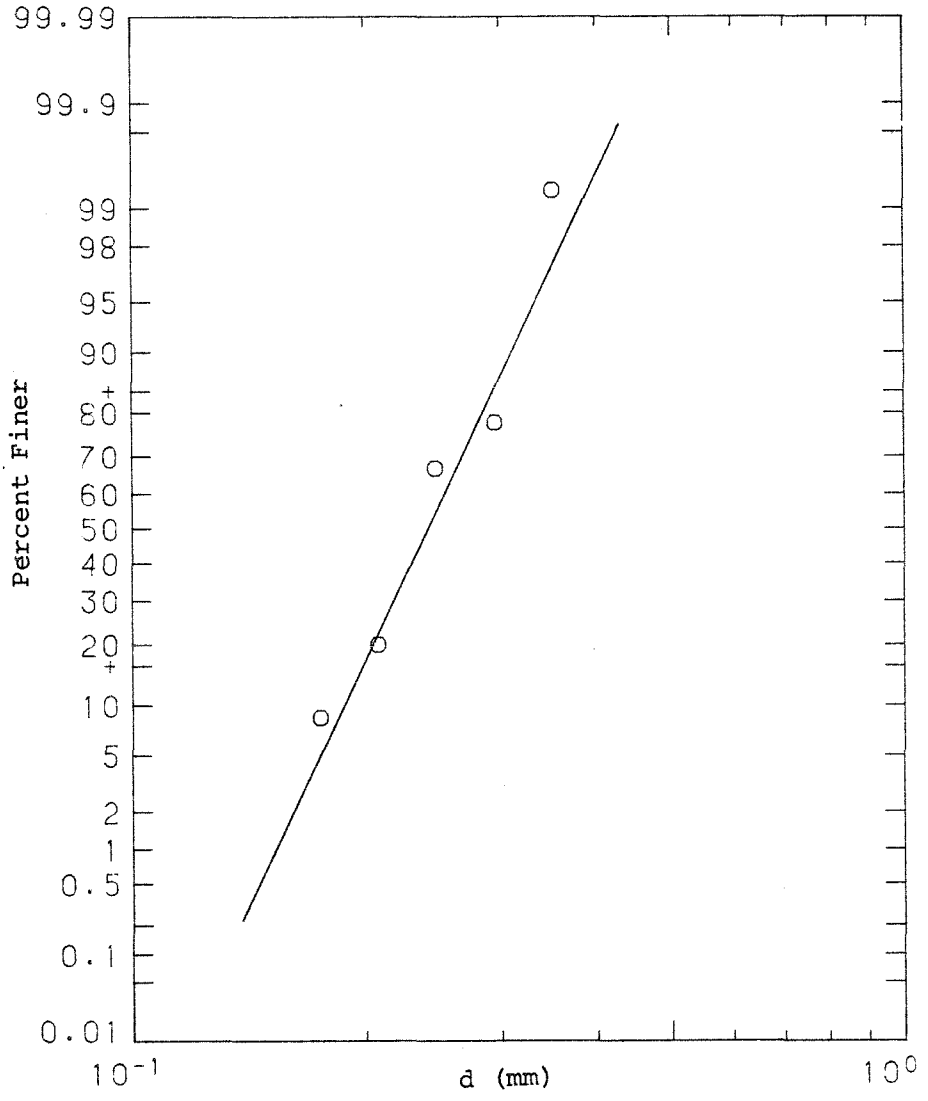

Figure 6.2.1 Sediment grain size distribution

nearest 0.2 mm with a vernier. The Venturi tube was calibrated prior to this study using clear water. The maximum error in the discharge measurement was judged to be approximately three per cent.

The mean water surface slope and sediment bed slope were determined from a series of point gage measurements at twenty locations along the flume. Measurements of the quiescent water surface were used as a horizontal reference. The reported surface slope, S=0.00275, is the average of ten sets of point gage measurements. The error in the reported slope measurement is judged to be approximately five per cent.

Local mean velocities were measured by a 0.63 cm (0.188 in) O.D. Prandtl-type Pitot tube. An air-water manometer was connected to the Pitot tube. The manometer can be read to the nearest 0.2 mm with a vernier. Due to the Froude number of the flow used in this study, Fr=0.75, small surface standing waves were often present. The mean velocity at a fixed point was observed to vary as much as eight per cent over several minutes.

Local mean sediment concentration measurements were made with the point sediment sampler shown in Figure 6.3.1. The sampler was made from 0.95 cm (0.375 in) O.D. brass tubing. The tip opening was flattened as shown. Samples were withdrawn at the local flow velocity (isokinetically) by a siphon arrangement as described by Brooks (1954).

Total load measurements were also made. A second brass sampling tube, shown in Figure 6.3.2, was suspended vertically in the outlet section throat. Sampling was again isokinetic as described by Vanoni and Brooks (1957).

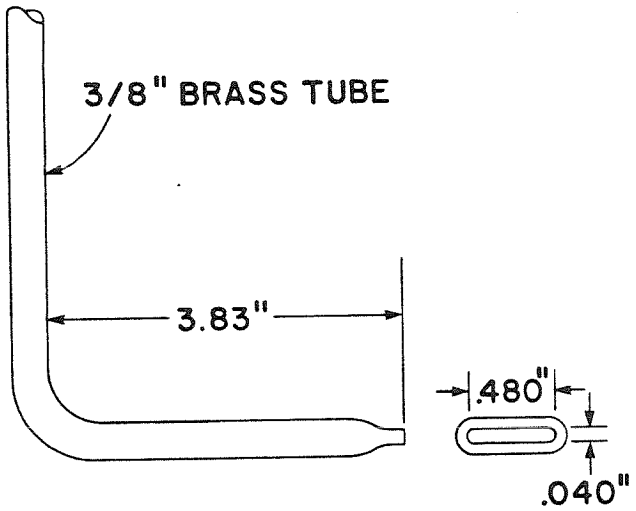

Figure 6.3.1. Sediment concentration point sampling tube

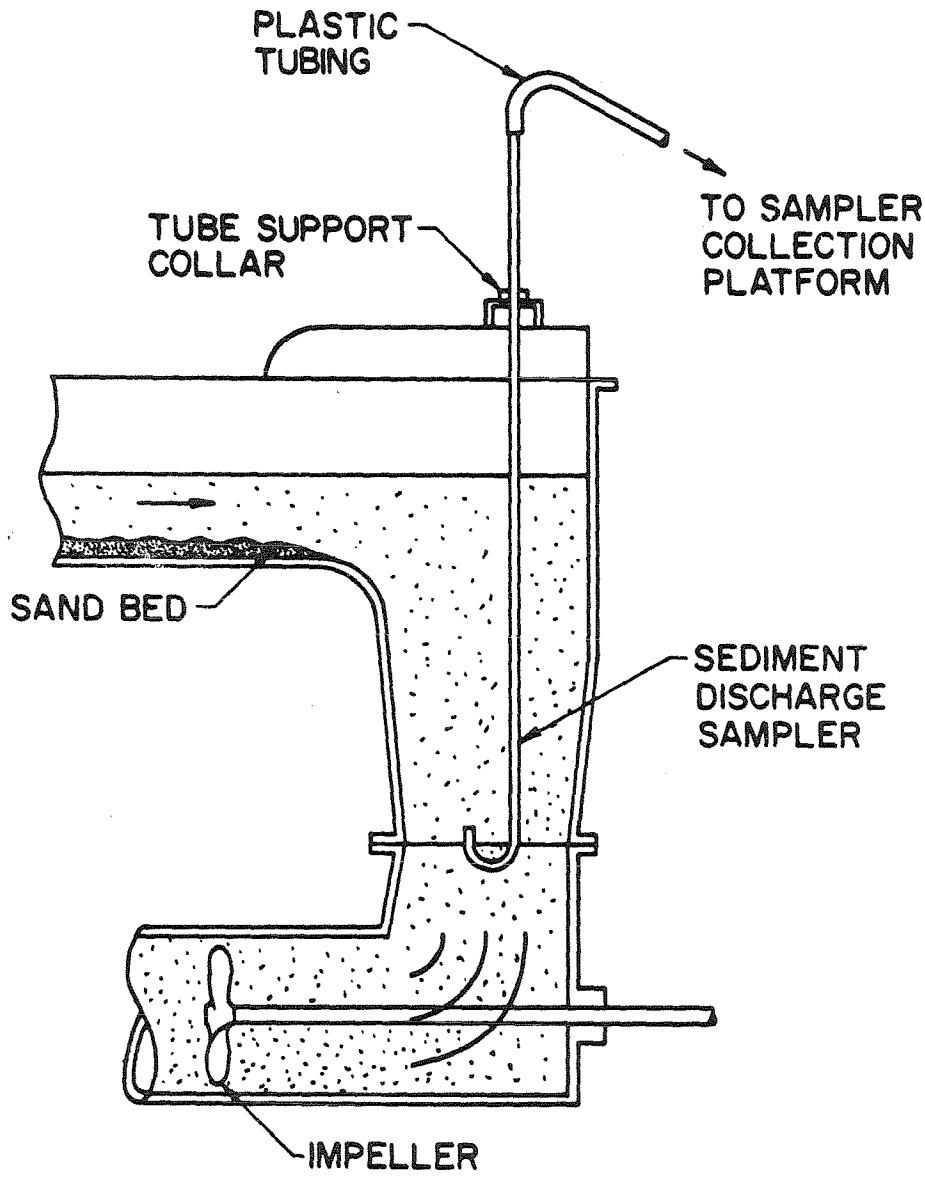

Figure 6.3.2 Sediment concentration total load sampling tube

6.4 Measurements of time-fluctuating flow characteristics

A laser-Doppler velocimeter, shown in Figures 6.4.1 and 6.4.2, was developed to measure the one-dimensional, time-varying characteristics of the flow at a fixed point. Direct, instantaneous measurements of fluid velocity, sediment grain velocity, and sediment grain inter-arrival time were made. The dual-scatter method was used. Some non-standard optics and processing electronics were developed due to the special problems inherent in applying the basic technique to sediment-laden flows, as described in Chapter 4 and Appendix A.

The light source for the system was a Spectra-Physics Model 162, argon ion laser. The laser was tuned to the 5145 Angstrom line. The output power was approximately 15 mW. As shown in Figure 6.4.2, the laser light was first passed through a cube beam splitter. Three resultant beams were produced, two of which have forty-five per cent of the intensity of the initial beam and one which has ten per cent. The two equal stronger beams were made parallel by two mirrors. The dimmer beam was not used. The beams were focused and made to intersect by a lens.

The transmitting optics were aligned as follows. The optical components were first firmly attached to a 1.25 cm (0.5 in) thick aluminum carrier plate. The plate was leveled using a precision level. The two beams were then made parallel to the carrier plate and to each other by adjusting the position of the two mirrors. The directions of the beams were checked by shining them across the laboratory to a wall 10 m from the carrier plate. The transmitting lens (250 mm diameter, 450 mm focal length) was then installed. The vertical position of the

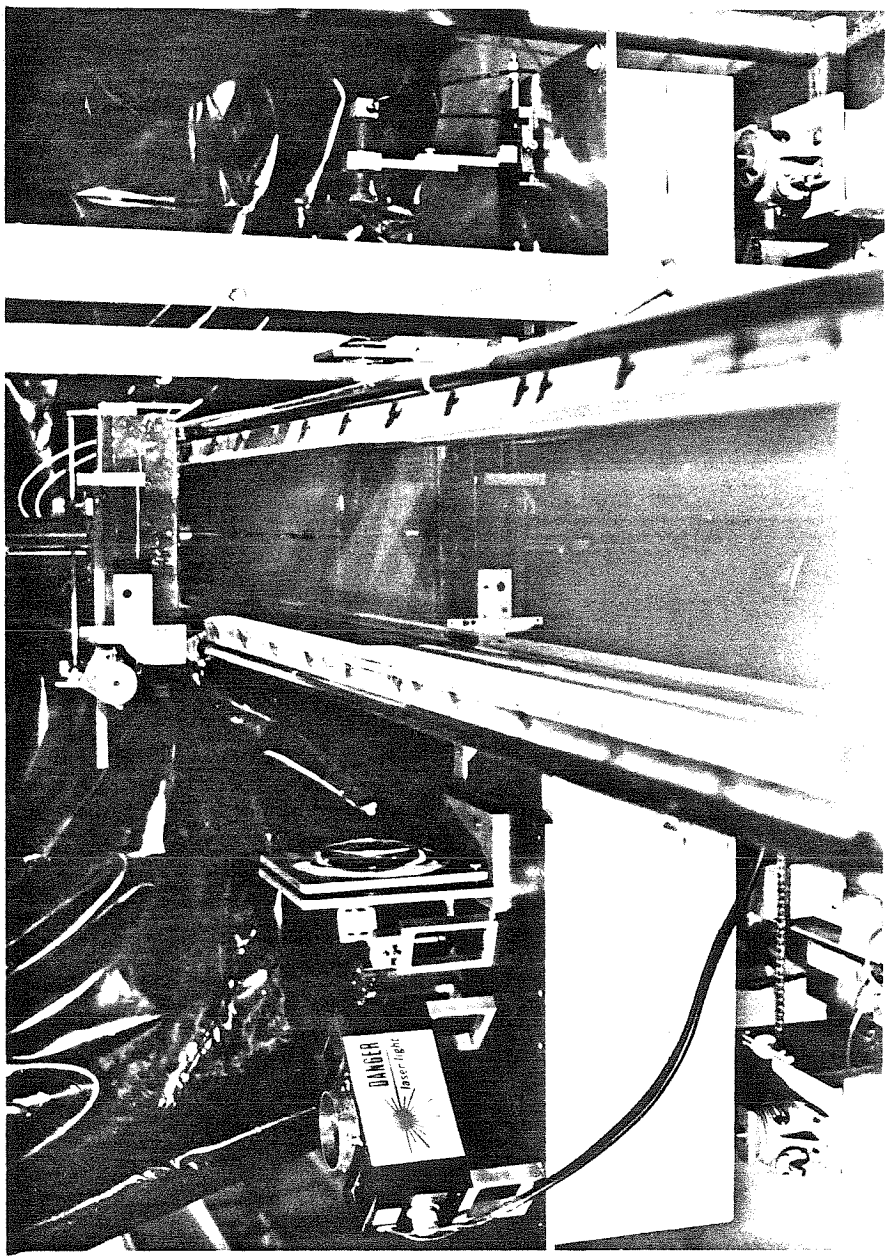

Figure 6.4.1 Photograph of the laser-Doppler velocimeter

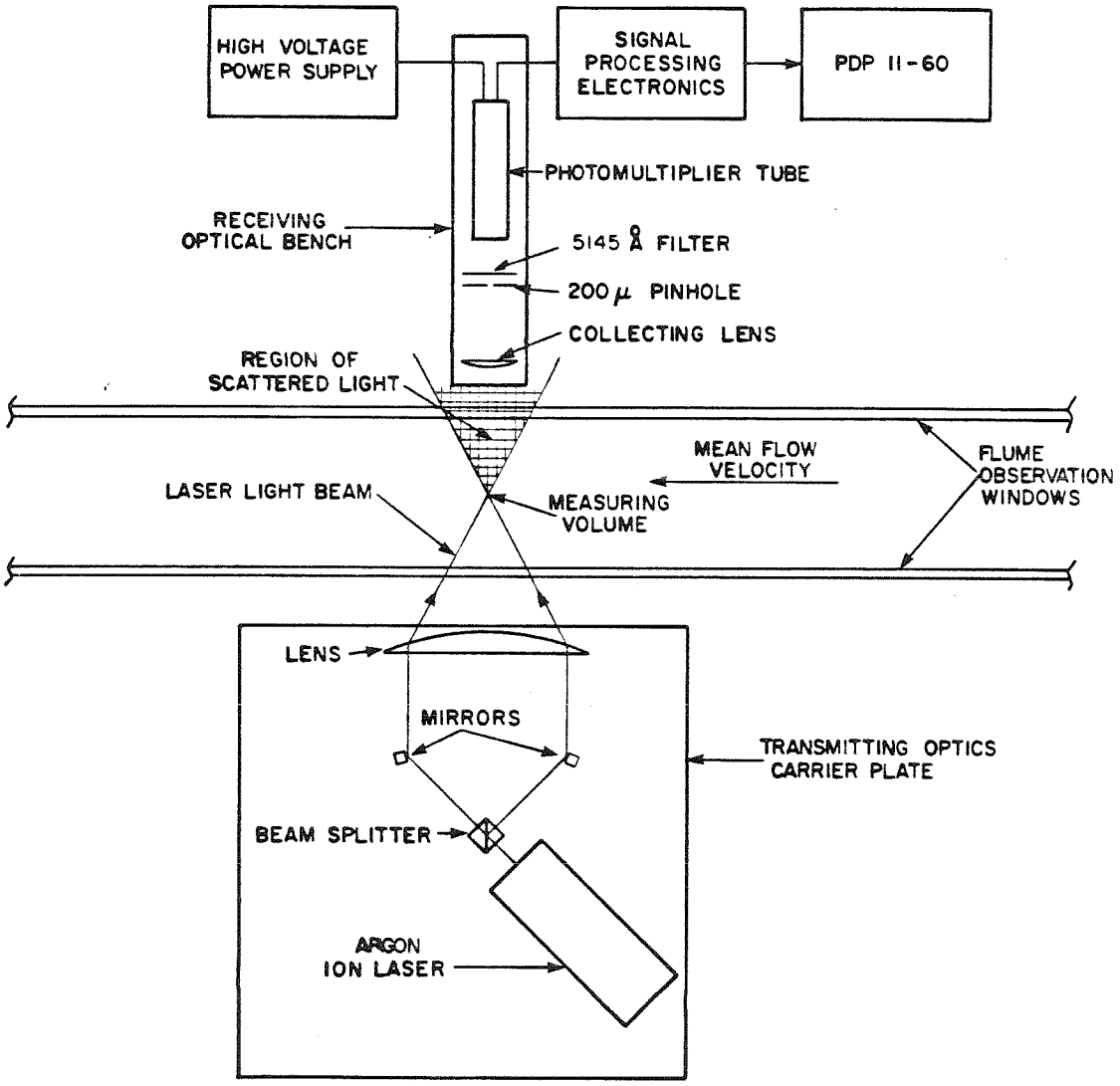

Figure 6.4.2 Laser-Doppler velocimeter plan-view schematic

lens was adjusted until the beams were not vertically refracted. As is likely in a lens of such size, some spherical aberration was noted. The beam separation distance was adjusted to achieve the desired beam intersection angle. The intersection angle was determined by measuring the resulting beam separation at the wall. The beam intersection angle was determined to be 10.70 degrees; the error was judged to be 0.025 degrees. The mean velocity determined by the laser-Doppler velocimeter was correlated to the velocity determined by a Pitot tube as a check on the beam survey. Good agreement was noted.

The diameters of the beams at the beam intersection volume and at the transmitting lens were measured using a precision optical slit. Using these measurements and the procedures given by Durst et al (1976), the minor diameter of the intersection volume was judged to be 0.6 mm. The length of the intersection volume was computed to be 3.2 mm and the maximum number of fringes contained within the volume was estimated at 216.

The receiving optical system consisted of a lens, a pinhole, a laser line filter and a photomultiplier. The lens collected a portion of the light scattered by each particle which passed through the laser beam intersection volume. The unscattered laser beams were masked and not collected by the receiving lens. The photocathode surface was placed at the image point of the laser beam intersection. The pinhole acted as an aperture, blocking light scattered from places other than the beam intesection. Additional apertures in combination with the pinhole were tried, but did not seem to improve the signal quality. The filter excludes the collection of the background lighting in the

laboratory. The mercury line from the fluorescent lighting in the laboratory is quite close to the argon line used, hence a narrow band pass filter was necessary. The photodetector, a RCA 8645 photomultiplier, converted the collected light intensity into an electrical current.

The transmitting and receiving optics were aligned as follows. The transmitting optics plate was mounted on one side of the special carriage described later in this chapter. The components of the receiving optics were mounted to a second aluminum plate which was then mounted to the carriage on the opposite side of the flume (see Figure 6.4.1). The receiving lens was placed as close as possible to the flume. This was done to minimize the total receiving optical pathlength. The pinhole and filter were fixed in place on the housing of the photomultiplier. The photomultiplier was positioned as accurately as possible at the calculated image point of the beam intersection volume. By trial and error, the position of the photomultiplier was adjusted to give the best signal.

The photomultiplier output current was amplified, filtered and processed electronically to yield digital velocimetry data. These data were sent to the laboratory mini-computer in real time for later analysis. The data from each particle consisted of three sixteen bit numbers. The relative size of the scattering particle, whether the scattering particle was a sand grain or a fluid tracer particle, is the four higher order bits of the first data word. The lower twelve bits of the first data word and the entire second data word are two independent measurements of the Doppler heterodyne frequency. Two

measurements are made to ensure the validity of the data as explained in Chapter 4. The velocity of a scattering particle is computed from the measured heterodyne frequency by

$$u = \frac{\lambda f}{2\sin\theta} \qquad (6.4.1)$$

where u is the streamwise component of particle velocity, f is the heterodyne frequency, λ is the laser light wavelength, and 2ϕ is the angle of the beam intersection. The time of measurement, as timed by the internal computer clock, is the fourth word. The processing electronics are described in detail in Appendix A. The subsequent analysis of the data has been discussed in Chapter 5.

6.5 The laser velocimetry carriage

A special carriage for the laser-Doppler velocimeter was designed and built to facilitate the velocity measurements. The carriage held the transmitting and receiving optics plates in rigid alignment and allowed the vertical positioning of the laser beam intersection volume within the water column. The carriage is shown in Figure 6.5.1. The carriage passed underneath and through the flume support truss near the flume window.

The transmitting and receiving optics mounting plates were fixed with aluminum channel spacers to an aluminum box beam. The flume support truss was altered to allow this beam to pass through the truss, just underneath the flume channel. The beam was supported by four precision screw jacks which were rigidly mounted on a steel plate which also passed underneath the flume support truss. The box beam, with the attached optical plates, can be raised and lowered smoothly by the

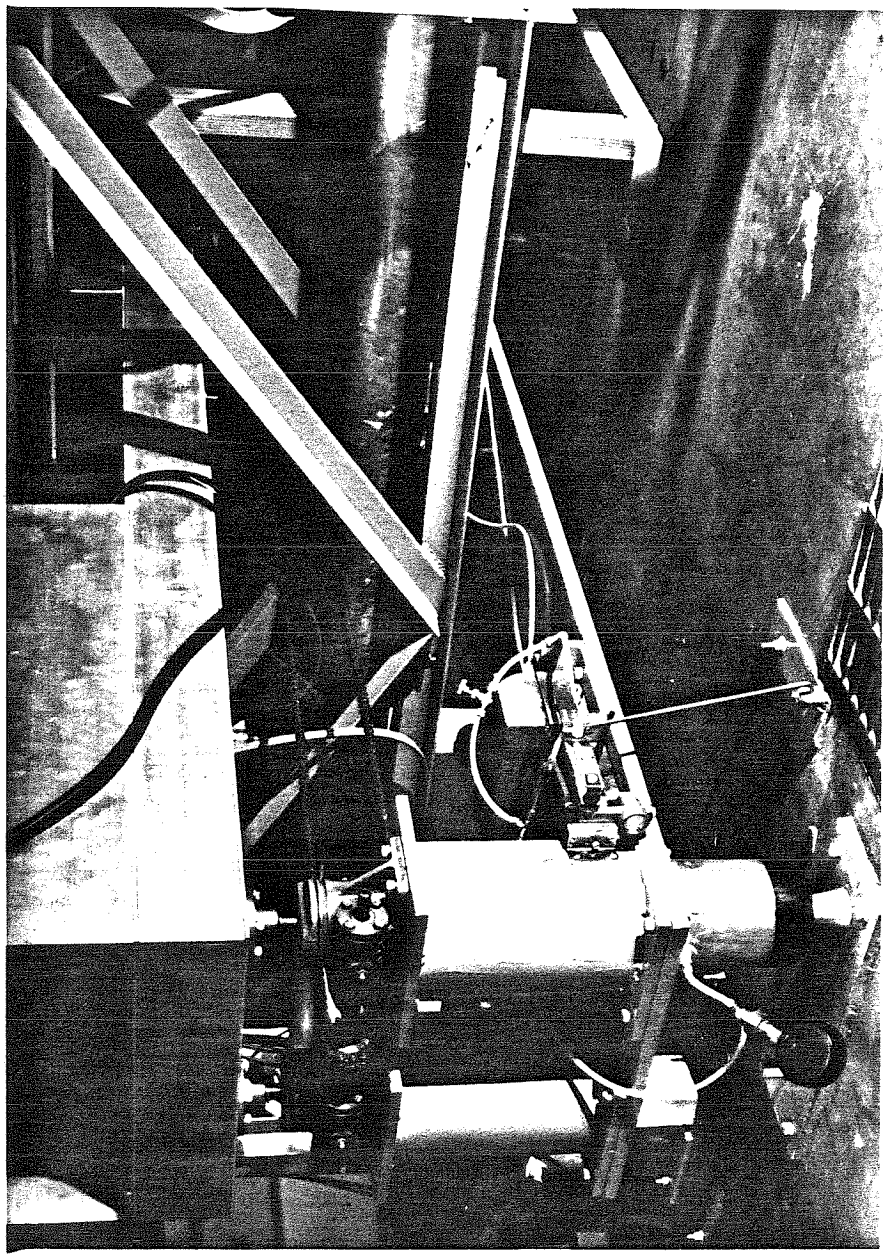

Figure 6.5.1 Photograph of the laser velocimetry carriage

jacks. The four jacks were connected and could be moved simultaneously by manually turning a master drive handle. The velocimeter measuring volume was positioned vertically within the water column by determining its location with the flume point gage.

The steel plate is supported by four Firestone Model IX84D Air Mount vibrational isolators. The flume glass, hence the velocimeter measuring volume, was located near the downstream flume pivot point. Using a Kinemetrics Model SS-1 Ranger Seismometer, it was found that the pump produces local vibrations in the laboratory floor at the pivot point. At the pump speeds commonly used in this study, the local floor vibrations had significant energy in the range of 5 to 15 Hz. Unfortunately, the laser velocimeter is a superior vibration detector, as it is incapable of distinguishing the scattering caused by a particle fixed in space seen from a vibrating carriage and the scattering caused by a moving particle seen from a fixed carriage. As the expected turbulence frequencies were of the same order as the floor vibrations, it was necessary to vibrationally isolate the velocimeter carriage from the floor. Using the isolators and weighting the carriage with lead bricks to give added mass, a 99.4 percent reduction in the amplitude of vibration of the velocimeter was achieved.

CHAPTER 7

EXPERIMENTAL PROCEDURE

A general description of the laboratory flow in which the velocimetry results were obtained is given in this chapter. Visual observations and conventional measurements of relevant flow properties are discussed. The laser-Doppler velocimetry data records are introduced.

7.1 General description of the flow conditions

The velocimetry results were obtained in a steady, uniform sediment-laden flow over a natural sand bed. The flow conditions, corrected for the side-wall effect following Vanoni and Brooks (1957), are summarized in Table 7.1.1. The flow was chosen to be in the high transport, flat bed regime to minimize flow disturbances due to sediment bed forms.

The sediment bed was flat in the center portion of the flume; small ripples projected from either side wall approximately four centimeters into the flume. Intermittently, the bed became undular. The undulations were approximately forty centimeters in length and less than one centimeter in height. These bed waves, when present, traveled slowly downstream. Sporadic surface waves, usually in phase with the bed waves, were also noted. These disturbances are primarily due to the relatively small size of the experimental flume. However, the waves were small with respect to large amplitude ripples or dunes found in other flow regimes.

Table 7.1 Mean flow conditions

Fluid discharge	Q	12.94	l/sec
Mean velocity	u	64.41	cm/sec
Mean depth	d	7.54	cm
Hydraulic radius	R	4.82	cm
Bed shear velocity	u_{*_b}	3.88	cm/sec
Bed friction factor	f_b	0.029	
Energy slope	S	0.00275	
Sediment discharge	Q_s	4.92	g/sec
Mean sediment concentration	$\bar{c}$	0.380	g/l
Geometric mean sediment size	d_g	0.245	mm
Geometric standard deviation	σ_g	1.22	
Sediment fall velocity	v_s	3.2	cm/sec
Water temperature	T	21	°C
von Karman constant	k	0.26	
Rouse exponent	z	1.67	
Froude number	Fr	0.75	
Reynolds' number	Re	1.24×10^5	

The suspended sediment concentration profile was measured by suction sampling tube. Three samples were obtained at each measurement location. The volume of each sample was one liter; the sample time on the order of three minutes. The results are shown in Figure 7.1.1. The mean of the samples is indicated by the plotting symbol; the range of the samples by the solid line. The variation noted is of the order of that commonly reported in similiar laboratory measurements.

Laser-Doppler velocimetry is dependent on the presence of a dilute concentration of small fluid tracer particles. If the particle number density of tracer particles becomes too large, the velocimetry signal deteriorates. The laser beams are diffused by repeated light scattering along the beam path. Multiple fluid tracer particles pass simultaneously through the beam intersection volume. The velocimetry signal is obscured.

Fluid tracer particles were continuously generated in the flume system by abrasion of sand grains and the flume return pipe. After several hours of recirculation in the flume, the flume water became visibly cloudy. Thus, it was repeatedly necessary to stop the circulating pump and change the water in the flume system. With care, it was possible to reproduce flow conditions to within the error inherent in measurement by point gage or pitot tube. That is, the errors which result from a change of the flume water were indistinguishable from the uncertainties which result from the repetition of a given measurement without disturbing the flowing flume.

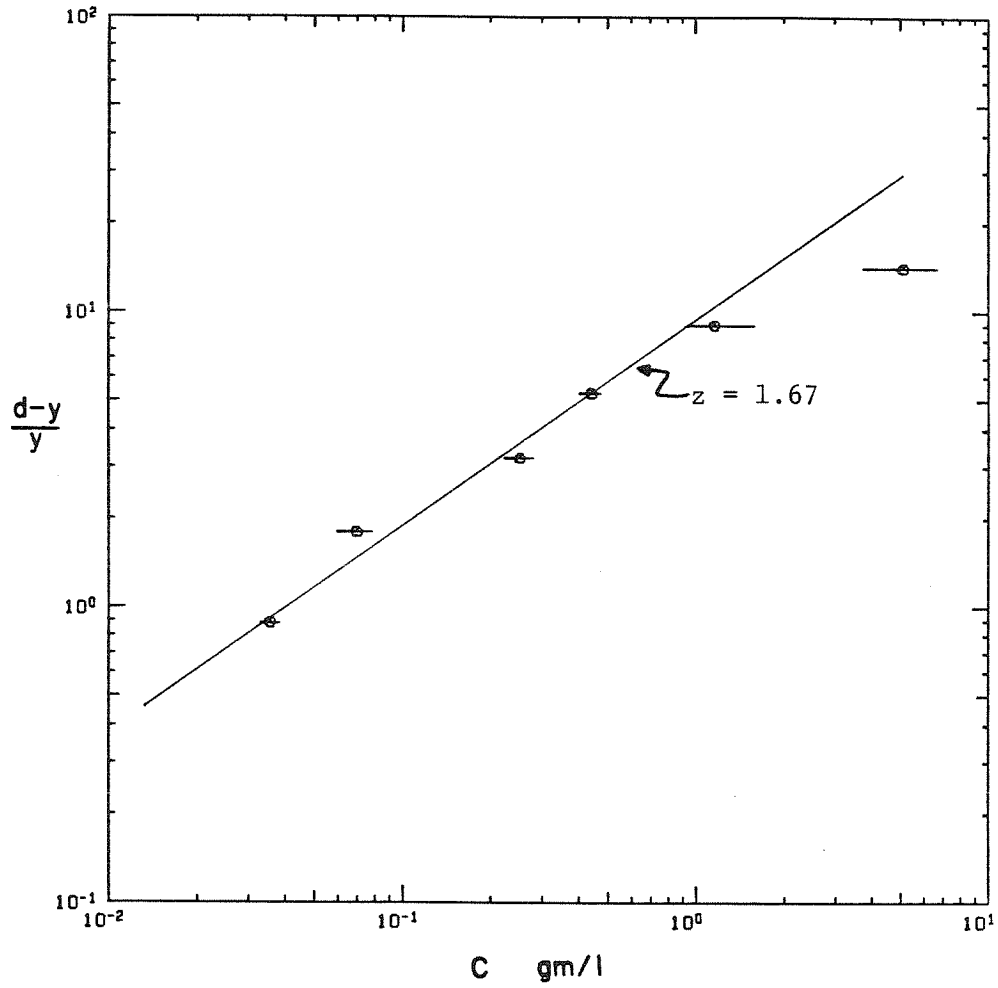

Figure 7.1.1 Suspended sediment concentration profile

7.2 Description of velocimetry procedures

A total of twenty-four velocimetry data records were obtained at six different vertical locations in the water column. The velocimetry measurements were all one-dimensional in the streamwise direction. Twelve data records were retained for later analysis; seven data records were discarded due to the dubious accuracy of the velocimetry data and five data records were discarded due to possible ambiguities in the identification of fluid and sediment grain measurements. The sampling procedure followed is detailed in Appendix B.

At each location in the water column, the laser beam intersection was positioned with the point gage. Several short exploratory test data records were taken with various combinations of the band-pass filter setting, the Doppler burst threshold level, and the preset number of zero-crossings. It is necessary to obtain and screen sample data records before a valid combination of the above instrumentation settings can be assured. After preliminary screening, the final instrumentation settings were selected. Long time sampled data records were then obtained at all chosen instrumentation settings. The sampling period of the long time sampled records ranged from five minutes to twenty minutes. Some duplicate data records, records with identical instrumentation settings, were taken as a check on the time variability of the data acquisition.

The flume water was changed before moving the velocimeter to the next vertical measurement location. All measurements at a given elevation were obtained without altering the flume flow in any manner. After refilling, the flow was allowed to stabilize for approximately

thirty minutes prior to the acquisition of new exploratory test data records. Velocimetry data were obtained at elevations of 6.00, 4.00, 2.70, 1.80, 1.20, and 0.75 cm above the sediment bed reference level. Beneath 0.75 cm, the laser beams were, more often than not, blocked by the sediment bed; no measurements were possible.

During the subsequent analysis, a data record was discarded if it was found to have an anomalously high fraction of invalid data events or if the probability density function of the Doppler burst signal frequency was markedly skewed with respect to the frequency pass band of the filter. The discarded records were generally obtained as the flow became overseeded with fluid tracer particles. The variability noted in the remaining data records is judged to be due to fluctuations in the flow, not to the velocimetry data acquisition. The measurement location, the number of measurements of each type of scattering particle, and the length of record of each of the twelve retained validated data records are summarized in Table 7.2.1.

Table 7.2.1 Velocimetry Data Records

Location (cm above the bed)	Record Name	Period (min:sec)	Number of Fluid Velocity Measurements	Number of Valid Sediment Grain Velocity Measurements	Total Number of Sediment Grains
6.00	SQ600	9:06	29883	422	1597
	SQ601	15:10	13352	551	5733
4.00	SQ401	12:01	14607	1213	12538
2.70	SQ271	10:31	12776	1737	15593
	SQ272	18:35	14808	3112	29366
1.80	SQ180	5:37	21203	1403	5405
	SQ181	6:53	9916	1143	9655
	SQ182	7:02	23585	1880	7881
1.20	SQ120	9:09	9763	1584	16115
	SQ121	9:17	9118	2131	19661
	SQ122	8:58	9566	2047	20967
0.75	SQ750	25:04	9320	1181	12997

CHAPTER 8

PRESENTATION OF THE RESULTS

The one-dimensional laser-Doppler velocimetry data are presented in this chapter. The fluid and sediment grain velocity records are discussed first. Sediment grain inter-arrival time data are then shown. Finally, sediment grain velocity and inter-arrival time correlation statistics are presented.

8.1 Representative velocimetry data records

Portions of one of the validated velocimetry records obtained at each of the vertical measurement locations are presented in Figures 8.1.1 through 8.1.6. The measurement locations are identified by their respective elevations in centimeters above the sediment bed reference level. The fluid velocity measurements are connected by a solid curve; the sediment grain velocity measurements are indicated with plotting symbols. The plotted fluid velocity measurements have been filtered by a running average technique. In Figure 8.1.1, location 6.00, the effect of water surface waves on the data may be clearly seen. These waves, when present, were visually observed to shift slowly downstream. Also note that the sediment grains are, more often than not, moving faster than the fluid. No such wavy character is evident in the sample record from location 4.00, Figure 8.1.2. The sediment grains occasionally move faster than the surrounding fluid. The data records at location 2.70, exemplified by Figure 8.1.3, show little or no wavelike motion. The sediment grains move at a velocity comparable to that of the surrounding fluid. The data records at

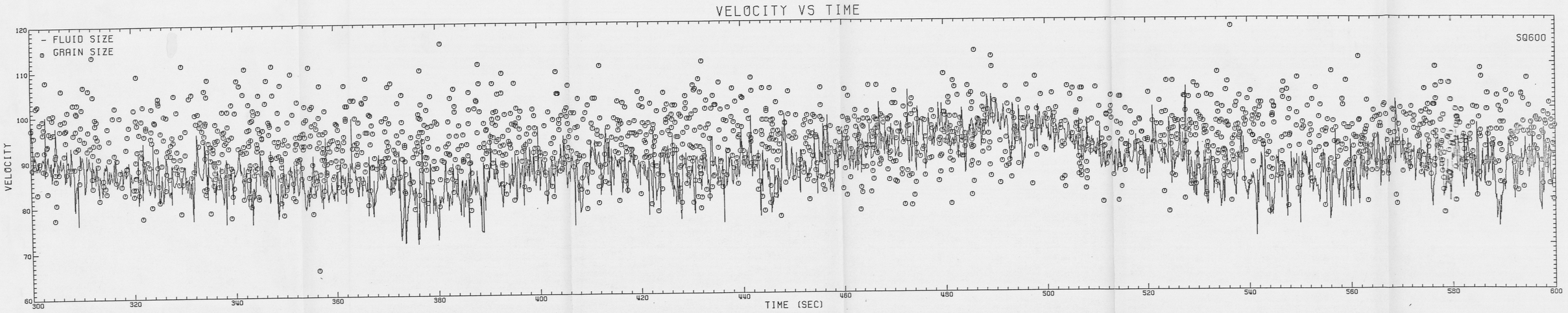

Figure 8.1.1 Sample velocimetry data record, location 6.00

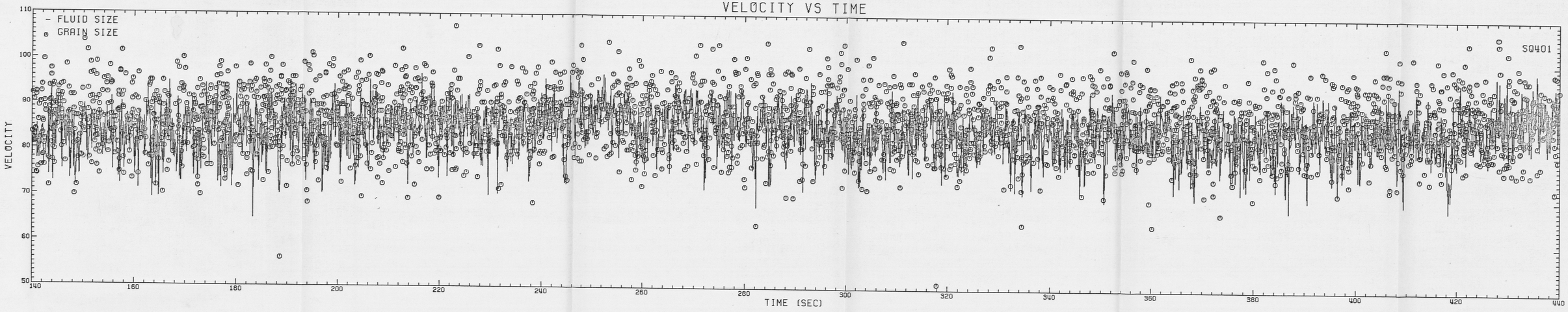

Figure 8.1.2 Sample velocimetry data record, location 4.00

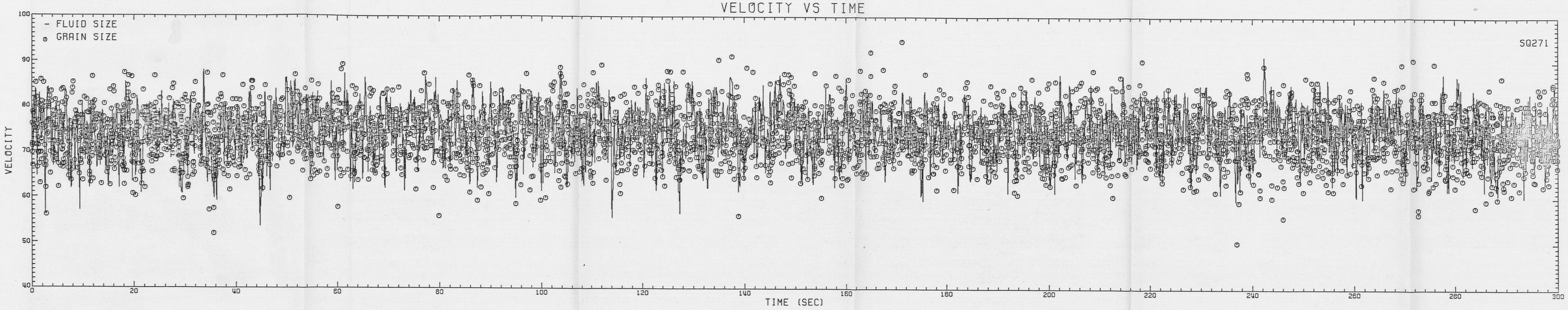

Figure 8.1.3 Sample velocimetry data record, location 2.70

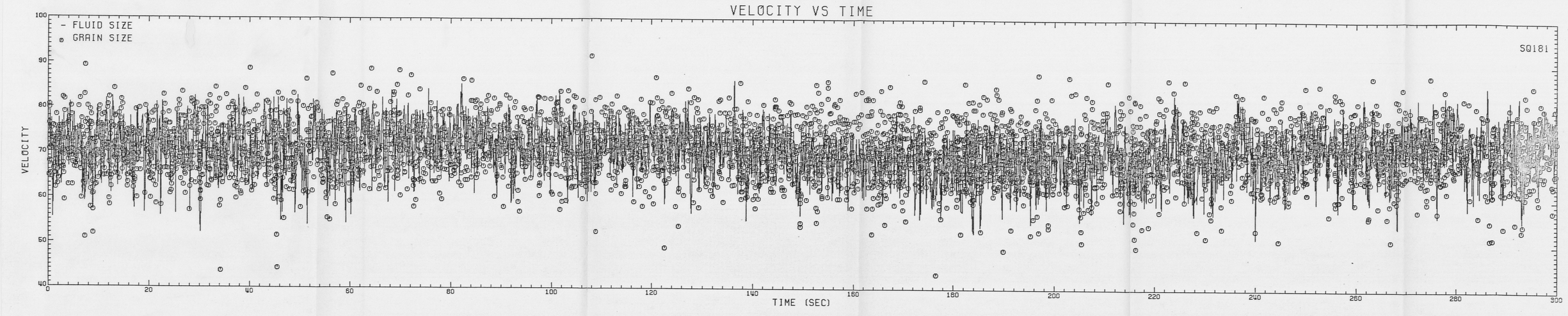

Figure 8.1.4 Sample velocimetry data record, location 1.80

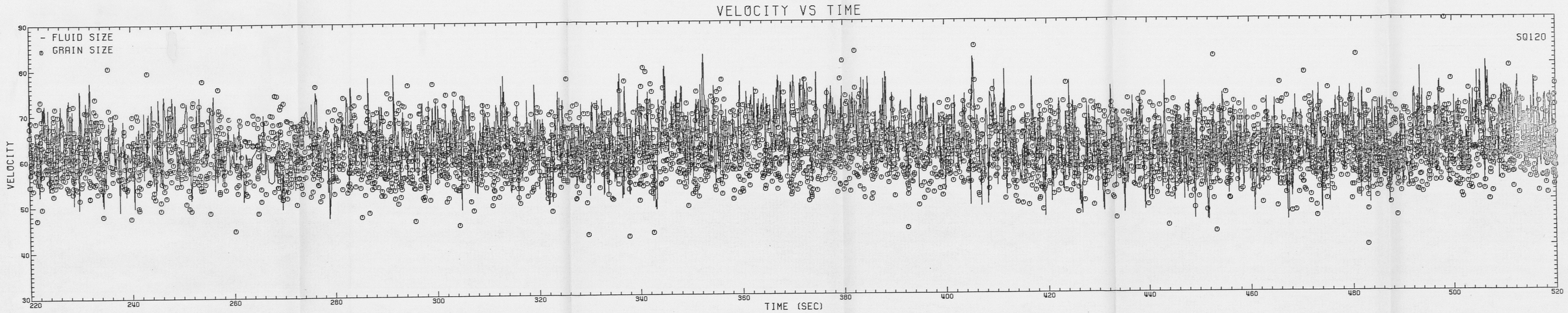

Figure 8.1.5 Sample velocimetry data record, location 1.20

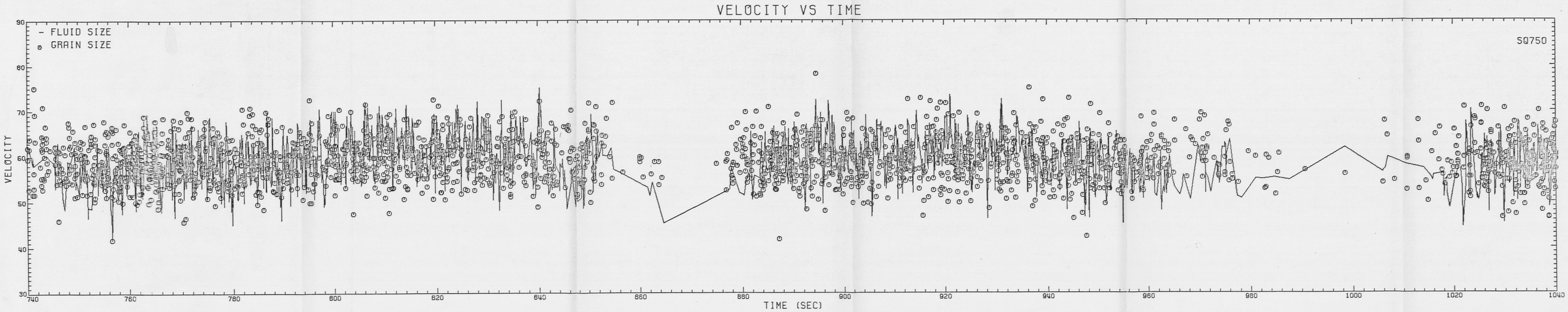

Figure 8.1.6 Sample velocimetry data record, location 0.75

location 1.80, Figure 8.1.4, are very similiar to those obtained at location 2.70. At location 1.20, Figure 8.1.5, a wavy character is again observed. The oscillations are now due to intermittent undulations in the sediment bed. Many of the sediment grains lag the nearby fluid. The effect of bed undulations is seen most clearly in Figure 8.1.6, location 0.75. The velocimetry record contains periods in which little or no data was collected. The gaps in the data are caused by undulations in the sediment bed which completely blocked the laser light beams.

Figures 8.1.7 and 8.1.8 illustrate the effects of the filter used on the fluid velocity measurements in the preceding figures. The unfiltered data appear in the lower plot of each figure. Trends in the fluid velocity data record are more easily seen in the filtered plot. The filtered plots must be viewed with care, however, when comparing the fluid and the sediment grain velocity. The velocity of some of the sediment grains seems very different from the nearby filtered fluid velocity measurements. Filtering the fluid velocity removes many of the extreme fluctuations. Comparison of the filtered plots to the unfiltered plots shows that this apparent difference in the sediment grain and fluid velocity is primarily due to the filtering. The sediment grain velocity is seen to be quite similiar, in most cases, to the nearby fluid velocity.

Some grains are observed to have a velocity different from that of the surrounding unfiltered fluid, but this still may not be the case within the flow. The fluid velocity data record may lack measurements of the "surrounding" fluid velocity. Portions of the unfiltered data

Figure 8.1.7 Sample velocimetery data record, filtered and unfiltered, location 6.00

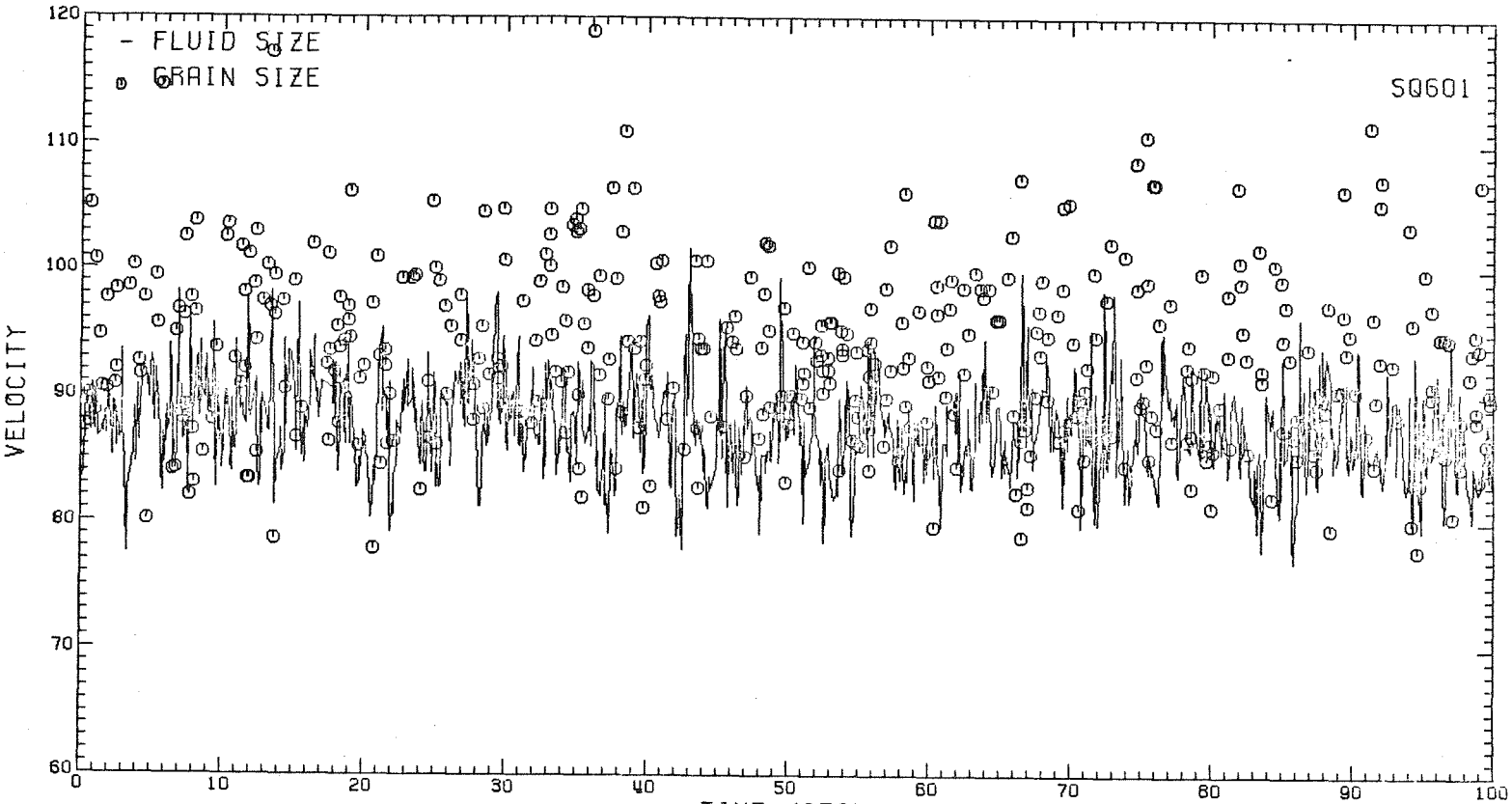

filtered

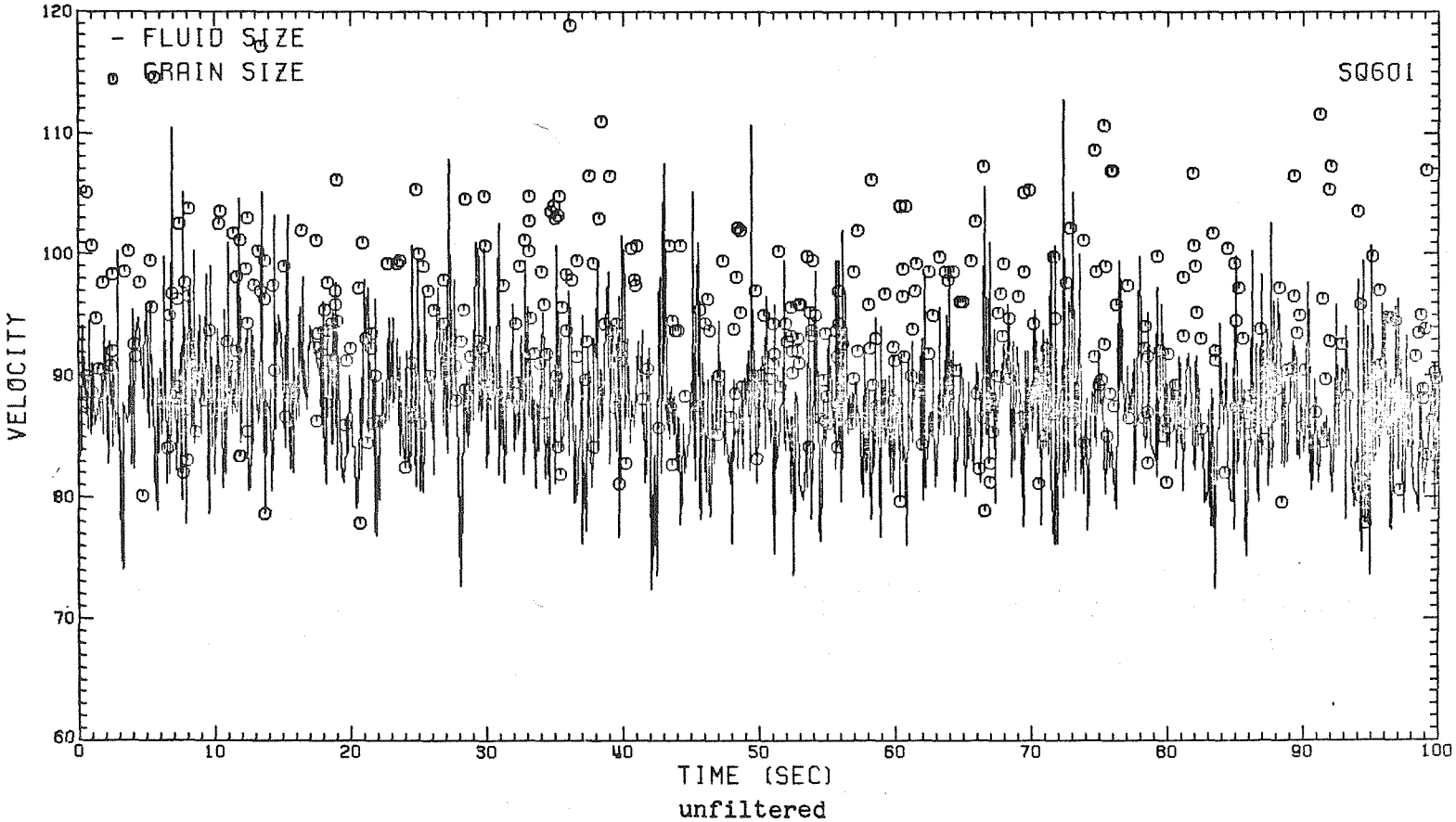

unfiltered

Figure 8.1.8 Sample velocimetery data record, filtered and unfiltered, location 1.80

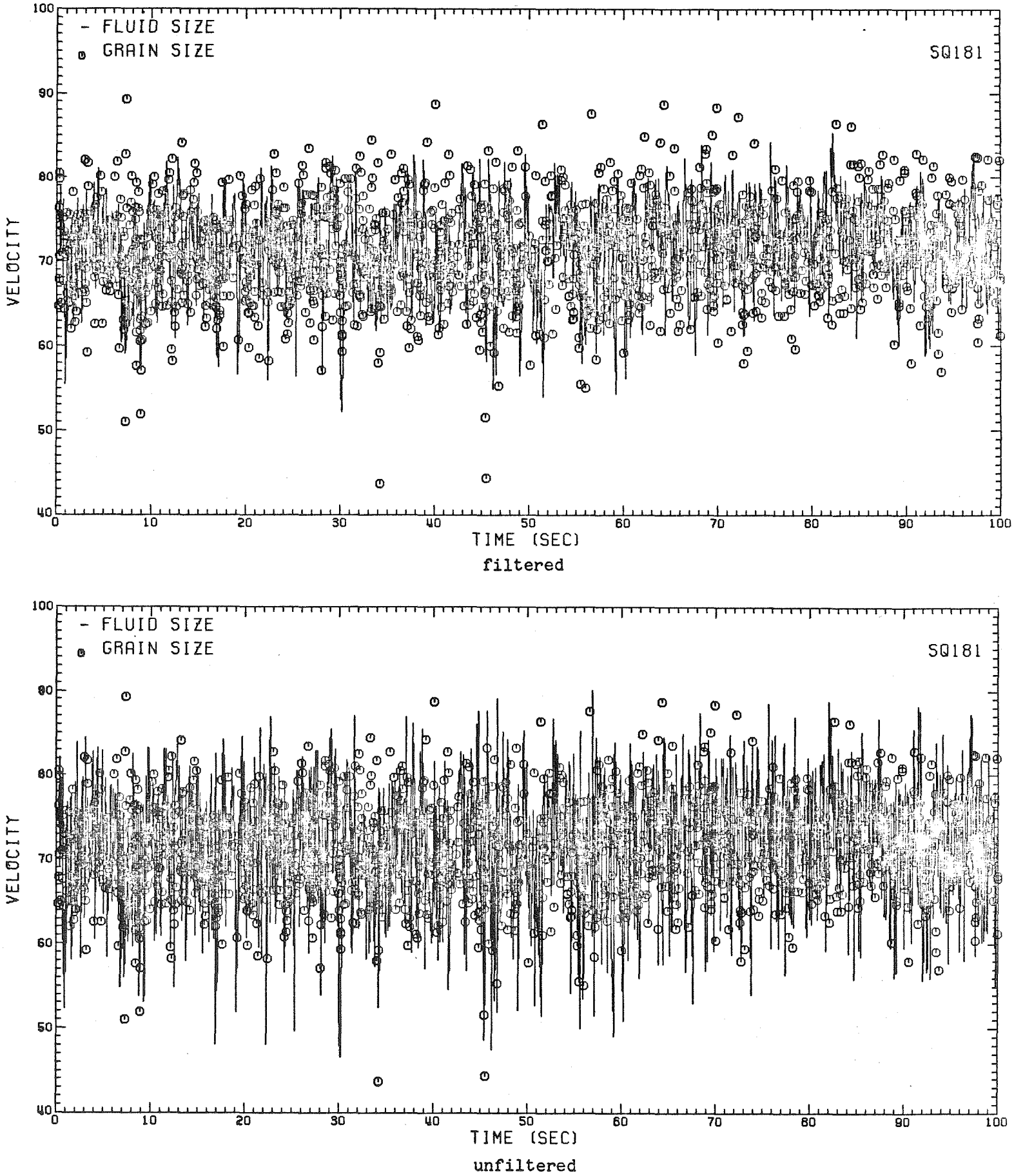

records shown in the previous Figures are expanded in Figure 8.1.9 to allow each fluid velocity measurement to be identified with a second plotting symbol. At approximately t=17 seconds the fluid velocity data record from location 6.00 contains a gap. No measurements of the fluid velocity were made. The sediment grain velocity recorded at this time seems to differ from the plotted fluid velocity, but there are no measurements of the fluid velocity very near to the grain. The times of measurement of fluid and sediment grain velocity are not coincident and the resulting data records are not continuous.

8.2 Measurements of fluid and sediment grain velocity

Profiles of the mean velocity of the fluid, $\overline{u}$, and the sediment grains, $\overline{u}_g$, are shown in Figure 8.2.1. The mean velocities computed from the different data records obtained at a single location are noted to vary. This is most probably due to slow, long time-scale fluctuations in the flow. A comparison of $\overline{u}$ and $\overline{u}_g$ is presented in Figure 8.2.2. In the lower portion of the flow, $\overline{u}_g$ is less than $\overline{u}$. At location 6.00, near the water surface, the sediment grains are observed to move significantly faster, in the mean, than the fluid.

Profiles of the standard deviation of the velocity of the fluid, $\sqrt{\overline{u'^2}}$, and the sediment grains, $\sqrt{\overline{u_g'^2}}$, are shown in Figure 8.2.3. Profiles of the relative velocity fluctuation, the local value of the standard deviation expressed as a percentage of the local mean, are given in Figure 8.2.4. The fluid velocity observations are in accordance with existing experimental measurements. Comparisons of $\sqrt{\overline{u'^2}}$ and $\sqrt{\overline{u_g'^2}}$ are given in Figure 8.2.5 and Figure 8.2.6. Throughout

Figure 8.1.9 Sample expanded scale velocimetry data records,
locations 6.00 and 1.80

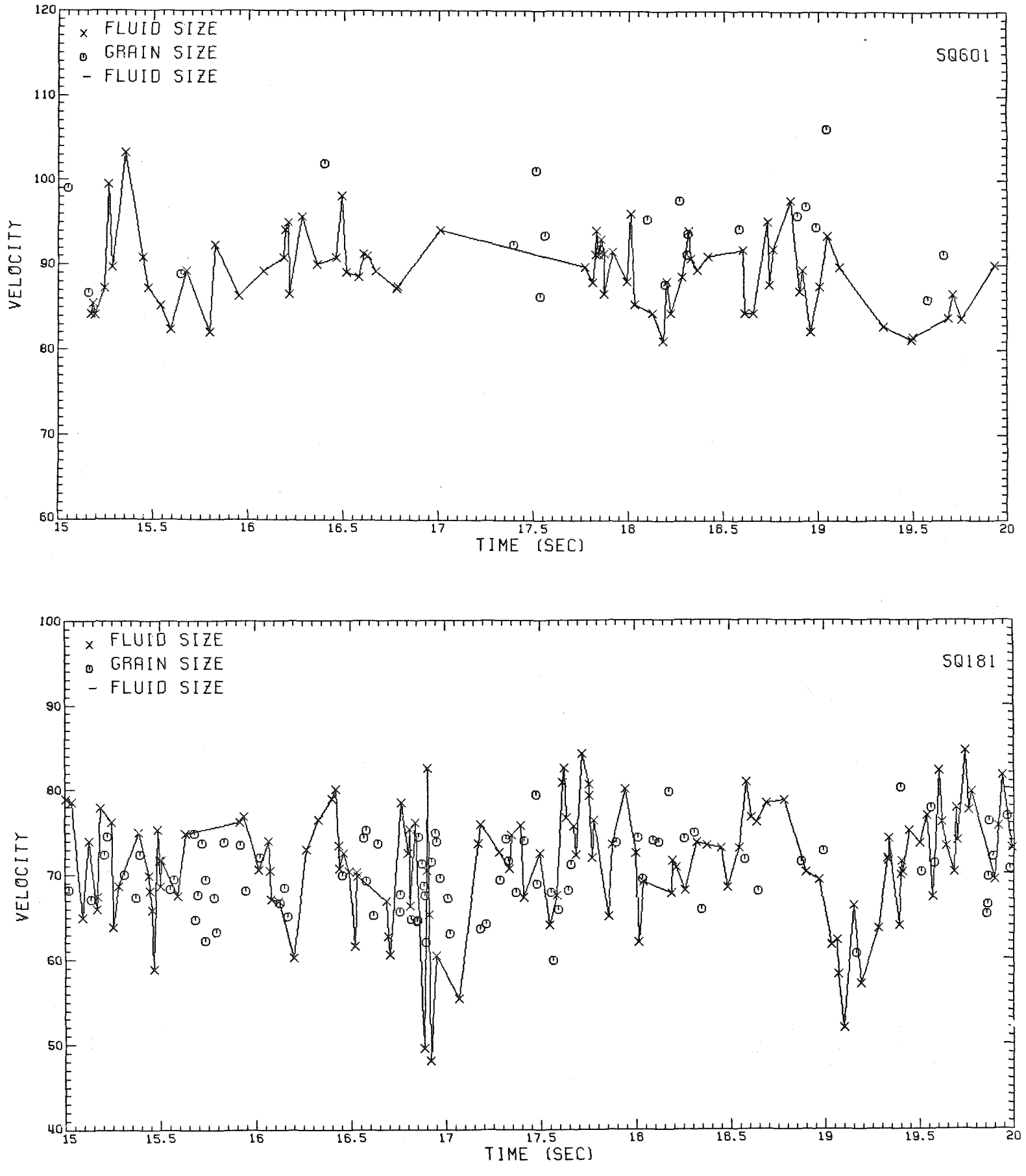

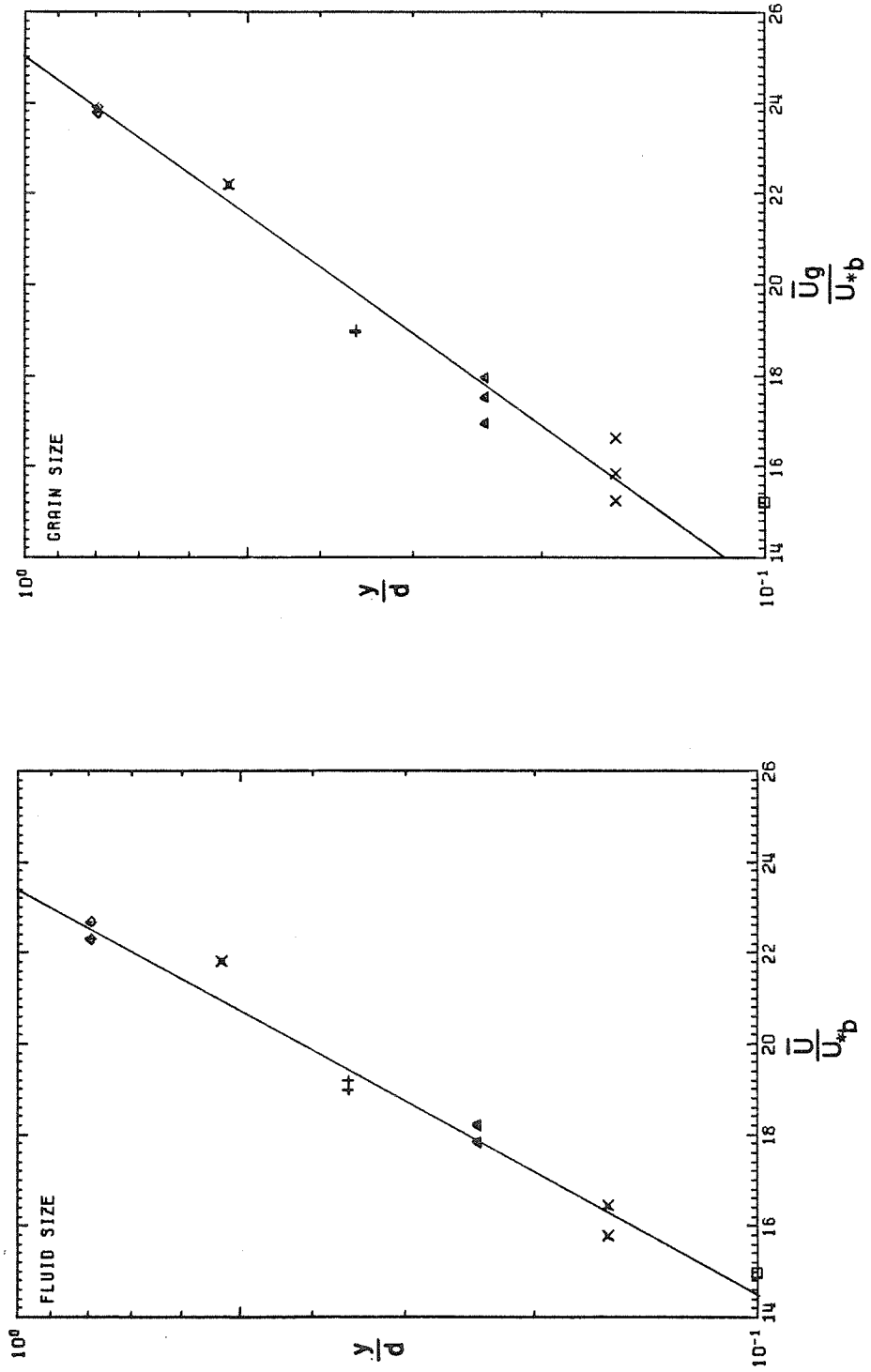

Figure 8.2.1 Profiles of mean velocity

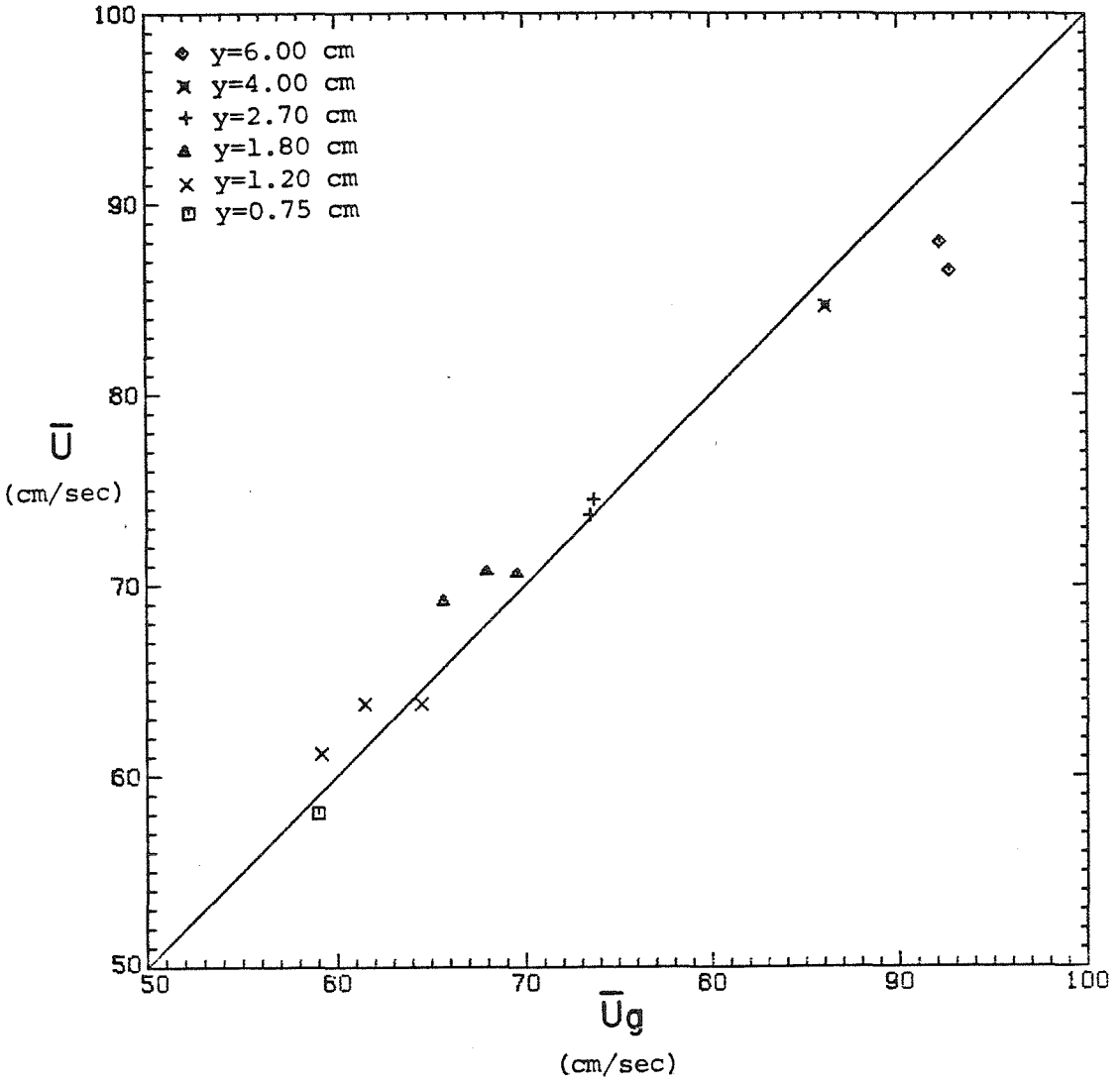

Figure 8.2.2 Comparison of fluid and sediment grain mean velocity

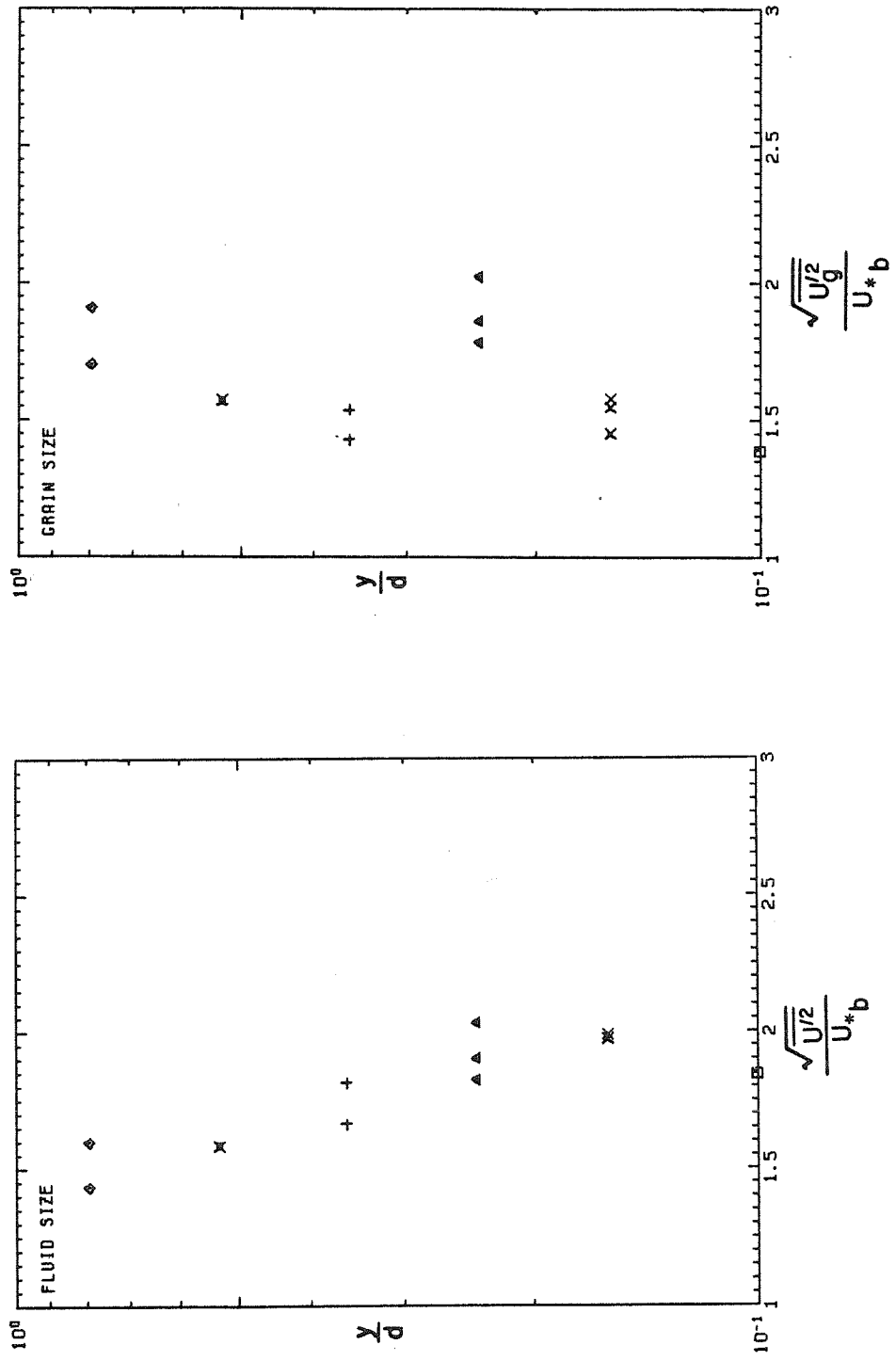

Figure 8.2.3 Profiles of velocity standard deviation

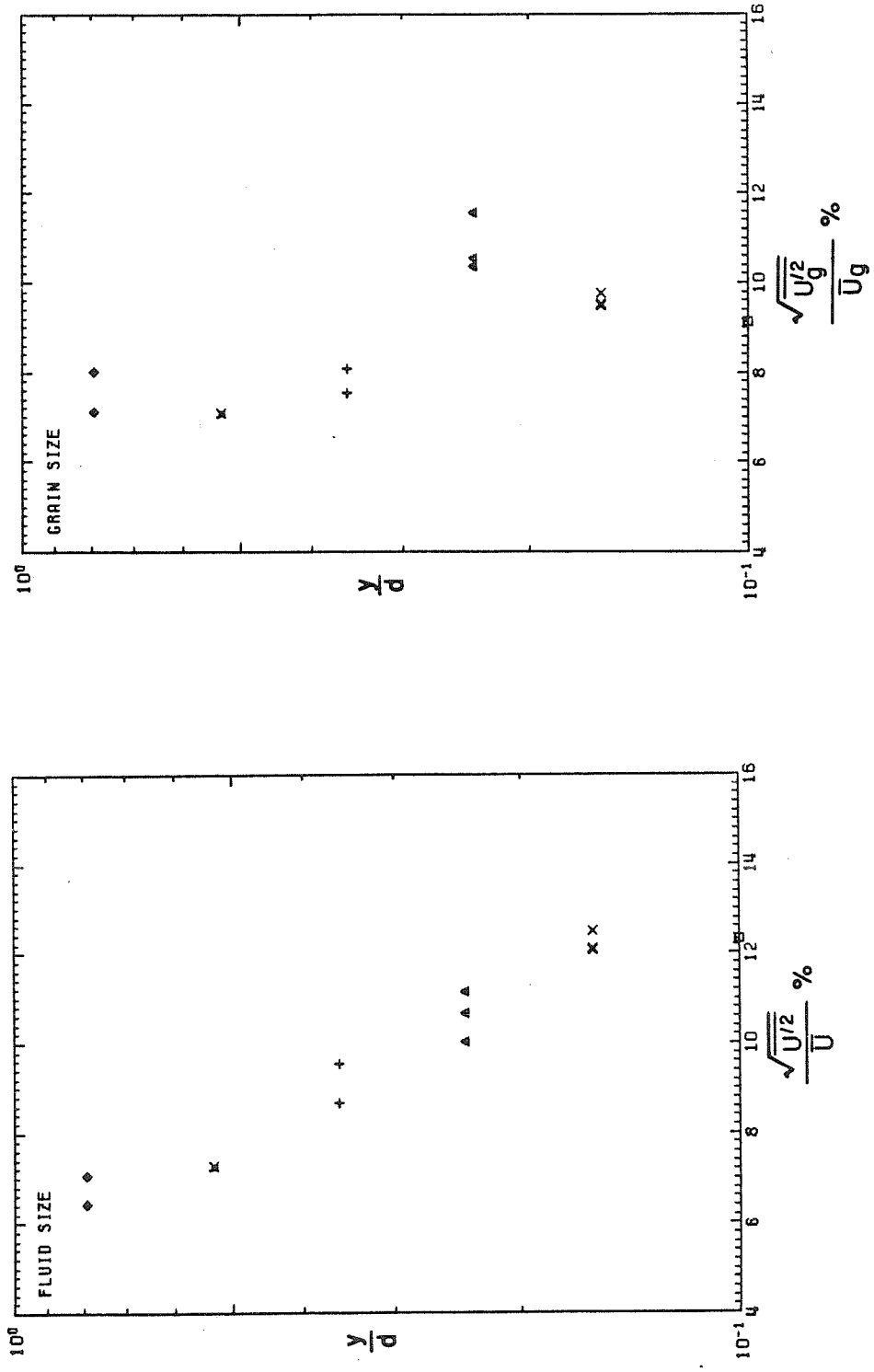

Figure 8.2.4 Profiles of relative velocity fluctuation

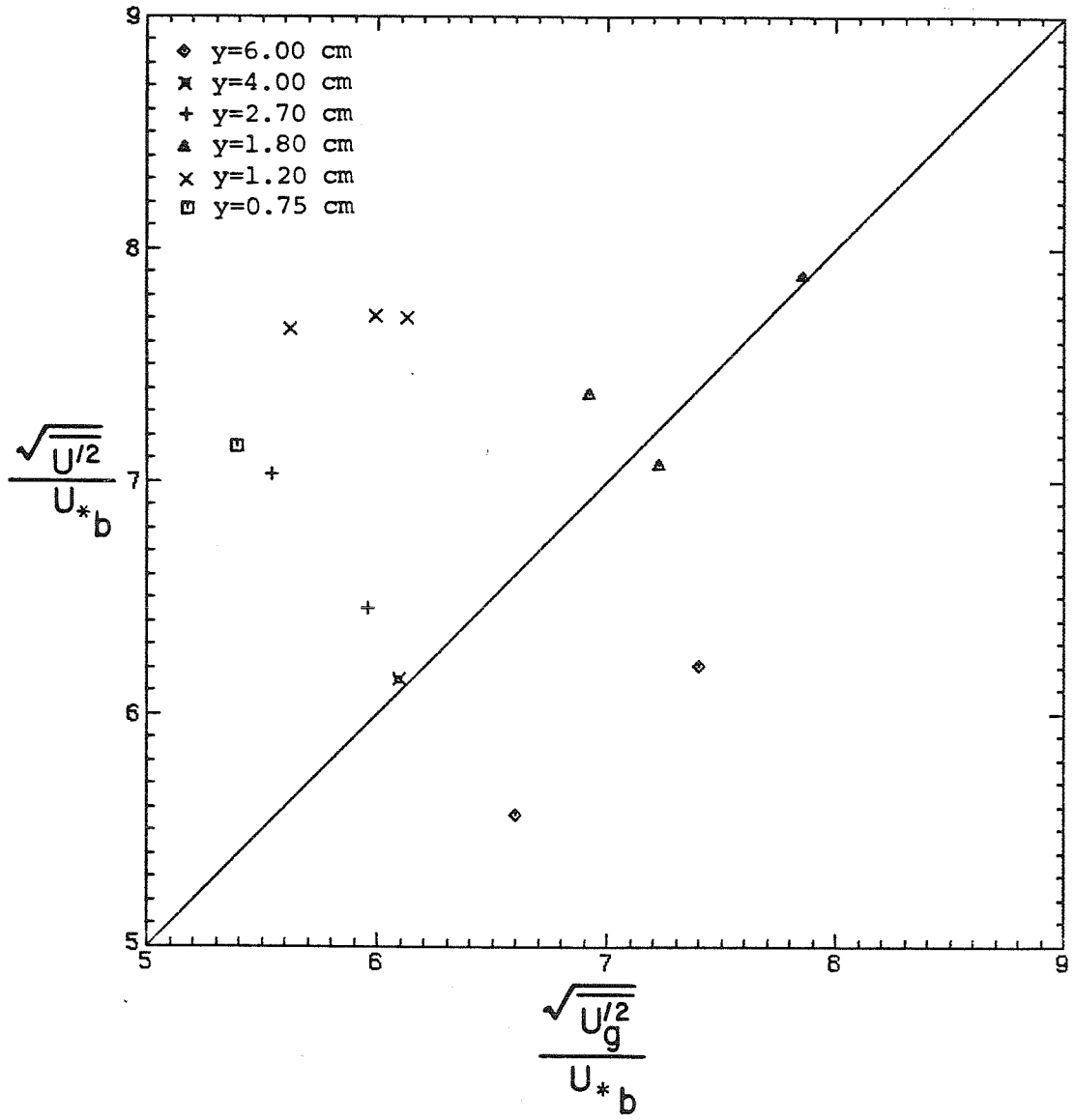

Figure 8.2.5 Comparison of fluid and sediment grain velocity standard deviation

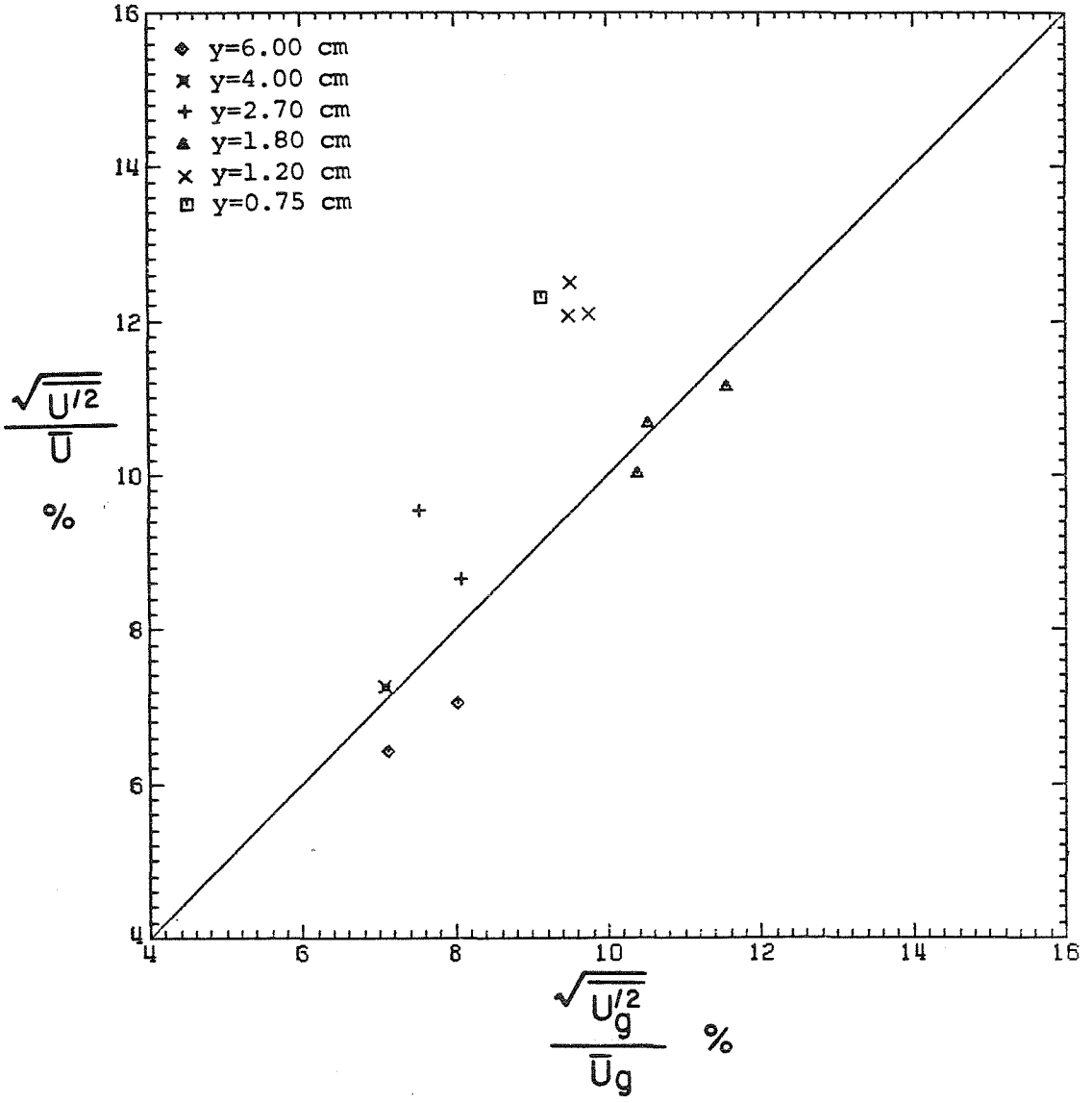

Figure 8.2.6 Comparison of relative fluid and sediment grain velocity fluctuation

most of the water column, $\sqrt{\overline{u'^2}}$ is greater than $\sqrt{\overline{u_g'^2}}$. Near the sediment bed, $\sqrt{\overline{u'^2}}$ and the relative fluctuation in the fluid velocity is much greater than $\sqrt{\overline{u_g'^2}}$. Near the water surface, $\sqrt{\overline{u_g'^2}}$ is much greater than $\sqrt{\overline{u'^2}}$, but their relative fluctuations are nearly equal.

The velocity probability density functions for each data record are shown in Figure 8.2.7. The fluid velocity probability density function is given by the solid line; that of the sediment grains by the dashed line. The mean fluid velocity and the mean sediment grain velocity are noted with plotting symbols. The probability density function of the fluid velocity near the sediment bed is broader than that near the free surface. The sediment grain velocity distribution does not exhibit such a trend. The sediment grain velocity tends to be less than the fluid velocity at locations 1.20 and 1.80. Also, at locations 1.20 and 0.75, the distribution of the fluid velocity is broader than distribution of the sediment grain velocity. The fluid velocity is clearly less than the sediment velocity at location 6.00. At the remaining locations, the probability density functions of the fluid velocity and the sediment grain velocity are quite similiar.

The simple lag correlation coefficients of velocity fluctuations computed for one of the data records from location 1.80 are shown in Figure 8.2.8. Similiar results were obtained for each of the remaining data records. No correlation in the velocity of successive sediment grains was found in any of the data. Unfortunately, the subsequent calculation of the true auto-correlation function proved unreliable. This calculation requires the inversion of a matrix with elements

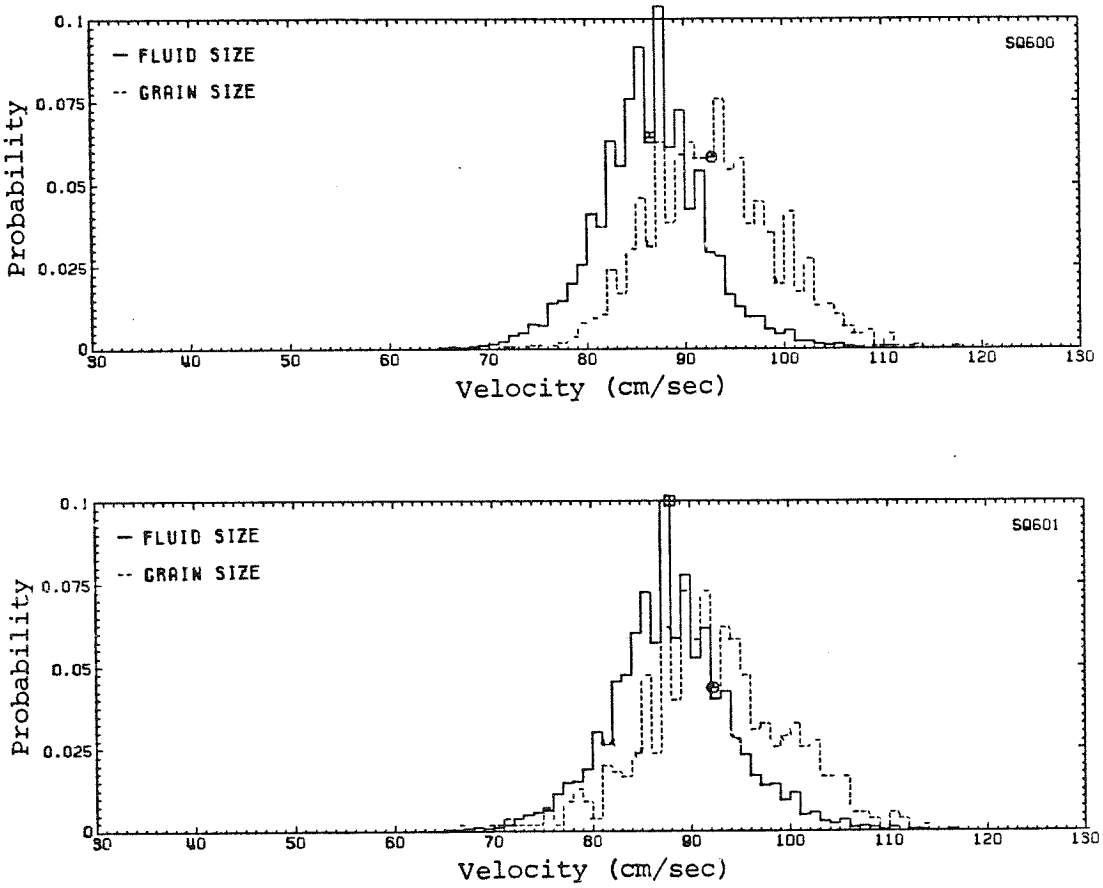

Figure 8.2.7.a Velocity probability density functions, location 6.00

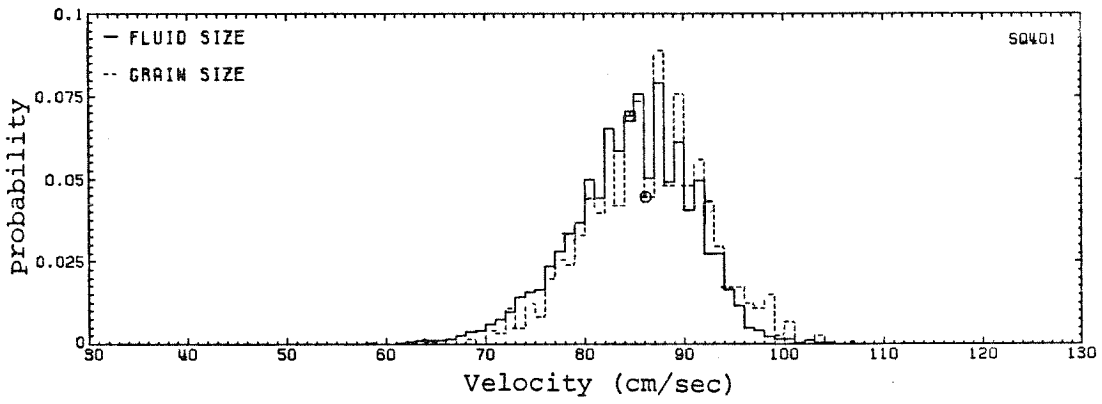

Figure 8.2.7.b Velocity probability density function, location 4.00

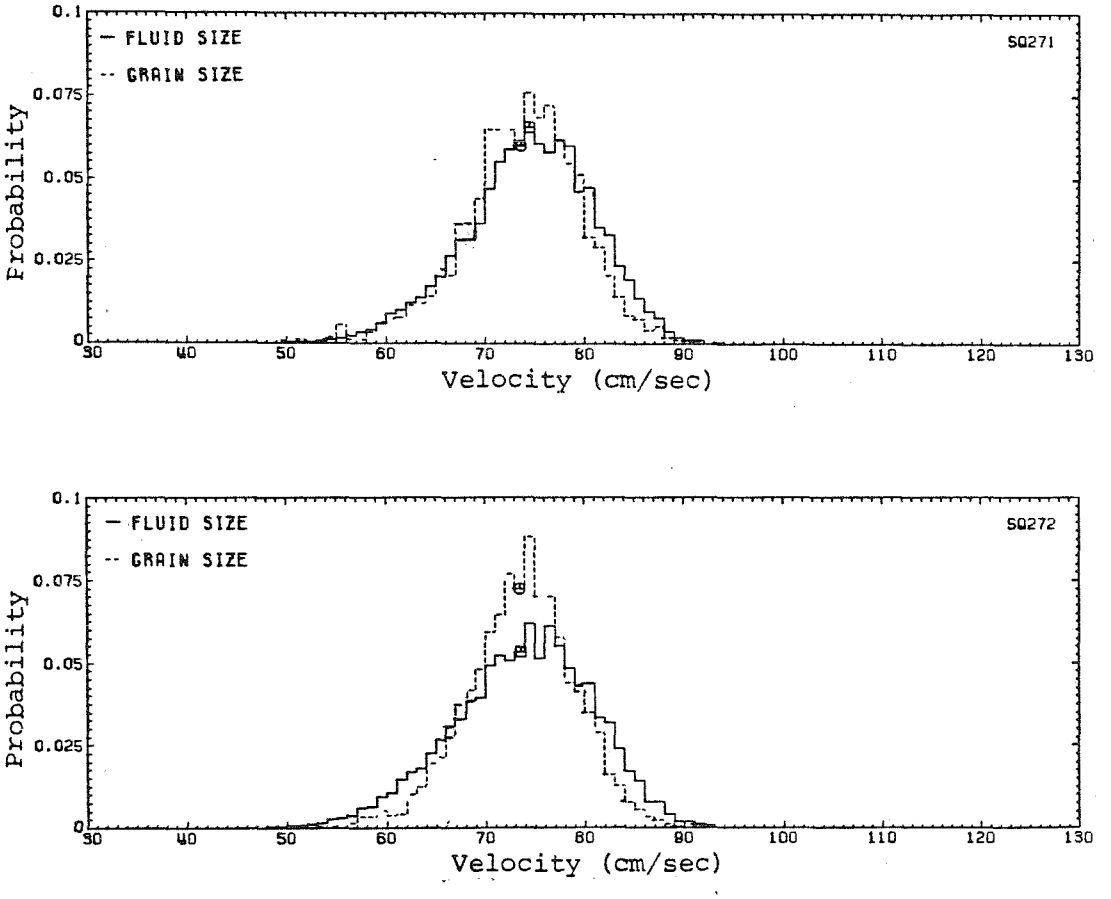

Figure 8.2.7.c Velocity probability density functions, location 2.70

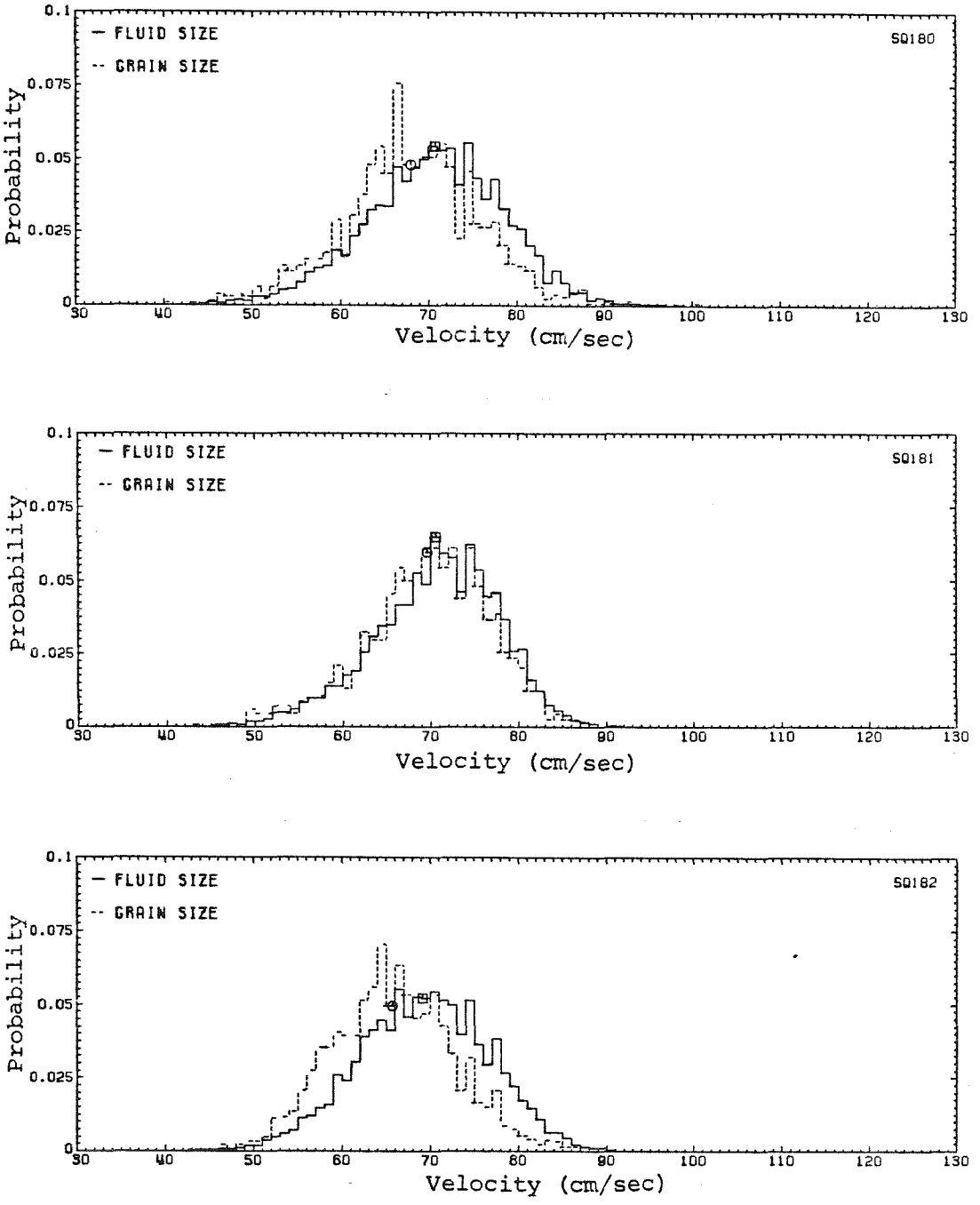

Figure 8.2.7.d Velocity probability density functions, location 1.80

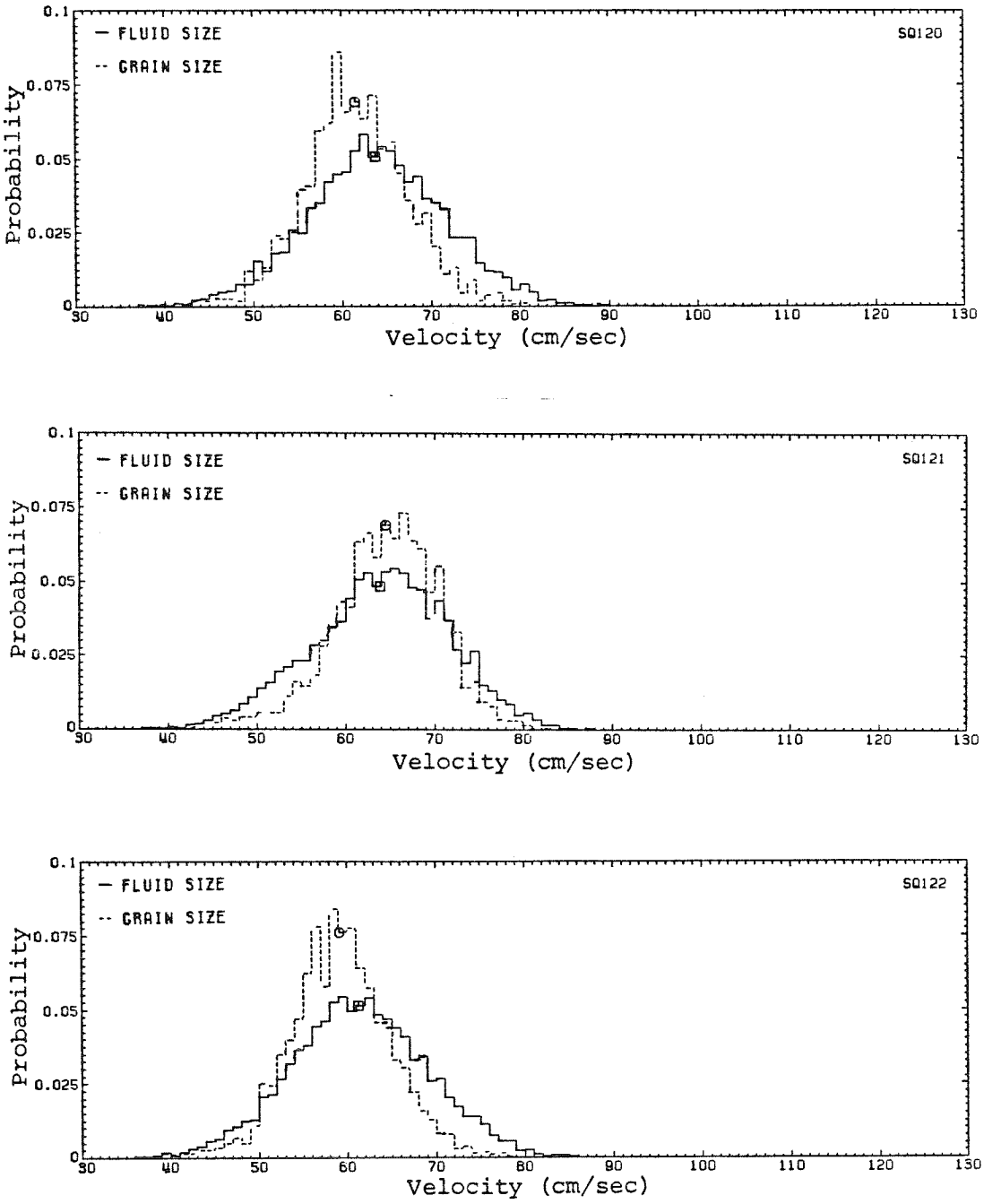

Figure 8.2.7.e Velocity probability density functions, location 1.20

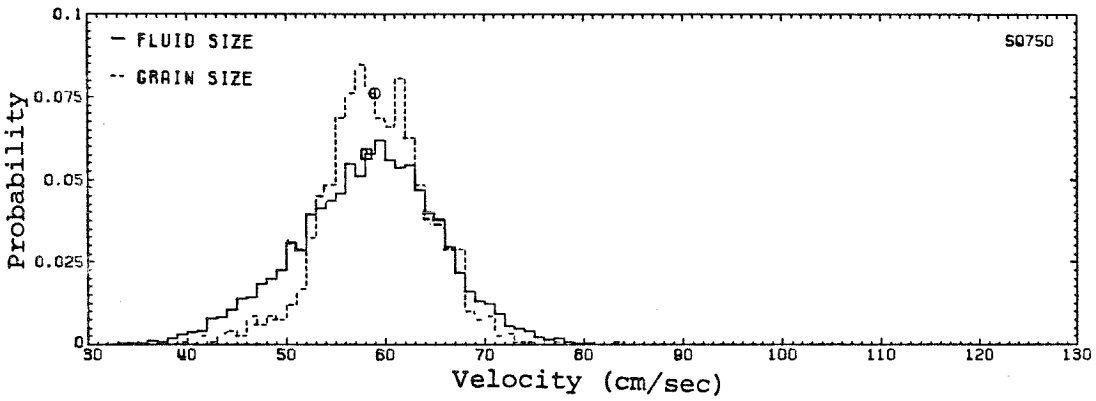

Figure 8.2.7.f Velocity probability density function, location 0.75

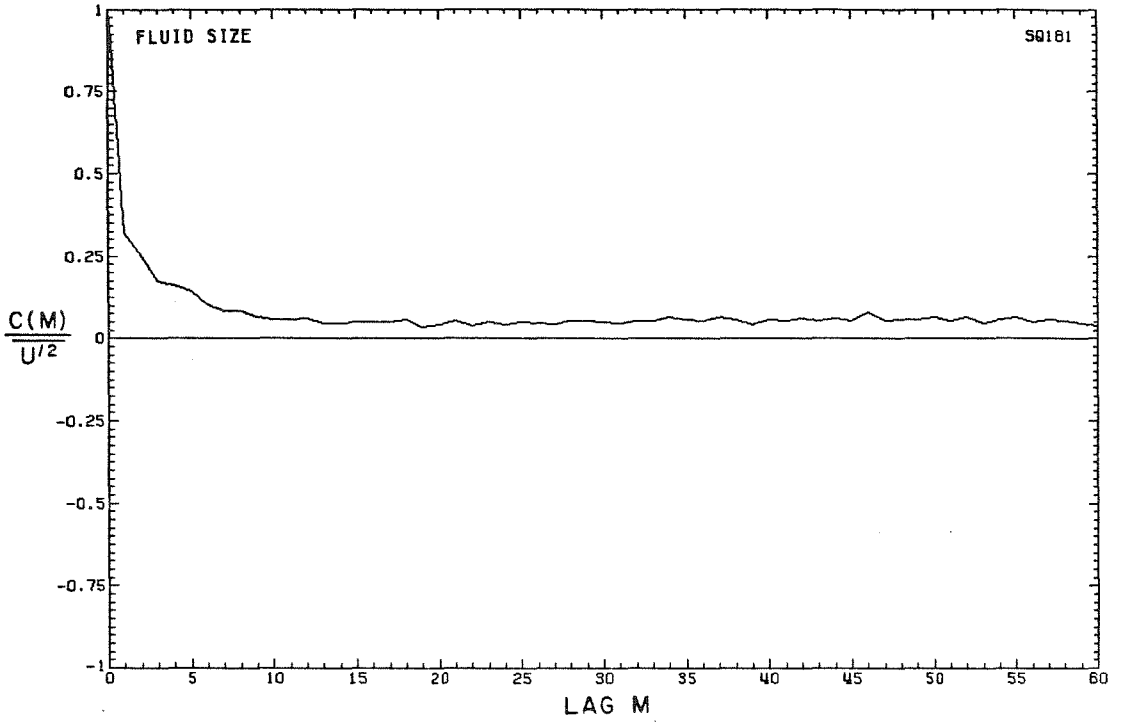

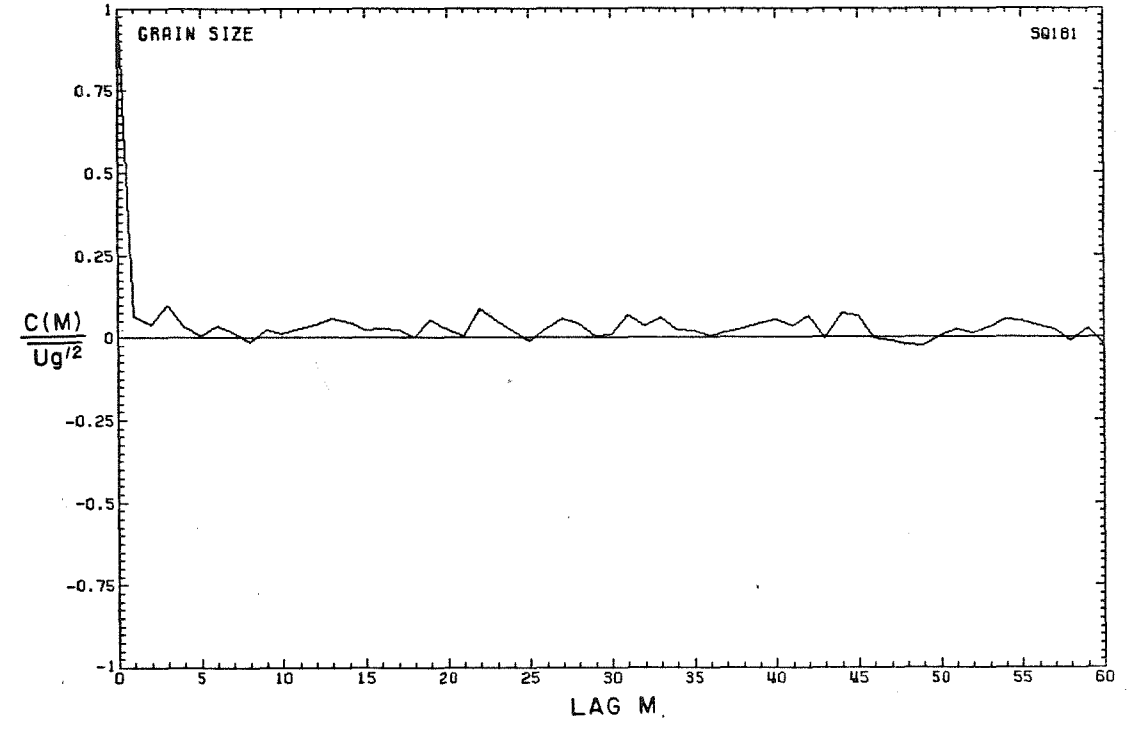

Figure 8.2.8 Sample simple lag correlation coefficients of velocity fluctuation, location 1.80

determined by the probability density functions of lag time τ at lag M. Such a matrix becomes more nearly singular as the sampling becomes more irregular in time. The numerical inversion of a nearly singular matrix is plagued by numerical instability. The computed inverted matrix, if obtained at all, bears little or no resemblance to the inverse of the initial matrix. The velocimetry events obtained in this study are quite irregularly spaced in time. The resulting matrices of lag time probability density for both the fluid and the sediment grain measurements in each data record are nearly singular. The computed true velocity auto-correlation functions were overwhelmingly dominated by the numerical errors and were physically meaningless.

The normalized power spectral estimate of the fluid velocity fluctuations and the relevant power spectral window function as computed for two of the data records are shown in Figure 8.2.9. The power spectral estimate is given by the solid line; the spectral window function is given by the dashed line. The mean sampling frequency is indicated with a plotting symbol. The results are presented for two of the data records with the most similiar time sampling characteristics.

The futility of the spectral computations is apparent. While the power spectral estimate generally decreases with increasing frequency, the expected error in the power spectral estimate is equal to the value of the estimate. There is no smoothing inherent in the direct computation of the power spectral estimate. The spectral window function does indicate a lower bound on the frequency for which the computation of the power spectral estimate should be performed. For

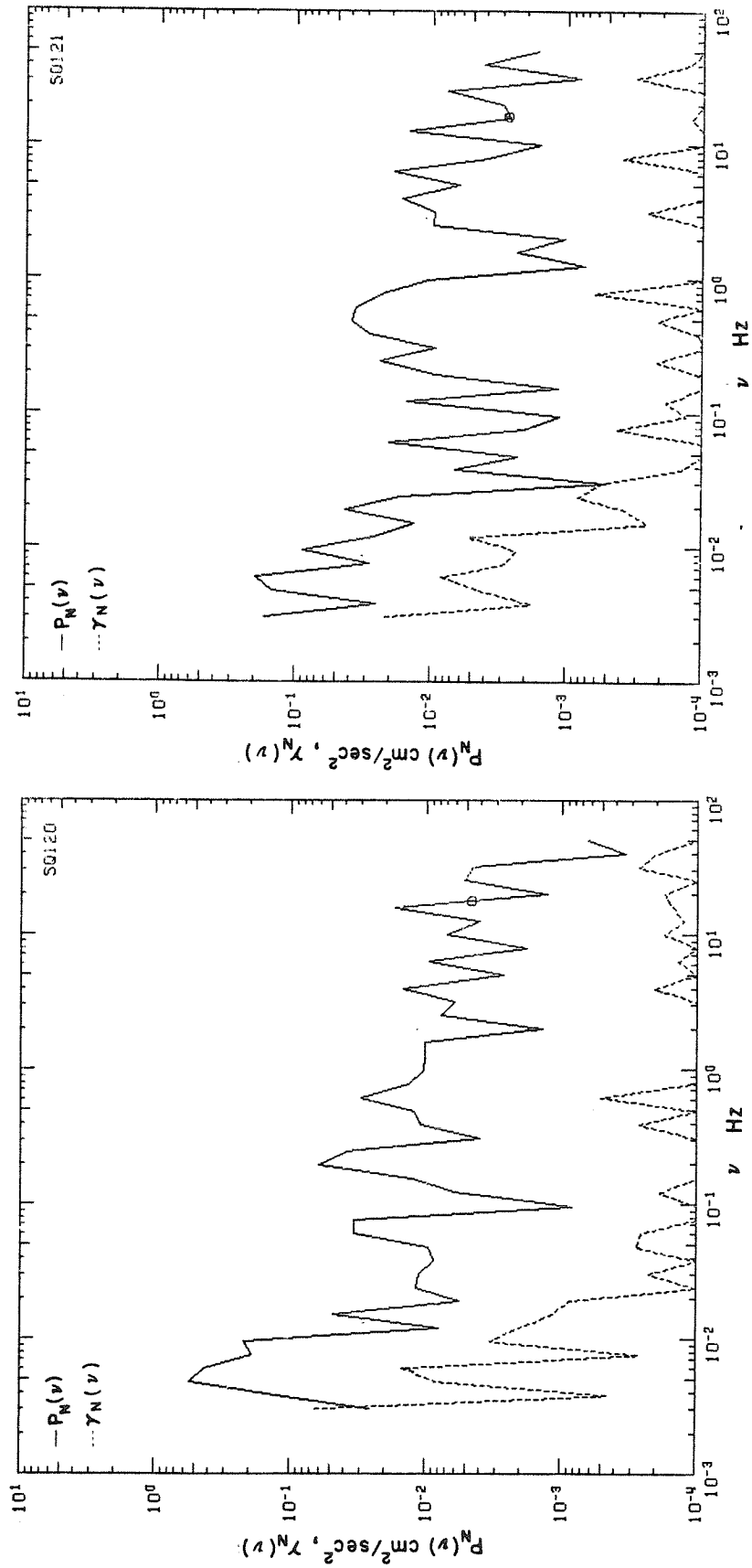

Figure 8.2.9 Sample fluid velocity fluctuation power spectral estimates and power spectral window functions, location 1.20

the presented data records, this lower bound is seen to be approximately 0.02 Hz, which corresponds to roughly one-tenth of the total sampling period.

The results of the spectral calculations of the sediment grain velocity fluctuations are still less instructive. Figure 8.2.10 shows the power spectral estimate and the power spectral window function corresponding to the fluid results shown in Figure 8.2.9. No trend in the power spectral estimate is at all apparent. The mean sampling frequency of the sediment grain velocity in the data records shown is approximately 4 Hz. Thus, at best, only long-time fluctuations in sediment grain velocity can be considered. The expected error in the sediment grain velocity spectral calculations is greater than that of the fluid velocity spectral estimates due to the relatively smaller number of sediment grain velocity measurements.

The effects of the bias correction procedures on the computed mean and standard deviation of the fluid velocity are shown in Figure 8.2.11. The result of the Mc Laughlin-Tiederman (1973) correction is given in Figure 8.2.11.a. The trapezoidal bias correction suggested by Dimotakis (1976) was applied to give Figure 8.2.11.b. Figure 8.2.11.c illustrates the effect of the procedure developed by Mc Dougall (1980). Little change in $\overline{u}$ results from any of the correction procedures. All of the bias corrections tend to increase $\sqrt{\overline{u'^2}}$ slightly. The trapezoidal averaging correction yields a slightly larger change in $\sqrt{\overline{u'^2}}$ than the other correction procedures; however, no significant difference among the three correction procedures is apparent.

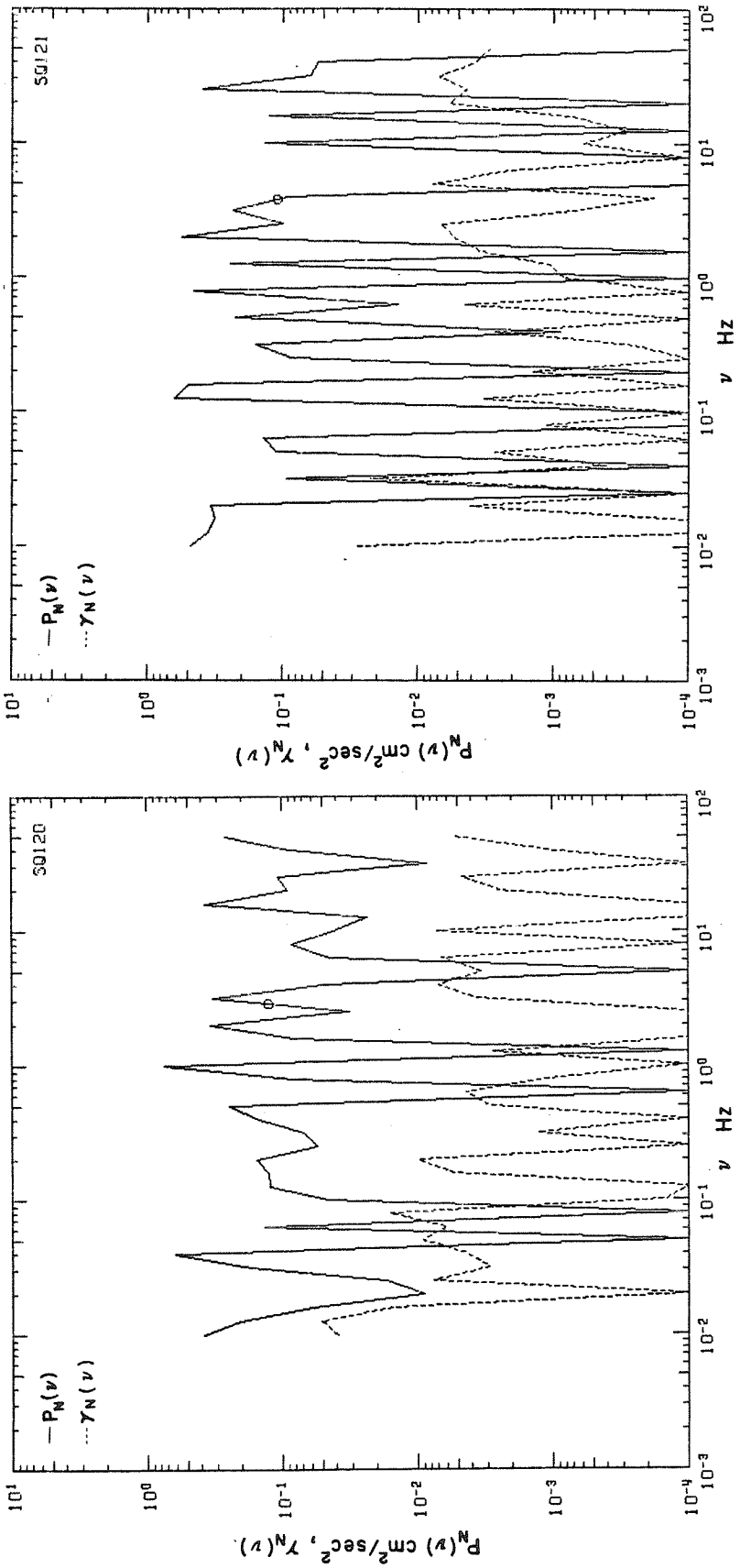

Figure 8.2.10 Sample grain velocity fluctuation power spectral estimates and power spectral window functions, location 1.20

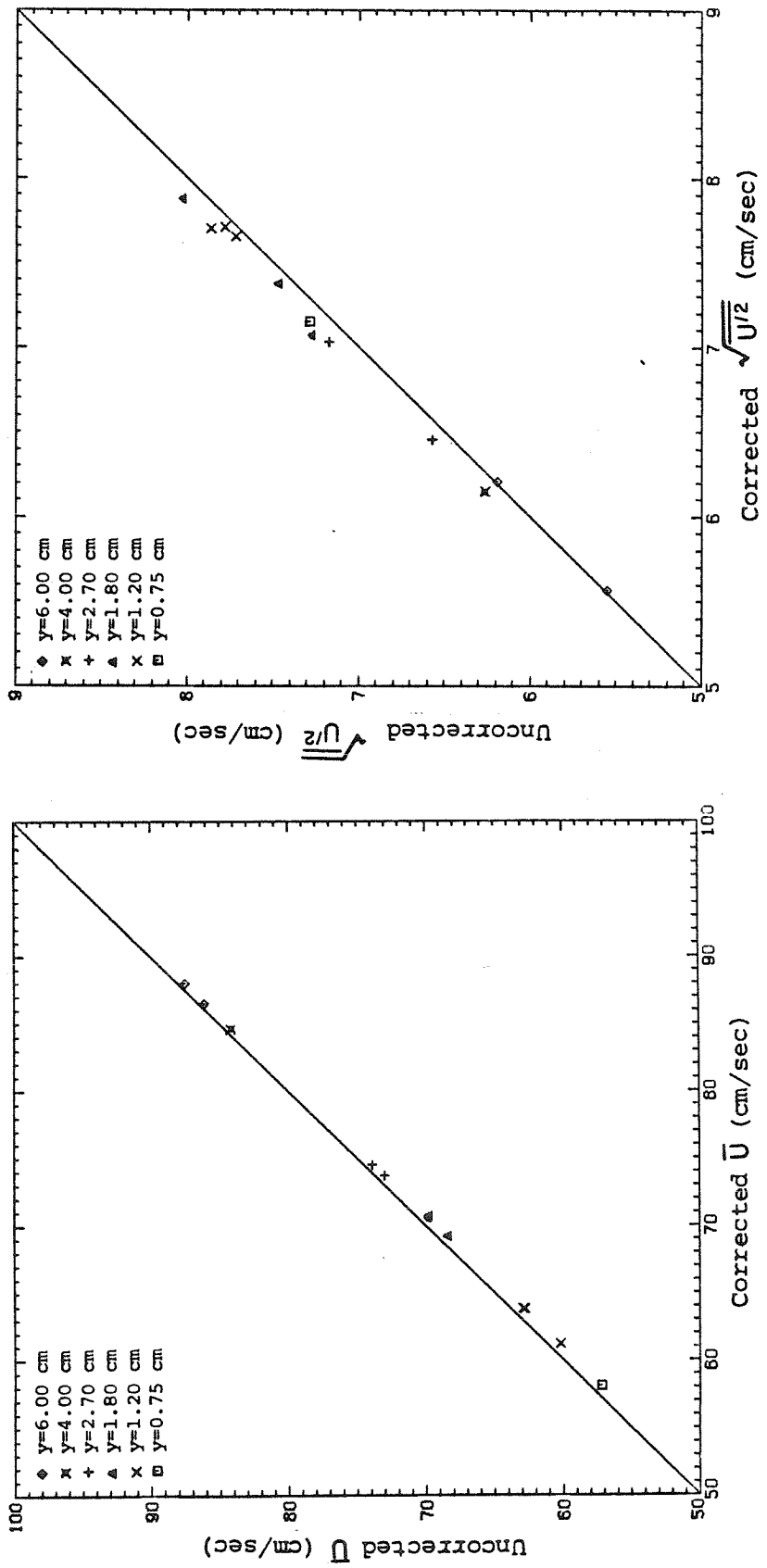

Figure 8.2.11.a Comparison of uncorrected and corrected fluid velocity mean and standard deviation, Mc Laughlin-Tiederman procedure

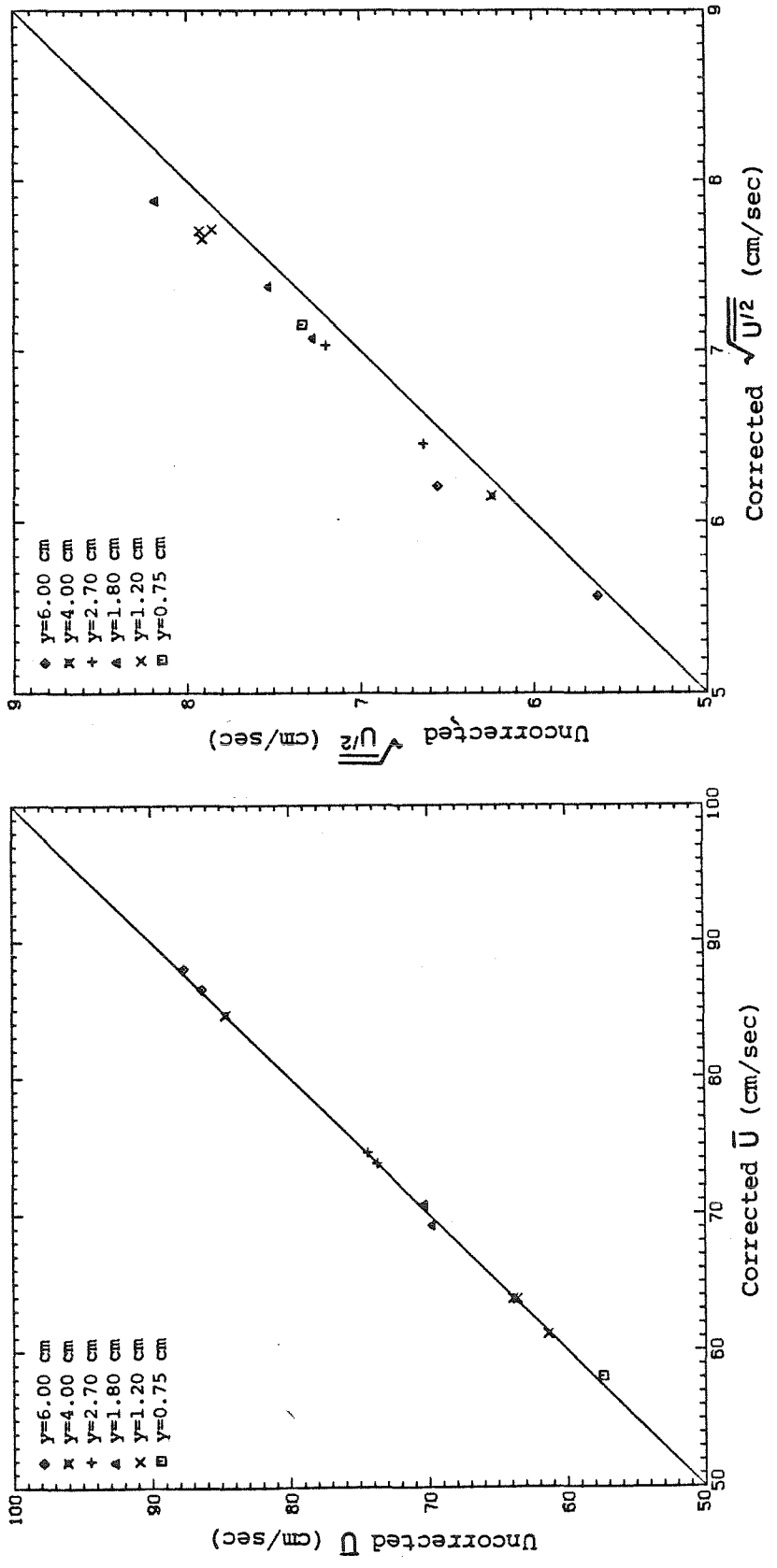

Figure 8.2.11.b Comparison of uncorrected and corrected fluid velocity mean and standard deviation, Dimotakis procedure

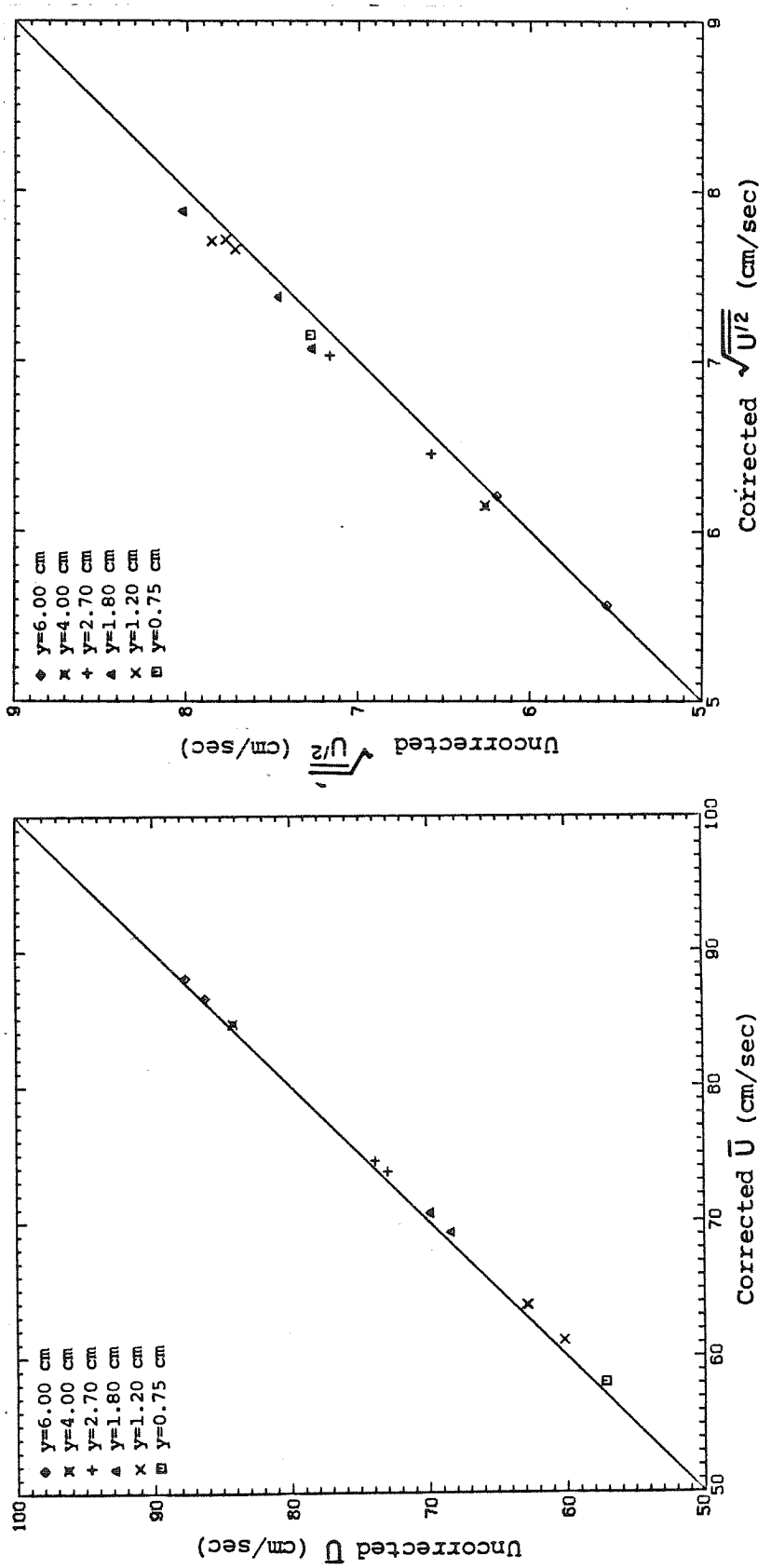

Figure 8.2.11.c Comparison of uncorrected and corrected fluid velocity mean and standard deviation, Mc Dougall procedure

The Mc Laughlin-Tiederman and the Dimotakis procedures procedures were also used to compute corrected velocity probability density functions. The results for one of the data records from each location are shown in Figure 8.2.12. The corrected velocity probability density functions are only very slightly broadened. Again, the two correction procedures are very similiar and have only minor effect compared to the uncorrected velocity distribution.

8.3 Representative sediment grain inter-arrival time records

Associated with each velocimetry data record is a sediment grain inter-arrival time data record. As discussed in Chapter 3, sediment transport rate is inversely related to the sediment grain inter-arrival time. The fluctuations in grain inter-arrival times give a measure of the small time-scale fluctuations in the sediment transport rate. The inter-arrival time data records corresponding to each of the previously given velocimetry data records are shown in Figures 8.3.1 through 8.3.6. The inter-arrival times for all detected the sediment grains, size class 4 G, are connected with a solid line; those sediment grains which generated good velocimetry signals, size class 9, are indicated with plotting symbols. Note that the inter-arrival time values for size class 9 are not plotted; only the occurrence of a valid velocimetry measurement at a given time is implied.

The time variability in sediment grain inter-arrival time at any one of the measurement locations is readily apparent from the figures. Also, the occurrence of a valid velocimetry data does not seem to be obviously correlated with long inter-arrival times.

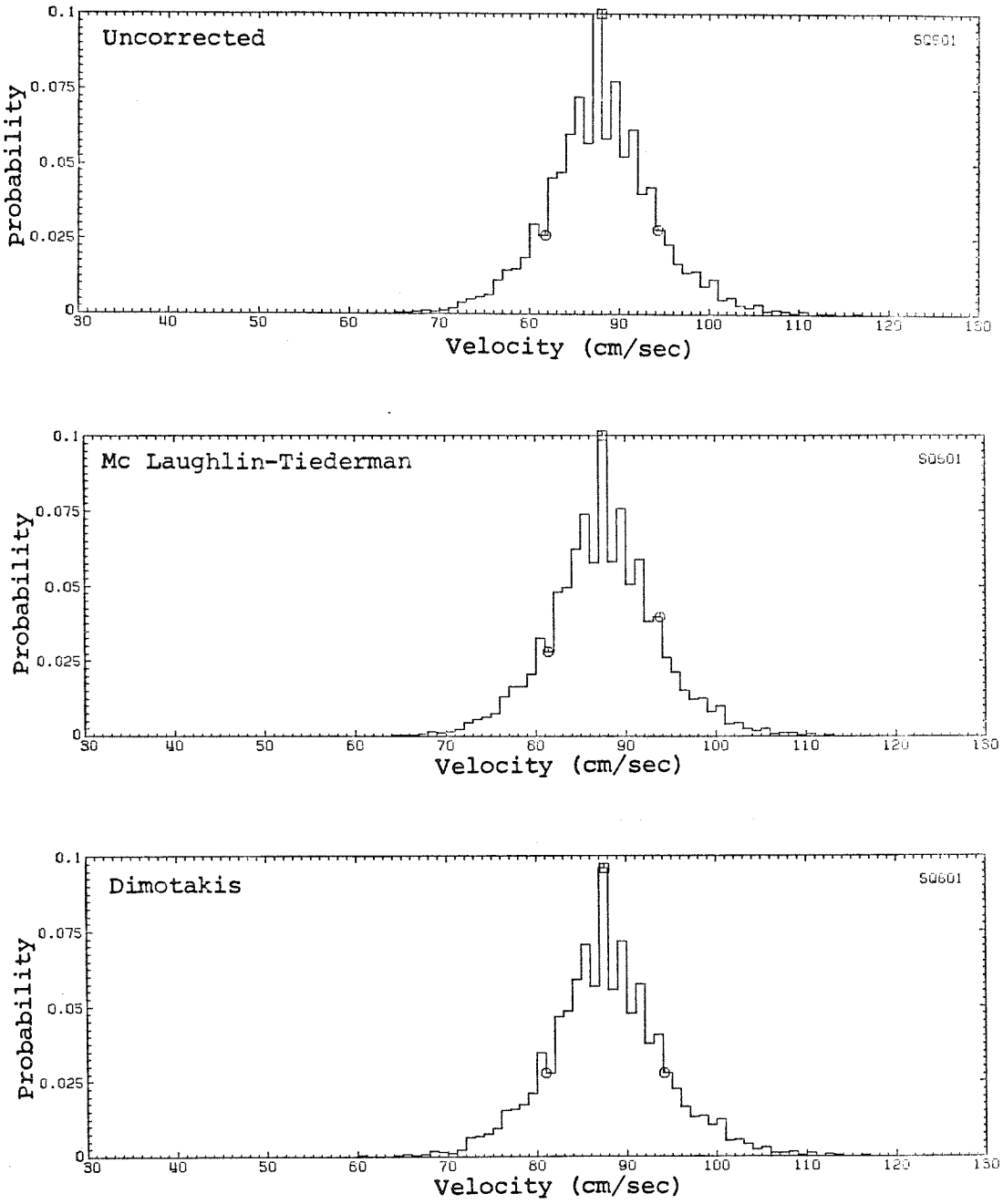

Figure 8.2.12.a Sample comparison of uncorrected and corrected fluid velocity probability density function, location 6.00

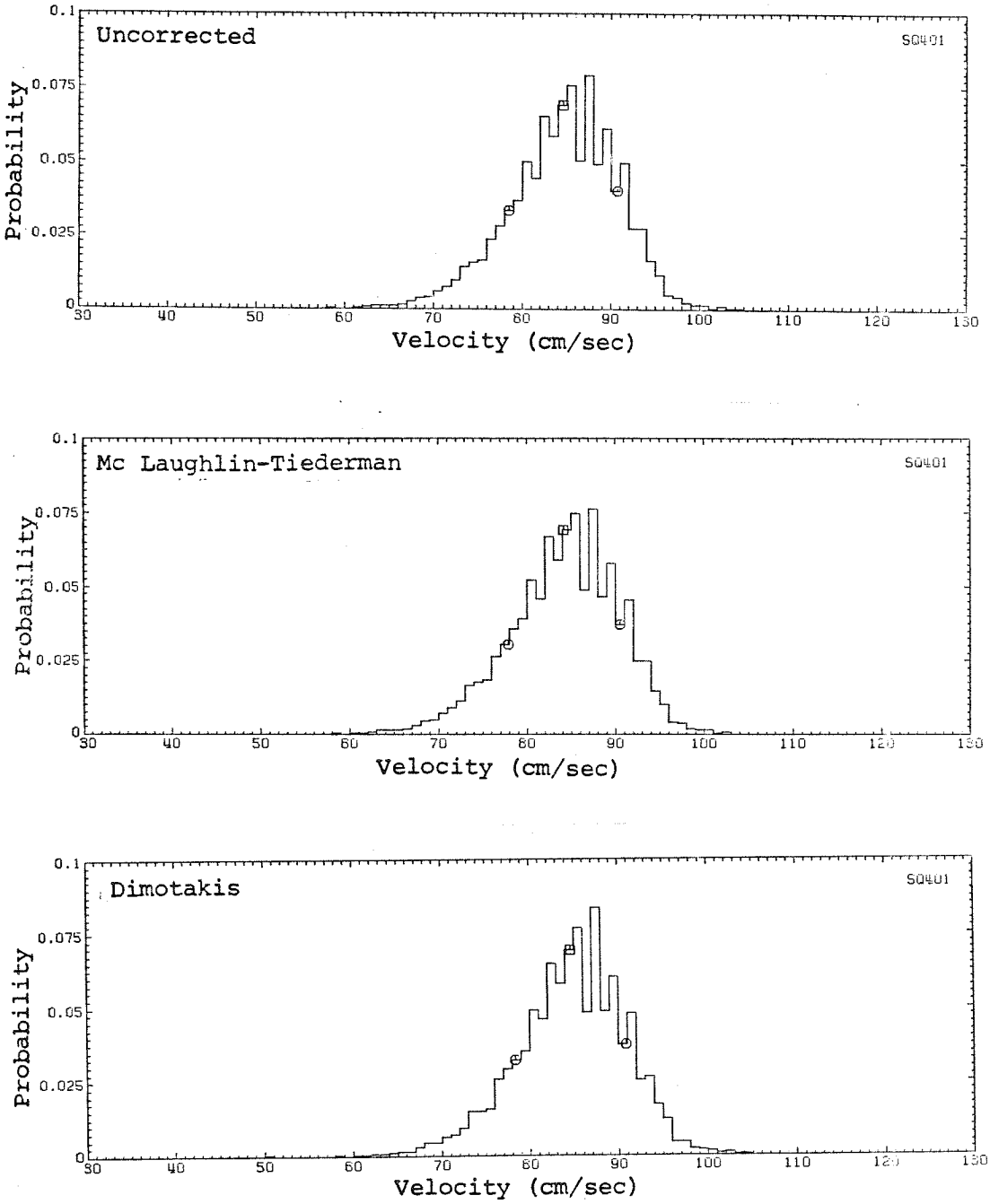

Figure 8.2.12.b Sample comparison of uncorrected and corrected fluid velocity probability density function, location 4.00

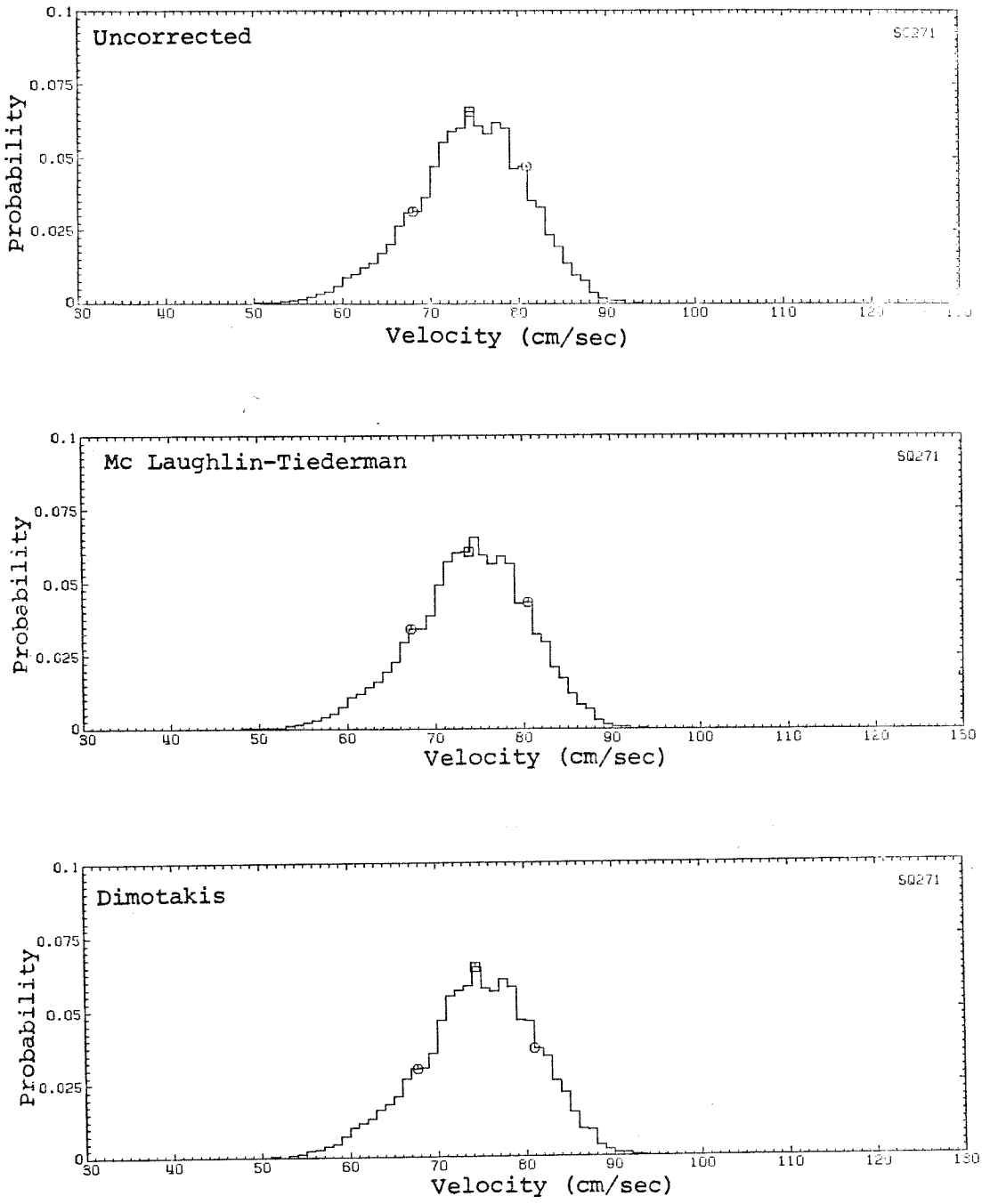

Figure 8.2.12.c Sample comparison of uncorrected and corrected fluid velocity probability density function, location 2.70

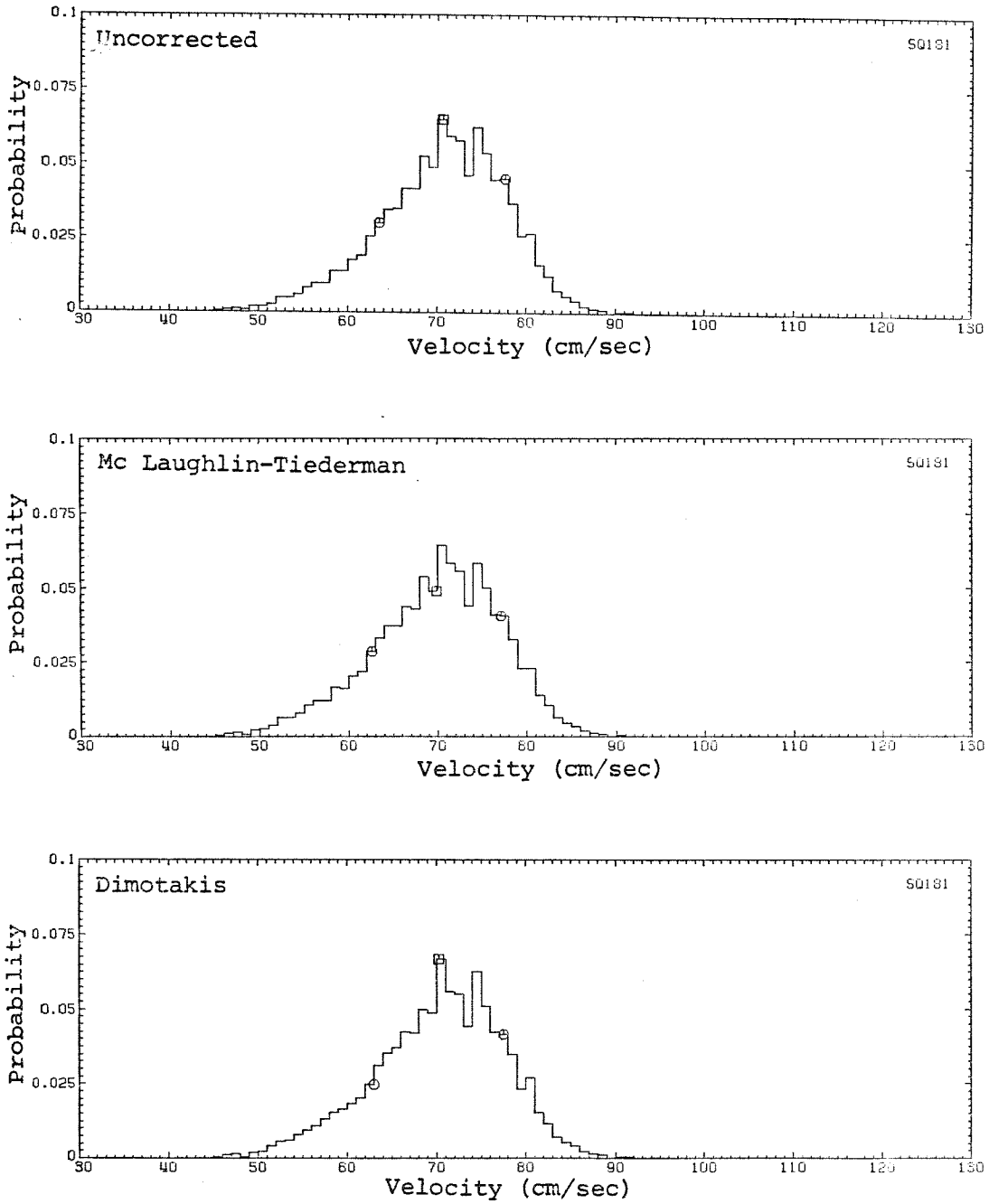

Figure 8.2.12.d Sample comparison of uncorrected and corrected fluid velocity probability density function, location 1.80

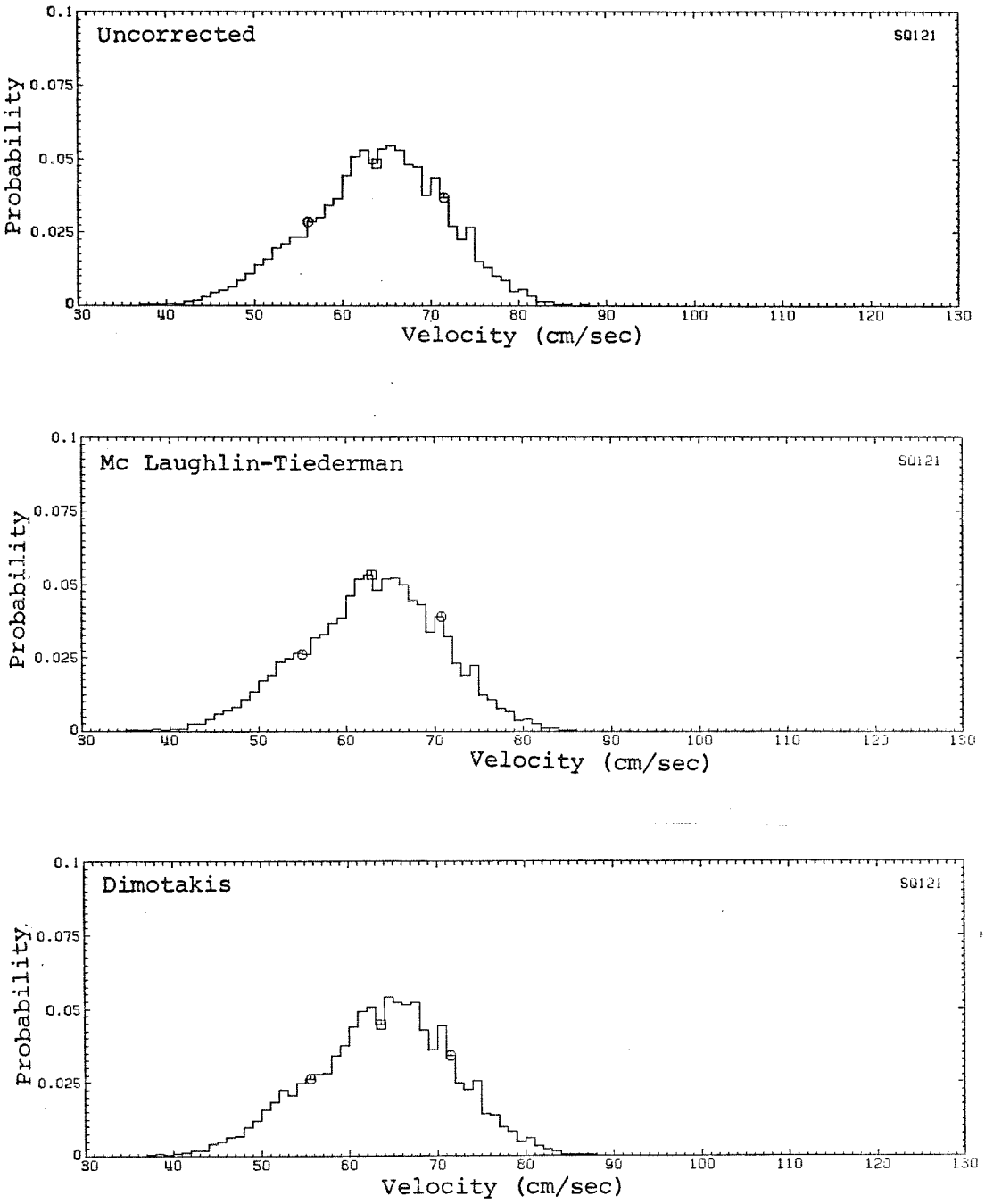

Figure 8.2.12.e Sample comparison of uncorrected and corrected fluid velocity probability density function, location 1.20

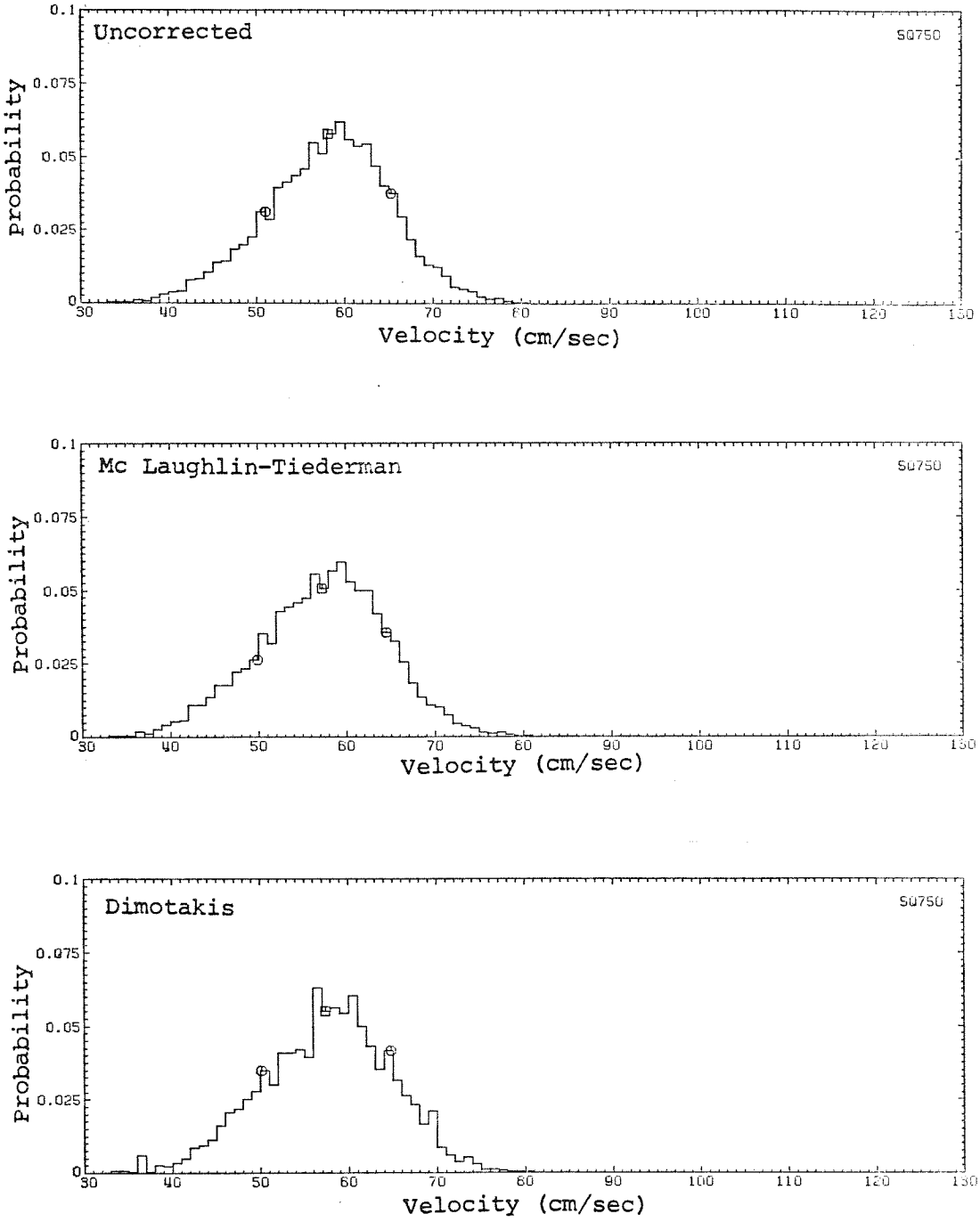

Figure 8.2.12.f Sample comparison of uncorrected and corrected fluid velocity probability density function, location 0.75

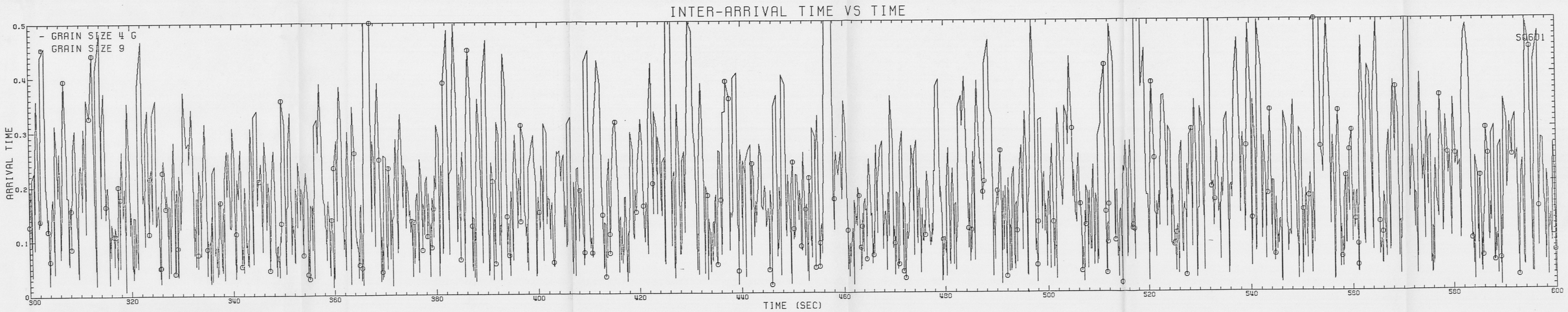

Figure 8.3.1 Sample sediment grain inter-arrival time data record, location 6.00

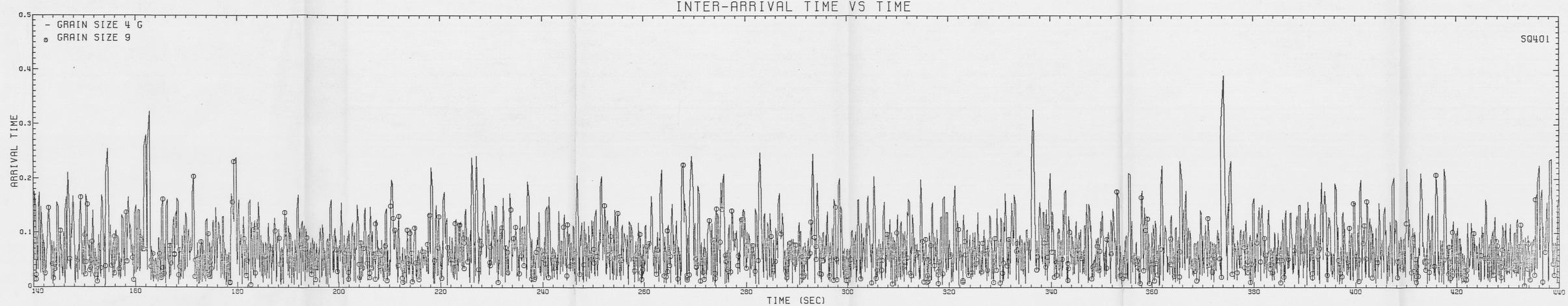

Figure 8.3.2 Sample sediment grain inter-arrival time data record, location 4.00

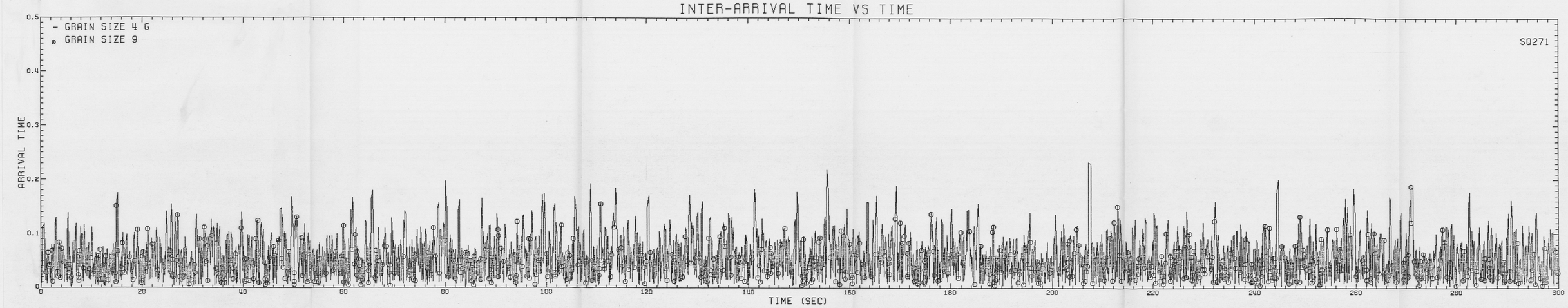

Figure 8.3.3 Sample sediment grain inter-arrival time data record, location 2.70

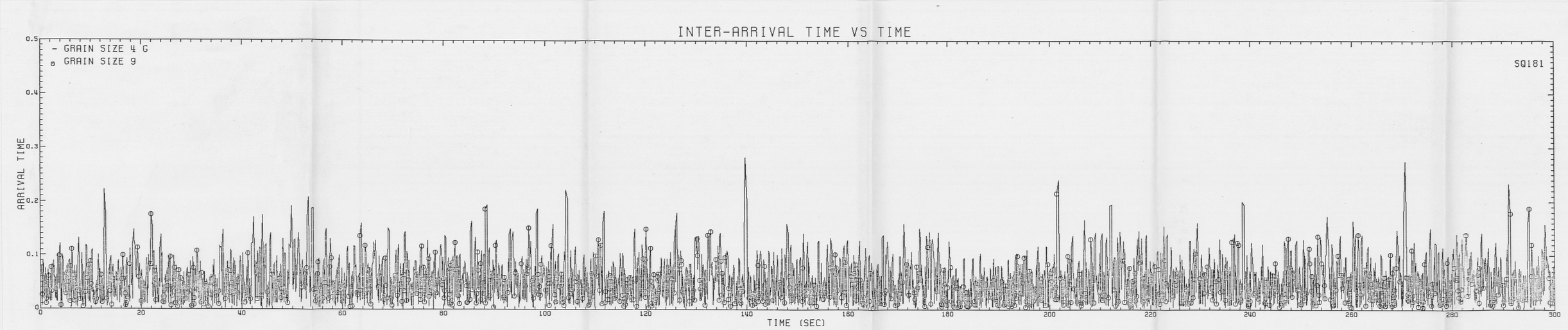

Figure 8.3.4 Sample sediment grain inter-arrival time data record, location 1.80

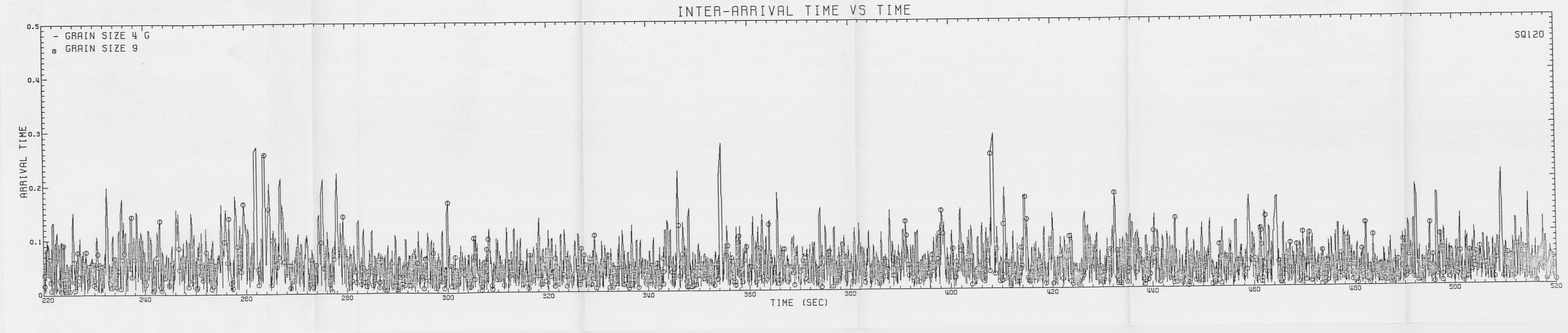

Figure 8.3.5 Sample sediment grain inter-arrival time data record, location 1.20

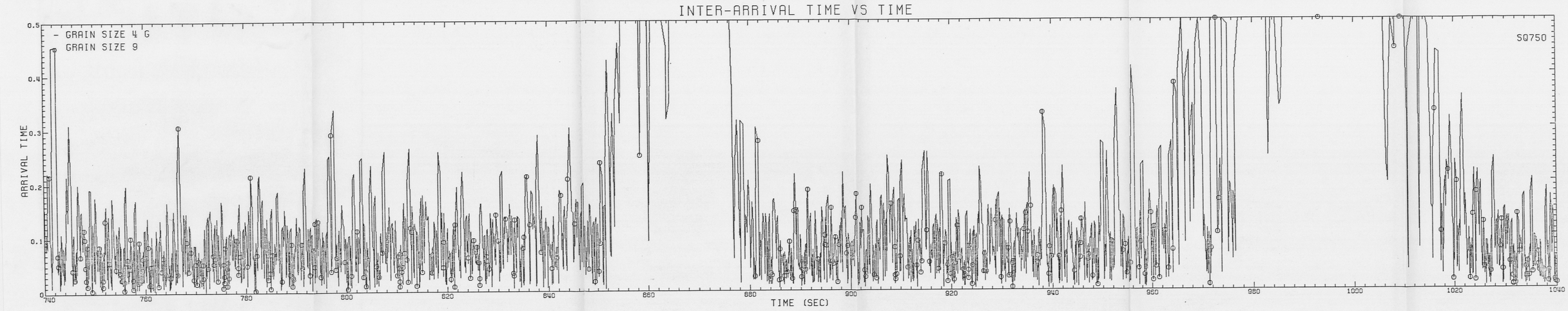

Figure 8.3.6 Sample sediment grain inter-arrival time data record, location 0.75

8.4 Measurements of sediment transport

Profiles of the mean sediment grain inter-arrival time, $\overline{\delta t_g}$, are shown in Figure 8.4.1 for size class 9 and size class 4 G. Some variations are noted in the different data records obtained at a single location. The inter-arrival time tends to decrease with proximity to the sediment bed, as the sediment grain inter-arrival time is inversely related to the sediment transport rate. Exceptions to this trend are noted in size class 4 G at location 1.80, in both size classes at location 0.75, and in size class 9 at location 1.20. No clear explanation for the observed value of $\overline{\delta t_g}$ in size class 4 G at location 1.80 is apparent.

The computed value of $\overline{\delta t_g}$ for location 0.75, appears to be anomalously high. As shown in Figure 8.1.6, the data record at this location contains periods in which no data events were collected. The gaps in the data record are associated with very long grain inter-arrival times as seen in Figure 8.3.6. The computed $\overline{\delta t_g}$ is biased by these long grain inter-arrival times. During the gaps, the actual sediment grain inter-arrival times are quite small; the laser beams are blocked by the sediment bed. A more representative value of $\overline{\delta t_g}$ may be computed by excluding those grain inter-arrival times caused by the record gaps. Determination of the true $\overline{\delta t_g}$ is not possible, however, as the number of sediment grains passing through the measurement volume during the gaps in the data record remains unknown.

In Figure 8.4.1.a, $\overline{\delta t_g}$ does not decrease from location 1.80 to location 1.20. Instead, a slight increase is observed. This may be caused by a decrease in the probability that a given sediment grain

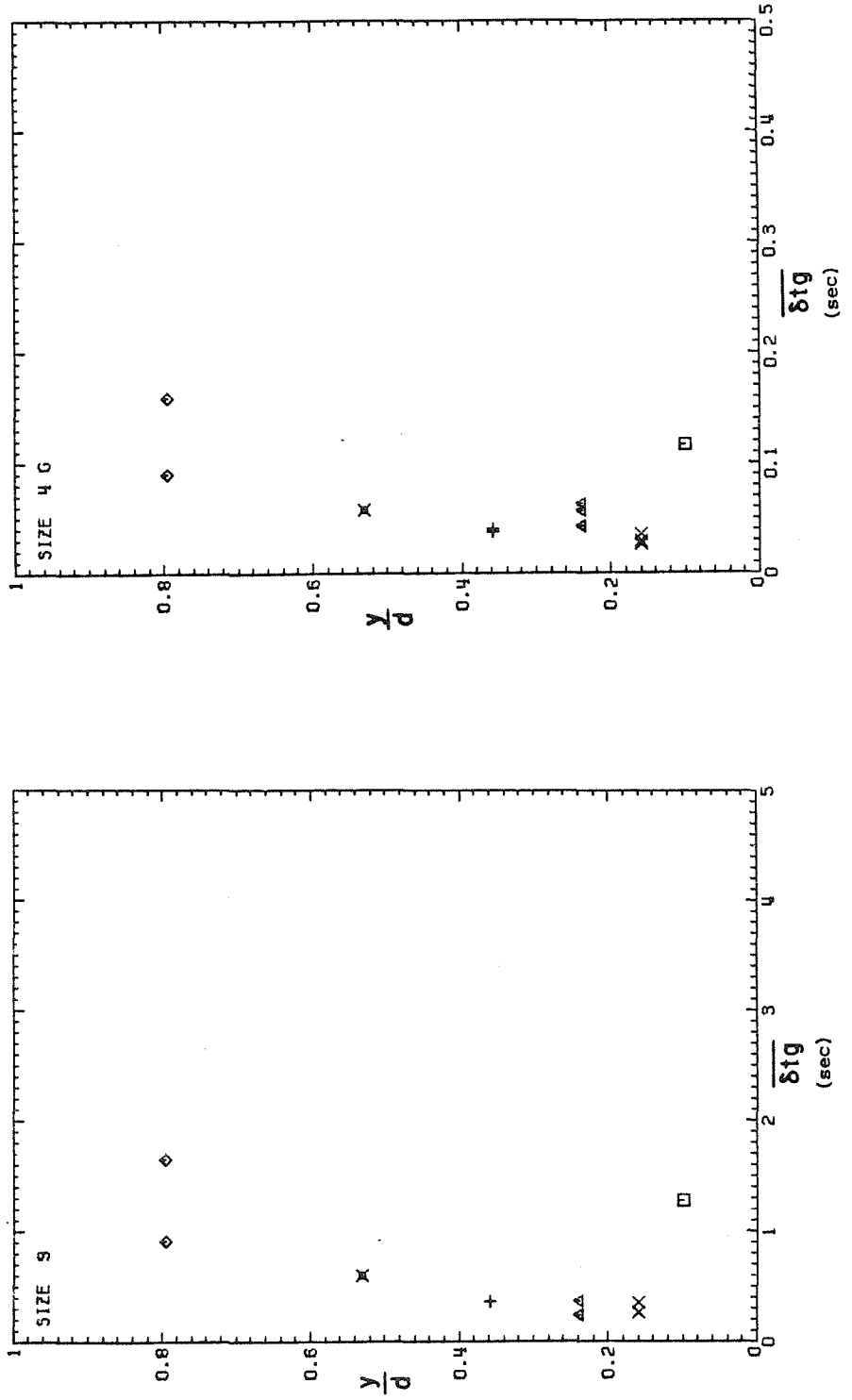

Figure 8.4.1 Profiles of mean sediment grain inter-arrival time

will generate a valid velocimetry data event. If the sediment transport rate becomes sufficiently high, multiple grains may simultaneously pass near the beam intersection volume. While the number of grains which pass through the volume increases, the number of grains which generate valid velocimetry events decreases. The time between good velocimetry events tends to increase.

Profiles of the standard deviation of the sediment grain inter-arrival times are shown in Figure 8.4.2. The mean and the standard deviation of the inter-arrival times are approximately equal. Examined on a granular scale, the fluctuations in the sediment transport are on the order of the mean sediment transport.

The mean sediment transport rate is compared to the mean sediment grain inter-arrival time in Figure 8.4.3. The transport rate, q_s, is computed as $\bar{u}\bar{c}$, where $\bar{u}$ is the mean fluid velocity and $\bar{c}$ is the local suspended sediment concentration as measured by suction tube sample. The range of the suction tube samples are indicated with error bars.

As discussed in Chapter 3, if at most one sediment grain passed through the beam intersection volume at any given instant, the velocimeter would be, effectively, a particle counter. The mean sediment transport rate would be inversely related to the mean sediment inter-arrival time by

$$q_s = \frac{m}{\overline{\delta t_g}\, dA} \qquad (8.4.1)$$

where m is the mean mass of the sediment grains and dA is the effective frontal area of the scattering volume. For size class 9, dA was

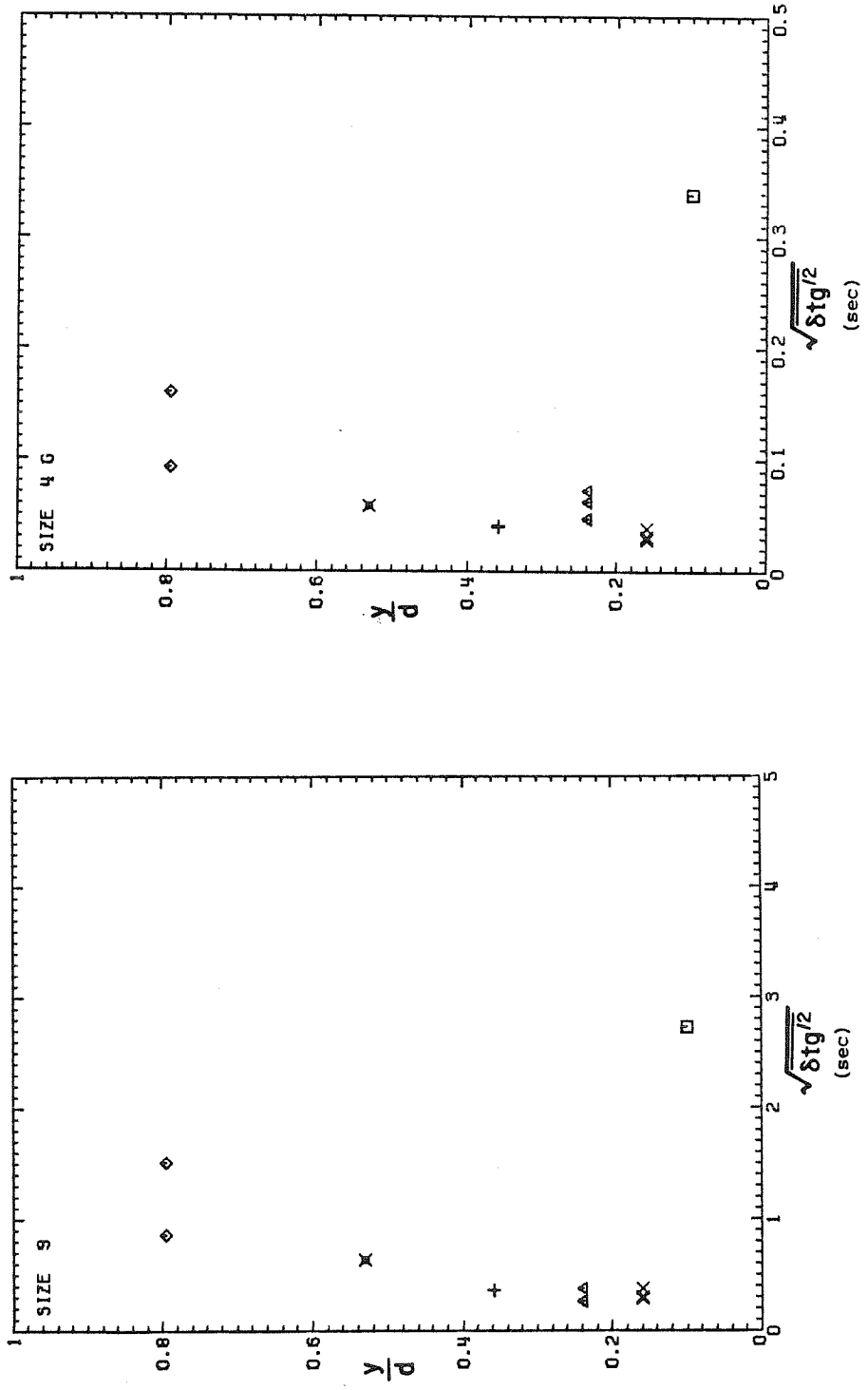

Figure 8.4.2 Profiles of sediment grain inter-arrival time standard deviation

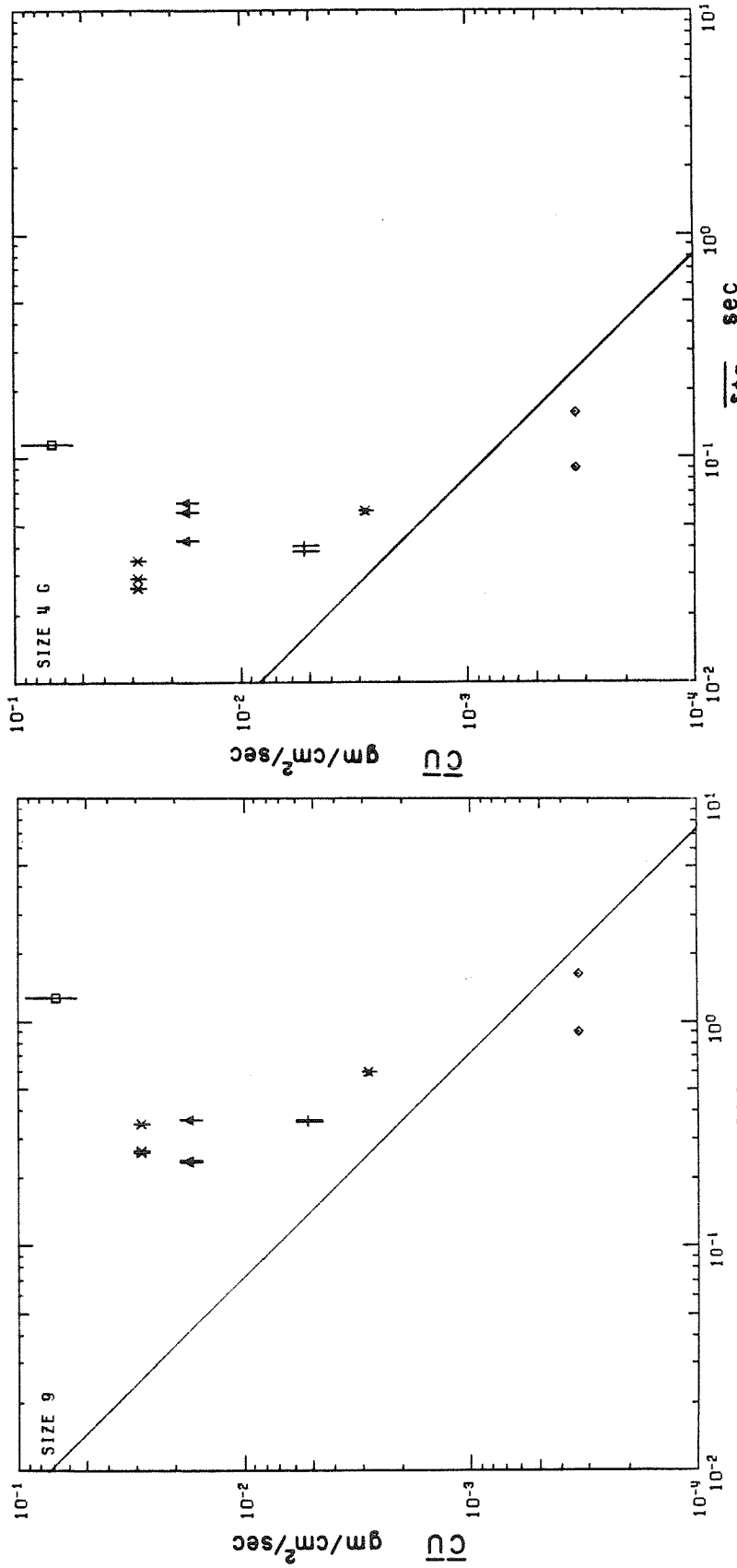

Figure 8.4.3 Comparison of mean sediment transport rate and mean sediment grain inter-arrival time

estimated to be 1.3 mm^2, based on the computed frontal area of the laser beam intersection volume and the sediment grain size. The area was estimated to be ten times larger for size class 4 G. The resulting estimated calibrations are plotted in Figure 8.4.3 with solid lines. Values near the water surface are in reasonable agreement with the crude estimated calibration. The values in the lower portion of the flow are in error by at least an order of magnitude. The sediment grain inter-arrival time is much too large, implying that the number of grains detected is much too small. The velocimeter is far from a simple particle counter.

Figure 8.4.4 gives the sediment grain inter-arrival time probability density functions for each data record. The mean inter-arrival time is indicated with a plotting symbol. The probability density functions are observed to be exponential in character. Little change in the probability density functions with elevation is noted in the lower portion of the flow. The velocimeter is failing to detect many, or even most, of the particles which pass through the beam intersection volume.

The simple lag correlation coefficients of the sediment grain inter-arrival times for two of the data records are shown in Figure 8.4.5. Similiar results were obtained for each of the remaining data records. Again, as discussed in Section 8.2, it was not possible to compute the true arrival time auto-correlation functions. While the sediment grain inter-arrival time data in the lower portion of the flow are not reliable due to the inability of the velocimeter to detect all sediment grains, the observations in the upper portion of the flow seem

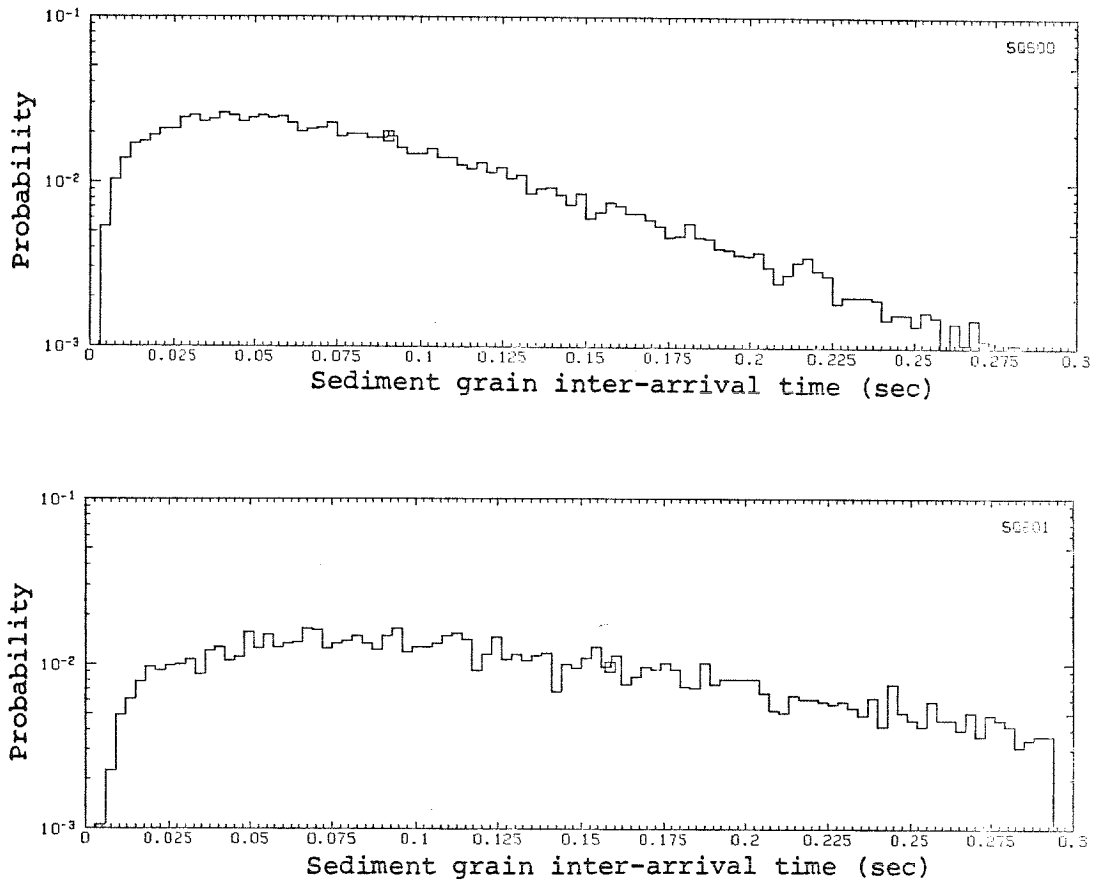

Figure 8.4.4.a Sediment grain inter-arrival time probability density functions, location 6.00

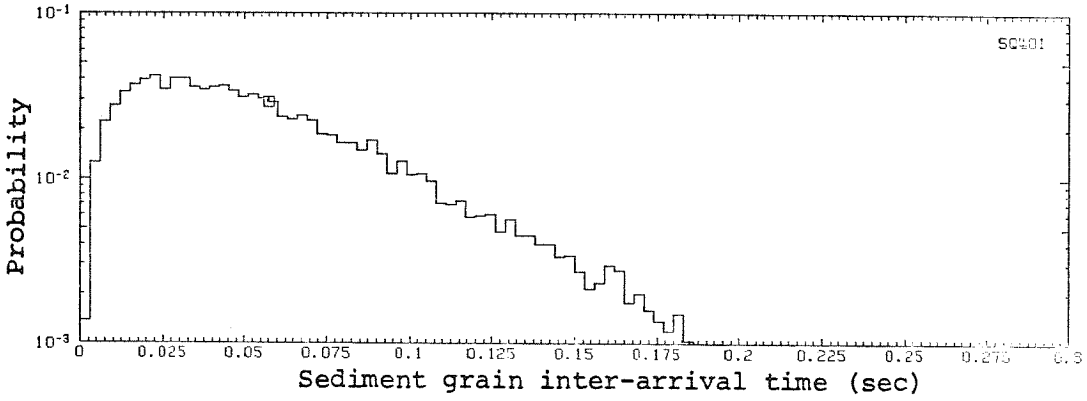

Figure 8.4.4.b Sediment grain inter-arrival time probability density function, location 4.00

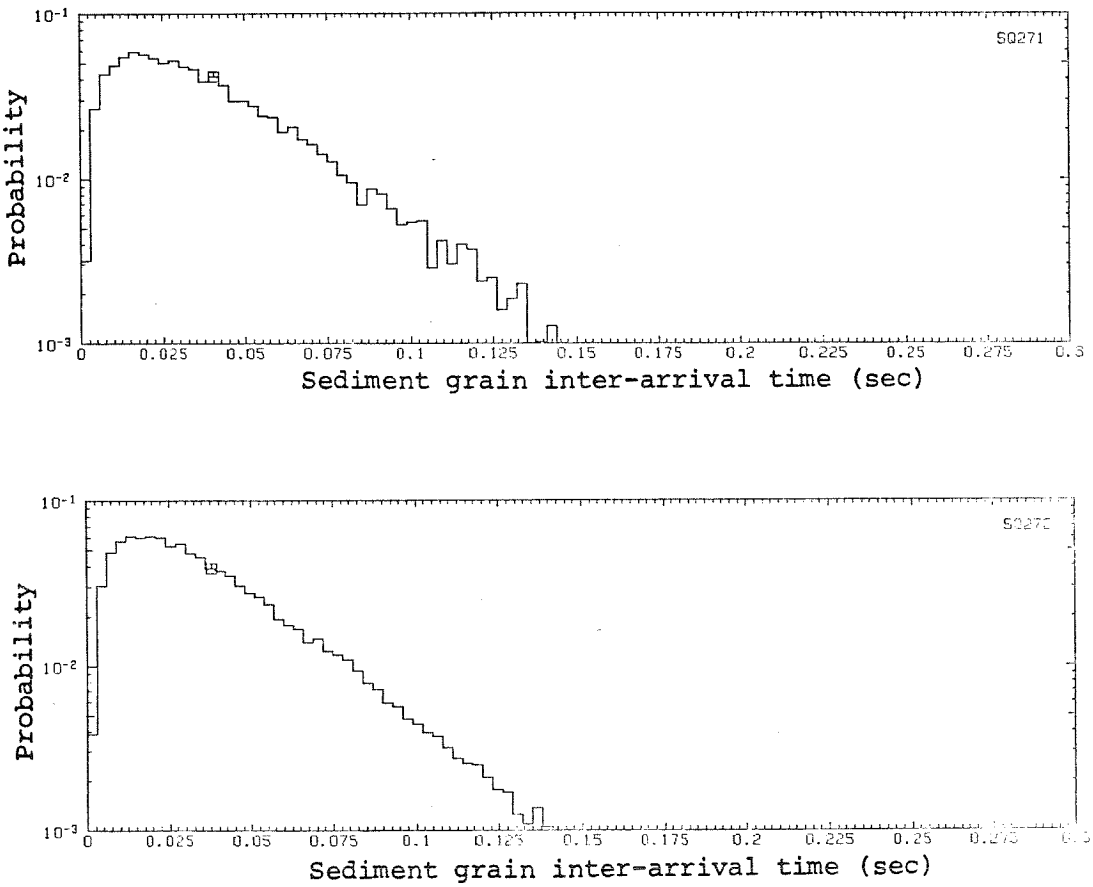

Figure 8.4.4.c Sediment grain inter-arrival time probability density functions, location 2.70

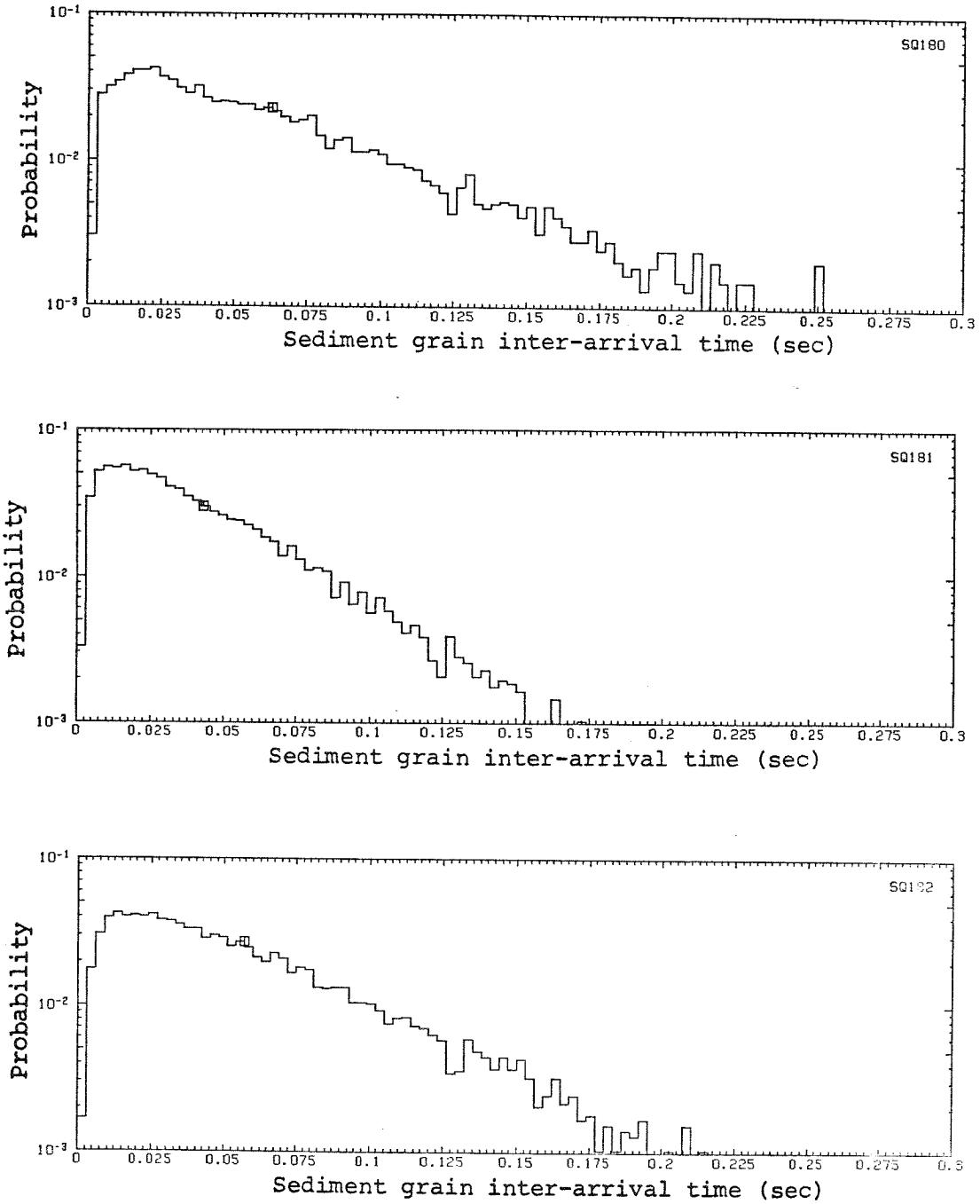

Figure 8.4.4.d Sediment grain inter-arrival time probability density functions, location 1.80

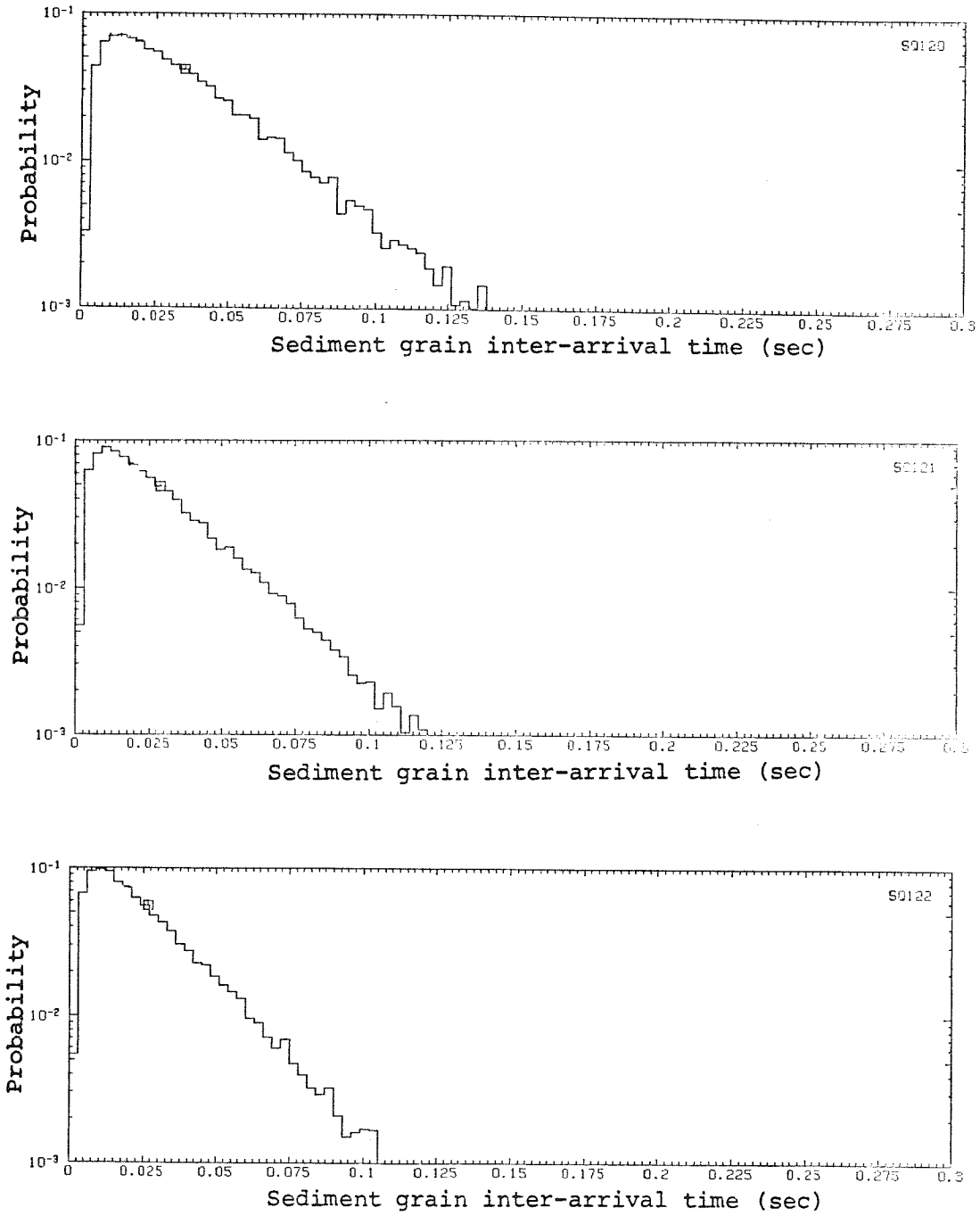

Figure 8.4.4.e Sediment grain inter-arrival time probability density functions, location 1.20

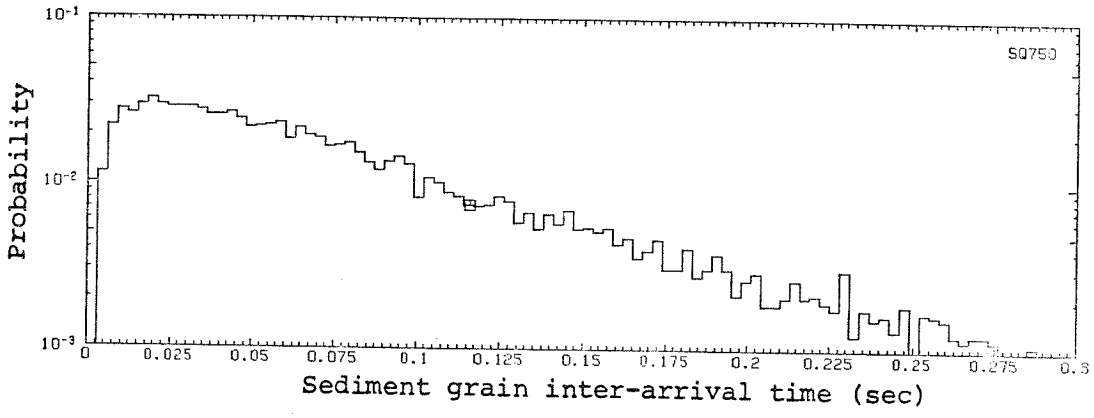

Figure 8.4.4.f Sediment grain inter-arrival time probability density function, location 0.75

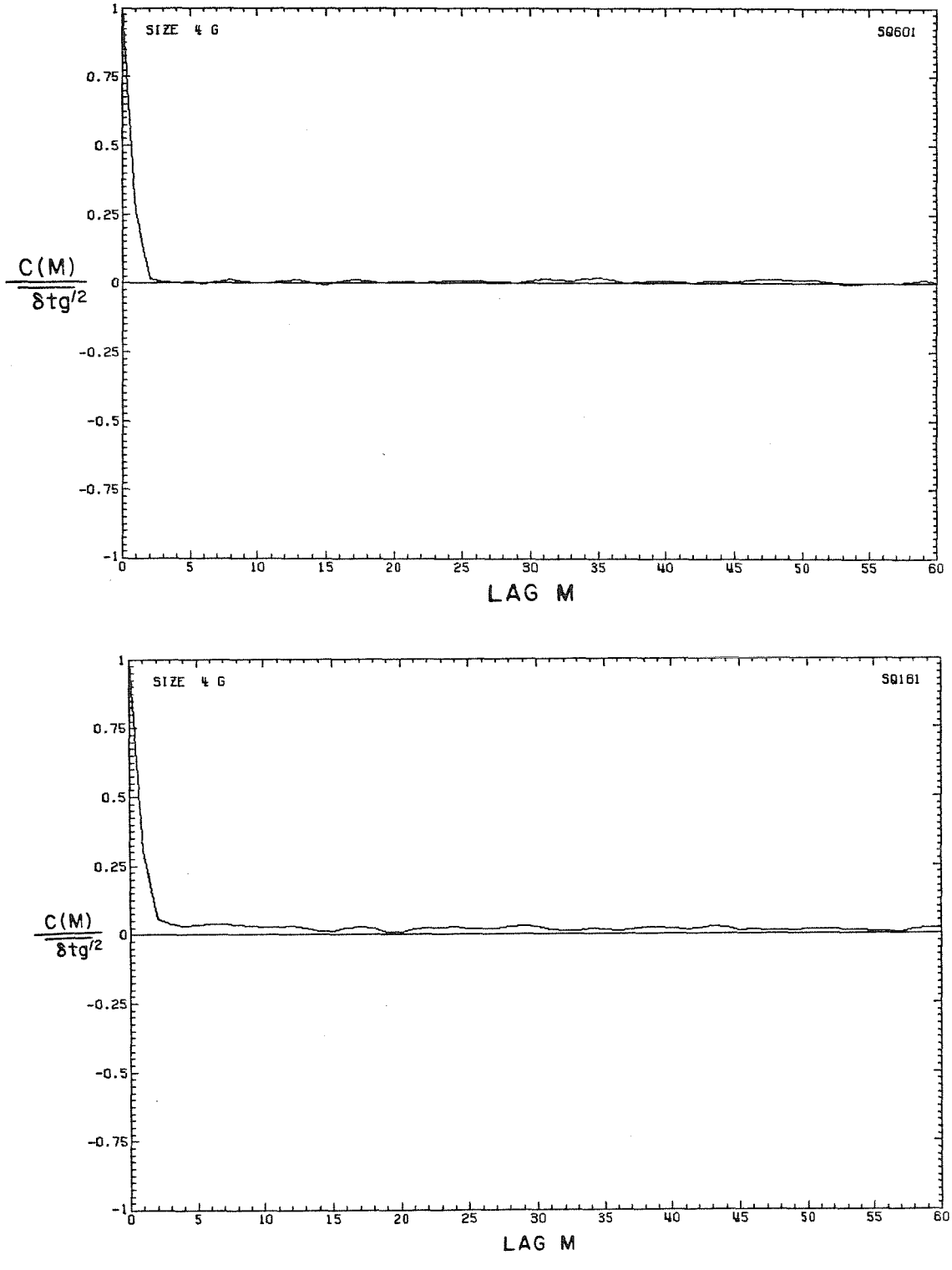

Figure 8.4.5 Sample simple lag correlation coefficients of sediment grain inter-arrival time fluctuations, locations 6.00 and 1.80

to be valid. Little or no correlation in the sediment grain inter-arrival times were observed. The passages of successive sediment grains through the measurement volume seem independent.

The normalized spectral estimate of the sediment grain inter-arrival time fluctuations and the relevant power spectral window function computed for one of the data records from location 6.00 are given in Figure 8.4.6. Theoretically, the power spectral estimate should reflect the contribution to the variance of the sediment grain inter-arrival times by the various time scales of the sediment movements. The power spectral window function should reflect the contributions to the mean sediment grain inter-arrival time. Again, however, the computed spectra are most likely dominated by computational errors. Physical interpretation of the spectra cannot be made with any degree of confidence.

No cross-correlations of fluid velocity and sediment grain velocity and inter-arrival time characteristics were computed with the data acquired in this study. Nor were any computations of the sediment grain slip velocity, defined by Equation 3.1.4, or any selective sampling of the fluid velocity data record based on chosen sediment transport characteristics performed. Such calculations require that the time between the measurement of the sediment grain velocity and the velocity of the associated fluid be small with respect to the turbulence time scale. The data records used in this study did not always have such time resolution. The time between the detection of a sediment grain and the closest fluid velocity realization was often larger than the turbulence time scale, estimated at approximately

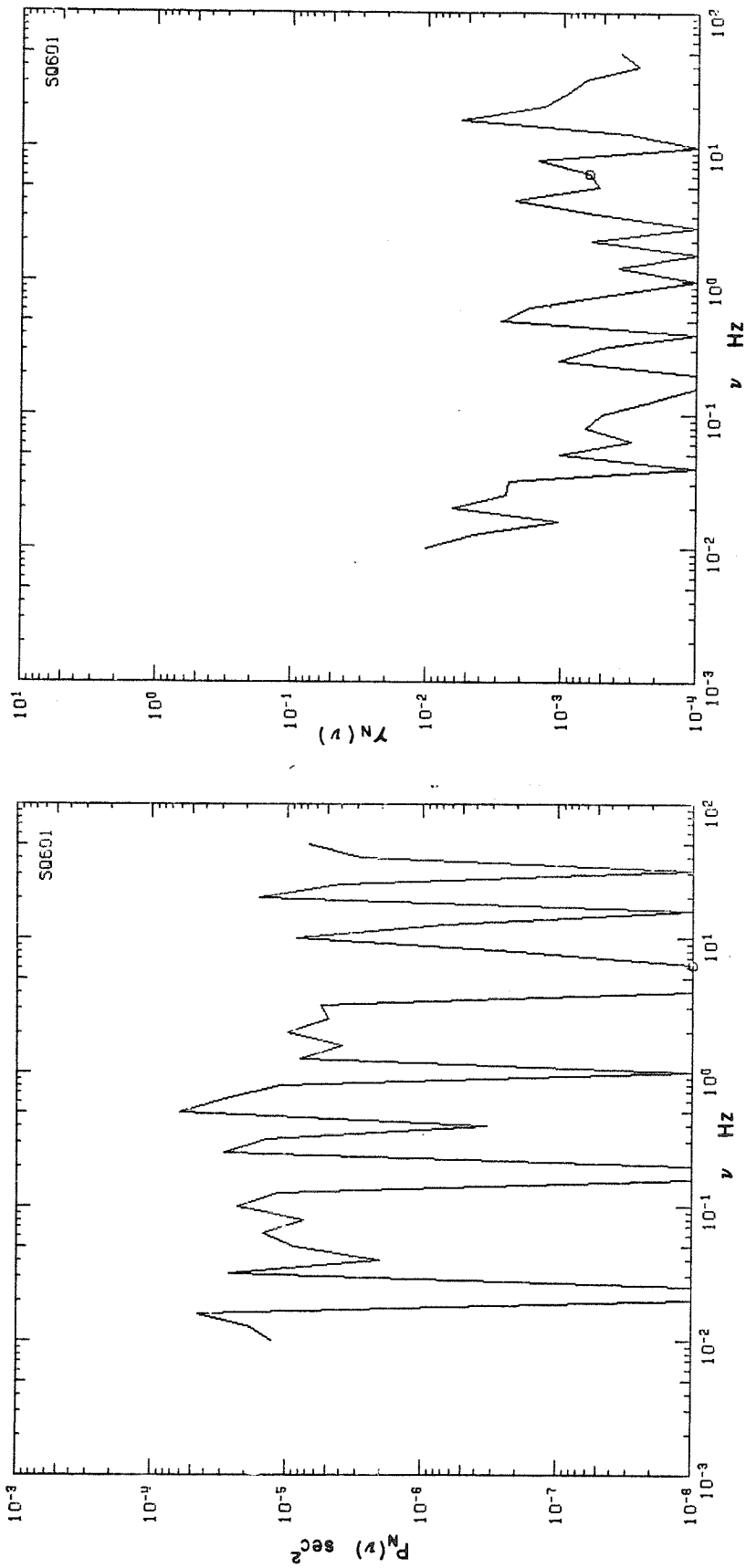

Figure 8.4.6 Sample sediment grain inter-arrival time fluctuation power spectral estimates and power spectral window functions, location 6.00

10 msec.

8.5 Summary

This chapter has presented the one-dimensional velocimetry data obtained in this study. Examples of the validated data records were given. The difficulties encountered in the computation of auto-correlations and power spectral estimates were discussed. The velocimeter was observed to be far from a simple grain counter. Further discussion of these results and suggestions for further work indicated by these results are given in the remaining chapters.

CHAPTER 9

DISCUSSION OF THE RESULTS

The results presented in Chapter 8 are discussed here. The applicability of the laser-Doppler technique for velocimetry to sediment-laden flows is assessed. The difficulties encountered in this study are reviewed. The implications of the data obtained are then examined for new insights into the mechanics of sediment suspension and entrainment. Specific suggestions for further research are given.

9.1 Discussion of the application of laser-Doppler velocimetry in sediment-laden flows

The advantages of the laser-Doppler velocimetry technique for use in sediment-laden flows were apparent prior to this study; certain disadvantages and uncertainties only became known during the research. This section details the discovered difficulties with the technique, evaluates their relative importance, and suggests improvements for subsequent applications of the technique to sediment-laden flows.

The first difficulty encountered in this study is the long length of record required for the investigation of fluid turbulence in sediment-laden flows. Such investigations require the acquisition and subsequent processing of a relatively large quantity of experimental data. This is due to the disparity between the time scales of the fine scale fluid turbulence and those of the sediment bed motions. To characterize accurately all of the time scales present, the flow velocity must be sampled at a relatively rapid rate, on the order of 100 Hz, for a relatively long observation period, at least greater than 10 minutes, at each measurement location. The quantity of data

required is, therefore, quite large with repect to that of previous investigations of sediment-laden flows or studies of turbulence in homogeneous fluid flows with fixed boundaries. For the small, preliminary experiment presented in this study over two million velocimetry events were recorded, even though the observation periods (5 to 20 minutes) were still too short to resolve fully the very slow transients in the sediment motion. The subsequent analysis of such an amount of data consumes both computer and human time.

The second difficulty encountered, also inherent in the investigation of fluid turbulence in sediment-laden flows, is gradual shifting of the sediment bed level, even in the nominally flat bed regime. Since the measurement location is fixed in space, the distance above the bed varies as the bed elevation changes, causing difficulties with the physical interpretation of the collected data. The understanding of the fine scale motions of a sediment-laden flow requires the appreciation of the larger scale features also.

The major difficulty encountered in this study is the possible conditional sampling of the flow velocity and is directly attributable to the laser-Doppler technique. The validated velocimetry events may be a conditionally selected subset of the recorded velocimetry events, which are, in turn, a conditionally selected subset of all possible velocimetry events. The resulting velocimetry data record is, possibly, biased in an unknown manner.

A velocimetry event is not validated if its Doppler burst signal does not remain regular in frequency during the time required to determine the Doppler burst frequency. Most probably, an irregular

Doppler burst signal is either the result of noise in the signal processing electronics or generated by multiple scattering particles passing simultaneously through or sufficiently near to the laser beam intersection volume. The primary source of electronic noise in apparatus employed in this study is the statistical quantum noise of the photodetector. While such noise may cause the loss of data, no biasing of the recorded data record will result. Biasing can, however, result from simultaneous scattering by multiple particles.

There is a particularly high occurrence of light scattering by multiple particles in the vicinity of the beam intersection volume in a sediment-laden fluid flow. The particle number density of the small fluid tracer particles is difficult to regulate and increases during the course of an experiment. The concentration of sediment grains is determined by the flow conditions; furthermore, a sediment grain need only graze the beam intersection volume to scatter sufficient light to mask that scattered by a particle passing directly through the volume. In this study, well over half of the recorded data events were not valid events. It is not possible to estimate the number of generated Doppler burst signals which were not recorded.

Simultaneous scattering by multiple particles is most likely to occur when the fluid flux is high and/or the sediment transport rate is high. In either case, the flux of scattering particles through the beam intersection region is relatively high. The velocimetry events generated in these instants are more likely to be invalid than those generated at other times. The validated velocimetry data record will tend to exclude the periods in which the sediment transport rate is

relatively high.

It is not possible to estimate accurately the relative importance of the two sources of invalid velocimetry events with the data obtained in this study. Further research in this direction is clearly required. The inherent noise in the photodetector was relatively high in the velocimeter employed in this study due to low incident light intensity and low light scattering efficiency resulting from the large beam intersection angle. Thus, the shot noise could be reduced by an increase in the laser light intensity. The detection of light scattered by sand grains passing near the beam intersection volume might be decreased by alterations to the receiving optical system to reduce the effective depth of field. Increased incident light intensity will allow the decrease of the solid collection angle. A smaller pinhole and other additional appertures between the collecting lens and the photodetector should be tried once again with the increased light scattered from more intense laser beams.

Given the possibility that the velocimetry data in sediment-laden flows may be conditionally sampled, the application of any bias correction procedure to the data does not seem warranted. Such correction procedures assume that the observed velocity is biased by the proportionately larger number of measurements generated by fluid tracer particles associated with fast-moving fluid parcels. In sediment-laden flows, the observed velocity may well be biased by the relative lack of those measurements. The corrected velocity may be more in error than the uncorrected velocity. Furthermore, as seen in Figures 8.2.11 and 8.2.12, the usual correction procedures have

relatively little impact on the observed velocimetry data. The application of a bias correction procedure to velocimetry data from a sediment-laden flow gives the impression of improved accuracy, without guarantee of any such improvement.

The velocimeter employed in this study is not an accurate sediment grain counter. As discussed in Section 8.4, the local mean sediment transport rate cannot be accurately estimated from the mean sediment grain inter-arrival time. Near the bed, the sediment transport rate estimated from the velocimeter measurements is one to three orders of magnitude lower than the transport rate as measured by suction sampling tube. Only a very small subset of the number of sediment grains which pass through the measurement volume during the period of data acquisition are counted by the velocimeter. The discrepancy between the estimated and the observed sediment transport rate may be attributed to two factors: the assumption that all of the recorded velocimetry events were generated by individual sediment grains and the rejection of Doppler burst signals which are highly irregular in frequency by the counter-processor. The first factor could account for a discrepancy of no more than a factor of two or three in the estimated and observed transport rates. The discrepancy is sufficiently large, see Figure 8.4.3, to imply that the data record is missing most of the sediment grains which actually passed through the measurement volume. Not all sediment grains which pass through the scattering volume are both detected by the counter-processor and reported to the mini-computer.

The development of the laser-Doppler technique for application to sediment-laden flows is still in the experimental phase. The simple system developed for this study may be greatly improved. The technique will never be without its particular disadvantages; however, no other approach currently holds as much promise for the measurement of the fine scale structure of sediment-laden flows.

9.2 Discussion of the mechanisms of sediment entrainment and suspension

Longitudinal velocity measurements alone are not sufficient to describe adequately even a two-dimensional fluid flow field. Measurements of the vertical motions are also necessary. Thus, the one-dimensional velocimetry results presented here can yield only limited insights into the mechanics of sediment suspension and entrainment. Nonetheless, the data do give some first glimpses into the time-varying nature of sediment-laden flows.

The observed longitudinal turbulence intensity, $\sqrt{\overline{u'^2}}$, does not differ significantly from measurements in clear water by previous investigators. In a clear water flow over a smooth boundary, Raichlen (1967) noted a steady increase in the relative longitudinal turbulence intensity, $\sqrt{\overline{u'^2}}/\overline{u}$, from a minimum of approximately 3.8% at y/d=0.8 to approximately 10% at y/d=0.16. Blinco and Partheniades (1971) report similiar values near the water surface, but a value of approximately 12% at y/d=0.14. The measurements obtained in this study, as illustrated in Figure 8.2.3, are seen to increase from values of nearly 6.4% at y/d=0.8 to values of approximately 12.6% at y/d=0.16. The data from these studies and the present study are drawn in Figure

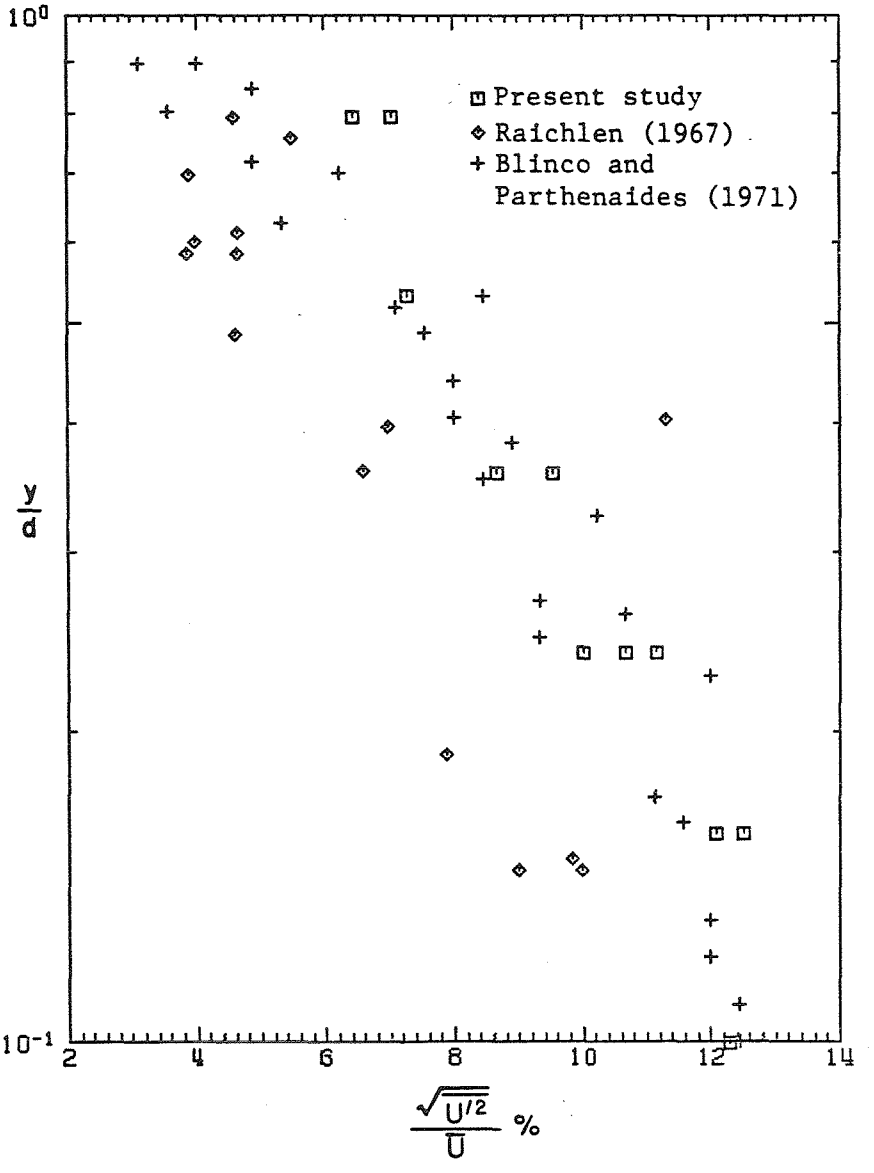

Figure 9.2.1 Comparison of longitudinal turbulence measurements

9.2.1. Since the fluid velocity fluctuations observed in this study are on the order of those observed in clear fluid flows, the presence of suspended sediment in the flow does not appreciably alter the longitudinal intensity of the fluid turbulence.

The longitudinal velocity of the sediment grains tends to be approximately 5 per cent less than that of the fluid in the lower half of the flow field. The variance of the sediment grain velocity is notably smaller than the variance of the fluid velocity. Near the water surface, the situation is reversed. The mean sediment grain velocity is greater than that of the fluid and the variance of the sediment grain velocity is significantly larger. To explain these observations, more experimental data are required. First, simultaneous vertical velocity measurements are essential. Second, data records should have sufficient time resolution or sampling frequency, to allow the cross-correlation or selected sampling of the velocities of the sediment grains and the closely surrounding fluid.

The sediment grain inter-arrival time data obtained in this study are not sufficiently reliable to yield much insight into the mechanics of sediment transport. Some of the recorded grain velocimetry events are caused by multiple grains passing simultaneously through the volume; hence, some fraction of the grain velocimetry events are not recorded. The grain inter-arrival data are only possibly valid in the upper portion of the flow (at locations 6.00 and 4.00). At these locations, as seen in Figure 8.4.3, the sediment transport rate as estimated from the mean sediment grain inter-arrival time is on the order of the mean sediment transport rate determined by suction sampling tube.

The sediment grain inter-arrival time data at these two upper locations do exhibit some interesting characteristics. The mean sediment grain inter-arrival time is approximately equal to the standard deviation. The probability density functions of the grain inter-arrival times are exponential in nature. The logarithm of the probability of a given grain inter-arrival time decays linearly with the grain inter-arrival time. Modeling the passage of successive sediment grains through the measurement volume as a Poisson process seems to be promising.

The ability to measure the motions of individual sediment grains forces thinking about the transport of sediment on the granular scale. Two-dimensional velocimetry measurements are required to begin to unravel the phenomena of sediment entrainment and suspension. The data of this study can only demonstrate the type of fluctuations which must be further investigated.

9.3 Suggestions for future work

This study is among the first attempts to apply the laser-Doppler velocimetry technique to two-phase flows. Furthermore, an attempt was made to obtain the time histories of the velocity measurements. The data reported here form one of very few sets of direct measurements of the small-scale characteristics of a fluid flow transporting relatively dense solid particles. Again, this work is only the preliminary portion of an ongoing research program.

The most pressing need in regard to the technique is an understanding of the causes of the invalid velocimetry events. Over

half of the recorded data events were not valid events. Both sediment grain and fluid velocimetry events were discarded. Invalid data events were present not only in the data records from locations near the sediment bed, where the sediment concentration is large, but also in data records from near the water surface. Following are four suggestions of further research to address this problem.

First, a more powerful laser should be used. Increasing the incident light intensity by increasing the laser power used should reduce any noise due to the photodetector and the first stage of the signal amplification electronics. Increased incident light intensity will also permit modifications to the receiving optics to reduce the optical depth of field. In other words, the detection of light scattered by particles passing through the laser beams outside of the beam intersection volume could be reduced. A smaller collection solid angle, additional and smaller apertures, and placing the axis of the receiving optical train at some angle to the transmitted laser beams should be tried. Unfortunately, such alterations must be done by trial and error.

Second, the band-pass filtered Doppler burst signal and the associated pedestal signal should be digitized directly and examined. The characteristics of the burst signal could then be quantitatively determined. The irregularity in the Doppler burst signal could be explicitly measured. Any correlation between pedestal amplitude and signal irregularity would be exposed. Simultaneous monitoring of the developed counter-processor would determine the relative number and characteristics of the incoming burst signals which are discarded by

the processor. Since the Doppler frequency is of the order of 500 KHz to ensure reasonable resolution of the burst signal, digitization at a rate of approximately 5 MHz would be desirable. Because of the acquisition rate and the quantity of the resulting data, disjoint portions of the incoming signal must be digitized at successive time intervals.

Third, an independent method of detecting the presence of sediment grains in the vicinity of the velocimetry measurement volume should be tried. Knowledge of the exact number of sediment grains scattering light at any given instant would allow an accurate determination of the local sediment transport rate. Independent measurements of both the velocimetry data and the local transport rate would determine if invalid velocimetry events are more often generated during instants of relatively high sediment transport. The nature of any biasing in the velocimetry data could be appreciated.

Lastly, the developed velocimeter should be applied to a less complex flow. Elimination of the movable sediment bed would allow some experimental control over the local sediment transport rate. The fluid could be seeded with sediment grains until the desired transport rate was achieved. The performance of the velocimeter at different local rates of sediment transport could be evaluated.

It is important to stress, however, that better understanding of the laser velocimetry technique applied to sediment-laden flows is primarily to allow the acquisition of better velocimetry data in such flows. Better velocimetry data, in turn, will allow better insights into the mechanics of sediment entrainment and suspension. Despite all

of the uncertainties with the technique as noted in this study, the implementation of a two-dimensional velocimeter for use in sediment-laden flows over movable sand beds is overwhelmingly recommended. Vertical velocity data are required to begin to understand the fundamental mechanics of sediment-laden flows. While the data acquired with a laser-Doppler velocimeter may be biased in an unknown manner, the observations can be made.

CHAPTER 10

SUMMARY

The basic laser-doppler velocimetry technique was adapted for use in sediment-laden flows. The developed instrumentation was employed to make one-dimensional, instantaneous measurements of both fluid and sediment grain velocity throughout the water column in such a flow. This work is the foundation of an ongoing program of experimental observations of the fine-scale, time-varying nature of sediment-laden flows.

This study has yielded information on three facets of the continuing effort. These aspects are: (1) the feasibility of laser-Doppler velocimetry in sediment-laden flows; (2) the inherent difficulties in direct experimental investigations of the mechanisms of sediment suspension and entrainment; and (3) the character of the interactions between the fluid turbulence and the motions of individual sediment grains.

10.1 Feasibility of laser-Doppler velocimetry in sediment-laden flows

Laser-Doppler velocimetry is particularly attractive for use in sediment-laden flows. No calibration is required and the flow field is not deformed in any way. The technique allows the measurement of the fluid velocity, the occurrence of individual sediment grains, and the velocity of those individual sediment grains. However, the resulting velocimetry data may be biased in some unknown manner; a large fraction of the measurements must be discarded due to the simultaneous light scattering by multiple sediment grains and fluid

particles. The resulting fluid velocity measurements may be biased in a manner different from the recognized bias inherent in the technique when applied to clear fluid flows. The sediment grain velocity data may also be biased. Also, the velocimeter is not a reliable particle counter, except possibly in the upper portions of the flow. The severity of these difficulties cannot be determined with the data obtained in this study. Even in light of these disadvantages, no other technique currently available allows such direct, instantaneous measurements.

10.2 Inherent difficulties in direct experimental investigations of the mechanisms of sediment suspension and entrainment

Since this study is among the first to measure directly the fine-scale motions of sediment-laden flows, it has pinpointed two difficulties inherent in such studies. First, the quantity of data required to describe adequately all of the processes present in the flow is quite large. The time scales of the flow range from the small-scale, relatively rapid fluctuations of the fluid turbulence to the long-scale, slowly varying changes in the sediment bed forms. Second, the subsequent physical interpretation of any data is complicated by the movements of the sediment bed. These problems are due to the complex nature of sediment-laden flows and are independent of the instrumentation used to observe the flow variables. Obtaining and interpreting measurements of the time-dependent characteristics of the interactions between the flowing fluid, the transported sediment and the accompanying motions of the sediment will always be difficult.

10.3 Interactions between fluid turbulence and the motions of individual sediment grains

Despite the various difficulties, the data obtained in this study do give insights into the mechanics of the suspension and entrainment of sediment. The values of $\sqrt{u'^2}$ determined for the sediment-laden flow observed in this study are on the order of those reported by previous investigators in clear fluid flows. The mean and standard deviation of the sediment grain velocity were observed to be less than those of the fluid velocity in the lower portion of the flow, but relatively greater near the water surface.

The data also demonstrates the shortcomings of the continuum approach to the mechanics of the suspension of sediment. A new conceptual model is required. The suspended load equation leads to an estimate of the vertical distribution of the mean concentration of suspended sediment for engineering purposes. It does not accurately reflect the mechanics of sediment suspension. The length, or time, scales of the fluid turbulence are much less than the length, or time, scales of the number of grains necessary to define the mean sediment concentration or its fluctuation. Computation of the term $\overline{v'c'}$ requires the correlation of two processes of widely disparate scale. Sediment suspension and entrainment should be explored on a granular scale.

In the upper portion of the flow, where the velocimeter apparently acts as a grain counter, the probability density functions of the recorded sediment grain inter-arrival times (the times between the detection of successive sediment grains) were observed to be

negative exponentials. The transport of sediment might be approached on a granular scale by modeling the sediment grain arrival as a Poisson process.

Direct observations of the turbulent structure of the fluid and the motions of the suspended sediment grains will contribute much to the knowledge of the small-scale, time-fluctuating characteristics of sediment-laden flows. Quantitative measurement may yield only qualitative insights into the complex phenomena of sediment suspension and entrainment. The instrumentation implemented in this study should be expanded to give two-dimensional velocimetry data and improved as a sediment grain counter.

REFERENCES

Bagnold, R. A., Experiments on a gravity free dispersion of large spheres in a Newtonian fluid under shear, Proceedings of the Royal Society of London, Series A, vol. 225, 1954, p. 49-70.

Blinco, P. H. and E. Partheniades, Turbulence characteristics in free surface flows over smooth and rough boundaries, Journal of Hydraulic Research, vol. 9, no. 1, 1971, p. 43-71.

Bohlen, W. F., Hot-wire anemometry study of turbulence in open-channel flows transporting neutrally buoyant particles, Report 69-1, Experimental Sedimentology Laboratory, Massachusetts Institute of Technology, Cambridge, Massachusetts, 1969.

Brooks, N. H., Laboratory studies of the mechanics of streams flowing over a movable bed of fine sand. Thesis presented to the California Institute of Technology, at Pasadena, California, in partial fulfillment of the requirements for the degree of Doctor of Philosophy, 1954.

Daily, J. W. and T. K. Chu, Rigid particle suspensions in turbulent shear flow: some concentration effects, Report Number 48, Hydrodynamics Laboratory, Massachusetts Institute of Technology, Cambridge, Massachusetts, 1961.

Daily, J. W. and R. L. Hardison, Rigid particle suspensions in turbulent shear flow: measurement of total-head, velocity and turbulence with impact tubes, Report Number 67, Hydrodynamics Laboratory, Massachusetts Institute of Technology, Cambridge, Massachusetts, 1964.

Daily, J. W. and P. Roberts, Rigid particle suspensions in turbulent shear flow: size effects with spherical particles, Report Number 69, Hydrodynamics Laboratory, Massachusetts Institute of Technology, Cambridge, Massachusetts, 1966.

Deeming, T. J., Fourier analysis with unequally-spaced data, Astrophysics and Space Science, vol. 36, 1975, p. 137-158.

Dimotakis, P. D., Single scattering particle laser-Doppler measurements of turbulence, AGARD Symposium on the Applications of Non-Intrusive Instrumentation in Fluid Flow Research, Saint-Louis, France, Paper Number 10, 1976.

Durst, F., A. Melling, and J. H. Whitelaw, Principles and Practice of Laser-Doppler Anemometry, Academic Press, New York, New York, 1976.

Durst, F., Studies of particle motion by laser-Doppler techniques, Proceedings of the Dynamic Flow Conference, I.M.S.T., Marseille,

France, September 11-14, and Johns Hopkins University, Baltimore, Maryland, September 18-21, 1978, p. 345-372.

Einstein, H. A. and N. Chein, Second approximation to the solution of the suspended load theory, Series 47, Issue 2, Institute of Engineering Research, University of California, Berkeley, California, January 31, 1952.

Einstein, H. A. and N. Chein, Effects of heavy sediment concentration near the bed on velocity and sediment distribution, MRD Series 8, University of California, Institute of Engineering Research and the United States Army Corps of Engineers, Omaha, Nebraska, August 1955.

Einstein, H. A. and H. Li, The viscous sublayer along a smooth boundary, Transactions, ASCE, vol. 123, paper 2992, 1958, p. 293-313.

Elata, C. and A. T. Ippen, The dynamics of open channel flow with suspensions of neutrally buoyant particles, Technical Report 49, Hydrodynamics Laboratory, Massachusetts Institute of Technology, Cambridge, Massachusetts, 1961.

Gartrell, G., Jr., A signal processor for a laser-Doppler velocimeter, Technical Memorandum 78-5, W. M. Keck Laboratory of Hydraulics and Water Resources, California Institute of Technology, Pasadena, California, 1978.

Gilbert, G. K., Transportation of debris by running water, United States Geological Survey, Professional Paper 86, 1914.

Hino, M., Turbulent flow with suspended particles, Journal of the Hydraulics Division, ASCE, vol. 89, HY 4, Proc. Paper 3579, July, 1963, p. 161-185.

Hunt, J., Private communication, 1980.

Ismail, H. A., Turbulent transfer mechanisms and suspended sediment in closed conduits, Transactions, ASCE, vol. 117, paper 2500, 1952, p. 409-454.

Jackson, R. G., Sedimentological and fluid dynamic implications of the turbulent bursting phenomenon in geophysical flows, Journal of Fluid Mechanics, vol. 77, part 3, 1976, p. 531-560.

Laufer, J., Recent measurement in a two-dimensional turbulent channel, Journal of Aeronautical Science, vol. 17, no. 5, May, 1950, p. 227-287.

Luque, R. F. and R. van Beek, Erosion and transport of bed-load sediment, International Association for Hydraulic Research, vol. 14, 1976, p. 127-144.

Mc Dougall, T. J., Bias correction for individual realization laser-Doppler anemometer measurements, Journal of Physics, Series E, Scientific Instruments, vol. 13, January, 1980, p. 53-60.

Mc Laughlin, D. K. and W. G. Tiederman, Biasing correction for individual realization of laser anemometer measurements in turbulent flows, Physics of Fluids, vol. 16, no. 12, December, 1973, p. 2082-2088.

Mc Quivey, R. S., Principles and measuring techniques of turbulence characteristics in open-channel flows, United States Geological Survey, Professional Paper 802A, 1973.

Müller, A., Turbulence measurements over a movable bed with sediment transport by laser-anemometry, Proceedings 15th Congress, International Association for Hydraulic Research, Istanbul, Turkey, September 3-7, 1973, p. 43-50.

Müller, A. and J. R. Glover, An LDA adapted to measure sediment-laden flows, Proceedings 17th Congress, International Association for Hydraulic Research, Baden-Baden, Germany, August 15-19, 1977, p. 647-650.

Nomicos, G., Effects of sediment load on the velocity field and friction factor of turbulent flow in an open channel, thesis presented to the California Institute of Technology, at Pasadena, California, in partial fulfillment of the requirements for the degree of Doctor of Philosophy, 1956.

O'Brien, M. P., Review of the theory of turbulent flow and its relation to sediment transportation, Transactions, American Geophysical Union, Washington, D. C., April 27-29, 1933, p. 487-491.

Offen, G. R. and S. L. Kline, A proposed model of the bursting process in turbulent boundary layers, Journal of Fluid Mechanics, vol. 70, part 2, 1975, p. 209-228.

Raichlen, F. R., Some turbulence measurements in water, Journal of the Engineering Mechanics Division, ASCE, vol. 93, EM 2, Proc. Paper 5195, 1967, p. 73-97.

Roberts, J. R. and M. Gaster, On the estimation of spectra from randomly sampled signals: a method of reducing variability, Proceedings of the Royal Society of London, Series A, vol. 371, 1980, p. 235-258.

Rouse, H., Modern conceptions of the mechanics of fluid turbulence, Transactions, ASCE, vol. 102, paper 1965, 1937, p. 463-543.

Shapiro, H.S. and R. A. Silverman, Alias-free sampling of random noise, Journal of the Society for Industrial and Applied Mathematics, vol. 8, no. 2, June, 1960, p. 225-248.

Sutherland, A. J., Proposed mechanism for sediment entrainment by turbulent flows, Journal of Geophysical Research, vol. 72, no. 24, 1966, p. 6183-6194.

Taylor, B. D., Temperature effects in alluvial streams, Report KH-R-27, W. M. Keck Laboratory of Hydraulics and Water Resources, California Institute of Technology, Pasadena, California, August, 1971.

Vanoni, V. A., Transportation of suspended sediment by water, Transactions, ASCE, vol. 111, Proc. Paper 2267, 1946, p. 67-133.

Vanoni, V. A. and N. H. Brooks, Laboratory studies of the roughness and suspended load of alluvial streams, Report E-68, Sedimentation Laboratory, California Institute of Technology, Pasadena, California, 1957.

von Karman, T., Turbulence and skin friction, Journal of Aeronautical Science, vol. 1, no. 1, January, 1934, p. 1-20.

APPENDIX A

A PROCESSING SYSTEM FOR LASER-DOPPLER VELOCIMETRY FOR SEDIMENT-LADEN FLOWS

A PROCESSING SYSTEM FOR LASER-DOPPLER VELOCIMETRY FOR SEDIMENT-LADEN FLOWS

by

Catharine van Ingen

Supported by:

National Science Foundation
Grant Numbers ENG75-15786 and ENG77-10182

W. M. Keck Laboratory of Hydraulics and Water Resources
Division of Engineering and Applied Science
California Institute of Technology
Pasadena, California

Technical Memorandum 80-1 June 1980

ACKNOWLEDGMENTS

The processing system herein described could not have been accomplished without the contributions of many people. First, and most importantly, Professor Ricardo Gomez. His most generous offer to teach the author electronics by example has given the author a valuable skill. The pre-amplifier, a Gomez magic box, makes this simple approach to laser velocimetry in sediment-laden flows possible. The good/bad approach to Doppler signal frequency determination was used in a previous counter used in the Keck Laboratory. That counter was developed by Greg Gartrell with Marc Donner and E. John List. Sven Sondergaard patiently taught the author the rudiments of printed circuit board layout and etching. The brute force approach to solving ground loop problems was contributed by Eric Siskind. The wire-wrap computer program was run with the help of William Kropac, Frank Nagy, and Eric Siskind. Norman Brooks made the original manuscript readable. Discussions with Alan Barnes and Robert Landau yielded many helpful suggestions and comments. This work was supported by the National Science Foundation under Grant Numbers ENG75-15786 and ENG77-10182 (Principal Investigator, Professor Norman Herrick Brooks) and was done in conjunction with the author's thesis research on the mechanisms of entrainment and suspension in sediment-laden flows.

TABLE OF CONTENTS

LIST OF FIGURES

LIST OF TABLES

1

SECTION I

INTRODUCTION

I.1 Introduction

The laser-Doppler technique has been used quite successfully in homogeneous fluid or gas-aerosol flows. The main advantage of the technique is that the flow field is not disturbed. No probe is introduced into the flow. This characteristic makes the technique particularly attractive for use in sediment-laden flows where the introduction of a probe, especially near the movable bed, can grossly deform the flow.

Due to lack of instrumentation, most previous experimental investigations of sediment-laden flows have been limited to time-averaged measurements of flow variables. Also, most measurements have averaged over a large spatial volume. The interactions between fluid turbulent structure and suspended sediment have been theorized from the mean sediment concentration and mean velocity profiles. Hot-film anemometry has been done in sediment-laden flows, but the technique has real disadvantages. Sediment grains collide with the probe tip, causing short voltage spikes in the signal. Rapid abrasion of the probe tip gives long term calibration difficulties. Morever, the sand grains are deflected by the probe, deforming the local flow field.

In homogeneous fluid flows, the laser-Doppler technique depends on the presence of small scattering particles. Ideally, these particles are diffuse, so that at any instant only one

particle is present in the measuring volume and small enough ($\sim$10μm) to follow the small scale fluid flow. In a sediment-laden flow, there are sand grains also in suspension. These grains are quite large with respect to the small scattering particles and need not follow the flow as the smaller particles do. Sand grain concentration is determined by the flow mechanics; near the bed, the concentration becomes large and the grains are not diffuse.

For the laser-Doppler technique to be useful in a sediment-laden flow, the signals generated by the two types of scattering particle must be detectable, distinguishable, and processable. The measuring volume must be such that the sand grains appear diffuse, that is, there are times in which only fluid tracer particles occupy the volume.

This report describes a simple system for obtaining and processing the signal obtained using the laser-Doppler velocimetry technique in a sediment-laden flow. Section I.2 describes the optical arrangement used to obtain the velocimetry signal. Section II gives an overview of the signal processing. The details of the processing electronics are given in Sections II.2 and II.3. Some general remarks on the technique and its difficulties are found in Section III.

It is not the intention of this report to describe in detail either laser-Doppler velocimetry or digital electronics. For a

discussion of the laser-Doppler technique, see Durst, Melling, and Whitelaw (1976). For an introduction to digital electronics, see Lancaster (1974).

I.2 Laser-Doppler Velocimetry Optics

Figure I.1 shows the basic dual-scattering optical arrangement used in one-dimensional laser-Doppler velocimetry. The laser light beam is split into two beams of equal intensity, then made to intersect at a point within the flow field. When a particle passes through the laser beam, it scatters light which is frequency shifted according to the Doppler principle. The frequency shift, Δf, is given by:

$$\Delta f = \frac{u \sin \phi}{\lambda}$$

where u is the particle velocity, ϕ the scattering angle, and λ the wavelength of the incident light. The frequency shift is small with respect to the frequency of the incident light. The beam intersection volume is imaged on the surface of a photodetector by a collecting lens. When a particle passes through the beam intersection, it scatters light from both beams simultaneously. The collected light focused at the photodetector is a combination of light scattered from both beams. The response of a photodetector is slow with respect to the frequency of light, but not slow with respect to the difference frequency of the combined light.

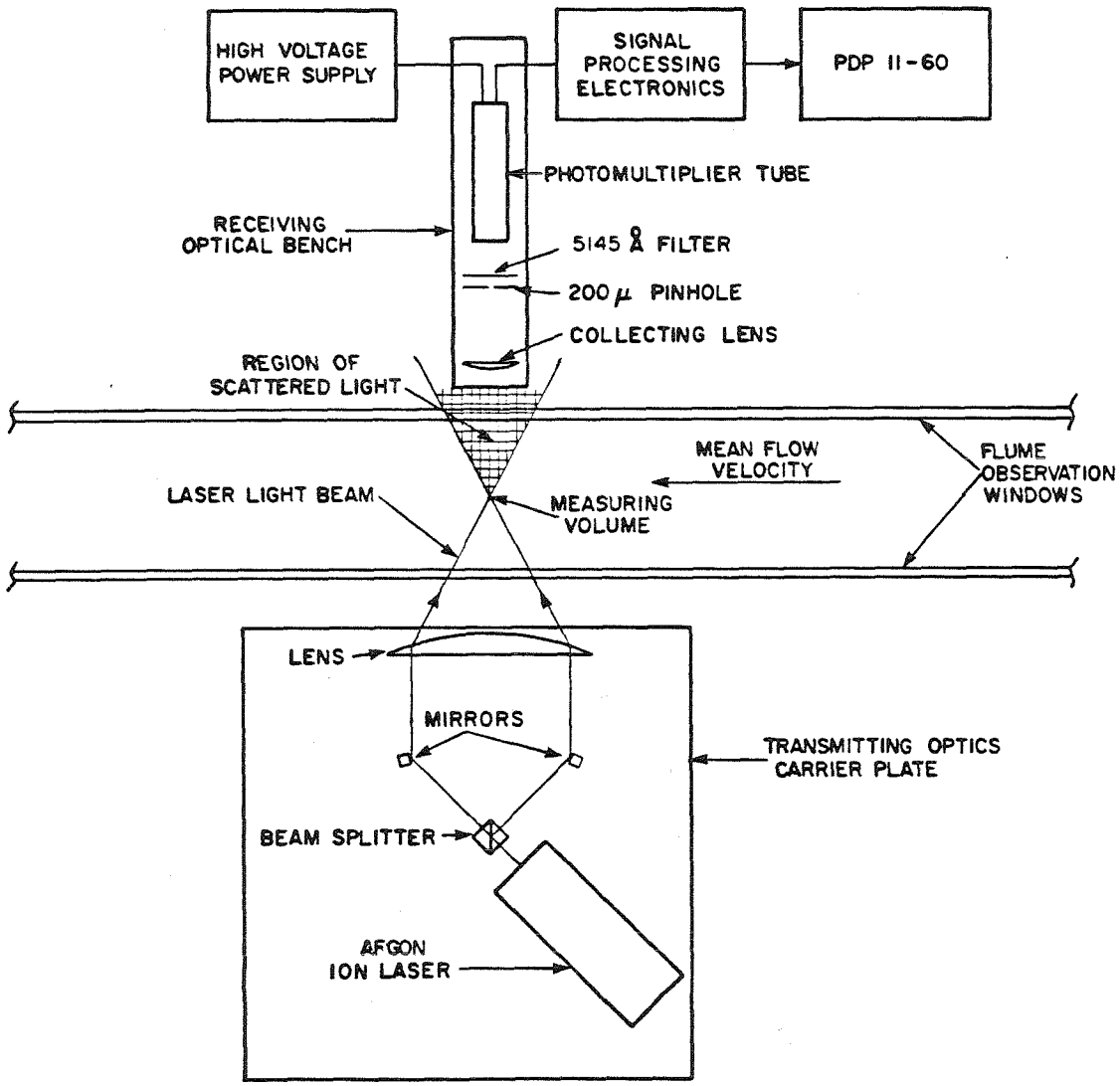

Figure I.1 One-dimensional dual-scatter optical arrangement (plan view)

5

The photodetector output current is proportional to the square of the intensity of the incident light. A typical photodetector output signal appears in Figure I.2.a. The signal consists of two parts: the pedestal or offset current and the Doppler modulated burst. The offset current is caused by the Gaussian light intensity of the laser light beams. The ratio of the pedestal amplitude to the Doppler burst amplitude is a function of the optical geometry and the scattering particle size.

In sediment-laden flows, the sorting of signals generated by sand grains and fluid tracer particles can be accomplished by measuring the pedestal amplitude. Large particles scatter more light. Since sand grains are commonly on the order of 300μm, they scatter much more light than 10μm fluid tracer particles. While it is not simple to distinguish various sand sizes, it is quite easy to distinguish signals generated by sand grains from signals generated by dust, polystyrene latex spheres, milk, latex paint particles or other commonly used fluid tracer particles.

Sand grains scatter so much more light than the smaller fluid tracer particles that detecting both types becomes a problem. The photodetector and processing electronics must be sufficiently sensitive to low amplitude scattering to detect the small particles, yet sufficiently insensitive such that the large grains do not saturate the system. A sand grain which passes through a beam just outside the measuring volume scatters enough light to mask the scattering by a tracer particle passing

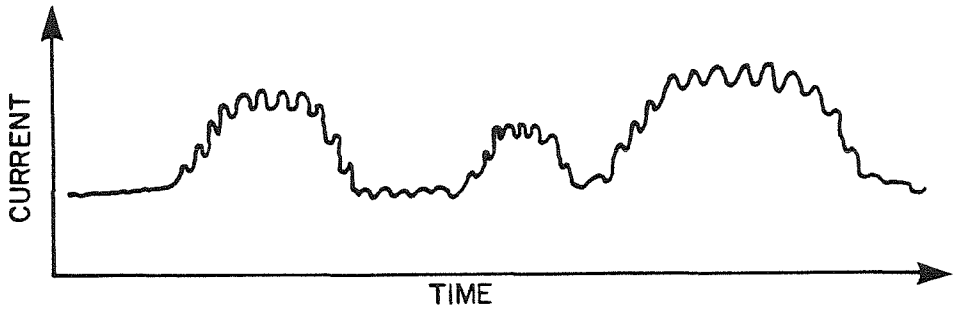

Figure I.2.a Photomultiplier output signal from typical LDV optics (beam intersection angle 4 degrees)

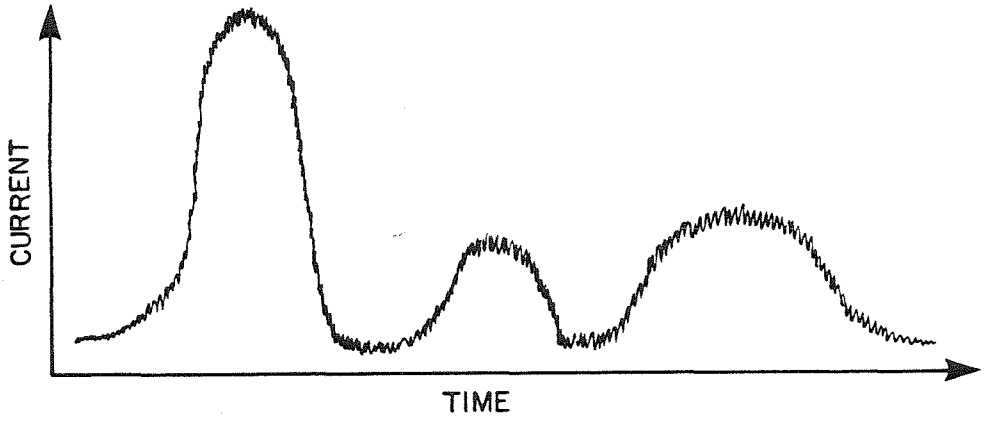

Figure I.2.b Photomultiplier output signal from LDV optics as used (beam intersection angle 22 degrees)

simultaneously through the beam intersection. Such a sand grain generates a burst of white noise which must be distinguished from the Doppler burst generated by the particles and grains passing through the beam intersection. The transmitting optics must be such that there exist instants when not only are there no sand grains within the measuring volume, but there are no sand grains in the beams near the volume.

In ordinary laser-Doppler applications, the angle of laser beam intersection is quite small ($\sim$2 degrees). This results in an elliptical measuring volume whose major diameter is on the order of fifty times the minor diameter. If an angle of beam intersection of 22 degrees is used, the major diameter is only five times the minor diameter. By minimizing the minor diameter, making it near the sand diameter, the measuring volume becomes small enough to allow fluid velocity measurement because sand particles are sometimes absent. The large beam angle also reduces the probability of a sand grain in the vicinity of the collected scattered light. Thus, the scattering from water tracer particles can also be detected. Other larger beam intersection angles may be used also. However, if the angle gets too large, the scattering efficiency of the smaller tracer particles lessens, making them quite hard to detect. An angle of 22 degrees was used as a compromise value.

I.3 Signal Processor Overview

A typical photodetector output signal from a sediment-laden flow appears in Figure I.2.b. Note that the ratio of pedestal amplitude

to Doppler burst amplitude may be as high as 100:1 as a result of the transmitting optics and large sand grain size.

Thus, the signal consists of Doppler modulated bursts, bursts of white noise and low level background noise. To accurately determine the velocity of the fluid and the sand grains, the signal processor must meet several criteria. These are:

1) Identification of the signal from a scattering particle passing through the beam intersection. It must recognize Doppler modulated bursts.
2) Detection of signals generated by both sorts of scattering particles. It must be sensitive to signals generated by fluid tracer particles and not saturated by signals from sand grains.
3) Identification of the relative size of the scattering particle which generated each Doppler modulated burst.
4) Accurate frequency determination over a wide range of relatively high frequencies. With the larger beam intersection angle, Doppler frequencies are in the range from 200 KHz to 900 KHz.

The signal processor developed in this study meets all these criteria and is detailed in Section II.

SECTION II

PROCESSOR SYSTEM DESCRIPTION

II.1 Counter System Overview

The signal processing system which has been developed is diagrammed in Figure II.1. The raw photomultiplier output current is first amplified and converted into a voltage, then the pedestal and Doppler burst portions of the signal are separated. The pedestal signal is isolated by low-pass filtering the amplifier output. As shown in Figure II.2.b, this removes the Doppler modulation. The Doppler burst signal is high-pass filtered, thus removing the pedestal, then further amplified and band-pass filtered. The band-pass filtering does two tasks. First it serves to clean up the burst signal, primarily removing high frequency white noise residuals. Second, if two-dimensional measurements are being made, the filtering separates the Doppler burst signal due to each component. A typical Doppler signal, amplified and filtered, appears in Figure II.2.c. These three signals, the two Doppler burst signals and the pedestal signal, are then input to the digital processing electronics.

The digital portion of the electronics can be broken into six parts. These are the two independent Doppler burst counters, the Doppler burst check counter, the particle relative size detector, the interface to the laboratory mini-computer, and the control logic. The digital electronics outputs three sixteen-bit words to the laboratory mini-computer for each velocity realization.

10

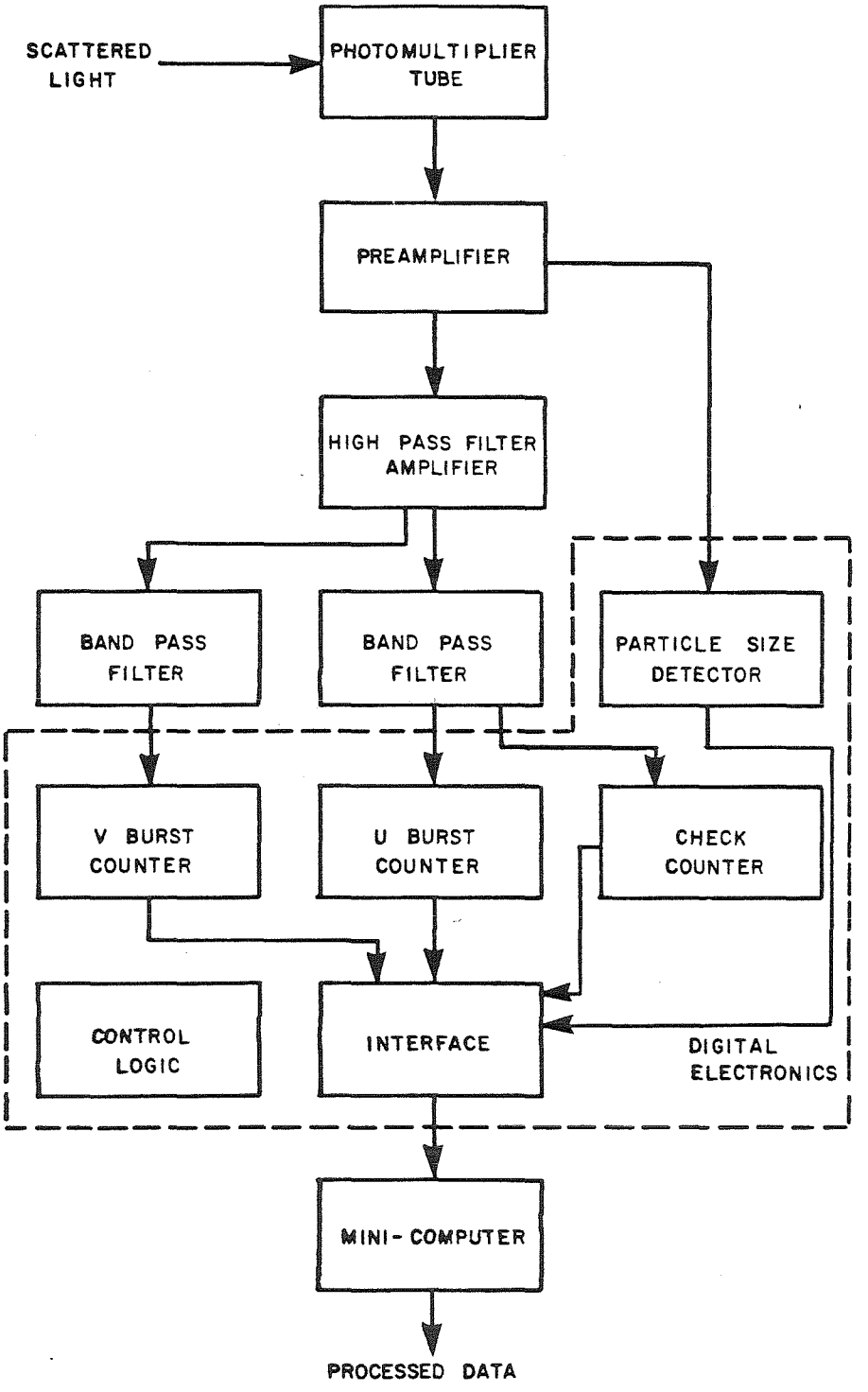

Figure II.1 Processor logic diagram

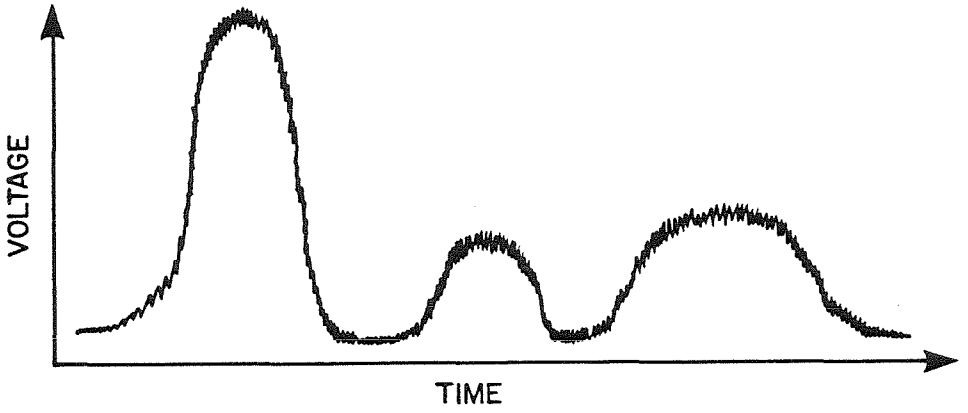

Figure II.2.a Simplified photomultiplier output signal

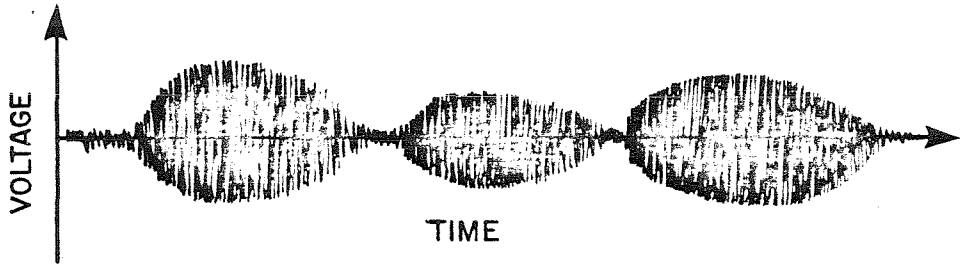

Figure II.2.b Doppler burst signal

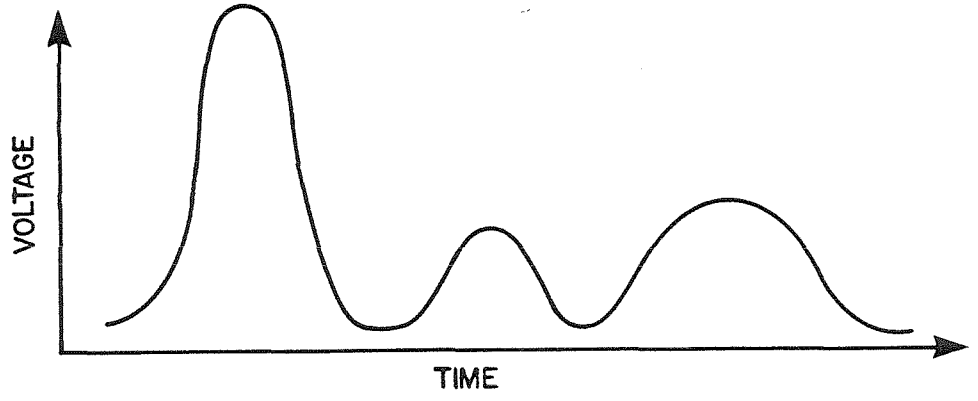

Figure II.2.c Pedestal signal

The upper four bits of the first word contain the particle size information. The lower twelve bits of the first word are the output of the Doppler burst check counter. The second and third words are the outputs of the two independent Doppler burst counters.

Each Doppler burst counter measures the frequency of the input Doppler burst by accurately measuring the time required for a preset number of signal zero-crossings to occur. During this counting process, the burst signal must remain larger than some threshold level and must be regular in frequency. This ensures that the signal being counted was generated by a scattering particle which passed through the beam intersection and was not generated by a sand grain passing near the volume.

A schematic of the counting system appears in Figure II.3. The incoming burst signal is fed into two different detectors. The output of the zero-crossing detector is high when the burst signal is greater than the analog ground. The burst level detector output is high when the burst amplitude is greater than an adjustable preset threshold level. When the level detector burst pulses occur sufficiently often, the level latch stays high. The time allowed between burst level pulses is adjustable and ensures that the frequency of the signal is regular. Zero-crossing pulses are counted only when the level latch is high. While zero-crossing pulses are being counted, a 10 MHz reference clock pulse is also being counted. The desired number of zero-crossing is preset. The velocity measurement is the number of reference clock pulses which

13

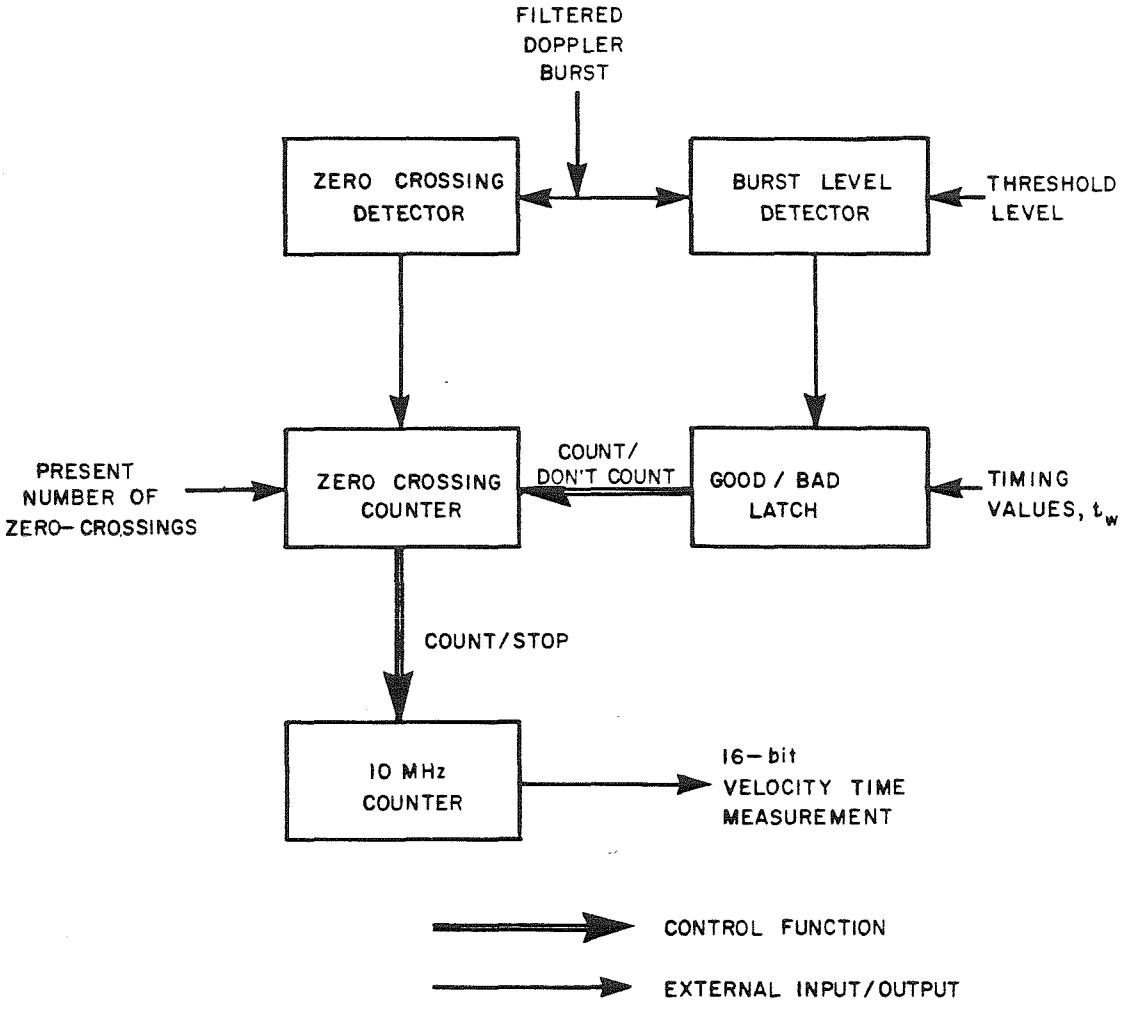

Figure II.3 Doppler burst counter logic diagram

occur in the time required to count the preset number of zero-crossings.

The Doppler burst check counter is quite similar to the two Doppler burst counters. Again, the time required for a preset number of zero-crossings is determined. The incoming signal to one of the burst counters is duplicated and counted by the check counter. By presetting a different number of zero-crossings, two different determinations of the burst frequency are made. If the incoming burst is regular in frequency, the two determinations will agree. The check counter is different fron the burst counters in that it does not feed into the counter control logic and its output is only twelve bits, not sixteen.

The particle relative size detector tags each velocity measurement as being generated by a sand grain, a fluid tracer particle, or an unidentified scatterer. The relative particle size is determined by the relative amplitude of the pedestal signal. Pedestal levels are measured only when the burst counters are on and counting. This ensures that the same scattering particle generates both measurements.

The Doppler burst counters and the particle size detector are controlled by the counter control logic. The control logic also runs the interface to the laboratory mini-computer. The control logic ensures that the burst counting and recording of counted bursts proceeds in an orderly fashion.

After initial acquisition, the data are analyzed by the computer. Mean fluid velocity, mean sediment grain velocity, sediment grain inter-arrival time and turbulence intensity can be calculated. The quantity of data and its rapid acquisition rate necessitate the use of a mini-computer or micro-processor.

II.2 Analog Electronics

The signal amplification takes place in two steps, as shown in Figure II.1. In the first step, the entire photodetector output current is amplified and converted into a voltage. In the second step, only the Doppler-modulated burst portion of the signal is amplified.

The circuit diagram for the pre-amplifier, or first step amplifier, is given in Figure II.4. The negative current of the photodetector yields a positive current at the input to the 72733. Two adjustments are provided. The 1 kilohm potentiometer determines the input impedence of the pre-amplifier. Adjusting this potentiometer varies the total gain of the pre-amplifier. This adjustment is required when changing sand sizes, or laser output power to avoid saturation of the 72733. By adjusting the 500 ohm potentiometer, the bias current of the photodetector can be removed. The 500 ohm potentiometer is mounted on the front panel. This allows a simple way to compensate for the change in photodetector bias current due to the change in total light level as the location of the scattering volume nears the sediment bed. Two output voltage signals, inverted and

16

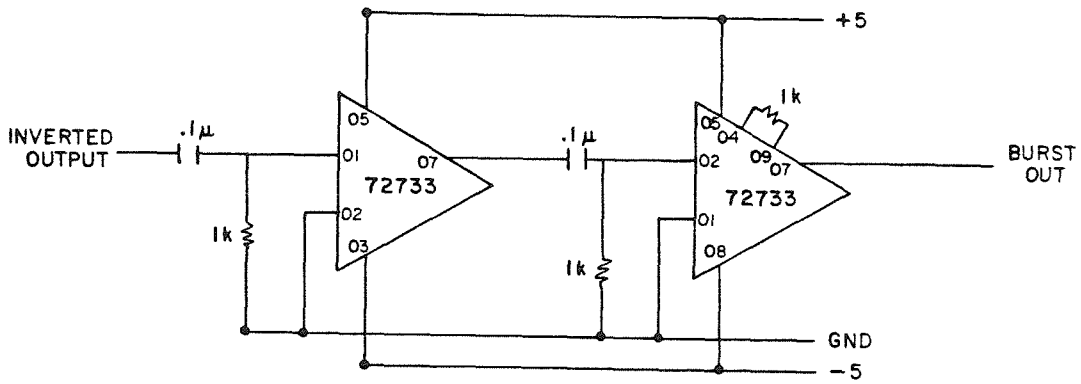

Figure II.4 Pre-amplifier circuit diagram

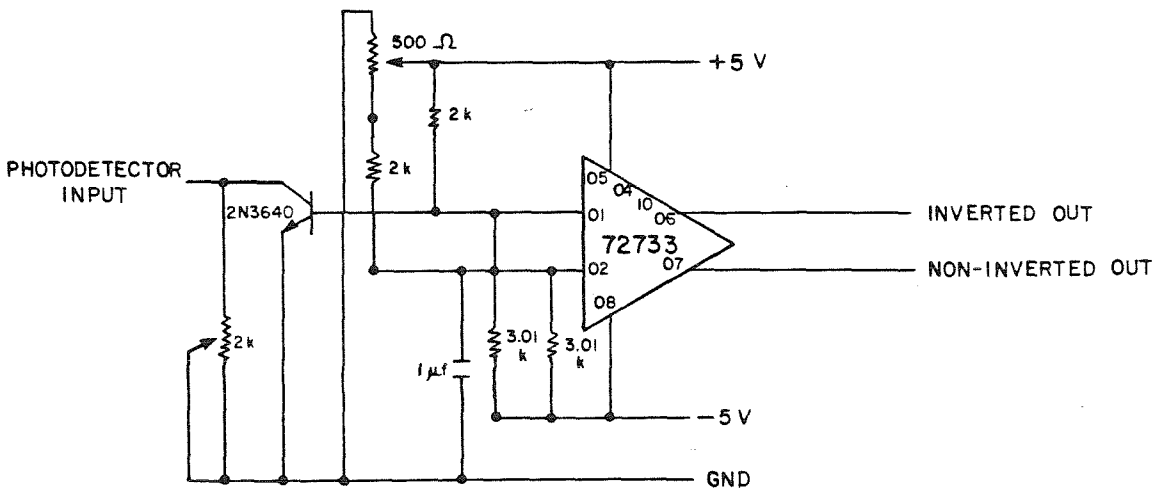

Figure II.5 Doppler burst amplifier circuit diagram

non-inverted result. The inverted, or positive going output, is input into the counter level detector circuit (described in Section II.3.3). The non-inverted signal is input to the second stage amplifier.

The pre-amplifier was tested using a Hewlett-Packard 3311A function generator. A 500 KHz sine wave with an amplitude of 10 millivolts and effset -150 millivolts was input to the pre-amplifier through a 19 megaohm resistor. Thus, the input to the pre-amplifier was a 630 picoampere sine wave with a -940 picoampere bias current. The resulting inverted output was a 3.1 millivolt sine wave with a +.53 volt bias.

The second stage, or Doppler, amplifier is shown in Figure II.5. Two 72733s are used for convenience. Only the inverted output is eventually used. The input from the pre-amplifier is high-pass filtered at 10 KHz, amplified by a 72733 with a gain of 10, again high-pass filtered and again amplified by a second 72733. The gain of the second 72733 was selected to be approximately 25 by a 1 kilohm resistor between pins 04 and 09. The two stages were used to achieve maximum amplification without saturation. The amplifier was tested with the output of the pre-amplifier described above. The amplifier output was measured to be 600 millivolts, giving a gain of 200.

The Doppler burst signal is filtered using two Kronite 3202 filters. These are infinitely variable, high or low pass filters with a 24dB per octave roll off. Other filters may be substituted.

High frequency (greater than ∿2 MHz) noise residuals inherent in the Doppler amplifier 72733 must be removed by low-pass filtering. The dc bias also inherent in the 72733 is removed by high-pass filtering.

II.3 Digital Processing Electronics

This section describes in detail the digital processing electronics. As shown in Figure II.1 and described in Section II.1, there are six principal parts: two identical Doppler burst counters, a Doppler burst check counter, a particle size detector, an interface to the laboratory mini-computer or other external device, and the control logic.

Physically, the digital electronics consists of three printed circuit boards, three wire-wrapped boards and a front panel containing various external switches, potentiometers, inputs, and outputs. Unless otherwise noted, all integrated circuit identification numbers are Texas Instrument numbers. To facilitate the design and fabrication of the processing electronics, particularly the wire-wrapped portion, all of the internal TTL signals were given names. For ease in explaining the processing electronics and inter-relating the various circuit diagrams, some of these names will be used here.

Each signal name describes in some way what the function of that signal is when high or logically true. For instance, the signal PDPRDY is high when the laboratory mini-computer is ready to receive new data. A signal name ending in BR is an inverted

signal. Hence, PDPRDYBR, the inverse of PDPRDY, is high when the mini-computer is not ready to receive new data. The two Doppler burst counters are differentiated on the basis of their respective signal names. The U counter signals have a "U" in their names. The signal names with a V originate in the V counter. The check counter signals are identified by a C. Thus, OVFLU is the counter overflow signal from the U counter, OVFLV that from the V counter and OVFLC that from the check counter.

Section II.3.1 describes the control logic. The Doppler burst counters and the check counter are described in Section II.3.2, followed by the description of the particle size detector in Section II.3.3. The interface to the laboratory mini-computer is described in Section II.3.4. All sections include the relevant circuit diagrams. A partial glossary of signal names is found in Appendix 1. A full listing of the wire-wrap signal names and pin interconnections is found in Appendix 2.

II.3.1 Control Logic

The control logic orders the tasks of the Doppler burst counters, the particle size detector and the computer interface. This is accomplished by imposing a set of "states" upon the above, ensuring that the data acquisition and processing proceeds in an orderly and electronically clean fashion. The eight states and their respective functions are block diagrammed in Figure II.6. The state number, in binary, appears in the upper left corner of each block. The output of the state logic is a set of eight sequence

20

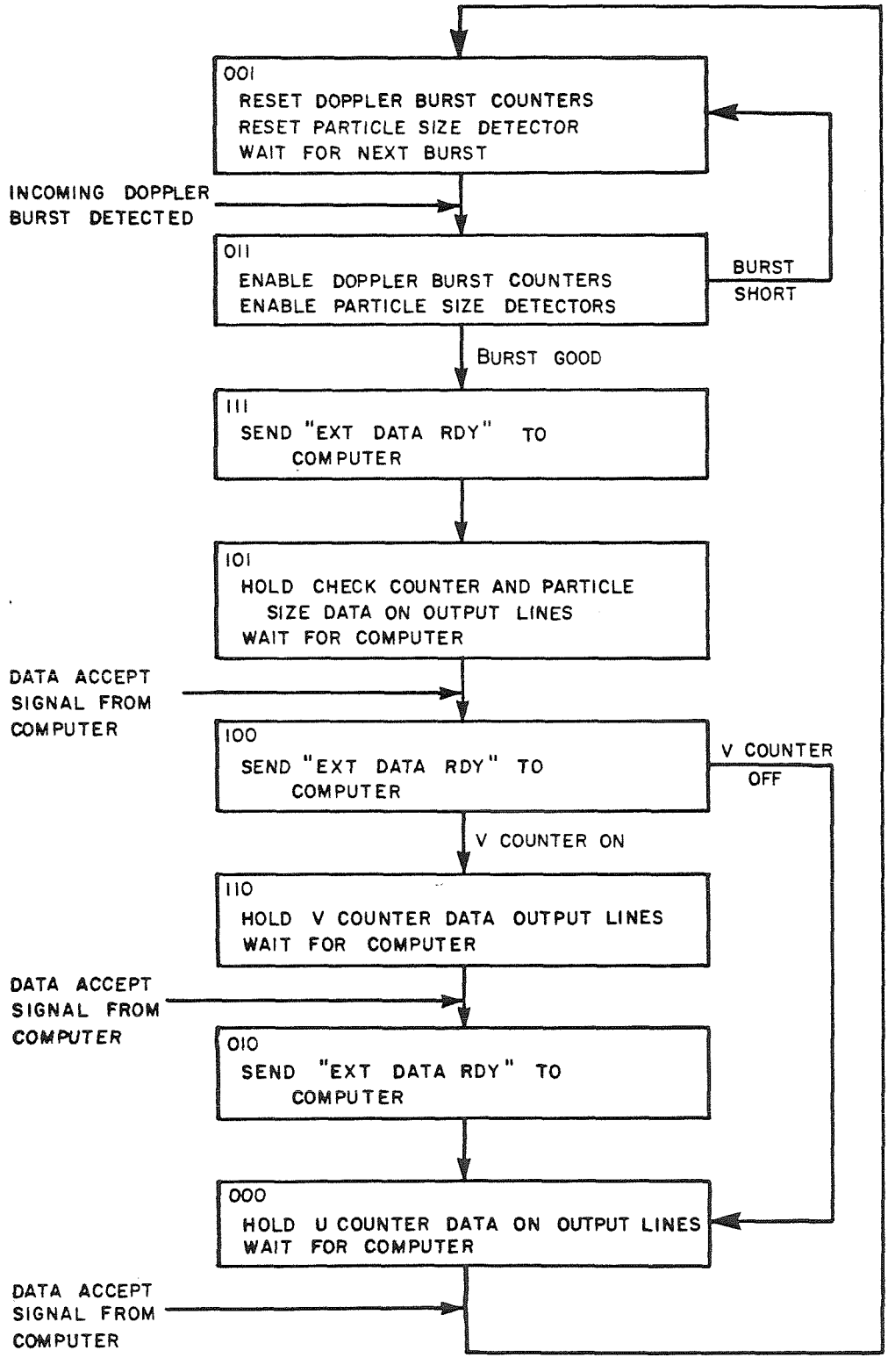

Figure II.6 Control logic states

signals, SEQ0 through SEQ7, to control the remaining electronics. The inputs to the state logic tell it what the incoming Doppler burst looks like, whether it is a good countable burst; what the computer, or other external recording device, is doing; and whether both of the burst counters are being used.

The state sequence codes are controlled by three J-K flip-flops, each one-half of a 74112, and a 7442 decoder. The circuit is shown in Figure II.7. The counter is said to be in a state upon when its sequence signal is high or, equivalently, when the SEQnBR signal is low. Only one sequence signal can be low at any given time. The state number is the value of the three bit number composed of the three flip-flop outputs. The 7442 outputs are inverted, hence when all flip-flop outputs are low, SEQ0BR will be low and the device will be in State 0. Similarly, State 3 occurs when FF0 and FF1 are high and FF2 is low.

The progression from state to state is grey coded, so that only one flip-flop changes at any given time. The cause of each flip-flop transition is given in Table II.1. Flip-flop transitions occur on the negative transition of the 10 MHz timing clock. The flip-flop output rises on the next clock pulse after the J input goes high. When the K input is high, the flip-flop output falls on the next clock pulse. Either input to each flip-flop is high in only one state. Both the J and K inputs to any flip-flop are never simultaneously high.

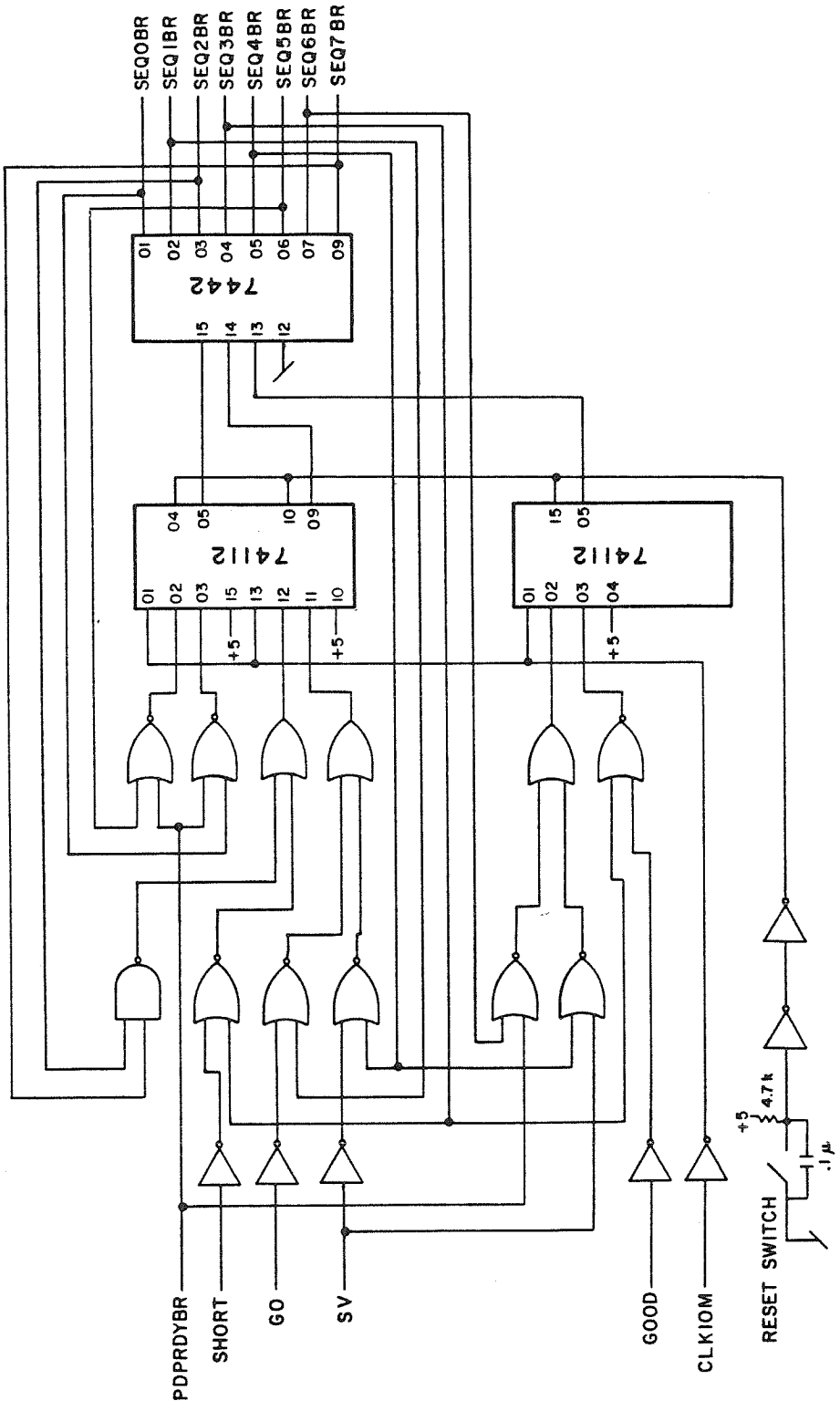

Figure II.7 Control logic circuit diagram

Table II.1 Flip-Flop transitions

STATE CHANGE	FLIP-FLOP	RELEVANT SIGNALS	CAUSE OF CHANGE
1 → 3	FF1	SEQ1BR = L GO = H	In State 1 and a new incoming Doppler burst signal is detected
3 → 7	FF2	SEQ3BR = L GOOD = H	In State 3 and the incoming Doppler burst signal is successfully counted
3 → 1	FF1	SEQ3BR = L SHORT = H	In State 3 and the incoming Doppler burst signal goes bad before being successfully counted
7 → 5	FF1	SEQ7BR = L	Transition automatic
5 → 4	FF0	SEQ5BR = L PDPRDYBR = L	In State 5 and computer signals that it has read the data on the output lines
4 → 6	FF1	SEQ4BR = L SV = L	In State 4 and two-dimensional measurements are being made
4 → 0	FF2	SEQ4BR = L SV = L	In State 4 and one-dimensional measurements are being made
6 → 2	FF2	SEQ6BR = L PDPRD4BR = L	In State 6 and computer signals that it has read the data on the output lines
2 → 0	FF1	SEQ2BR = L	Transition automatic
0 → 1	FF0	SEQ0BR = L PDPRD4BR = L	In State 0 and computer signals that it has read the data on the output lines

The 10 MHz timing clock signal is generated with a Motorola MC4024 multi-vibrator as shown in Figure 11.8.a. For simplicity, a single clock signal, CLK10M, is used to time the control logic and serve as a reference clock signal for the Doppler burst counters. The frequency is crystal-controlled by an external 10 MHz crystal connected across pins 3 and 4. During the initial development and testing of the digital electronics, the circuit shown in Figure II.8.b was used to slow the clock frequency. This simplifies the debugging process by making the internal logical signals much easier to observe.

The remaining portion of the control logic interprets signals from the two Doppler burst counters and the mini-computer for the J-K flip-flops. Four signals in particular are important. The PDPRDYBR signal informs the state logic that the computer is ready to receive data. If there is no external recording device, PDPRDYBR is always low. In this case, the transitions from State 0 to State 1, State 5 to State 4, and State 6 to State 2 will be automatic, requiring a single 10 MHz clock pulse. Otherwise the processing electronics will wait until the computer is ready before counting a new Doppler burst. This is further described in Section II.3.4.

The signals GO, GOOD, and SHORT tell the state logic what the incoming Doppler burst signal looks like. GO is high only during the time that the amplitude of the Doppler burst signal is greater than the preset threshold level, that is, the incoming signal is a

25

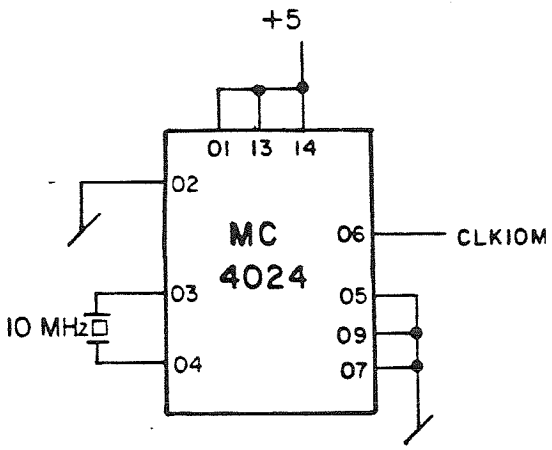

Figure II.8.a 10 MHz crystal-controlled frequency

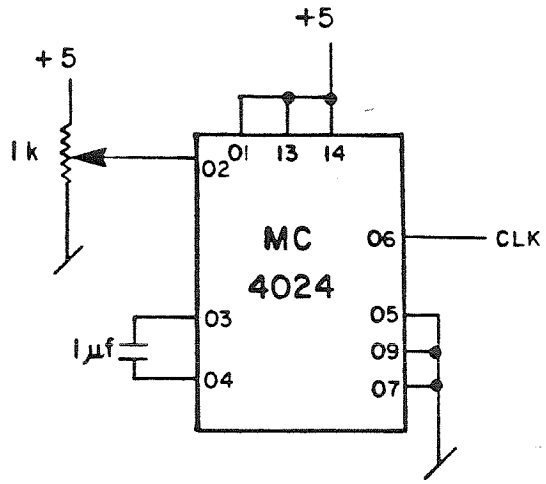

Figure II.8.b Debugging circuit

countable Doppler burst. Each countable burst is either good or short. GOOD goes high when the preset number of zero-crossings have been successfully counted; a good velocity measurement has been made. If the Doppler burst signal level falls below the threshold level before the preset number of zero-crossings have been counted, SHORT goes high. The signal was too short to be good. If the signal is good, State 3 gives way to State 7 and the good data are sent to the computer. If the signal is short, the counter returns to State 1 to wait for the next incoming burst. Both GOOD and SHORT reset to low upon entering State 1.

Each of these three signals is the output of a multiplexor. Two multiplexors are contained on a single 74153 chip as shown in Figure II.9. The multiplexing allows the U counter to be used independently to make one-dimensional measurements or ties the U and V burst counters together when making two-dimensional measurements, thus ensuring that a single scattering particle generates both velocity measurements. Three front panel switches select which counters are being used. Closing the switch, SU, SV, or SC, turns off the respective counter. Thus, the U counter signals are selected when SU is open and SV is closed. If both the SU and SV switches are open, two-dimensional measurements are being made, the multiplexor selects the input which is an appropriate combination of signals from both counters. Closing SC does not affect the multiplexor, but does disable the check counter.

27

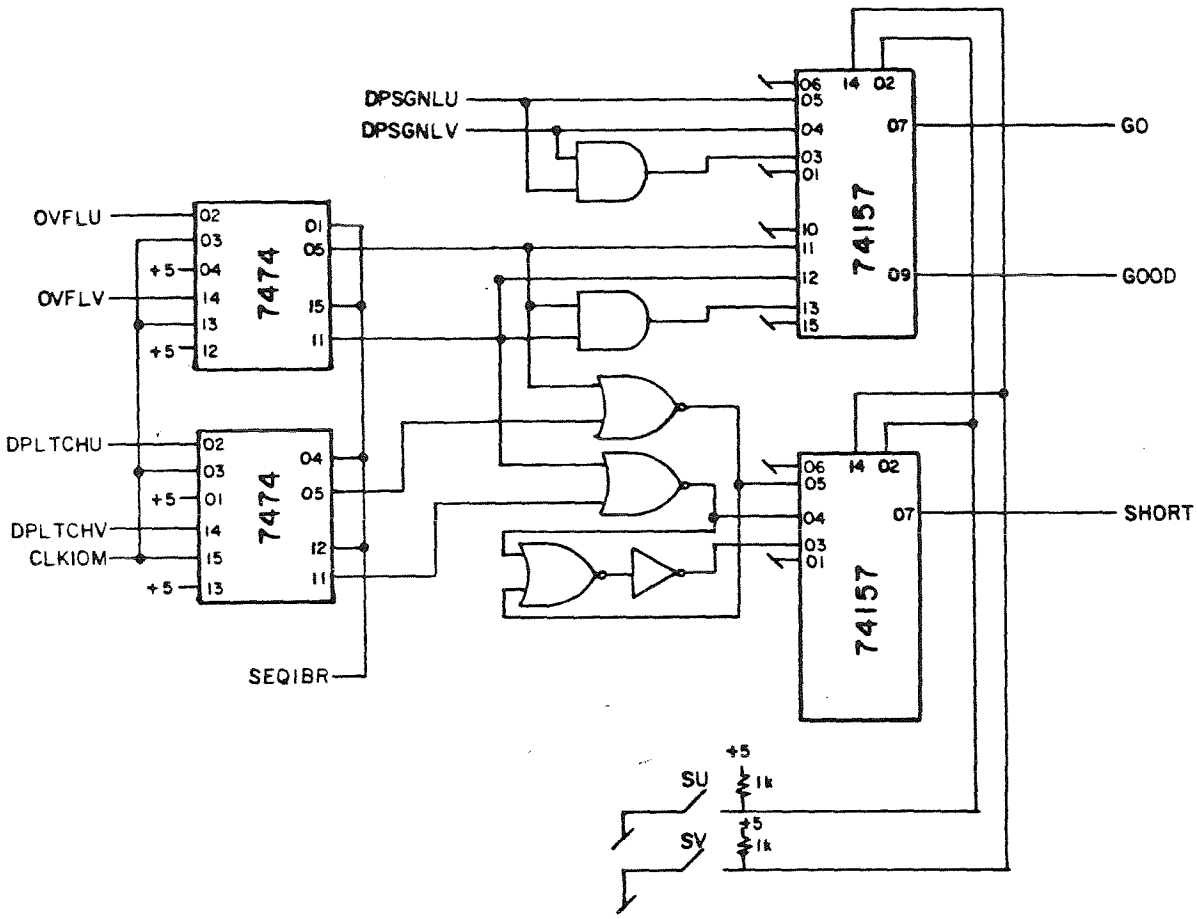

Figure II.9 Control logic circuit diagram (counter signals)

The burst counter signals, DPSGNLU, DPSGNLV, OVFLU, OVFLV, DPLTCHU, and DPLTCHV, are explained in more detail in the discussion of the Doppler burst counters, Section II.3.2. Briefly, the DPSGNLn signal from each burst counter is equivalent to GO for that burst counter. When high, the incoming signal to that burst counter is a countable Doppler burst. The OVFLn signal, when high, indicates that the preset number of zero-crossings for that burst counter have been successfully counted. Thus, OVFLn is equivalent to GOOD for a particular burst counter. The DPLTCHnBR signals are roughly inverted DPSGNLn signals. The signal from a burst counter is short if the DPLTCHnBR signal goes high before the OVFLn signal goes high. That is, the preset number of zero-crossings were not successfully counted before the incoming signal went bad. This is the result of a logical not of DPLTCHnBR and OVFLnBR. This is the logic which yields SHORT.

When two-dimensional measurements are made, the incoming signals to both burst counters must be countable and be successfully counted when a measurement is made. Thus, GO is the result of a logical and of DPSGNLU and DPSGNLV. Similarly, GOOD is the and of OVFLU and OVFLV. If the incoming signal to either counter is short, however, the measurement should be discarded. Therefore, SHORT is the result of a logical or of the DPLTCHnBR-OVFLnBR nored signals.

II.3.2 Doppler Burst Counters

This section describes in more detail the Doppler burst counters and the check counter. As noted previously, the two burst

counters are identical. The names for the U counter signals will be used. The counter logic is shown in Figure II.3. The circuit diagram for the Doppler burst counter is shown in Figure II.10. The circuit diagram for the check counter is given in Figure II.10.b. An expanded diagram of the internal logical signals is shown in Figure II.11.

Figure II.11.a shows three simplified Doppler bursts after amplification and filtering. The actual input to the counter is different only in that it contains more zero-crossings per burst, The burst on the left was generated by a scattering particle, most likely a fluid tracer particle, passing through the beam intersection volume. The burst in the center was generated by a sand grain passing through the intersection. The burst on the right was caused by a sand grain passing near or grazing the intersection. The burst counters must distinguish these three sorts of bursts, process the first two sorts and reject the third. Two criteria are used. A countable burst must first be greater in amplitude than the noise remaining in the system when no scattering particle is in the beam intersection. Second, a countable signal must be regular in frequency.

A 72311 voltage comparator is used to detect the signal amplitude. The incoming burst signal is fed into the non-inverting input. A reference voltage is fed into the inverting input. The reference voltage level is controlled by a ten-turn 500 ohm

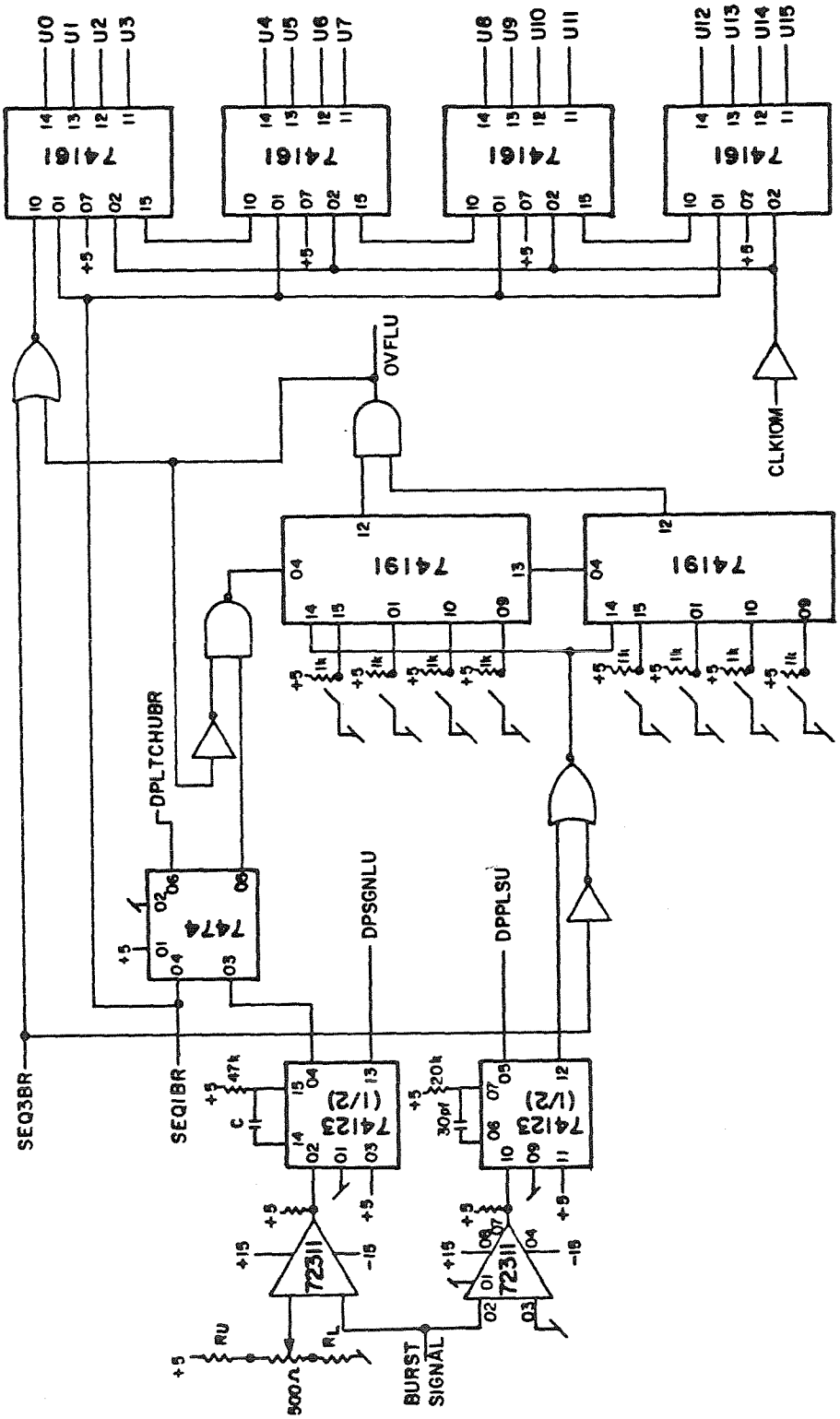

Figure II.10.a Doppler burst counter circuit diagram

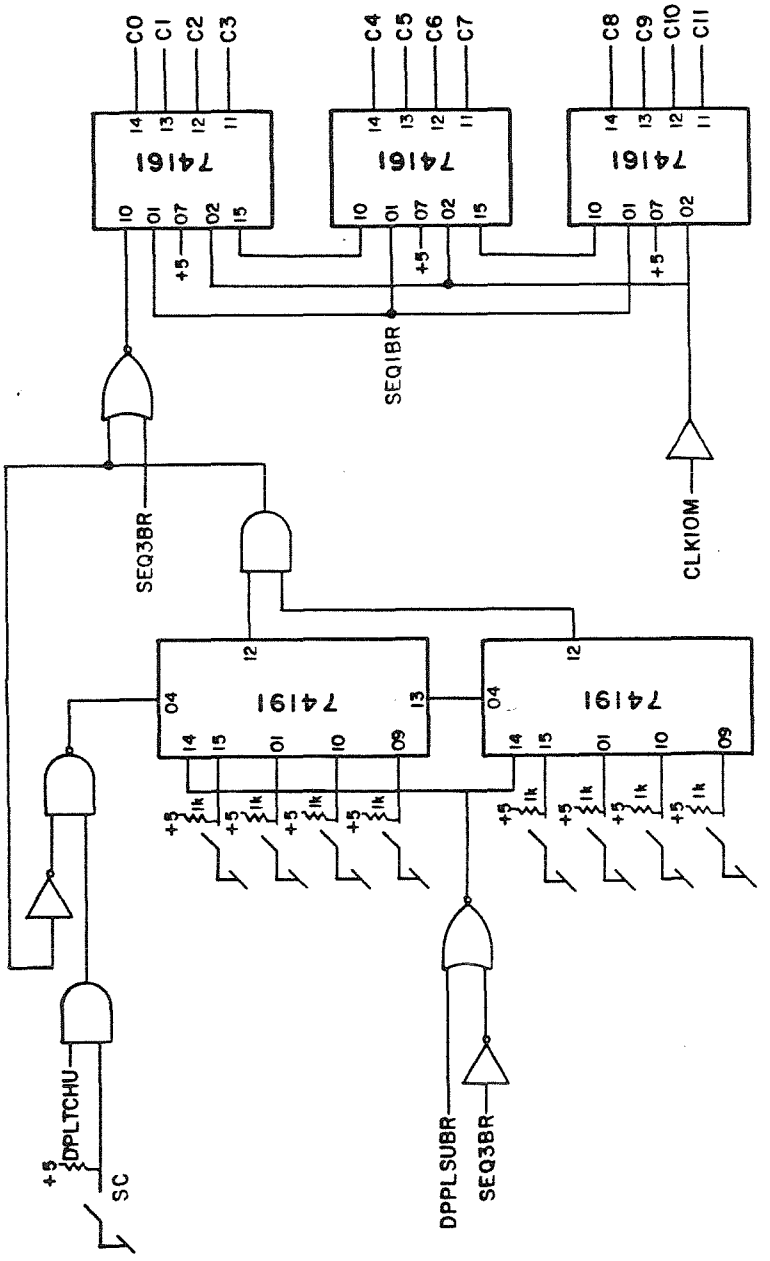

Figure II.10.b Check counter circuit diagram

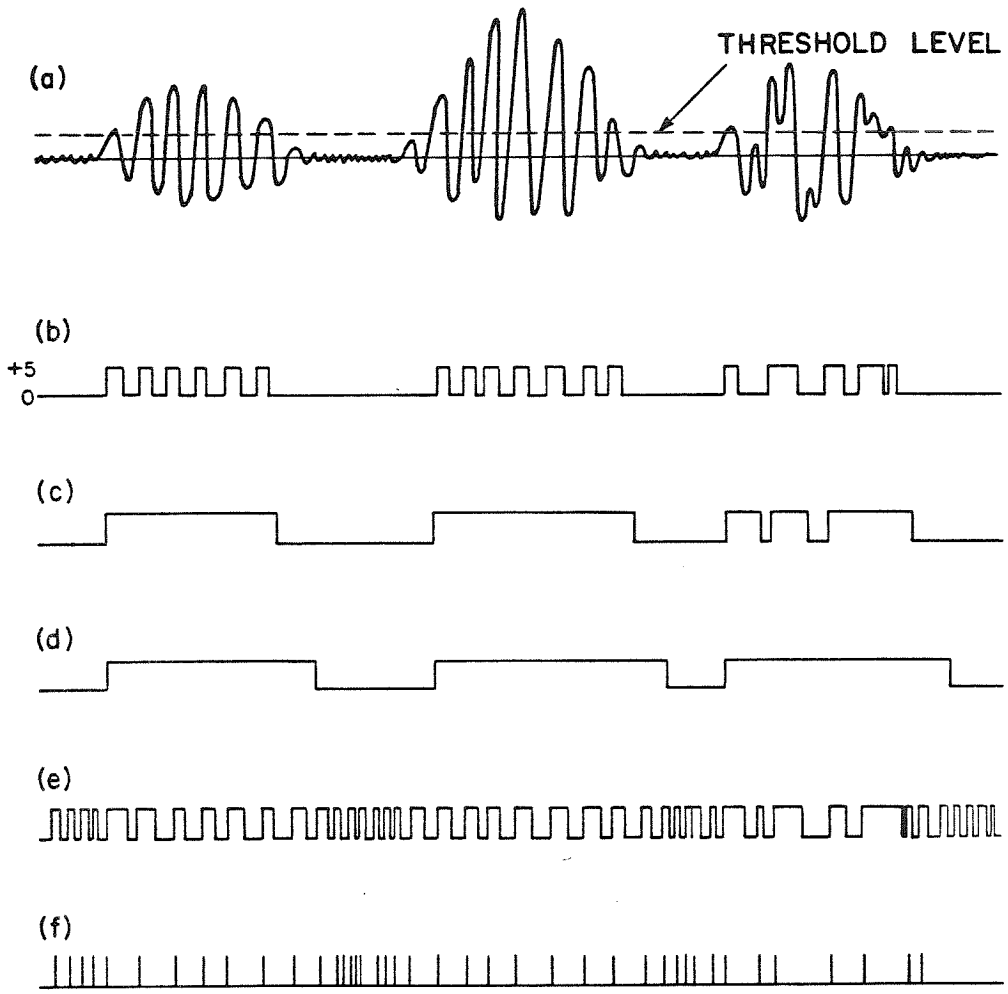

Figure II.11.a Simplified Doppler burst signal

b Level detector comparator output

c DPSGNL1 (appropriate t_w)

d DPSGNL1 (t_w too long)

e Zero-crossing comparator output

f Zero-crossing pulses

potentiometer on the front panel. As implemented, a reference voltage of from +310 mV to ground may be obtained. To change the range of the threshold reference voltage, the resistor, R1, is changed. The new voltage upper limit is given by:

$$V = \frac{2500}{500 + R1}$$

When the incoming burst voltage is higher than the reference voltage, a TTL compatible pulse is generated. This is shown in Figure II.11.b. The circuit is not a true Schmidt-trigger, in that it tests only the amplitude of the positive portion of the burst signal without hysteresis. In early experiments, it was noted that the Doppler bursts generated by sediment grains were often not cleanly modulated in amplitude. By insisting that the absolute value of the burst signal be greater than the reference threshold, most grain generated Doppler bursts would be discarded because they would not seem sufficiently regular.

The regularity of the level pulses is checked by a 74123 one-shot. When the input to a one-shot makes a positive transition, the output either changes from low to high, or, if already high, remains high. The output remains high for a time, t_w, after each positive transition of the input. The time t_w is determined by the resistor and capacitor timing circuit connected between pins 6 and 7 or pins 12 and 13. There are two timing circuits as there

are two independent one-shots in a single 74123 chip. The value of t_w is given by:

$$t_w = .25RC(1 + .7/R)$$

where t_w is in nano-seconds, R in kilohms, and C in pico-farads. To optimize the response, particularly for the higher burst frequencies, the maximum allowable resistance should be used.

The time t_w should be selected with care. The one-shot output will be low until the incoming burst signal amplitude is greater than the reference voltage signal. When the first pulse from the 72311 arrives, the incoming burst amplitude is greater than the reference voltage, the one-shot will go high. It will remain high as long as pulses from the 72311 arrive more often that time t_w. When the one-shot output, DPSGNLU, is high, the incoming signal is identified as a countable Doppler burst. Thus, t_w must be longer than the expected period of the signal. The resulting DPSGNLU for an appropriate choice of t_w is shown in Figure II.11.c. The time t_w should not be too much larger than the expected signal period, however. If t_w is too long, DPSGNLU will remain high even though the incoming signal is no longer a Doppler burst. In this way, one burst may end and a new burst begin, yet be identified as a single burst. The rejection of bursts of noise, the third signal in Figure II.11.a, is also regulated by the choice of t_w.

If too long a t_w is chosen, the noise bursts will be identified as countable bursts and processed as such. This may cause difficulty in later processing the data, as each measurement is somewhat suspect.

The pulse width is adjusted by changing the capacitor C shown in Figure II.10. A rotary wafer switch is mounted on the front panel for this reason. Table II.2 lists the capacitors currently available on the switch and their respective pulse times.

To further ensure that only one countable Doppler burst is processed in State 3, DPSGNLU is latched to produce DPLTCHU. A 7474 D flip-flop is used. When the control logic enters State 1, SEQ1BR goes low and DPLTCHU, DPLTCHU remains high until DPSGNLU goes low, until the incoming signal is no longer countable. It then remains low, regardless of DPSGNLU, until the control logic again enters State 1. In this way, only one burst can be counted in each pass through the State 3. The incoming signal is ignored until the control logic and counter are ready to process it.

The zero-crossing pulses which are counted are also generated by a 72311 voltage comparator. When the input to the comparator is above the analog ground, the output is high. Figure II.11.e shows the output of the comparator. A 74123 one-shot makes all the comparator output pulses the same length. Figure II.11.f shows the one-shot output pulses, the signal DPPLSU. As shown in Figure II.10, the pulse width is 350 nano-seconds.

Table II.2 Timing capacitors for DPSGNLn as implemented

c (pf)	t_w (μ sec)	f (KHz)
820	10.96	91
500	6.68	150
430	5.75	174
370	4.94	241
310	4.14	202
220	2.94	340
160	2.14	470
125	1.67	599
100	1.34	750
95	1.27	788
83	1.11	902

Zero-crossing pulses are counted by two 74191 programmable counters, making an eight-bit counter. The desired number of zero-crossings to be counted is set by eight front panel mounted switches. When a particular switch is open, the bit is set. Thus, if all switches are open, 255 zero-crossings will be counted. When SEQ1BR goes low, the switch setting is loaded into the counters. The counters count down from the loaded setting. When zero is reached, the "min" output, pin 12, goes high. When both 74191s reach zero, the preset number of crossings has been counted. Therefore, the OVFLU signal is generated by the logical and of the min outputs from both 74191s. Incoming zero-crossing pulses, DPPLSU, are logically anded with SEQ3, so that pulses reach the counters only during State 3. The counter is enabled, allowed to count, only while DPLTCHU is high, the incoming signal is countable, and OVFLU is low, the preset number of crossings has not yet been counted. If the signal is short, DPLTCHU will go low to disable the counter. If the signal is good, OVFLU will go high to disable the counter.

While the zero-crossing pulses are being counted, the 10 MHz reference clock pulses are also being counted by four 74161 counters. These are joined to make a sixteen-bit counter. The clock pulses count up from zero. When State 1 is entered, the outputs are cleared. The counters are enabled only while both SEQ3BR and OVFLU are low. If the incoming burst is short, DPLTCHU goes low, the control logic returns to State 1 and the clock pulse

counters are disabled and cleared. If the incoming burst signal is good, OVFLU goes high and the clock pulse counters are disabled, but not cleared. The output bit signals, U0 through U15, form the sixteen-bit number of reference clock pulses which occurred during the time required to count (N-1) zero-crossing pulses. Note that N is the switch set number of zero-crossing pulses. No buffering of the data are required, as the pulse counters are not cleared until the control logic again enters State 1, after sending the data to the mini-computer.

For oscilloscope observations of the data, or if no external digital recording device is available, the data may be output through a digital-to-analog converter. One such circuit appears in Figure II.12. The data bits, U0 through U15, are first latched using three 74174 hex latches. Each 74174 contains six independent latches with a common clock. The inputs become the outputs on the positive transition of the clock signal SEQ7. Since the inputs from the burst counters are clocked in State 7, only good counted bursts are latched.

For oscilloscope viewing, a Motorola MC3410 10-bit digital-to-analog converter may be used. This chip is common, inexpensive and gives sufficient precision for viewing of the signal. If the data is to be recorded in analog fashion, a 12-bit converter, such as a DATEL 6912B, should be substituted. The higher order bits should be used as inputs to the converter. The output current of

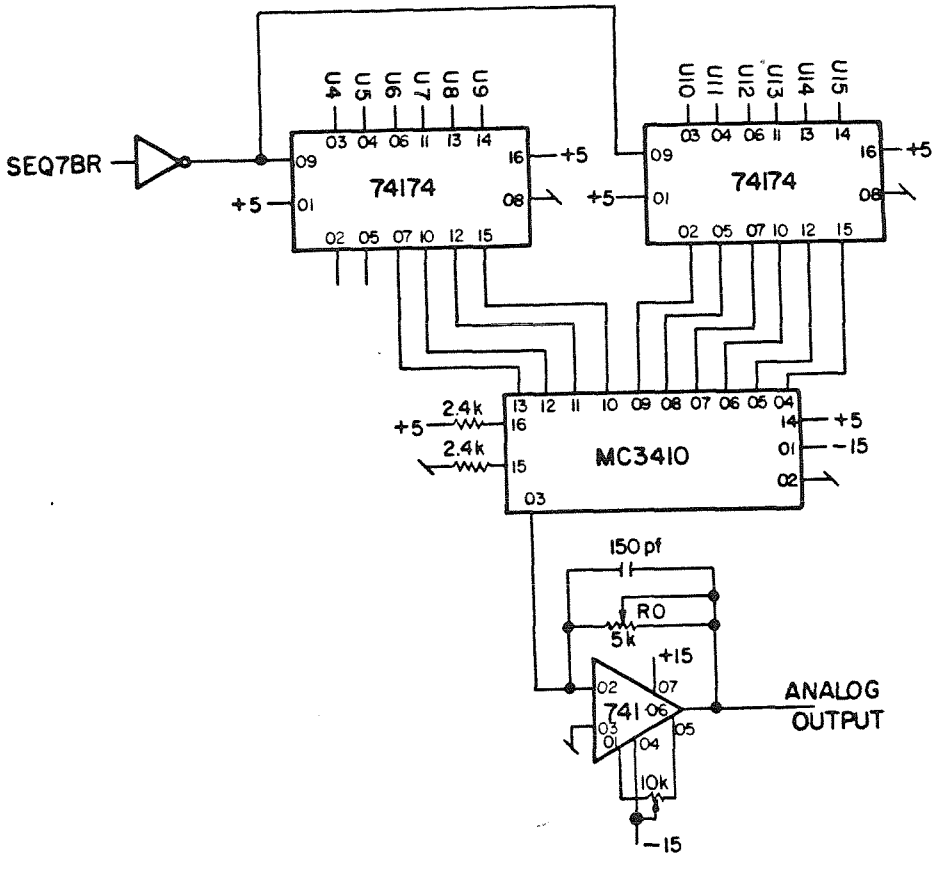

Figure II.12 Doppler burst counter analog output circuit diagram

the MC3410 is converted into a voltage by a 72741 amplifier. Two potentiometers are used to adjust the output voltage bias and range. The 10 kilohm potentiometer is used to adjust the output bias. The 5 kilohm potentiometer adjusts the sensitivity of the voltage output. The voltage output is given by:

$$V = \frac{2R_o}{2.4\times10^3} \times 5\left[\frac{U6}{2} + \frac{U7}{4} + \frac{U8}{8} + \ldots + \frac{U15}{2048}\right]$$

where R_o is the resistance to the 5 kilohm potentiometer as indicated in Figure II.12.

II.3.3 Particle Size Detector

The particle size detector measures the relative size of the scattering particles which generate the velocity measurements. Again, it is very difficult, if not impossible, to accurately size all scattering particles over the range of interest in a sediment-laden flow. This is particularly true for the larger sand grain sizes. The maximum amplitude of light scattering is dependent on the exact trajectory of the particle through the beam intersection. Knowledge of the trajectory of each particle is quite difficult to obtain. When the grains in motion become larger than the beam intersection volume, greater than 300 μm, the problem is even more complicated. It is, however, not difficult to distinguish the scattering from a fluid tracer particle and a sand grain.

The size detector consists of a set of four independent voltage comparators and latches. Each of the comparators produces one bit of the four bit size detector output. Thus, it is possible to divide the signals into five size groups. In practice, only three are needed. In order of increasing pedestal size, these are fluid tracer particles, unidentified scatterers, and sand grains.

The size detector circuit is shown in Figure II.13. The output of the initial 72733 amplifier is a-c coupled to remove the bias voltage, then low-pass filtered at 10 KHz to remove the Doppler modulation. The output of each of the 72810 comparators is low while the incoming filtered pedestal is less than the reference threshold voltage. The 72810 output is high while the pedestal is higher than the threshold. Each threshold level is adjusted by a 500 ohm potentiometer on the front panel. The voltage range on each is adjusted by selecting the resistors R_U and R_L. The upper and lower voltages are given by:

$$V_U = 5(500 + R_L)/500 + R_U + R_L$$

$$V_L = 5R_L/500 + R_U + R_L$$

The resistors and resulting voltage ranges as currently implemented are given in Table II.3. The outputs from the voltage comparators are latched by a 7496 shift resistor so that the maximum pedestal level is measured. The latch outputs are reset in State 1. The

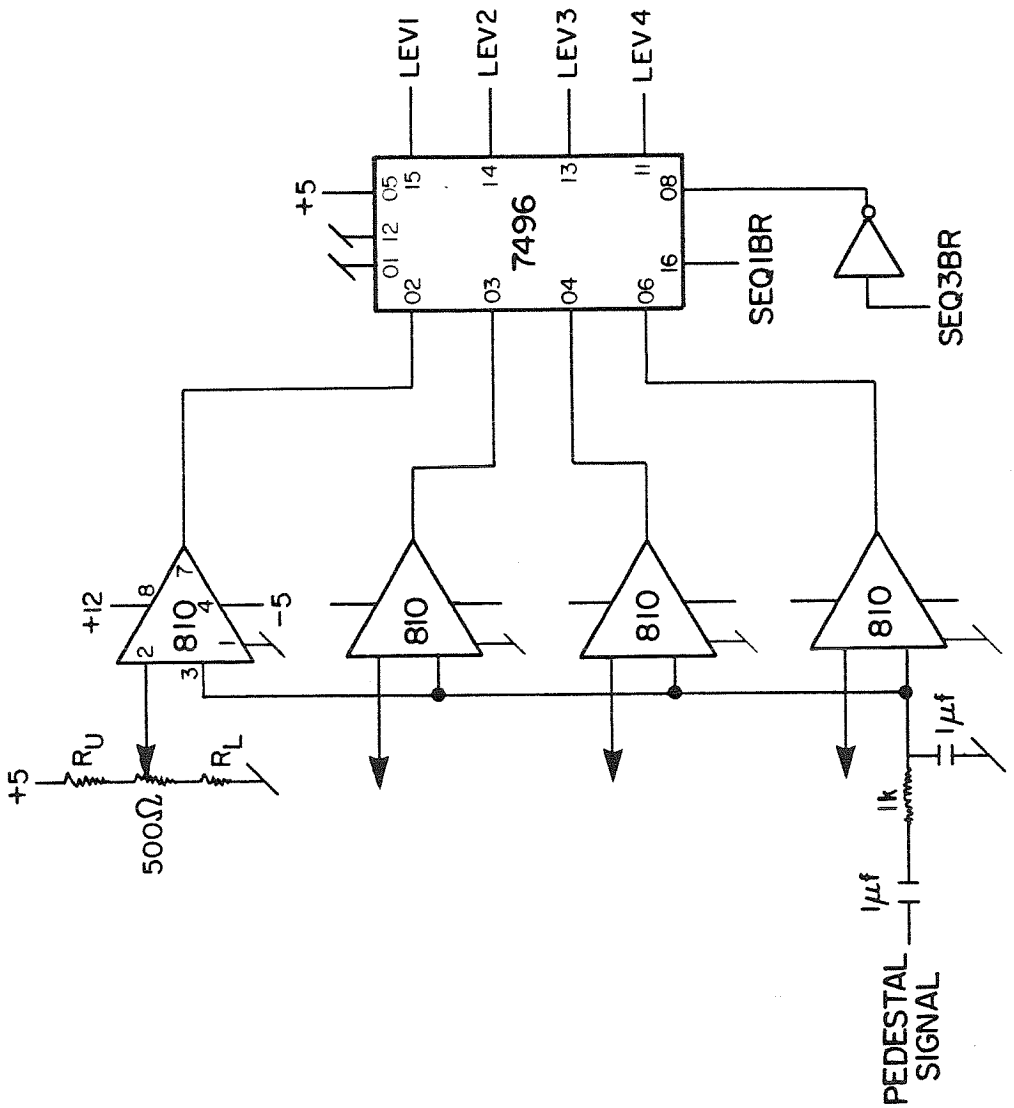

Figure II.13 Pedestal level detector circuit diagram

Table II.3 Resistors and resultant voltages for level detectors

$R_U(\Omega)$	$R_L(\Omega)$	V_U(mV)	V_L(mV)
6.2k	0	370	0
5.6k	0	410	0
3.0k	0	710	0
1.5k	0	1250	0

latches are enabled only in State 3, when an incoming Doppler burst is detected. The latch output is high if, at any instant during State 3, the corresponding voltage comparator output was high.

An example of how the size detector works is contained in Figure II.14. The solid line in Figure II.14.a is the filtered pedestal signal. The dotted lines are the preset thresholds. Two relevant state signals, SEQ1BR and SEQ3BR, are shown in Figures II.14.b and II.14.c. The output of each comparator is shown in Figure II.14.d. The resulting latched binary data are indicated.

By setting the threshold levels appropriately, it is possible to distinguish the very small fluid tracer particles. It is necessary to count enough zero-crossings to ensure that the maximum pedestal amplitude will occur during the counting period, State 3. A bit of experimentation is advised.

II.3.4 Interface to the PDP 11

The state control logic makes the interfacing of the two Doppler burst counters, the check counter and the particle size detector to an external data recording device simple. While the electronics were designed to interface to the laboratory PDP 11/60 via a DR11-K, the design is sufficiently general to allow the use of other interfaces, or, with slight modifications, other external devices.

The DR11-K is a digital interface with sixteen parallel data lines and two control lines. The first control line, EXT DATA RDY,

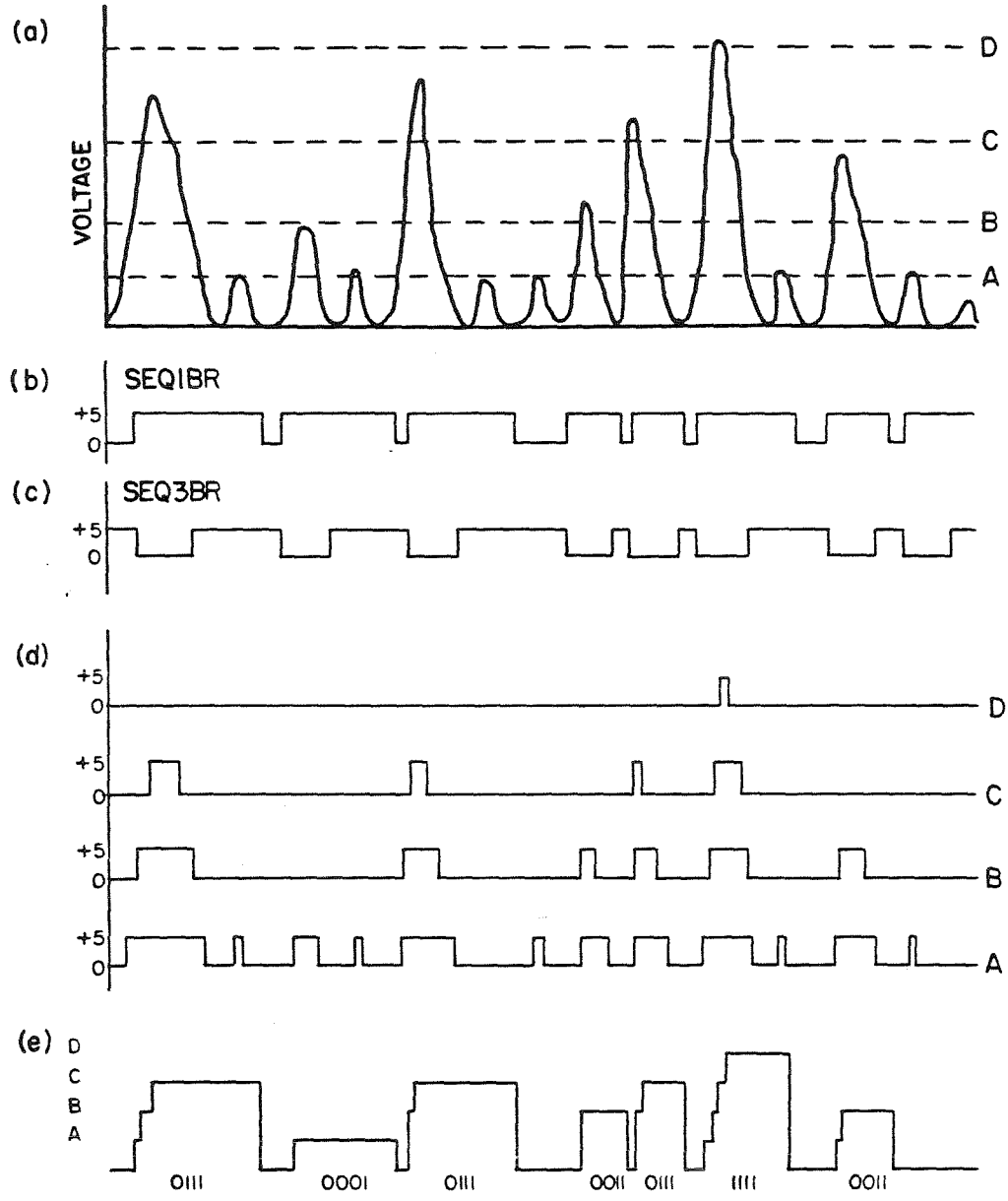

Figure II.14.a Incoming filtered pedestal signal

b SEQ1BR

c SEQ3BR

d Level detector outputs

e Latches particle size output (binary data indicated)

allows the external generation of an interrupt causing the signals on the data lines to be read into a word in memory under software control. The INT DATA ACC control line signals to the data transmitting device that the data lines have been read. Using both control lines, a handshaking process--"data ready"-"okay, data taken"--results. Data cannot be lost and the transmission is relatively free from transients on the data lines. It is the negative transition on either control line which forces the action. Similarly, bits in the resulting data word are set (made equal to 1) if the corresponding data line is low. This logic is used to give better immunity to transmission noise.

The transmission of data to the computer occurs during State 7 through State 0. In State 7, the internal PDPRDYBR signal is reset to high and an EXT DATA RDY signal is sent to the computer. The control logic enters State 5; the check counter and particle size measurement is held on the data lines. On receipt of the INT DATA ACC signal from the computer, PDPRDYBR goes low and the control logic enters State 4. The internal PDPRDYBR signal is again reset to high and a second EXT DATA RDY signal is sent to the computer. If two-dimensional measurements are being made, the control logic enters State 6 and the V burst counter measurement is held on the data lines. The control logic remains in State 6 until the computer responds with a second INT DATA ACC signal. On receipt of the new signal, the state logic enters State 2. The internal PDPRDYBR signal is reset, and a new EXT DATA RDY signal is sent to the

computer. The control logic enters State 0, and the U counter data is held on the output lines. The control logic waits in State 0 until the computer again responds with an INT DATA ACC signal. Thus, each cycle through the control logic states produces three data words. As explained previously, the first 16-bit data word consists of the 12-bit output of the check counter in the lower order bits and the relative particle size information in the upper 4 bits. The second and third words are the outputs of the V and U Doppler burst counters. If one-dimensional measurements are being made, the control logic does not enter States 6 and 2, but goes directly from State 4 to State 0. Two data words result, as the V counter output is not sent to the computer. The arrival of the data words may be timed using a KW11-K programmable clock or other similar peripheral device.

The EXT DATA RDY signal is the result of a logical nand of SEQ4BR, SEQ2BR, and SEQ7BR. The DR11-K expects an EXT DATA RDY signal lasting at least 0.5 microseconds. A 74123 one-shot is used to give the required pulse width. As shown in Figure II.15, the pulse width is 0.7 microseconds. To drive the signal over the transmission line, a 7406 is used. The 7406 inverts the incoming signal. A positive transition on the input to the one-shot will cause a negative transition at the DR11-K, forcing the data lines to be read.

The internal PDPRDYBR signal is the output of a 7474 flip-flop. The output is reset to high upon entry into State 4, State 2, or

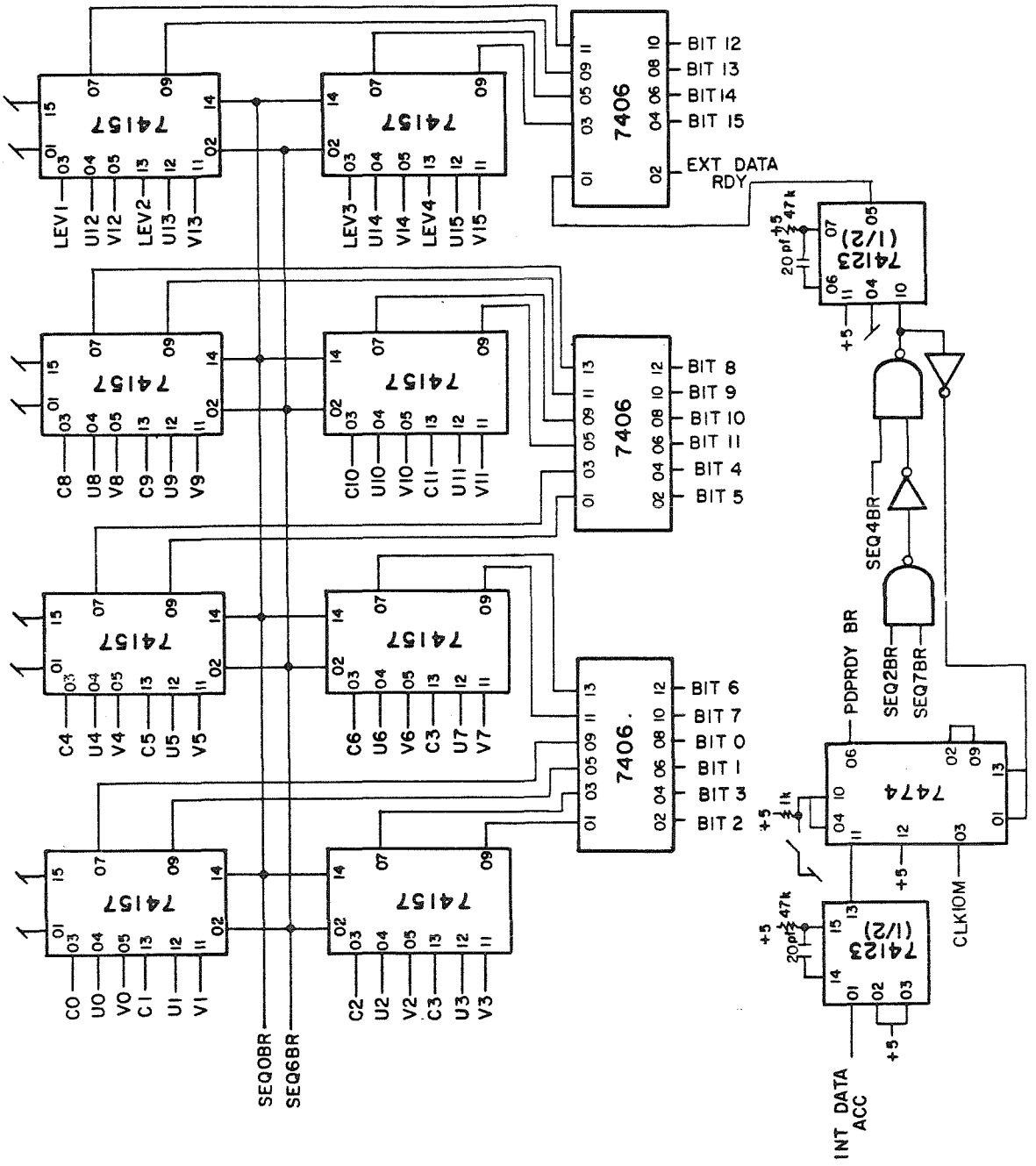

Figure II.15 Interface to DR-11-K circuit diagram

State 7. When the INT DATA ACC from the computer goes low, the computer should again be ready to receive new data. With some external devices or some computer operating systems, RSX-11M in particular, this may not be the case. A longer time delay between the receipt of an INT DATA ACC signal and the generation of the next EXT DATA RDY may be necessary. A 74123 one-shot is provided for this purpose. When the INT DATA ACC signal goes low, a longer negative going pulse is generated by the 74123. When this pulse goes high, PDPRDYBR goes low. The time delay is given by:

$$t_d = .25RC(1 + .7/R)$$

As shown, t_d is 3 microseconds. An external front panel switch, when closed, allows PDPRDYBR to be held low. This allows the processing electronics to be used without an external recording device.

The binary burst counter data is multiplexed onto the data lines by three 74157 chips, as shown in Figure II.15. When SEQ0BR is low, the U counter inputs are the outputs. When SEQ2BR is low, the V counter inputs are the outputs. Otherwise, the check counter and particle size detector inputs are the outputs. Again, 7406s are used to drive the data to the computer.

SECTION III

USAGE GUIDELINES

III.1 User Information

This section describes the use of the signal processing system documented in the previous section. Laser-Doppler velocimetry is not, alas, straightforward or foolproof in sediment-laden flows. Much trial and error is required. This section describes some of the difficulties involved and gives guides for their solution.

The largest problem encountered is identifying and discarding bursts generated by sand grains grazing the scattering volume without discarding the bulk of good fluid tracer particle bursts. Care must be taken not to band-pass filter the Doppler burst signal too sharply. If the pass band is too narrow, the mean measured Doppler frequency becomes a function of the filter settings, as the grazing grain generated bursts appear to be regular in frequency.

The relative occurrence of such bad bursts is primarily determined by the receiving optics. Accurate positioning of the pinhole is critical. The pinhole location determines the volume in the flow that is imaged by the collecting lens. If the imaged position is not within the beam intersection, scattering from the grazing grains predominates. The size of the pinhole determines the depth of field of the image. The smaller the pinhole, the smaller the depth of field. Thus, a small pinhole is desirable

because the imaged volume is minimized. However, the total intensity of collected light is also a function of the pinhole size. The smaller the pinhole, the less light is collected. It is recommended that the pinhole be roughly one-half the size of the image of the scattering volume at the pinhole. Experimentation with a few different pinhole sizes is recommended.

The use of a small pinhole may require the adjustment of the pinhole location as the scattering volume is moved vertically in the water column. Seldom are flume windows precisely parallel or optically flat. It is desirable that the pinhole at least remain in the focal plane of the scattering volume image as the volume is moved in the water column. The adjustment in this direction is the most critical and most difficult. Much trial and error is required. Horizontal and vertical adjustment of the pinhole within the focal plane of the image is not difficult and requires minimal time.

Selection of the number of fringes to be counted, the Doppler burst threshold level and the time constant, t_w, of Doppler signal regularity must be done with some care. A bad burst may remain somewhat regular for short periods of time, or may have many zero-crossings in a very short period of time. By counting a large number of zero-crossings, the inherent irregularity of a bad burst is more likely to become apparent. In addition, if an insufficient number of fringes is counted, the pedestal will not always achieve maximum amplitude while the burst is being counted. Particle size information will be unreliable. Counting at least 50 zero-crossings

is recommended. The threshold level must be set sufficiently low that scattering from the fluid tracer particles is not discarded. A low data acquisition rate may well be due to too high a threshold level. Also, the flow must be seeded correctly. It is tracer particle number density, not volumetric concentration, which is important. The timing constant, t_w, should be set as close to the expected period of the Doppler modulation as possible. The frequency as measured by the check counter and the U counter should agree. If the two measurements do not agree, most likely the signal was not regular in frequency and should be discarded by the data processing software.

Finally, note that the measured time for the preset number of counted zero-crossings in the check counter has only twelve bits. Thus, the maximum duration of counted zero-crossings that can be measured is 0.4095 msec. The reference time counter will continue to count beyond this time, but the user must realize that an overflow has taken place. For example, if 101 zero-crossings are counted and the reported time is 0.2572 msec, the actual Doppler frequency may be either 389 KHz or, if an overflow has occurred, 150 KHz.

III.2 Wiring Guidelines

Suggestions to aid in the construction of the electronics described in Section II are given in this section. Because of the high frequency and small amplitude of the Doppler modulated burst signal, reasonable care must be taken when constructing the processor.

The signal amplifiers should be physically separated from the digital electronics. In fact, it was found that the preamplifier should be separated from the Doppler burst amplifier. Each should be mounted in a separate, shielded box. Double-sided, ground plane printed circuit boards should be used. Breadboarding is not recommended. The two amplifiers may share a common ±5 volt power supply, but the power supply should not be shared with the digital electronics.

The digital electronics require ±5, ±15, and + 12 volt power supplies. A Power One model D5 used for the +5 volt power supply and two Standard Power model SPS 30D supplies used for the remaining voltages were more than adequate.

The bulk of the digital electronic connections were wire wrapped. This method allows easy alteration of the circuit. Three EECO model 55643 boards were used. These boards hold twenty-four sixteen-pin sockets. Pin assignments and connections are given in Appendix 1. Printed circuit boards were used for the 72810 chips in the particle size detector circuit and for the 72311 chips in the Doppler burst counter circuit. Again, the boards were ground plane boards. No shielding was found to be required. A single-sided printed circuit board was used for the Doppler burst counter D/A converter circuit and several additional 74128 line drivers. The added line drivers were used to display various signals on a small separate panel. The addition of this display ability is strongly

suggested. The choice of which signals to display will be left to the user. Signals which were found to be helpful in using the processor were GO, GOOD, SHORT, OVFL1, OVFL2, and SEQO.

Care must be taken when connecting the amplifiers to the digital electronics. Grounding the system was a problem. All ground connections should use 12 gage solid core wire. There are three grounds in the system: the analog ground, the digital logic ground, and the chassis ground. Keeping the digital ground completely separated from the analog ground is recommended. The filter should be grounded to the analog ground. The twisted pair cabling connects the digital ground to the ground of the computer or other external recording device. This connection must be made carefully, as the output signal cabling will act as an antenna otherwise.

REFERENCES

Digital Equipment Corporation (1978) Peripherals Handbook.

Durst, F., Melling, A., and Whitelaw, J. H. (1976) Principles and Practices of Laser-Doppler Anemometry. Academic Press, London.

Lancaster, D. (1974) TTL Cookbook.

Texas Instruments, Inc. (1976) The Linear and Interface Data Book for Design Engineers.

Texas Instruments, Inc. (1976) The TTL Data Book for Design Engineers.

APPENDIX 1

SIGNAL NAME GLOSSARY

CLK10M	10 MHz clock signal
DPSGNLU	when high, the incoming signal is a Doppler burst
DPLTCHUBR	when low, the incoming signal is a Doppler burst and the control logic is in State 3
DPPLSU	Doppler burst zero-crossing pulses
EXT DATA RDY	when high, a data word is ready to be sent to the mini-computer, the control logic is in State 7, State 4, or State 2
GO	when high, an incoming Doppler burst has been detected
GOOD	when high, a Doppler burst has been successfully counted, a good velocity measurement was made
INT DATA ACC	when low, the computer has read the counter data on the output lines
LSQBRST	Doppler burst level pulses, when high, the amplitude of the incoming signal is greater than the preset threshold level
OVFLU	when high, the preset number of zero-crossing pulses were successfully counted by the U burst counter
OVFLV	similar to OVFLU, but for the V burst counter
OVFLC	similar to OVFLU, but for the check counter
PDPRDYBR	when low, the mini-computer is ready to accept new data
SEQ0BR	when low, control logic is in State 0; control logic is holding U counter data on output lines
SEQ1BR	when low, control logic is in State 1, control logic is waiting for an incoming Doppler burst

SEQ2BR	when low, control logic is in State 2; control logic has sent EXT DATA RDY to the computer for V burst counter data
SEQ3BR	when low, control logic is in State 3; burst counters are counting a new Doppler burst
SEQ4BR	when low, control logic is in State 4; control logic has sent EXT DATA RDY to the computer for U burst counter data
SEQ5BR	when low, control logic is in State 5; control logic is holding check counter data on output lines
SEQ6BR	when low, control logic is in State 6; control logic is holding V counter data on output lines
SEQ7BR	when low, control logic is in State 7; control logic has sent EXT DATA RDY to the computer for check counter and particle size data
SU	U burst counter switch; when low, the U counter is not used
SV	similar to SU, but for the V burst counter
SC	similar to SU, but for the check counter
SHORT	when high, the Doppler burst could not be successfully counted, the signal level fell below the preset threshold level before the preset number of zero-crossings were counted

APPENDIX 2

WIRE-WRAP LISTING

MODULE PLACEMENT

SLOT	MODULE	DESCRIPTION
01A		RESISTOR NETWORK
02A	74123	ONE-SHOT
03A		COMPONENT CARRIER
04A	7474	D FLIP-FLOP
05A	7474	D FLIP-FLOP
06A	74161	COUNTER
11A	74161	COUNTER
12A	74161	COUNTER
13A	7408	2IN AND
14A	7496	SHIFT REGISTER
15A	7408	2IN AND
16A	7408	2IN AND
21A	7474	D FLIP-FLOP
22A	7408	2IN AND
23A	74153	MULTIPLEXER
24A	7402	2IN NOR
25A	74123	ONE-SHOT
26A		COMPONENT CARRIER

SLOT	MODULE	DESCRIPTION
01B		RESISTOR NETWORK
02B	74191	COUNTER
03B	74191	COUNTER
04B	74191	COUNTER
05B	7408	2IN AND
06B	74161	COUNTER
11B	74161	COUNTER
12B	74161	COUNTER
13B	74153	MULTIPLEXER
14B	74153	MULTIPLEXER
15B	74153	MULTIPLEXER
16B	74153	MULTIPLEXER
21B	MC4024	OSCILLATOR
22B	7404	INVERTER
23B	74153	MULTIPLEXER
24B	74S112	JK FLIP-FLOP
25B	7474	D FLIP-FLOP
26B	7432	2IN OR

SLOT	MODULE	DESCRIPTION
01C	7400	2IN NAND
02C	74191	COUNTER
03C	74191	COUNTER
04C	74191	COUNTER
05C	7400	2IN NAND
06C	74161	COUNTER
11C	74161	COUNTER
12C	74161	COUNTER
13C	74153	MULTIPLEXER
14C	74153	MULTIPLEXER
15C	74153	MULTIPLEXER
16C	74153	MULTIPLEXER
21C	7408	2IN AND
22C		COMPONENT CARRIER
23C	7442	BCD DECODER
24C	74S112	JK FLIP-FLOP
25C	7400	2IN NAND
26C	7404	INVERTER

SLOT	MODULE	DESCRIPTION
01D		
02D		
03D		
04D	7408	2IN NAND
05D	7404	INVERTER
06D	7474	D FLIP-FLOP
11D	74161	COUNTER
12D	74161	COUNTER
13D	—	
14D	7406	LINE DRIVER
15D	7406	LINE DRIVER
16D	7406	LINE DRIVER
21D	74128	LINE DRIVER
22D	74123	ONE-SHOT
23D	7474	D FLIP-FLOP
24D	7402	2IN NOR
25D	7402	2IN NOR
26D	7474	D FLIP-FLOP

01A RESISTOR NETWORK	02A 74123 ONE-SHOT	03A COMPONENT CARRIER
PIN SIGNAL	PIN SIGNAL	PIN SIGNAL
01 S1U	01 G02A08	01 R02A07
02 S2U	02 SQBRSTU	02 C02A06
03 S3U	03 VCC02A16	03 R02A15
04 S4U	04 DPPLSUBR	04 C02A14
05 S5U	05 DPPLSV	05
06 S6U	06 C02A06	06
07 S7U	07 R02A07	07
08	08 G02A08	08
09 S8U	09 G02A08	09
10 S1C	10 SQBRSTV	10
11 S2C	11 VCC02A16	11
12 S3C	12 DPPLSVBR	12
13 S4C	13 DPPLSU	13 R02A15
14 S5C	14 C02A14	14 VCC03A16
15 S6C	15 R02A15	15 R02A07
16	16 VCC02A16	16 VCC03A16

11A 74161 COUNTER	12A 74161 COUNTER	13A 7408 2IN AND
PIN SIGNAL	PIN SIGNAL	PIN SIGNAL
01 SEQ1BRU	01 SEQ1BRV	01 VCC13A16
02 CLK10MU	02 CLK10MV	02 SEQ1BRU
03	03	03 SEQ1BRU
04	04	04 VCC13A16
05	05	05 SEQ1BRU
06	06	06 SEQ1BRV
07 VCC11A16	07 VCC12A16	07 G13A08
08	08	08 G13A08
09	09	09
10 ENBLTMU	10 ENBLTMV	10 CLK10MU
11 U3	11 V3	11 VCC13A16
12 U2	12 V2	12 CLK10M
13 U1	13 V1	13 CLK10MV
14 U0	14 V0	14 VCC13A16
15 RPLUT1	15 RPLVT1	15 CLK10M
16 VCC11A16	16 VCC12A16	16 VCC13A16

21A 7474 D FLIP-FLOP	22A 7408 2IN AND	23A 74153 MULTIPLEXER
PIN SIGNAL	PIN SIGNAL	PIN SIGNAL
01 VCC21A16	01 DPSGNLU	01 G23A08
02 DPLTCHU	02 DPSGNLV	02 SV
03 CLK10M	03 DPSGNLUV	03 LTCHOVUV
04 SEQ1BR	04 OVFLUS	04 LTCHOVV
05 DPLTCHUS	05 OVFLVS	05 LTCHOVU
06	06 OVFLUV	06 G23A08
07 G21A08	07 G22A08	07 SHORT
08 G21A08	08 G22A08	08 G23A08
09	09	09
10	10	10
11 DPLTCHVS	11	11
12 SEQ1BR	12	12
13 CLK10M	13	13
14 DPLTCHV	14	14 SU
15 VCC21A16	15	15
16 VCC21A16	16	16

04A
7474 D FLIP-FLOP

PIN	SIGNAL
01	SEQ3
02	VCC04A16
03	DPPLSU
04	VCC04A16
05	SEQPLSU
06	
07	G04A08
08	G04A08
09	
10	
11	SEQPLSV
12	VCC04A16
13	DPPLSV
14	VCC04A16
15	SEQ3
16	VCC04A16

05A
7474 D FLIP-FLOP

PIN	SIGNAL
01	SEQ3
02	VCC05A16
03	CLKU
04	VCC05A16
05	CLKUQ
06	
07	G05A08
08	G05A08
09	
10	
11	CLKVQ
12	VCC05A16
13	CLKV
14	VCC05A16
15	SEQ3
16	VCC05A16

06A
74161 COUNTER

PIN	SIGNAL
01	SEQ1BRC
02	CLK10MU
03	
04	
05	
06	
07	VCC06A16
08	
09	
10	ENBLTMC
11	C3
12	C2
13	C1
14	C0
15	RPLCT1
16	VCC06A16

14A
7496 SHIFT REG

PIN	SIGNAL
01	G14A08
02	LEV1
03	LEV2
04	LEV3
05	VCC15A16
06	LEV4
07	
08	SEQ3L
09	
10	
11	C15
12	G14A08
13	C14
14	C13
15	C12
16	SEQ1BRL

15A
7408 2IN AND

PIN	SIGNAL
01	VCC15A16
02	SEQ1BRD
03	SEQ1BRF
04	VCC15A16
05	SEQ1BRD
06	SEQ1BRC
07	G15A08
08	G15A08
09	
10	SEQ1BRL
11	SEQ1BRD
12	VCC15A16
13	
14	VCC15A16
15	
16	VCC15A16

16A
7400 2IN NAND

PIN	SIGNAL
01	SEQ6BR
02	SEQ5BR
03	MUXBB
04	SEQ6BR
05	SEQ5BR
06	MUXBC
07	G16A08
08	G16A08
09	
10	MUXAB
11	SEQ5BR
12	SEQ0BR
13	MUXAC
14	SEQ5BR
15	SEQ0BR
16	

24A
7402 2IN NOR

PIN	SIGNAL
01	LTCHOVUVBR
02	LTCHOVV
03	LTCHOVU
04	LTCHOVUV
05	LTCHOVUVBR
06	G24A08
07	G24A08
08	G24A08
09	
10	DPLTCHUS
11	OVFLUS
12	LTCHOVU
13	DPLTCHVS
14	OVFLVS
15	LTCHOVV
16	

25A
74123 ONE-SHOT

PIN	SIGNAL
01	G25A08
02	LBRSTU
03	VCC25A16
04	DPSGNLUBR
05	DPSGNLV
06	C25A06
07	R25A07
08	G25A08
09	G25A08
10	LBRSTV
11	VCC25A16
12	DPSGNLVBR
13	DPSGNLU
14	C25A14
15	R25A15
16	VCC25A16

26A
COMPONENT CARRIER

PIN	SIGNAL
01	R26A15
02	R26A07
03	SU
04	SV
05	SC
06	SRSTB
07	SRSTB
08	
09	
10	SRT
11	VCC26A16
12	VCC26A16
13	VCC26A16
14	VCC26A16
15	VCC26A16
16	VCC26A16

60

01B
RESISTOR NETWORK

PIN	SIGNAL
01	S7C
02	S8C
03	S1V
04	S2V
05	S3V
06	S4V
07	S5V
08	
09	S6V
10	S7V
11	S8V
12	
13	
14	
15	
16	

02B
74191 COUNTER

PIN	SIGNAL
01	S2U
02	
03	
04	ENBLPLU
05	VCC02B16
06	
07	
08	
09	S4U
10	S3U
11	SEQ1BRP
12	MINU1
13	RPLU
14	CLKU
15	S1U
16	VCC02B16

03B
74191 COUNTER

PIN	SIGNAL
01	S2C
02	
03	
04	ENBLPLC
05	VCC03B16
06	
07	
08	
09	S4C
10	S3C
11	SEQ1BRP
12	MINC1
13	RPLC
14	CLKU
15	S1C
16	VCC03B16

11B
74161 COUNTER

PIN	SIGNAL
01	SEQ1BRU
02	CLK10MU
03	
04	
05	
06	
07	VCC11B16
08	
09	
10	RPLUT1
11	U7
12	U6
13	U5
14	U4
15	RPLUT2
16	VCC11B16

12B
74161 COUNTER

PIN	SIGNAL
01	SEQ1BRV
02	CLK10MV
03	
04	
05	
06	
07	VCC12B16
08	
09	
10	RPLVT1
11	V7
12	V6
13	V5
14	V4
15	RPLVT2
16	VCC12B16

13B
74153 MULTIPLEXER

PIN	SIGNAL
01	G13B08
02	MUXBB
03	C0
04	V0
05	U0
06	G13B08
07	M0
08	G13B08
09	M1
10	G13B08
11	U1
12	V1
13	C1
14	MUXAB
15	G13B08
16	

21B
OSCILLATOR

PIN	SIGNAL
01	VCC21B16
02	CLKP
03	CLKC1
04	CLKC2
05	G21B08
06	CLK10M
07	G21B08
08	G21B08
09	
10	
11	G21B08
12	
13	
14	
15	
16	VCC21B16

22B
7404 INVERTER

PIN	SIGNAL
01	SRSTB
02	MSTRST
03	MSTRST
04	MSTRSTBRI
05	DTRDY
06	DTRDYBR
07	G22B08
08	G22B08
09	
10	
11	
12	
13	
14	CLK10MBR
15	CLK10M
16	

23B
74153 MULTIPLEXER

PIN	SIGNAL
01	G23B08
02	SV
03	DPSGNLUV
04	DPSGNLV
05	DPSGNLU
06	G23B08
07	GO
08	G23B08
09	GOOD
10	G23B08
11	OVFLUS
12	OVFLVS
13	OVFLUV
14	SU
15	G23B08
16	

04B	05B	06B
74191 COUNTER	7408 2IN AND	74161 COUNTER
PIN SIGNAL	PIN SIGNAL	PIN SIGNAL
01 S2V	01 CLKUQ	01 SEQ1BRC
02	02 OVFLUBR	02 CLK10MU
03	03 ENBLTMU	03
04 ENBLPLV	04 CLKUQ	04
05 VCC04B16	05 OVFLCBR	05
06	06 ENBLTMC	06
07	07 G05B08	07 VCC06B16
08	08 G05B08	08
09 S4V	09	09
10 S3V	10 ENBLTMV	10 RPLCT1
11 SEQ1BRP	11 OVFLVBR	11 C7
12 MINV1	12 CLKVQ	12 C6
13 RPLV	13	13 C5
14 CLKV	14	14 C4
15 S1V	15	15 RPLCT2
16 VCC04B16	16	16 VCC06B16

14B	15B	16B
74153 MULTIPLEXER	74153 MULTIPLEXER	74153 MULTIPLEXER
PIN SIGNAL	PIN SIGNAL	PIN SIGNAL
01 G14B08	01 G15B08	01 G16B08
02 MUXBB	02 MUXBB	02 MUXBB
03 C2	03 C4	03 C6
04 V2	04 V4	04 V6
05 U2	05 U4	05 U6
06 G14B08	06 G15B08	06 G16B08
07 M2	07 M4	07 M6
08 G14B08	08 G15B08	08 G16B08
09 M3	09 M5	09 M7
10 G14B08	10 G15B08	10 G16B08
11 U3	11 U5	11 U7
12 V3	12 V5	12 V7
13 C3	13 C5	13 C7
14 MUXAB	14 MUXAB	14 MUXAB
15 G14B08	15 G15B08	15 G16B08
16	16	16

24B	25B	26B
74S112 JK FLIP-FLOP	7474 D FLIP-FLOP	7432 2IN OR
PIN SIGNAL	PIN SIGNAL	PIN SIGNAL
01 CLK10MBR	01 VCC25B16	01 FF1JA
02 FF2K	02 G25B08	02 FF1JB
03 FF2J	03 DPSGNLUBR	03 FF1J
04 VCC24B16	04 SEQ1BR	04 FF2KA
05 FF2	05 DPLTCHU	05 FF2KB
06	06 DPLTCHUBR	06 FF2K
07	07 G25B08	07 G26B08
08	08 G25B08	08 G26B08
09	09	09
10	10 DPLTCHVBR	10
11	11 DPLTCHV	11
12	12 SEQ1BR	12
13	13 DPSGNLVBR	13 FF1K
14	14 G25B08	14 FF1KB
15 MSTRSTBRI	15 VCC25B16	15 FF1KA
16 VCC24B16	16 VCC25B16	16

01C	02C	03C
7400 2IN NAND	74191 COUNTER	74191 COUNTER
PIN SIGNAL	PIN SIGNAL	PIN SIGNAL
01 SEQPLSV	01 S6U	01 S6C
02 DPPLSVBR	02	02
03 CLKV	03	03
04 SEQPLSU	04 RPLU	04 RPLC
05 DPPLSUBR	05 VCC02C16	05 VCC03C16
06 CLKU	06	06
07 G01C08	07	07
08 G01C08	08	08
09	09 S8U	09 S8C
10	10 S7U	10 S7C
11	11 SEQ1BRP	11 SEQ1BRP
12	12 MINU2	12 MINC2
13	13	13
14	14 CLKU	14 CLKU
15	15 S5U	15 S5C
16	16 VCC02C16	16 VCC03C16

11C	12C	13C
74161 COUNTER	74161 COUNTER	74153 MULTIPLEXER
PIN SIGNAL	PIN SIGNAL	PIN SIGNAL
01 SEQ1BRU	01 SEQ1BRV	01 G13C08
02 CLK10MU	02 CLK10MV	02 MUXBB
03	03	03 C8
04	04	04 V8
05	05	05 U8
06	06	06 G13C08
07 VCC11C16	07 VCC12C16	07 M8
08	08	08 G13C08
09	09	09 M9
10 RPLUT2	10 RPLVT2	10 G13C08
11 U11	11 V11	11 U9
12 U10	12 V10	12 V9
13 U9	13 V9	13 C9
14 U8	14 V8	14 MUXAB
15 RPLUT3	15 RPLVT3	15 G13C08
16 VCC11C16	16 VCC12C16	16

21C	22C	23C
7408 2IN AND	COMPONENT CARRIER	7442 BCD ENCODER
PIN SIGNAL	PIN SIGNAL	PIN SIGNAL
01 VCC21C16	01 SMAN	01 SEQ0BR
02	02 R22D07	02 SEQ1BR
03	03 R22D07	03 SEQ2BR
04 VCC21C16	04 R22D15	04 SEQ3BR
05 SEQ1BR	05 R22D15	05 SEQ4BR
06 SEQ1BRO	06 CLKP	06 SEQ5BR
07 G21C08	07 CLKC2	07 SEQ6BR
08 G21C08	08	08 G23C08
09	09	09 SEQ7BR
10	10 CLKC1	10
11 VCC21C16	11 VCC22C16	11
12	12 C22D14	12 G23C08
13 MSTRSTBR	13 VCC22C16	13 FF2
14 VCC21C16	14 C22D06	14 FF1
15 MSTRSTBRI	15 VCC22C16	15 FF0
16 VCC21C16	16 VCC22C16	16

04C
74191 COUNTER

PIN	SIGNAL
01	S6V
02	
03	
04	RPLV
05	VCC04C16
06	
07	
08	
09	S8V
10	S7V
11	SEQ1BRP
12	MINV2
13	
14	CLKV
15	S5V
16	VCC04C16

05C
7400 2IN NAND

PIN	SIGNAL
01	OVFLUBR
02	DPLTCHU
03	ENBLPLU
04	OVFLCBR
05	DPLTCHU
06	ENBLPLC
07	G05C08
08	G05C08
09	
10	
11	
12	
13	ENBLPLV
14	DPLTCHV
15	OVFLVBR
16	

06C
74161 COUNTER

PIN	SIGNAL
01	SEQ1BRC
02	CLK10MU
03	
04	
05	
06	
07	VCC06C16
08	
09	
10	RPLCT2
11	C11
12	C10
13	C9
14	C8
15	
16	VCC06C16

14C
74153 MULTIPLEXER

PIN	SIGNAL
01	G14C08
02	MUXBB
03	C10
04	V10
05	U10
06	G14C08
07	M10
08	G14C08
09	M11
10	G14C08
11	U11
12	V11
13	C11
14	MUXAB
15	G14C08
16	

15C
74153 MULTIPLEXER

PIN	SIGNAL
01	G15C08
02	MUXBB
03	C12
04	V12
05	U12
06	G15C08
07	M12
08	G15C08
09	M13
10	G15C08
11	U13
12	V13
13	C13
14	MUXAB
15	G15C08
16	

16C
74153 MULTIPLEXER

PIN	SIGNAL
01	G16C08
02	MUXBB
03	C14
04	V14
05	U14
06	G16C08
07	M14
08	G16C08
09	M15
10	G16C08
11	U15
12	V15
13	C15
14	MUXAB
15	G16C08
16	

24C
74S112 JK FLIP-FLOP

PIN	SIGNAL
01	CLK10MBR
02	FF0K
03	FF0J
04	MSTRSTBR
05	FF0
06	
07	
08	
09	FF1
10	VCC24C16
11	FF1J
12	FF1K
13	CLK10MBR
14	MSTRSTBR
15	VCC24C16
16	VCC24C16

25C
7400 2IN NAND

PIN	SIGNAL
01	SEQ2BR
02	SEQ7BR
03	FF1KBR
04	SEQ4BR
05	DTRDYI
06	DTRDY
07	G25C08
08	G25C08
09	
10	DTRDYI
11	FF1KB
12	VCC25C16
13	
14	
15	
16	VCC25C16

26C
7404 INVERTER

PIN	SIGNAL
01	GO
02	GOBR
03	GOOD
04	GOODBR
05	SHORT
06	SHORTBR
07	G26C08
08	G26C08
09	
10	VOFF
11	SV
12	
13	
14	
15	
16	

64

01D	02D	03D
PIN SIGNAL	PIN SIGNAL	PIN SIGNAL
01	01	01
02	02	02
03	03	03
04	04	04
05	05	05
06	06	06
07	07	07
08	08	08
09	09	09
10	10	10
11	11	11
12	12	12
13	13	13
14	14	14
15	15	15
16	16	16
11D	12D	13D
74161 COUNTER	74161 COUNTER	
PIN SIGNAL	PIN SIGNAL	PIN SIGNAL
01 SEQ1BRU	01 SEQ1BRV	01
02 CLK10MU	02 CLK10MV	02
03	03	03
04	04	04
05	05	05
06	06	06
07 VCC11D16	07 VCC12D16	07
08	08	08
09	09	09
10 RPLUT3	10 RPLVT3	10
11 U15	11 V15	11
12 U14	12 V14	12
13 U13	13 V13	13
14 U12	14 V12	14
15	15	15
16 VCC11D16	16 VCC12D16	16
21D	22D	23D
74128 LINE DRIVER	74123 ONE-SHOT	7474 D FLIP-FLOP
PIN SIGNAL	PIN SIGNAL	PIN SIGNAL
01 EXDTRDYO	01 INTDTACC	01 DTRDYBR
02 EDTDRY	02 VCC22D16	02 PDPI
03 EDTRDY	03 VCC22D16	03 CLK10MBR
04 SEQ3D	04 STDRY	04 SMAN
05 SEQ3BR	05 EDTRDY	05 PDPRDY
06 SEQ3BR	06 C22D06	06 PDPRDYBR
07 G21D08	07 R22D07	07 G23D08
08 G21D08	08 G22D08	08 G23D08
09	09 G22D08	09
10 SEQ1BR	10 DTRDY	10
11 SEQ1BR	11 VCC22D16	11 PDPI
12 SEQ1D	12	12 SMAN
13	13 SPDPRDY	13 STDRY
14	14 C22D14	14 VCC23D16
15	15 R22D15	15 DTRDYBR
16	16 VCC22D16	16 VCC23D16

04D
7408 2IN AND

PIN	SIGNAL
01	MINU1
02	MINU2
03	OVFLU
04	MINV1
05	MINV2
06	OVFLV
07	G04D08
08	G04D08
09	
10	OVFLC
11	MINC1
12	MINC2
13	
14	
15	
16	

05D
7404 INVERTER

PIN	SIGNAL
01	SEQ3BR
02	SEQ3
03	OVFLU
04	OVFLUBR
05	OVFLC
06	OVFLCBR
07	G05D08
08	G05D08
09	
10	OVFLVBR
11	OVFLV
12	SEQ3L
13	SEQ3BR
14	
15	
16	

06D
7474 D FLIP-FLOP

PIN	SIGNAL
01	SEQ1BRU
02	OVFLU
03	CLK10MU
04	VCC06D16
05	OVFLUS
06	
07	G06D08
08	G06D08
09	
10	
11	OVFLVS
12	VCC06D16
13	CLK10MV
14	OVFLV
15	SEQ1BRV
16	VCC06D16

14D
7406 LINE DRIVER

PIN	SIGNAL
01	
02	M2
03	BIT2
04	M3
05	BIT3
06	M8
07	BIT8
08	
09	BIT9
10	M9
11	BIT0
12	M0
13	BIT1
14	M1
15	VCC14D16
16	VCC14D16

15D
7406 LINE DRIVER

PIN	SIGNAL
01	
02	M4
03	BIT4
04	M5
05	BIT5
06	M10
07	BIT10
08	
09	BIT11
10	M11
11	BIT12
12	M12
13	BIT13
14	M13
15	VCC15D16
16	VCC15D16

16D
7406 LINE DRIVER

PIN	SIGNAL
01	
02	M6
03	BIT6
04	M7
05	BIT7
06	EDTRDY
07	EXDTRDY
08	
09	
10	
11	BIT14
12	M14
13	BIT15
14	M15
15	VCC16D16
16	VCC16D16

24D
7402 2IN NOR

PIN	SIGNAL
01	FF0J
02	SEQ0BR
03	PDPRDYBR
04	FF0K
05	PFPRDYBR
06	SEQ5BR
07	G24D08
08	G24D08
09	
10	PDPRDYBR
11	SEQ6BR
12	FF2KA
13	SEQ3BR
14	GOODBR
15	FF2J
16	

25D
7402 2IN NOR

PIN	SIGNAL
01	FF1KA
02	SEQ3BR
03	SHORTBR
04	FF2KB
05	SV
06	SEQ4BR
07	G25D08
08	G25D08
09	
10	SEQ1BR
11	GOBR
12	FF1JA
13	SEQ4BR
14	VOFF
15	FF1JB
16	

26D
7474 D FLIP-FLOP

PIN	SIGNAL
01	VCC26D16
02	GOBR
03	CLK10MBR
04	VCC26D16
05	GOBRS
06	
07	G26D08
08	G26D08
09	
10	
11	
12	
13	
14	
15	
16	

66

PIN INTERCONNECTIONS

01C06=03C14=02C14=02B14=03B14-05A03

13B02=14B02=15B02=16B02=16A03

13C02=14C02=15C02=16C02=16A06

21C06=15A05=15A02=13A02=13A05-15A11

11D01=11C01=11B01=11A01=13A03-06D01

12A02=13A06=12B02=12C02=12D02-06D13

12D01=12C01=12B01=12A01=13A06-06D15

04A15=04A01=05A01-05A15=05D02

13B14=14B14=15B14=16B14=16A10

13C14=14C14=15C14=16C14=16A13

06D05=23B11=22A04=24A11=23B11

06D11=24A14=22A05=23B12=24A14

28D05=26C11=26A04=23D02=28B02

11D02=06C02=11C02=11B02=06B02=06A02=11A02=13A10-06D03

04C11=03C11=02C11=02B11=03B11=04B11=15A03

21D10=21D11=21C05=23C02=25B04=25B12=25D10-21A04-21A12

24D13=05D01=25D02=23C04=21B05=21D06=05D13=

05A16-05A14-05A12-05A04-05A02

67

21B11-21B05-21B07-21B08

21C07-21C08

22B02-22B03

21D07-21D08

15A07-15A08

24A06-24A07-24A08

15B01-15B15-15B10-15B06-15B08

15C01-15C15-15C06-15C08-15C10

15D07-15D08

24D07-24D08

01C07-01C08

04A07-04A08

13A07-13A08

22A07-22A08

13B01-13B15-13B10-13B06-13B08

22B07-22B08

13C15-13C01-13C06-13C08-13C10

04D07-04D08

13D07-13D08

22D08-22D09

16A07-16A08

25A01-25A08-25A09

16B01-16B15-16B10-16B06-16B08

25B02-25B14-25B07-25B08

16C01-16C15-16C06-16C08-16C10

25C07-25C08

16D07-16D08

25D07-25D08

04B12-04D04

04C12-04D05

11C13-13C11

11C11-14C11

12C14-13C04

06C11-14C13

11A11-14B11

06A12-14B03

12C12-14C04

02B04-05C03

03B04-05C06

04B04-05C13

11A10-05B03

06A10-05B06

12A10-05B10

14A15-15C03

11B14-15B05

16C05-11D12

14A16-15A10

12A11-14B12

12A12-14B04

23C03-25C01

15C12-12D13

14A08-05D12

14A11-16C13

23C15-24C05

06B13-15B13

68

02A11-02A03-02A16

02B05-02B16

04A16-04A12-04A14-04A02-04A04

02C05-02C16

06A07-06A16

06B07-06B16

06C07-06C16

03B05-03B16

03C05-03C16

04B05-04B16

04C05-04C16

03A14-03A16

02A01-02A08-02A09

24A01-24A05

11A07-11A16

11B07-11B16

13A11-13A14-13A16-13A01-13A04

11C07-11C16

15A04-15A12-15A14-15A16-15A01

06D04-06D12-06D16

11D07-11D16

12A07-12A16

12B07-12B16

12C07-12C16

12D07-12D16

21C11-21C14-21C16-21C01-21C04

22D16-22D02-22D03-22D11

25A04-25B03

25A12-25B13

02A12-01C02

02A04-01C05

02A13-04A03

02A05-04A13

23C14-24C09

03B13-03C04

06A15-06B10

06B15-06C10

06B12-16B03

11A14-13B05

22C10-21B03

22C07-21B04

15C04-12D14

06B14-15B03

03B12-04D11

03C12-04D12

23D02-23D11

04D10-05D05

11C14-13C05

22A06-23B13

11C12-14C05

12H11-16B12

20C10-25D14

06A13-13B13

69

22C04=22C05=22D15

13C09=14D10

14C09=15D10

01A11=03B01

01A01=02B15

16C04=12D12

26B10=24C02

22A03=23B03

24C05=24D04

06D07-06D08

15C05=11D14

21A06-24A10

21A11-24A13

12C13=13C12

12C11=14C12

06A11=14B13

14A14=16C13

23D06=24D03=24D05=24D10

16A12=16A15=23C01=24D02

22B15=21B06=13A12=13A15-21A03-21A13

15A06=06A01=06B01=06C01

24B01=22B14=24C01=24C13-24D03-23D03

26A06=26A07=22B01

25D06=25D13=25C04=23C05

24D11=23C07=16A01=16A04

21A02=25B05=05C02=05C05

23B14-26A03=23A14

23D01-23D15-22B06

01A05=02C15

01B07=04C15

13B07=14D12

01A09=02C09

13C07=14D06

01B11=04C09

14C07=15D06

01A10=03B15

23A04=24A02=24A15

23A05=24A03=24A12

14B09=14D04

15C09=15D14

22A01=23B05=25A13

25A05=23B04=22A02

01A13=03B09

01A03=02B10

01B05=04B10

22B05=25C06=22D10

05B05=05C04=05D06

16B07=16D02

01B01=03C10

05B02=05C01=05D04

05B11=05C15=05D10

01A06=02C01

01B09=04C01

13B09=14D14

22C02-22C03=22D07

70

01B03-04B15

15B07-15D02

16C07-16D12

05A05-05B01-05B04

26B14-25C03-25C11

01A14-03C15

01A04-02B09

22C01-23D04-23D12

24B15-22B04-21C15

21C13-24C04-24C14

02A07-03A01-03A15

02A15-03A03-03A13

01B06-04B09

21D02-21D03-22D05

04B14-04C14-01C03-05A13

01B02-03C09

16B09-16D04

01A07-02C10

01B10-04C10

14B07-14D02

15C07-15D12

01A12-03B10

01A02-02B01

01B04-04B01

16C09-16D14

05C14-21A14-25A11

15A09-15D04

04A05-01C04

05A07-05A08

02A06-03A02

02A14-03A04

22C06-21B02

11B12-16B05

26A03-24C11

26B01-25D12

26B02-25D15

04A11-01C01

06C13-13C13

16C12-12D11

26B13-24C12

26B15-25D01

12B13-15B12

24B05-23C13

02B13-02C04

11A15-11B10

11B15-11C10

11C15-11D10

06A11-16B13

04A13-04C04

11A13-13B11

12A15-12B10

12A15-12C10

12C15-12D10

02A12-04D01

02C12-04D02

12A14-13B04

05B12-05A11

25D11-26D05

23D14-23D16

24B04-24B16

25B15-25B16-25B01

24C10-24C15-24C16

25A11-25A03-25A16

21B01-21B16

21A15-21A16-21A01

26A13-26A14-26A15-26A16

22C13-22C15-22C16

14A01-14A12-15A08

05B07-05B08

23A01-23A06-23A08

14B01-14B15-14B10-14B06-14_B08

05C07-05C08

23B01-23B15-23B10-23B06-23_B08

14C01-14C15-14C06-14C08-14_C10

05D07-05D08

23C08-23C12

14D07-14D08

23D07-23D08

26B07-26B08

26C07-26C08

26D07-26D08

05D03-06D02-04D03

05D11-06D14-04D06

26D01-26D04-26D16

15C11-11D13

23C06-24D06

24B03-24D15

11B11-16B11

23C09-25C02

24B02-26B06

26B04-24D12

26B05-25D04

12B12-16B04

06A14-13B03

14A13-16C03

23B09-26C03

26C06-25D03

23B07-26C01

23A07-26C05

06C14-13C03

24C03-24D01

12B14-15B04

11A12-14B05

06C12-14C03

12A13-13B12

26C02-26D02

26C04-24D14

25C05-25C10

25C12-25C16

23A03-24A04

16C11-11D11

11H13-15B11

APPENDIX B

GUIDELINES FOR THE ACQUISITION AND PRELIMINARY ANALYSIS OF LASER-DOPPLER VELOCIMETRY DATA IN SEDIMENT-LADEN FLOWS

GUIDELINES FOR THE ACQUISITION AND PRELIMINARY ANALYSIS OF LASER-DOPPLER VELOCIMETRY DATA IN SEDIMENT-LADEN FLOWS

by

Catharine van Ingen

Supported by:

National Science Foundation
Grant Numbers ENG75-15786 and ENG77-10182

W. M. Keck Laboratory of Hydraulics and Water Resources
Division of Engineering and Applied Science
California Institute of California
Pasadena, California

Technical Memorandum 81-1 October 1981

ACKNOWLEDGEMENTS

The methodology herein described was developed with the assistance of several people. Most importantly, the author would like to thank Dr. Eric Siskind of N.Y.C.B., Inc. His many clear explanations of software-hardware interactions, or non-interactions, continue to amaze and educate the author. Discussions with Mark Bartelt, Robert Landau, Greg Gartrell and E. John List yielded many helpful suggestions. Pat Houseworth, Melinda Hendrix-Werts and Phil Dube assisted in the preparation of the manuscript. This work was supported by the National Science Foundatation under Grant Numbers ENG75-15786 and ENG77-10182 (Principal Investigator Norman Herrick Brooks) and was done in conjunction with the author's thesis research on the mechanisms of entrainment and suspension in sediment-laden flows.

TABLE OF CONTENTS

LIST OF FIGURES

LIST OF TABLES

I. Introduction

Laser-Doppler velocimetry has become a standard technique for the measurement of velocities in homogeneous fluid flows. Application of the technique to two-phase flows, particularly those flows transporting solid particles, is not yet so common.

In homogeneous fluid flows, the laser-Doppler technique depends on the presence of small light scattering particles. These scattering particles are small enough, typically on the order of a few microns, to follow the small scale fluid flow. Ideally, their particle number density is arranged such that only one particle is present in the beam measurement volume at any given time and particles pass through the beam measurement volume sufficiently often to give the desired time resolution to the velocimetry record. In fluid flows transporting solid particles, the solid particles also scatter light, thus generating velocimetry data. The solid particles need not be small with respect to the small scale fluid motion and their particle number density is determined by the nature of the flow. For the laser-Doppler technique to be useful in solid-fluid flows, the signals generated by the two types of scattering particles must be distinguishable.

A simple system for laser-Doppler velocimetry in sediment-laden flows has been developed and described in a previous report, van Ingen (1980). That report described the optical arrangement and signal processing electronics. This report discusses the use of the system for one-dimensional velocimetry in sediment-laden flows. The procedures described may be simply extended for a two-dimensional velocimetry system. The form of the data, the difficulties involved,

and the philosophy behind the data acquisition and processing are given in Section II. The details of the initial data acquisition and data checking are discussed in Section III. Suggestions for the improvement of the counter-processor are given. Section IV describes the final data validation procedures.

This report is not meant as an introduction to laser-Doppler velocimetry, digital electronics, real-time data acquisition, or computer programming techniques. The reader is assumed to be familiar with the contents of the previous report.

II. System Use Overview

The velocimetry data are obtained in real time using the counter-processor and the laboratory mini-computer. A velocimetry event occurs when the counter-processor successfully detects a burst signal, determines the burst frequency, and reports the measurement to the computer. Each event generates a set of three data words. The upper four bits of the first word contain the output of the particle size detector. The remaining bits contain the output of the "C", or check, Doppler burst counter. The second word is the output of the "U" Doppler burst counter. The third word is the relative time of the measurement as determined by the internal computer clock.

The relative size of the scattering particle is determined by the relative amplitude of the light scattered by that particle. Sand grains scatter more light than fluid tracer particles. There are four amplitude discriminators in the processing electronics. Thus, the measurements may be sorted into five size classes. In order of

increasing pedestal signal amplitude, the size classes used were: probable fluid measurements, definite fluid measurements, measurements of scattering particles of unidentifiable size, probable sand grain measurements, and definite sand grain measurements. The two fluid size classes are chosen to reflect the amount of noise inherent in the data. Unidentifiable scattering particles are those which scatter too much light to be classified as fluid tracer particles, but not enough light to be positively identified as sand grains. Two sand grain sizes were used to allow an added check on the separation of the fluid and sand grain measurements. Setting of the amplitude discriminators proved to be relatively simple. The light scattered by sand grains is very much larger than that scattered by the fluid tracer particles.

A zero-crossing counter is used to determine the Doppler burst frequency. The time required for a preset number of signal zero-crossings to occur is determined. The signal frequency is then given by

$$f = \frac{N-1}{\Delta t}$$

where f is the signal frequency, N is the preset number of zero-crossings, and Δt is the determined time. Two realizations of the Doppler burst frequency are made simultaneously.

The major difficulty with the laser-Doppler technique in sediment-laden flows is the low signal-to-noise ratio in the amplified photodetector output signal. Minor contributors to the signal noise are the photodetector dark current noise, noise due to background light sources, and electronic amplification noise inherent in any

laser-Doppler velocimeter. The major source of signal noise in sediment-laden flows is the simultaneous light scattering by multiple particles.

Scattering by two fluid tracer particles passing simultaneously through the beam intersection volume occurs occasionally in laser-Doppler applications in homogeneous fluid flows. The error so introduced is usually quite minor and can be minimized by reducing the particle number density. In sediment-laden flows, however, the situation is more complex. A sand grain which passes through a laser beam outside of the beam intersection volume scatters enough light to mask that scattered by a fluid tracer particle passing simultaneously through the beam intersection. This occurrence generates a burst of noise, which, after band pass filtering, is similiar to a valid Doppler burst signal. In fact, if the trajectory of the grain is very close to the beam intersection volume, the grain alone may generate a noise burst. The predominate frequency of a filtered noise burst is determined by the pass band of the filter and does not reflect the velocity of the generating scattering particles. Also, depending on the trajectory of the grain, the noise burst may appear to be either a fluid or sand grain measurement.

The majority of noise bursts are distinguishable from valid Doppler bursts. Unless the filter pass band is extremely sharp, the noise bursts are not quite regular in frequency. The most irregular of the noise bursts are eliminated by the counter-processor. The bulk of those recorded are identified in the data validation by insisting that the two different realizations of the burst signal frequency agree, as

delineated in Section IV. Some small fraction of the noise bursts, however, will undoubtedly be indistinguishable from valid Doppler bursts. The number of such noise bursts hidden within the validated data record is minimized by judicious choice of the band pass filter setting, the Doppler burst threshold level, the preset number of zero-crossings, and the particle size discriminators as discussed in Section III.

The preliminary data analysis produces a record of validated data events: scattering particle identity and velocity as a function of time, from the record of observed data events. The data from an event are discarded if the two realizations of the Doppler frequency do not agree and the particle is not identified as a sand grain. If the particle is a sand grain and the two realizations of the Doppler frequency do not agree, the event is retained in the data record, but the velocity measurement is tagged as unreliable. The detection of a sand grain, regardless of its velocity, allows for more accurate computation of the sediment transport rate and later analysis for possible conditional sampling errors in the velocimetry process.

III. Data Acquisition

The acquisition of data events occurring at irregular time intervals must be done in an electronically clean and orderly fashion. This is particularly true if the loss of any given data event is to be avoided. In sediment-laden flows, it is impossible to predict when a given event will have been generated by a sand grain. Hence, it is important that every event is capable of being successfully recorded.

The counter-processor is interfaced to the laboratory mini-computer through a general purpose digital interface with sixteen parallel data lines and two control lines. The first control line, EXT DATA RDY, allows the external generation of a processor interrupt causing the signals on the data lines to be read into memory under software control. The second control line, INT DATA ACC, signals to the external device that the data lines have been read. Each velocimetry event requires the transmission of two data words from the counter-processor to the computer. The internal computer programmable real time clock is used to time the arrival of the second data word.

Ideally, the use of the two control lines sets up a handshaking process --"data ready"-"okay, data received"-- between the counter-processor and the computer. Ideally also, because of the state logic of the counter-processor, data cannot be lost and the transmission of the correct data word is ensured. In practice, however, this was found not to be the case.

The first problem which was detected arises from the fact that the INT DATA ACC signal is generated electronically by the reading of the data lines by the computer. The signal may be generated before the computer is ready to receive another data word, or before the computer is able to detect another EXT DATA RDY signal. Before receiving another data word, the computer must write the data word into memory and, when necessary, read the internal clock and signal the completion of a data buffer. If an EXT DATA RDY signal is sent to the computer by the counter-processor before the computer is actually ready, one of two things result. Either the computer cannot detect the EXT DATA RDY

signal, or the signal is detected, and the computer is unable to respond properly. In either case, the data acquisition ceases.

This problem has been circumvented by setting the response time of the counter-processor to be sufficiently long that a new EXT DATA ACC signal cannot be generated before the computer is in actual fact ready. A maximum mean data event acquisition rate of approximately 1.5 KHz was obtained. This data rate is clearly adequate to characterize the fluid motion. Also, the transit time of a sediment grain through the measurement volume was of the order of one millisecond, so the number of grain measurements that might be missed is minimal. The data rate was therefore judged sufficient.

A better solution to this problem would be to implement a true handshake process. One of the bits in the data output buffer of the same general purpose digital interface should be used to generate a true "okay, data received" signal. The INT DATA ACC control line should be connected to the chosen output data bit. The bit should be set by the computer upon receipt of the EXT DATA RDY signal. After reading the data lines and recording the data, just prior to returning from the interrupt, the computer should clear the bit, thereby generating a signal electronically similiar to the INT DATA ACC signal currently in use. This signal would reflect the true capacity of the computer to accept new data.

The second difficulty encountered in the data acquistion was incorrect reporting of the data by the counter-processor. Approximately 0.05 per cent of the data words recorded as data from the "C" counter were, in fact, data words from the "U" or "V" counters.

This is due to fluctuations in the timing of the data select signals to the output multiplexers of the counter-processor. Altering these multiplexer data select signals, MUXAB and MUXBB, as shown in Figure III.1 would reduce the occurrence of this error. An additional estimated 0.1 per cent of the data words, at most, were recorded incorrectly due to transients on the data lines. The estimation was made on the basis of the data words which were observed to have incorrect data bits in the particle size information position of the first data word. Nothing was done to prevent the misreporting, as the amount of the erroneous data from these sources was not judged to be large and the data validation procedures used identify and or discard these events. Implementation of the suggested change to the multiplexer data select signals should reduce the misreporting.

The data are recorded for later processing in 256 word buffers. Each buffer contains the data from 85 consecutive velocimetry events (three words per event, a total of 255 words), and one word containing the number of buffers to follow. A pre-selected number of buffers are recorded. Note that while the number of events observed is pre-selected, the exact duration of the data record cannot be predicted. The period of observation is dependent on the incoming (variable) data rate.

At each location in the water column, the data acquisition proceeds as follows. First, several short sample data records are obtained. Various combinations of filter setting, Doppler burst threshold level, and preset number of zero-crossings are tried. Because of the high incidence of noise bursts, it is absolutely

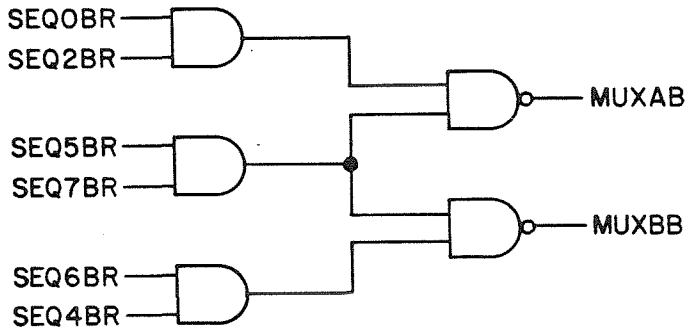

Figure III.1 Circuit diagram for the alteration of MUXAB and MUXBB

necessary to actually obtain and screen sample data records before a valid combination of the above instrumentation settings can be assured. After the determination of a valid setting or settings, data records of the desired time duration may be obtained. The approximate time duration of a record is predicted on the basis of the observed time duration of the relavant sample data record.

Again, the primary problem is distinguishing the good Doppler burst signals from the noise burst signals. Data acquisition is simple; the acquisition of valid data is not simple. Furthermore, since the primary source of noise is present only when sand is in motion, it is not possible to check the instrumentation settings by simple comparison with a clear water flow. It is quite possible to record data which, at first glance, appears to be turbulent velocimetry data, but which is only filtered noise. If the filter pass band is not centered at or near the mean Doppler burst frequency, if the Doppler burst threshold level is too low, or if the preset number of zero-crossings is too small, the noise bursts will predominate. If the Doppler burst threshold level is too high, good fluid Doppler bursts may be ignored; the valid data rate will be too low. If the preset number of zero-crossings is too large, the probability of valid Doppler bursts also decreases, as the effective measurement volume decreases; the valid data rate will again be too low. The lowest amplitude discriminator of the particle size detector may be used to set a lower bound on the pedestal amplitude of the signals identified as fluid measurements; burst signals with amplitudes less than some lower limit are more likely to be noise bursts. In practice it was found that, even with valid instrumentation settings, fifty to sixty per cent of

the data events obtained will not yield valid velocity measurements.

To determine the validity of a given setting, the data in each of the sample records are examined as follows. The mean and standard deviation of the number of counts (one count = one clock tick = 0.1 sec) required for the occurrence of the preset number of zero-crossings of the "U" counter are determined. Next, the deviation between the realization by the "U" counter and the "C" counter are computed and displayed. The deviation of a given measurement is given by

$$DEV = T_u - \left(\frac{N_u - 1}{N_c - 1}\right) T_c$$

where DEV is the deviation, Tu is the number of counts required by the "U" counter, Tc is the number of counts required by the "C" counter, Nu is the number of preset zero-crossings for the "U" counter and Nc is the number of preset zero-crossings for the "C" counter. The diagnostic display gives the probability distribution of the deviation as a function of the fluctuation in the "U" counter measurement (all entries are percentages summing to 100).

Four samples of the diagnostic display are given in Table III.1. The data records which generated these figures were obtained at a single location in the water column. All the data records contain the same total number of recorded events. The row of a given entry in the table is determined by its deviation; the column by its "U" counter measurement. The counter measurement is displayed in units of standard deviation. Thus "BAR" denotes the mean number of counts and "S" the standard deviation of the number of counts. Table III.1.a displays

COUNT	3800.	MEAN	226.41	SIGMA	20.42	MIN	156	MAX	511
		DMEAN	-1.09	DSIGMA	26.43	DMIN	-111	DMAX	222

	<-2S	>-2S	>-3S/2	>-S	>-S/2	>BAR	>+S/2	>+S	>+3S/2	>+2S
<-100	0.00	0.00	0.00	0.00	0.00	0.05	0.03	0.00	0.00	0.00
< -75	0.00	0.03	0.00	0.05	0.16	0.34	0.13	0.11	0.00	0.03
< -50	0.00	0.05	0.29	0.50	1.03	1.92	0.55	0.16	0.08	0.05
< -45	0.00	0.03	0.16	0.18	0.29	0.58	0.16	0.00	0.03	0.00
< -40	0.00	0.11	0.13	0.34	0.37	0.61	0.16	0.08	0.05	0.05
< -35	0.03	0.11	0.16	0.34	0.47	0.68	0.18	0.13	0.00	0.00
< -30	0.00	0.00	0.21	0.42	0.87	0.95	0.26	0.16	0.08	0.00
< -25	0.00	0.08	0.11	0.42	0.79	1.26	0.39	0.21	0.08	0.08
< -20	0.05	0.05	0.21	0.63	0.89	1.84	0.42	0.21	0.18	0.03
< -15	0.03	0.16	0.18	0.34	0.92	1.95	0.71	0.32	0.13	0.08
< -10	0.05	0.05	0.18	0.63	1.05	3.82	1.47	0.92	0.47	0.37
< -5	0.05	0.08	0.13	0.42	1.82	7.53	2.21	1.32	0.58	0.47
< 0	0.00	0.05	0.24	0.58	1.95	7.61	2.18	1.58	0.76	0.53
< 5	0.05	0.21	0.24	0.47	1.42	3.61	1.87	0.95	0.39	0.39
< 10	0.05	0.11	0.29	0.39	0.68	1.84	0.53	0.42	0.37	0.18
< 15	0.00	0.03	0.24	0.39	0.61	1.29	0.39	0.18	0.11	0.08
< 20	0.00	0.03	0.16	0.39	0.42	0.87	0.21	0.32	0.05	0.03
< 25	0.00	0.08	0.13	0.21	0.63	1.08	0.11	0.18	0.05	0.08
< 30	0.03	0.05	0.13	0.26	0.53	0.97	0.24	0.13	0.00	0.08
< 35	0.00	0.08	0.05	0.24	0.39	0.92	0.08	0.13	0.08	0.08
< 40	0.00	0.03	0.03	0.21	0.50	0.82	0.13	0.03	0.03	0.03
< 45	0.05	0.00	0.11	0.13	0.42	0.58	0.11	0.05	0.03	0.00
< 50	0.00	0.00	0.05	0.13	0.16	0.45	0.21	0.03	0.00	0.03
< 75	0.00	0.03	0.00	0.18	0.45	0.84	0.37	0.05	0.05	0.05
< 100	0.00	0.00	0.00	0.00	0.03	0.26	0.16	0.03	0.05	0.03
> 100	0.00	0.00	0.00	0.00	0.00	0.00	0.00	0.00	0.00	0.03

Doppler burst threshold: +3 Band pass filter: 500-700 KHz

Table III.1.a Sample test data diagnostic display
Valid instrumentation setting

COUNT	3902.	MEAN	245.56	SIGMA	21.45	MIN	189	MAX	510
		DMEAN	-1.21	DSIGMA	28.65	DMIN	-231	DMAX	309

	<-2S	>-2S	>-3S/2	>-S	>-S/2	>BAR	>+S/2	>+S	>+3S/2	>+2S
<-100	0.00	0.00	0.00	0.00	0.05	0.08	0.13	0.13	0.08	0.00
< -75	0.00	0.00	0.00	0.05	0.05	0.38	0.26	0.13	0.15	0.15
< -50	0.00	0.03	0.05	0.23	0.79	2.56	0.90	0.31	0.38	0.13
< -45	0.00	0.00	0.03	0.03	0.18	0.64	0.21	0.23	0.10	0.03
< -40	0.00	0.05	0.00	0.08	0.13	0.64	0.28	0.23	0.13	0.05
< -35	0.00	0.00	0.03	0.10	0.23	0.49	0.28	0.08	0.03	0.08
< -30	0.00	0.05	0.05	0.18	0.38	1.15	0.36	0.08	0.10	0.03
< -25	0.00	0.00	0.21	0.28	0.54	1.15	0.31	0.21	0.15	0.13
< -20	0.00	0.00	0.18	0.41	0.62	1.67	0.41	0.21	0.21	0.08
< -15	0.00	0.03	0.15	0.95	1.15	2.28	0.85	0.59	0.28	0.08
< -10	0.00	0.00	0.31	1.18	2.05	3.20	0.72	0.56	0.26	0.21
< -5	0.00	0.00	0.46	2.15	2.87	5.05	1.03	0.64	0.36	0.23
< 0	0.00	0.00	0.26	2.31	2.72	5.69	0.92	0.64	0.54	0.28
< 5	0.00	0.00	0.51	1.87	2.00	4.28	0.85	0.46	0.23	0.28
< 10	0.03	0.05	0.26	0.82	1.00	2.82	0.79	0.46	0.21	0.18
< 15	0.00	0.00	0.13	0.56	0.64	2.13	0.62	0.44	0.23	0.23
< 20	0.00	0.00	0.00	0.15	0.77	1.64	0.46	0.38	0.13	0.10
< 25	0.00	0.00	0.13	0.13	0.41	1.23	0.41	0.28	0.10	0.15
< 30	0.00	0.00	0.00	0.18	0.26	1.13	0.56	0.23	0.10	0.13
< 35	0.00	0.00	0.03	0.05	0.28	0.54	0.44	0.23	0.08	0.05
< 40	0.00	0.00	0.03	0.08	0.05	0.67	0.21	0.13	0.10	0.00
< 45	0.00	0.00	0.00	0.03	0.03	0.38	0.15	0.18	0.10	0.10
< 50	0.00	0.00	0.03	0.05	0.10	0.28	0.13	0.18	0.10	0.03
< 75	0.00	0.00	0.00	0.08	0.08	0.69	0.41	0.31	0.21	0.15
< 100	0.00	0.00	0.00	0.00	0.03	0.21	0.15	0.03	0.08	0.05
> 100	0.00	0.00	0.00	0.00	0.00	0.00	0.03	0.00	0.03	0.08

Doppler burst threshold: +3 Band pass filter: 400-600 KHz

Table III.1.b Sample test data diagnostic display
Low band pass filter setting

COUNT	3958.	MEAN	194.08	SIGMA	15.99	MIN	122	MAX	250
		DMEAN	-1.45	DSIGMA	21.65	DMIN	-92	DMAX	85

	<-2S	>-2S	>-3S/2	>-S	>-S/2	>BAR	>+S/2	>+S	>+3S/2	>+2S
<-100	0.00	0.00	0.00	0.00	0.00	0.00	0.00	0.00	0.00	0.00
< -75	0.00	0.00	0.03	0.03	0.05	0.08	0.10	0.03	0.03	0.00
< -50	0.00	0.10	0.38	0.53	0.61	0.99	0.15	0.20	0.05	0.03
< -45	0.00	0.00	0.13	0.25	0.30	0.30	0.08	0.00	0.00	0.00
< -40	0.05	0.05	0.20	0.40	0.48	0.45	0.05	0.13	0.00	0.00
< -35	0.03	0.05	0.18	0.45	0.66	0.73	0.15	0.08	0.03	0.00
< -30	0.10	0.08	0.23	0.35	0.63	0.96	0.23	0.15	0.08	0.05
< -25	0.03	0.10	0.25	0.53	0.81	1.52	0.43	0.10	0.00	0.03
< -20	0.08	0.10	0.48	0.35	0.86	2.17	0.38	0.30	0.05	0.03
< -15	0.03	0.10	0.43	0.63	0.91	2.50	0.81	0.38	0.18	0.03
< -10	0.03	0.08	0.51	0.66	1.06	3.39	2.20	0.96	0.53	0.18
< -5	0.10	0.03	0.56	0.61	1.19	5.58	4.27	2.27	0.78	0.33
< 0	0.05	0.28	0.38	0.38	0.88	6.42	4.40	2.48	0.71	0.28
< 5	0.10	0.20	0.48	0.71	0.78	3.39	2.32	1.04	0.58	0.23
< 10	0.03	0.15	0.48	0.43	0.63	1.84	0.93	0.28	0.23	0.03
< 15	0.05	0.15	0.28	0.58	0.61	1.29	0.48	0.28	0.08	0.00
< 20	0.05	0.13	0.35	0.61	0.51	0.83	0.30	0.13	0.05	0.03
< 25	0.03	0.15	0.18	0.51	0.53	1.06	0.33	0.05	0.03	0.00
< 30	0.00	0.15	0.10	0.40	0.33	0.81	0.20	0.05	0.05	0.00
< 35	0.00	0.05	0.05	0.38	0.30	0.71	0.13	0.08	0.05	0.03
< 40	0.00	0.05	0.15	0.13	0.53	0.48	0.23	0.00	0.00	0.00
< 45	0.00	0.00	0.13	0.13	0.30	0.35	0.18	0.10	0.05	0.00
< 50	0.03	0.00	0.03	0.05	0.05	0.28	0.08	0.05	0.00	0.00
< 75	0.00	0.00	0.03	0.08	0.13	0.25	0.13	0.08	0.00	0.00
< 100	0.00	0.00	0.00	0.03	0.00	0.00	0.03	0.00	0.00	0.00
> 100	0.00	0.00	0.00	0.00	0.00	0.00	0.00	0.00	0.00	0.00

Doppler burst threshold: +3 Band pass filter: 600-800 KHz

Table III.1.c Sample test data diagnostic display
High band pass filter setting

COUNT	3952.	MEAN	225.61	SIGMA	19.72	MIN	160	MAX	511	
		DMEAN	-0.96	DSIGMA	26.02	DMIN	-123	DMAX	260	
	<-2S	>-2S	>-3S/2	>-S	>-S/2	>BAR	>+S/2	>+S	>+3S/2	>+2S
<-100	0.00	0.00	0.00	0.00	0.00	0.05	0.00	0.00	0.00	0.00
< -75	0.00	0.03	0.03	0.03	0.10	0.18	0.10	0.05	0.00	0.03
< -50	0.05	0.15	0.15	0.53	0.61	2.18	0.23	0.23	0.03	0.00
< -45	0.00	0.00	0.15	0.20	0.30	0.58	0.10	0.00	0.05	0.00
< -40	0.00	0.08	0.18	0.18	0.40	0.84	0.13	0.10	0.00	0.00
< -35	0.00	0.08	0.20	0.40	0.53	0.91	0.20	0.15	0.03	0.00
< -30	0.03	0.03	0.10	0.30	0.78	1.49	0.15	0.20	0.05	0.05
< -25	0.00	0.10	0.15	0.35	1.06	1.49	0.38	0.30	0.13	0.03
< -20	0.00	0.10	0.13	0.73	1.14	2.58	0.46	0.33	0.23	0.03
< -15	0.00	0.13	0.18	0.23	1.01	2.78	1.06	0.46	0.23	0.18
< -10	0.03	0.03	0.33	0.58	1.32	4.81	1.47	0.91	0.30	0.38
< -5	0.03	0.10	0.13	0.33	1.57	6.17	2.07	1.44	0.58	0.56
< 0	0.05	0.10	0.23	0.38	1.57	5.24	1.67	1.04	0.51	0.40
< 5	0.05	0.08	0.15	0.40	1.09	3.95	1.37	0.81	0.51	0.30
< 10	0.03	0.08	0.30	0.30	0.81	2.78	0.99	0.48	0.15	0.08
< 15	0.05	0.00	0.20	0.43	0.63	1.82	0.68	0.30	0.23	0.18
< 20	0.00	0.08	0.15	0.30	0.68	1.11	0.35	0.13	0.08	0.03
< 25	0.00	0.08	0.23	0.38	0.51	1.24	0.25	0.18	0.05	0.03
< 30	0.00	0.00	0.10	0.33	0.56	1.14	0.10	0.08	0.03	0.03
< 35	0.00	0.03	0.15	0.15	0.48	0.86	0.18	0.08	0.00	0.00
< 40	0.00	0.00	0.15	0.20	0.35	0.63	0.18	0.03	0.05	0.00
< 45	0.00	0.08	0.10	0.10	0.35	0.61	0.20	0.08	0.03	0.00
< 50	0.00	0.00	0.03	0.03	0.25	0.40	0.08	0.05	0.05	0.03
< 75	0.00	0.00	0.03	0.10	0.56	0.94	0.43	0.13	0.08	0.03
< 100	0.00	0.00	0.00	0.00	0.03	0.13	0.05	0.03	0.03	0.03
> 100	0.00	0.00	0.00	0.00	0.00	0.00	0.00	0.00	0.00	0.05

Doppler burst threshold: +2 Band pass filter: 600-800 KHz

Table III.1.d Sample test data diagnostic display
Low Doppler burst threshold setting

data obtained with a valid instrumentation setting. When the deviation is in the range -5<DEV<+5, the distribution of Tu is centered and symmetric with respect to its mean. Table III.1.b illustrates the effect of setting the pass band of the filter too low. The distribution of Tu is skewed toward a low number of counts. For the data record shown in Table III.1.c, the pass band of the filter was set too high. The distribution of the number of counts is skewed in the opposite sense to the distribution in Table III.1.b. If the Doppler burst threshold level is set too low, a result similiar to Table III.1.d results. The distribution of Tu is symmetric, but flatter than that of Table III.1.a. Valid bursts become lost in noise.

IV. Data Validation

After the initial acquisition, the data are validated and a file containing valid velocimetry events is written. At the same time, some simple statistics are computed. Two processed data files result from each raw data file. The first file summarizes the simple statistics for each of the five primary size classes, six additional velocimetry size classes and six grain size classes. The second file contains the validated data events and the tagged invalid sediment grain events. The data are grouped in buffers of 16 events; the data from each event consist of the scattering particle identity, particle velocity in cm/sec, and time of measurement in seconds from the initial measurement (taken as t=0.000).

In addition to the five primary size classes stemming from the four amplitude discriminators in the particle size detector, several

additional size classes have been defined. Six additional sizes of valid data events are formed by combinations of the five primary sizes as shown in Figure IV.1 and Table IV.1. The additional size classes ease the grouping of the data for later display and analysis. Note that none of these cumulative size classes include size class three, as those data were generated by scattering particles of unidentifiable size. A sand grain which does not generate valid velocity data is tagged by negating its initial size. Thus, an invalid velocimetry event of size class 5 is entered into the validated data file as size class -5. To ease the manipulation of the grain events, six cumulative sand grain size classes were defined as shown in Table IV.2.

The data is validated in much the same way as the sample data records are examined. A maximum allowable deviation, or tolerance, is chosen. Typically, a value equal to one-half of the number of counts required by one zero-crossing was used. The deviation of each event is computed as before. If the absolute value of the deviation is less than the chosen tolerance value, the event is considered to be valid. If not, the deviation is recomputed to allow for the limiting error in the "C" counter. Counter-processors, by nature, have an inherent error of one count, or clock tick. While this is normally negligible, since the total number of counts is large, this was not true for the "C" counter. The "C" counter was used to count only a very few, typically three, zero-crossings, and the error introduced may be of the order of the chosen tolerance. This problem could be reduced by changing the 10 MHz clock currently used in the counter-processor with a 20 MHz clock as shown in Figure IV.2 The new deviation is computed as

$$NDEV = DEV + DSIGN * \left(\frac{N_u - 1}{N_c - 1}\right)$$

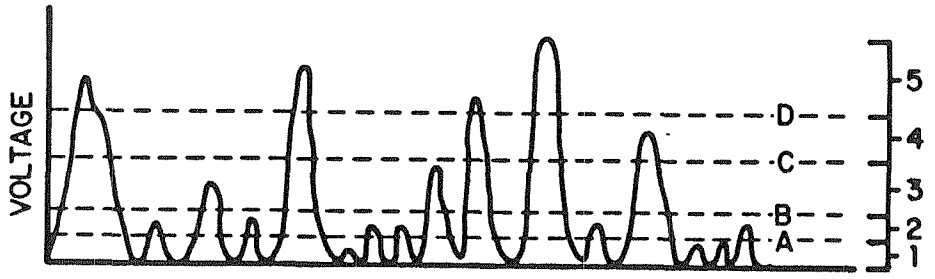

Figure IV.1 Velocity size classes

Table IV.1 Velocity size class sorting

Pedestal size \ Velocity size class	I	2	3	4	5	6	7	8	9	10	11
Less than threshold A	x					x		x		x	
Between thresholds A and B		x				x	x	x		x	x
Between thresholds B and C			x								
Between thresholds C and D				x		x	x		x		
Greater than threshold D					x	x	x		x	x	x

Table IV.2 Sand grain size class sorting

Initial velocity size class \ Cumulative grain size class	1	2	3	4	5	6
4				x	x	
5				x		x
-4	x		x	x	x	
-5		x	x	x		x

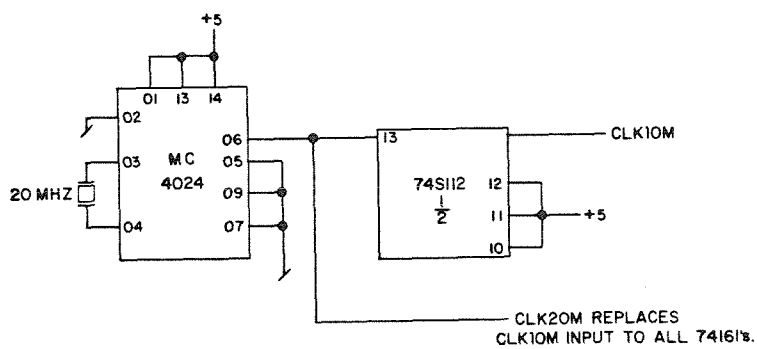

Figure IV.2 Circuit diagram for a 20 MHz reference clock oscillator

where NDEV is the new deviation and DSIGN is the sign of the deviation value, DEV. If the absolute value of the new deviation is less than the chosen tolerance value, the event is then considered validated.

The velocity is then computed for the validated fluid data and all sand grain data. The velocity is related to the Doppler burst frequency by

$$u = \frac{f\lambda}{2\sin\phi}$$

where f is the observed Doppler frequency, u is the velocity of the scattering particle, 2ϕ is the angle of the beam intersection, and λ is the wavelength of the laser light. For this system, the velocity is computed by

$$u = 1386 \frac{N_u - 1}{T_u}$$

where u is the velocity in centimeters/second, Nu is the preset number of zero-crossings for the "U" counter, and Tu is the number of counts reported by the "U" counter.

The summary file contains a file identification label and the number of buffers in the validated data event file. During the validation processing, the number of data events, mean velocity, velocity standard deviation, mean weighted velocity, weighted velocity standard deviation, mean inter-arrival time, and inter-arrival time standard deviation are computed for each of the eleven velocimetry size classes. Weighted velocities are computed to correct for the well known inherent bias in laser-Doppler velocimetry data. The weighting follows Mc Laughlin and Tiederman (1973). The mean and standard deviation of the inter-arrival times are computed for each of the six

cumulative grain size classes. These results are also written into the summary file. The maximum and minimum velocity, maximum and minimum inter-arrival time, total time of record, fraction of the data events discarded, and the skew and curtosis of the velocity for each size class are also determined, printed after the validation processing, but not stored in the summary file.

The validated data record is then screened for multiple measurements generated by a single scattering particle. Again, the Doppler modulated burst signal generated by a sand grain is longer in duration and greater in amplitude than that generated by a fluid tracer particle following the same trajectory through the measurement volume. Each sand grain may generate more than one velocity measurement. The data record is examined and measurements generated by a single grain are consolidated. If the time between successive data events is less than the mean time required for a grain to pass through the measurement volume, those events are assumed to be caused by the same grain.

Summarizing, the high probability of simultaneous light scattering by multiple particles is a major source of difficulty in laser-Doppler velocimetry in sediment-laden flows. Light scattered by multiple particles generates electronic signals which are quite similiar to valid Doppler burst signals; the frequency of such signals, however, is not simply related to the velocity of the generating scattering particles. The probability of the bursts of noise is a function of the local sediment concentration, the sediment grain size, the optical geometry of the laser velocimeter, and the local concentration of fluid tracer particles. Acquisition of valid velocity measurements can only

be assured by experimentation and subsequent careful data checking.

The validated data obtained at a single vertical location within the flow field consists of a time series of velocity measurements, each of which is identified as either a fluid measurement or a sand grain measurement. If the grain velocity measurement is not reliable, the measurement is so tagged. Each data record is not regular in time, nor does it include data from every scattering particle which passed through the velocimetry measurement volume. A data record does contain all or nearly all of the sand grains which passed through the measurement volume during the observation time. The validated data records obtained at locations throughout the water column may then be analyzed by various techniques to directly examine the small scale interactions between fluid turbulence and sediment motions.

REFERENCES

Mc Laughlin, D.K. and Tiederman, W.G., Biasing correction for individual realization of laser anemometer measurements in turbulent flows, Phys. Fluids, vol. 16, p. 2082-2088, 1973.

van Ingen, C., A processing system for laser-Doppler velocimetry for sediment-laden flows, W.M. Keck Laboratory if Hydraulics and Water Resources, California Institute of Technology, Technical Memorandum 80-1, 1980.